EFFECT OF GEOSYNTHETIC REINFORCED FILL ON THE FREQUENCY CONTENT OF EARTHQUAKE ZONES

by

Zeynep Esmerer

B.S., Civil Engineering, Boğaziçi University, 2015

Submitted to the Institute for Graduate Studies in
Science and Engineering in partial fulfillment of
the requirements for the degree of
Master of Science

Graduate Program in Civil Engineering

Boğaziçi University

2019

ACKNOWLEDGEMENTS

First and foremost, I am grateful to God for the good health and wellbeing that were necessary to complete this thesis.

I would like to express my special thanks to Prof. Erol Güler, my thesis advisor, for the sincere and valuable guidance and the continuous encouragement.

I am also grateful to my parents for accepting nothing less than excellence from me. I am extremely thankful and indebted to my mother and father for supporting me spiritually throughout writing this thesis and my life in general.

I would like to thank to Selim Sağlam, Yasin Toksoy and Kezban Kubalas, my colleagues and Ferit Yardımcı, my classmate, and also Ayşe Aydın for supporting my work and helping me throughout the school life.

I also place on record my sense of gratitude to one and all, who directly or indirectly have lent their hand in this venture.

ABSTRACT

EFFECT OF GEOSYNTHETIC REINFORCED FILL ON THE FREQUENCY CONTENT OF EARTHQUAKE ZONES

Destructive seismic loadings pose a great threat to the structural integrity of the soft soils underlying foundations in terms of service quality and serviceability. One of the effective means of improving soil is to make use of geosynthetic materials. Geosynthetics are commonly used as a reinforcement element in reinforced soil underlying foundations, to diminish the effects of earthquakes on structures. It is a proven fact that geosynthetics increases the bearing capacity of the soil and decreases the overall or partial settlement of soil under static loadings. The aim of the presented thesis is to understand the effect of the geosynthetic reinforcement, particularly geogrid, on the seismic behavior of the soft clayey soil underlying gravel fill, and examine the seismic performance of the geogrid reinforced soil under different ground motions. The identical prototypes of unreinforced and geogrid reinforced fill were numerically modelled using the finite element software. The focus of the study is to determine the impacts of different peak ground accelerations under different frequency of motions on the seismic performance of unreinforced and reinforced cases on the same model made up of soft clayey soil overlain by gravel. The comparison of unreinforced and reinforced cases were evaluated following numerical analyses of the average values of acceleration for the selected points and average energy values were computed with Arias Intensity. The hypothesis was that geogrid would absorb the energy and thus the energy at the selected points would be lessened in the reinforced case. Results show that most of the reinforced cases decreased the transmitted energy through the soil and the proposition is true for 70% of the results. However, the energy difference between the reinforced and the unreinforced cases is so minimal that gravel overlying soft clayey soil may have a greater influence than geogrid on the seismic behavior of soil.

ÖZET

FREKANS İÇERİĞİNİN DEPREM BÖLGELERİNDE GEOSENTETİKLERLE GÜÇLENDİRİLMİŞ DOLGUYA ETKİSİ

Yıkıcı deprem yükleri, temel altındaki zayıf zeminlerin yapısal bütünlüğüne karşı hizmet kalitesi ve hizmetedebilirlik açısından büyük bir tehlike oluşturmaktadır. Zemin iyileştirmeleri için geosentetik malzemeler verimli çözümlerden birisidir. Geosentetikler, depremlerin yapılar üzerindeki etkilerini azaltmak için donatı olarak temel altındaki güçlendirilmiş zeminlerde sıkça kullanılır. Geosentetiklerin toprağın taşıma kapasitesini arttırdığı ve statik yükler altında toprağın tüm veya kısmi oturmalarını azalttığı kanıtlanmış bir gerçektir. Sunulan tezin amacı, geosentetik takviyenin özellikle geogridin çakıl dolgu altındaki gevşek killi zeminin sismik davranışı üzerindeki etkisini anlamak ve geogridli zeminin sismik performansını farklı yer hareketleri altında incelemektir. Takviyesiz ve geosentetikli dolgunun birebir aynı prototipleri, sonlu elemanlar yazılımı kullanılarak sayısal olarak modellenmiştir. Araştırmanın odak noktası, farklı maksimum zemin ivmesi ve farklı frekansların, donatısız ve donatılı durumlardaki çakıl ile örtülmüş yumuşak killi zeminden oluşan aynı modeller üzerindeki sismik performansdaki etkilerini belirlemektir. Güçlendirilmemiş ve güçlendirilmiş durumların karşılaştırılması, seçilen noktalar için ortalama ivme değerleri ve Arias Yoğunluğu ile hesaplanan ortalama enerji değerleri açısından sayısal analizlere bakarak değerlendirildi. Varsayım, geogridin enerjiyi emmesidir ve bu nedenle seçilen noktalardaki enerjinin geogridli durumda azalmış olması gerekir. Sonuçlar, geogridli durumların çoğunun zemin yoluyla iletilen enerjiyi azalttığını ve önermenin sonuçların %70'i için doğru olduğunu göstermektedir. Fakat geogridli ve donatısız durumlar arasındaki enerji farkı öylesine az ki, belki yumuşak killi zeminlerin üzerindeki çakıl, zeminin deprem davranışında geogridden daha fazla etkiye sahip olabilir.

TABLE OF CONTENTS

LIST OF FIGURES

LIST OF TABLES

LIST OF SYMBOLS

a	Acceleration
$a(t)$	Function of acceleration with respect to time
C_{ref}	Cohesion of soil
$d(t)$	Incremental Change in Time
E_{ref}	Stiffness
g	Acceleration of gravity
I_A	Arias Intensity
kN	kilo Newton
$K_{x,y}$	Coefficient of Permeability in x and y direction
m	meter
s	Second
T_d	Duration of signal
$v(nu)$	Poisson Ratio
γ_{sat}	saturated unit weight of soil
γ_{unsat}	unsaturated unit weight of soil
$\Phi(phi)$	Friction angle

LIST OF ACRONYMS/ABBREVIATIONS

EPS	Expanded Polystyrene
FEM	Finite Element Method
GCL	Geosynthetic Clay Liner
GSI	Geotechnical Seismic Isolation
HZ	Hertz
PGA	Peak Ground Acceleration
SA	Spectral Acceleration
SI	Seismic Isolation
UHMWPE	Ultrahigh Molecular Weight Polyethylene

1. INTRODUCTION

1.1. General

Civil engineering structures are exposed to static and dynamic loadings. An earthquake is the most common and destructive dynamic loading. An earthquake is the shaking of the surface of the Earth, resulting from the sudden release of energy in the Earth's Lithosphere, which creates seismic waves. Earthquakes can range in size from those that are so weak that they cannot be felt to those violent enough to toss people around and destroy entire cities. As the wave travels from the lithosphere to the surface, it changes in character and amplitude depending on the soil layers. Therefore, the effect of the investigated ground is generally analyzed by modelling the soil under static and dynamic conditions with the help of computer programs.

At the Earth's surface, earthquakes are manifested on soil in the form of shakes, displacement or disruption of the ground. That is why, researchers try to reduce the effects of hazardous earthquakes, thereby minimizing the cost of engineering applications.

Soil failures have a great impact on the structures that are built on it. Before deciding on soil improvement, geological, geotechnical, environmental and economical parameters should be taken into consideration in detail. Geosynthetic material is a very effective solution for soft foundation soil improvement with a relatively low cost compared to many other ground improvement methods. Since the stability of soil is a serious problem especially under seismic loading, it may be a good idea to deal with it through the use of geosynthetic reinforcement.

1.2. Statement of the Problem

Earthquakes are the most dangerous and common threats especially to the stability of man-made engineering structures. Because of the propagating ground motions

followed by their secondary effects, earthquakes are one of the most destructive natural disasters. Despite the fact that there are numerous studies in the literature that focus on how to mitigate related earthquake hazards on engineering structures and enhance performance, as in the case of load settlement of the foundation soil system under monotonic loadings, the dynamic behavior of geosynthetic reinforced soft foundation soils is one of the least studied cases. Soft soils are encountered very frequently. Before constructing the structure on the ground, it is essential that the soil be investigated and, if necessary, improved. And geosynthetic reinforcement is an effective way of ground improvement. It is common practice to place a granular fill (usually gravel) on soft soil and carry out geosynthetic reinforcement within this granular fill. Since the dynamic behavior of the soft clayey soil may change in case a geosynthetic reinforced gravel layer is placed on the top, it is important to investigate and understand the seismic response of reinforced soft clayey soil overlain by gravel.

1.3. Objective of the Thesis

The aim of this study is to determine the effect of the geosynthetic reinforcement on the seismic performance of the soils and evaluate the seismic performance of the geogrid reinforced soft soil under different earthquake motions. Specifically, this study aims at identifying the effects of the ground motion (peak ground acceleration) of different frequencies of motion as well as the amplitude of the earthquake. To this end, models composed of soft clayey soil overlain by gravel layer were analyzed for results both with and without a geogrid reinforcement.

It is expected that transmitted accelerations using energy absorbent geosynthetic materials namely geogrid will ultimately be minimized to maintain soil stability under different earthquake conditions. To measure energy absorption and compare it with the unreinforced case, the theory of Arias Intensity was utilized. The Arias Intensity (IA) is a measure of the total energy of the ground motion. The Arias Intensity will be explained further in Specification Part 2.1. Arias Intensity values are calculated with the help of Matlab 2018. Results can give an insight into whether the geogrid can change the seismic response of reinforced soft soils overlain by gravel.

It should be noted that in the presented thesis, the effects of the number of layers of geosynthetic reinforcement (N) are not examined.

1.4. Organization of the Thesis

This study investigates the effect of geosynthetic reinforced fill on the frequency content of earthquake zones. The thesis involves numerical analysis including reinforced and unreinforced cases to evaluate the effect of geosynthetic reinforcement. Through the use of the numerical dynamic analysis program, Plaxis 2D developed on the finite element model, acceleration data at selected points have been obtained to determine the energy in the form of Arias Intensity. The influence of geosynthetic reinforcement, peak ground acceleration (PGA) and frequency of the motion on the soft clayey soil overlain by gravel have been examined in detail.

2. SEISMIC ANALYSIS

In geotechnical engineering, bearing capacity can be defined as the capacity of the soil to resist the loads transmitted to the ground. In other words, bearing capacity is the capability of the soil to carry out the loads/stresses/pressures applied to the soil by any engineering structure without undergoing shear failure or unacceptable large settlements.

An extreme building distortion and even toppling may originate from a soil shear failure. Excessive settlements can lead to structural damage to the framework of a building, such as cracks in tile or plaster. It is strongly recommended that investigation of both base shear resistance, bearing capacity of soil and soil settlements under static as well as dynamic conditions for any structure be made. Guler and Cicek (2018) investigated the load-settlement-failure behavior of a shallow strip footing on an unreinforced and reinforced medium dense sand by performing laboratory plate load tests and finite element analyses with the help of Plaxis. The study only dealt with static condition. The effects of changes in bearing capacity due to reinforcement configuration were examined. It was shown that type and configuration of reinforcement affect bearing capacity, settlements and the failure mode.

Although, researchers place great importance on static stability problems associated with geosynthetic reinforced foundation systems, there isn't sufficient attention paid to the dynamic response of superstructures incorporating geosynthetics. In the presented master's thesis, the concern regarding the dynamic response of a geotechnical facility combined with geosynthetic systems to energy thorough acceleration output is examined in detail.

Seismic waves can trigger destructive inertial forces in natural or artificial slopes, embankments, soil in general and superstructures. Earthquake ground motions may lead to destabilization problems especially for the soil under foundation. Instantaneous and severe earthquake loads might affect the shear strength of the soils by producing

excessive pore water pressure. The combined impact of the seismic loads and the alteration in the shear strength may lead to an overall decrease in the stability of the soils. On the other hand, generation of the high pore water pressure due to the cyclic loads may cause transformation of the soft as well as cohesionless and saturated materials (sand, silt etc.) into a liquefied condition where the shear strength of the soil is nearly zero.

In the literature review, the stability of slopes or soils in general during an earthquake are examined with the help of four basic methods of analyses (Houston *et al.* 1987):

- Pseudostatic Method: The earthquake inertial forces are simulated through containment of a static horizontal and vertical force in a limit equilibrium analysis.
- Newmark's Displacement Method: This method focuses on the idea that the actual slope acceleration may exceed the static yield acceleration at the expense of generating permanent displacements (Newmark,1965).
- Post-Earthquake Stability (Weakening Slope Stability): This is calculated using laboratory undrained strengths, using representative soil samples that have been subjected to cyclic loads comparable to those arising during an anticipated earthquake (e.g. Castro *et al.*, 1985).
- Dynamic Finite Element Analysis: A coupled two or three dimensional analysis using an appropriate constitutive soil model will provide details of stresses, strains, and permanent displacements (e.g. Finn, 1988; Prevost *et al.*, 1985) Since in this thesis, software based on finite element method was used, finite element method will be dealt with below comprehensively.

Finite element method allows engineers to evaluate the stability of complex structures. The method was first introduced to geotechnical engineering by Clough and Woodward (1967) and today it is commonly used in soil engineering analyses software especially for the analyses of complex earth structures like piles or earth dams. Finite Element Method (FEM) divides soil continuum into discrete elements that are called finite elements. These elements are interconnected at nodes (Figure 2.1). The FEM

assumes a simple approximation of unknown variables to transform partial differential equations into algebraic equations. Physical laws and numerical methods are developed based on the necessary solutions, and calculations are carried out on the computer (Dhatt, 2012 (Finite Element Method)). In this thesis, to analyze the soil and to examine the response of the soil under earthquake motions, Finite Element Method was used along with the Plaxis 2D software.

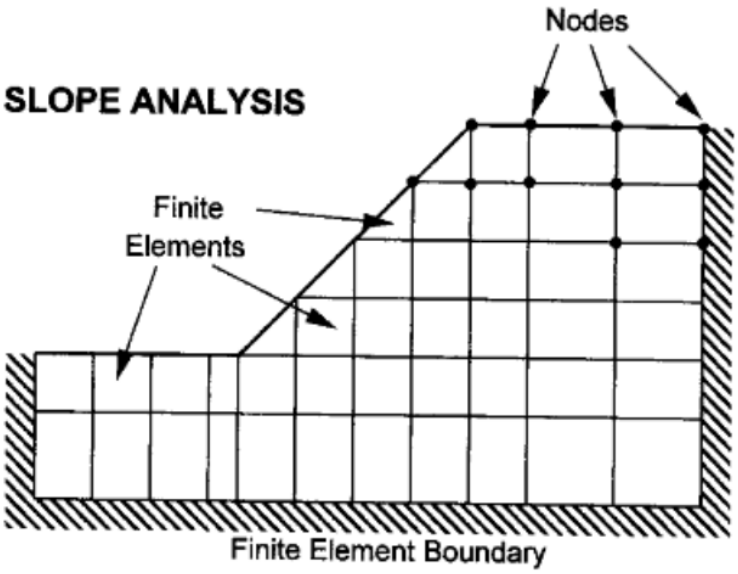

Figure 2.1. Basis of Finite Elements Method for slope analysis (Abramson, 2002).

The finite element analysis is time consuming and requires results of detailed field or laboratory testing to be obtained. Toksoy (2014) examined the performance of geosynthetic reinforced (geotextile) highway embankments under static and dynamic loading conditions. In that research, finite element method was utilized for analysis. Experimental and numerical analyses were conducted for both static and dynamic cases. The research was carried out based on finite element method and it demonstrated that geosynthetic reinforcement is an effective way to achieve the desired factor of safety.

3. SEISMIC ISOLATION

It is an indisputable fact that earthquakes have destructive effects on and cause damage to structures. Strong ground motion may lead to damage costing billions of dollars to local or global economy. Thus, it is important to minimize the effects of earthquake with the help of site improvement methods like geosynthetics if possible.

For many years, mechanical-base isolators have been designed and used by structural earthquake engineers to protect superstructures from seismic damage. Basically seismic isolation system of a structure aims at creating discontinuity between the superstructure and the ground, so that the amount of the transmitted energy, force and its acceleration from ground to the superstructure is restricted.

Recently in earthquake engineering practices, seismic base isolation has been used as the most suitable technique for vibration control. Base isolation can be described as a flexible material that is placed on the ground to decrease the transmitted seismic forces of any structure. The main aim of seismic isolation is to place laterally flexible but vertically stiff elements (base isolators) on the foundation of a building to significantly minimize the effect of a high-frequency earthquake on the superstructure. The basic principle of base isolation system is to extend the natural period of the fixed base building. This way, the sufficient stretched period of vibration of the superstructure allows a decrease in the force response where base isolator acts as energy dissipater. In other words, its essential function is to reduce the harm it does to structures subjected to intense ground motions by means of both an increase in the length of the fundamental period of vibration and additional damping, which results in fewer floor accelerations. Currently, many earthquake-prone countries in the world utilize this technology. Today, geosynthetics can also be used as base isolators but because the methodology is not fully mature yet, it is rarely utilized for this purpose.

Geosynthetic reinforced fill underlying the foundation is another alternative method that can be used to decrease destructive effects of earthquakes on the superstructure.

It is important to realize that base isolation is different from geosynthetic reinforced soil. Geosynthetic reinforced soil under superstructure has been frequently used to ensure resistance against destabilizing forces. It can be defined as replacing a mass of weak soil with geosynthetic reinforced fill. In this research, geogrid reinforced soil (which can underlie the superstructure) under seismic load will be examined for its role in earthquake hazard mitigation.

4. GEOSYNTHETICS

For engineering applications, geosynthetics in general corresponds to materials which are made of polymers and are used as key components in a structural system. The prefix "geo" refers to applications that have to do with soil, earth... etc. Some of the main functions of geosynthetics can be listed as filtration, drainage, reinforcement, isolation, separation and protection. Geosynthetics can be utilized for one or more of the functions at the same time. Geosynthetic applications are widely used in several areas such as transportation, geotechnical, civil, environmental, and hydraulics engineering to name a few. Geosynthetics are mainly divided into eight main product categories: geotextiles, geogrids, geonets, geomembranes, geosynthetic clay liner, geofoam, geocells and geocomposites

4.1. Geotextiles

Geotextiles are thin, flexible and porous sheets of synthetic material used to stabilize the soil and improve the strength of soil utilized in engineering applications. Geotextiles may filter, drain, reinforce and separate the soil under correct application. A combination of these functions may be utilized in one application. For instance, while laying down geotextile at the base of granular fill embankment constructed over soft clay, all the above mentioned functions can be carried out.

4.2. Geogrids

Geogrids are mainly made up of polymer materials in the shape of grids. Geogrids are generally used to reinforce retaining walls, subbases as well as subsoils below roads or structures. Soils pull apart under tension. Compared to soil, geogrids are stronger in the face of tension. That is why, they are likely to be used as reinforcement for soil.

4.3. Geonets

Geonets are made of polyethylene resin. A geonet is similar in structure to a geogrid in that it is composed of interconnected parallel sets of ribs overlying similar sets as a homogenously netlike configuration. They are commonly used for drainage purposes.

4.4. Geomembranes

A geomembrane is a thin impermeable or very low permeable synthetic membrane barrier used for mainly blocking migration of fluid (or gases) in engineering projects or structural systems. Possible areas of usage can be canals, landfills, and reservoirs especially those with leakage or contamination problems.

4.5. Geosynthetic Clay Liners (GCL)

Geosynthetic clay liners (GCLs) are factory manufactured hydraulic barriers consisting of a layer of bentonite or other very low-permeability material supported by geotextiles and/or geomembranes, mechanically held together by needling, stitching, or chemical adhesives (Koerner, 2012).

Any leakage from landfills must be collected and properly disposed of in accordance with environmental laws. Otherwise, contamination of the surrounding ground water may lead to major environmental and ecological problems. GCLs are frequently used and are the best choice for these environmental containment disposal applications.

4.6. Geopipe

Geopipe is specifically designed and manufactured to be a practical solution to all drainage problems. The 70% open area of the geopipe allows for a significant increase in the rate of water infiltrating into the pipe. It is used in many geotechnical, environmental and transportation applications such as wastewater, sewer, irrigation

systems and so forth.

4.7. Geofoam

Geofoam is a long lasting and lightweight material produced by EPS (expanded polystyrene foam). It is used in roads and many construction areas as a backfill behind retaining walls, lightweight fill on the road, building fill for floor elevations, slope stabilization and so on.

4.8. Geocomposites

When two or more types of geosynthetics are used in combination, geocomposites form. Basic functions of geocomposites are separation, reinforcement, filtration, drainage, and containment. Some of the common types of geocomposites can be listed as below:

- 1 Geotextile-geonet composites
- 2 Geotextile-geomembrane composites
- 3 Geomembrane-geogrid composites
- 4 Geotextile-geogrid composites
- 5 Geotextile-polymer core composites

5. RELATED SEISMIC PARTS OF THE NEW TURKISH SEISMIC SPECIFICATION 2018

The thesis has been analyzed in detail for the compliance of the modelling suggested here with the Seismic Specification Part 2-Earthquake Ground Motion, since the New Seismic Specification (2018) was put into force as of January, 2019.

The AFAD seismic map used in this study is shown in Figure 5.1. The soft clay soil type has been chosen as a typical case for this study. The values for the parameters obtained from the seismic map and the spectral acceleration graph provided as output have been checked to see whether the values match the horizontal elastic design spectrum that we have come up with using the parameters of our modelling. In Turkish Seismic Specification Part 2.2, level of earthquake ground motions have been categorized as DD-1, DD-2, DD-3, DD-4. For each the horizontal elastic design spectrums can be drawn manually; but on the AFAD map, level of earthquake ground motion is selected as DD-4 to see the accuracy of drawn horizontal elastic design spectrum with the program spectrum output corresponding to 0.2g PGA in the selected region. The related part of the Specification is given in Part 5.1. The 0.2g PGA horizontal elastic design spectrum figure of the program output has been found to be matching with the one given in Figure 5.4 according to the Seismic Specification.

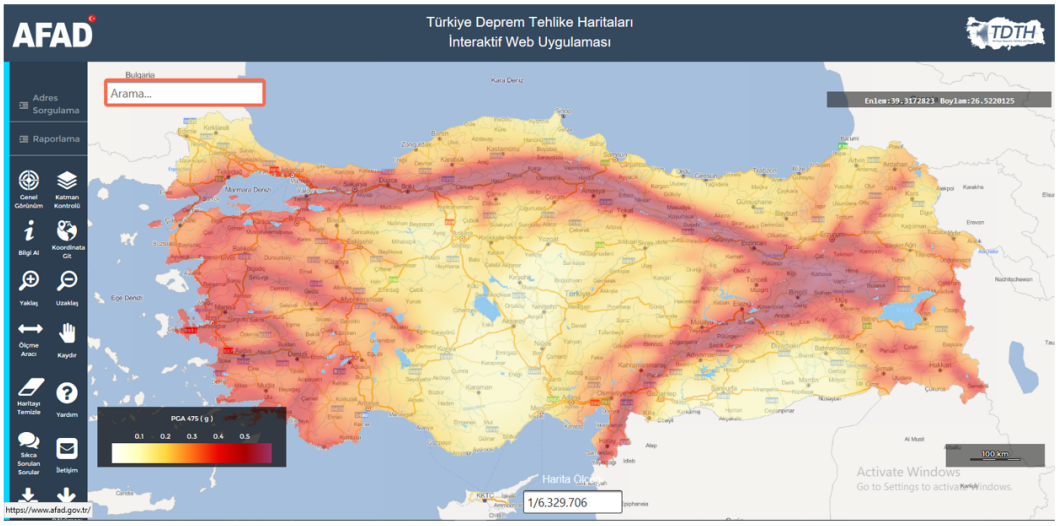

Figure 5.1. Earthquake Hazard Map. (https://tdth.afad.gov.tr).

5.1. The Seismic Specification Part 2.2.4 Seismic Earth Movement Level-4 (DD-4)

DD-4 Seismic Earth Movement refers to the very frequent Seismic Earth Movement, for which the possibility of excess of spectral sizes in 50 years is 68% (with a 50% possibility of excess within 30 years), with the relevant recurrence period being 43 years. Such seismic earth movement is also called service seismic earth movement.

Afterwards, in Specification Part 2.3 titled Standard Seismic Movement Spectrum has been examined. The related part of the New Seismic Specification has been given in the Part 5.2.

5.2. The Seismic Specification Part 2.3.2. Map Spectral Acceleration Coefficients and Design Spectral Acceleration Coefficients

The Seismic Specification Part 2.3.2.1 Dimensionless map spectral acceleration coefficients have been identified in accordance with Turkish Maps of Seismic Risks for 4 different levels of seismic movement described in Specification Part 2.2.

- Short period map spectral acceleration coefficient S_s
- Map spectral acceleration coefficient for a period of 1.0 second S_1

Map spectral acceleration coefficients that provide the geometric average of the effects of perpendicular two horizontal earthquakes have been identified as dimensionless coefficients that have been obtained by means of the division of map spectral accelerations by the gravitational acceleration for an acceleration rate of 5% using the reference ground condition of [$(Vs)_{30}$=760 m/s] for a given seismic earth movement.

The map spectral acceleration coefficients S_s and S_1 described in Specification Parts 2.3.2.2-2.3.2.1 are converted to design spectral acceleration coefficients S_{DS} and

S_{D1}.

$$S_{DS} = S_{S*}F_S$$
$$S_{D1} = S_{1*}F_1 \tag{5.1}$$

Here, F_S and F_1 refer to the local ground effect coefficients described in Specification part 2.3.3. In Specification part 2.3.2.3. Horizontal and vertical elastic design spectra have been identified in Specification parts 2.3.4 and 2.3.5 respectively using spectral acceleration coefficients obtained through Equation 5.1.

5.3. Specification Part 2.3.3. Local Ground Effect Coefficient

In Specification part 2.3.3.1, in accordance with the local ground classes described in Specification Part 16.4, local ground effect coefficients F_S and F_1 can be seen in Table 5.1 and Table 5.2 respectively. Linear interpolation can be performed for the intermediate value of the map spectral acceleration coefficients.

In order to use the values in Table 5.1, initially, the local ground class was identified using Specification Table 5.2 in part 16.4. As the value of the soft clay ground c_u (cohesion) is 24 kPa, the values below 70 kPa cohesion in Table 16.1 are in line with the ZE ground class. The relevant parameter values needed for ZE ground class have been bolded in Table 5.1 and Table 5.2.

Table 5.1. Local Ground Effect Coefficients for the Short Period Area.

Local Ground Class	Local Ground Effect Coefficient F_s for the Short Period Area					
	$S_S \leq 0.25$	$S_S = 0.50$	$S_S = 0.75$	$S_S = 1.00$	$S_S = 1.25$	$S_S \geq 1.50$
ZA	0.8	0.8	0.8	0.8	0.8	0.8
ZB	0.9	0.9	0.9	0.9	0.9	0.9
ZC	1.3	1.3	1.2	1.2	1.2	1.2
ZD	1.6	1.4	1.2	1.1	1.0	1.0
ZE	**2.4**	**1.7**	**1.3**	**1.1**	**0.9**	**0.8**
ZF	Field- specific ground behaviour analysis will be carried out (See 16.5)					

Table 5.2. Local Ground Effect Coefficients for a 1.0 second-period

Local Ground Class	Local Ground Effect Coefficient F_1 for a 1.0-second-period					
	$S_1 \leq 0.10$	$S_1 = 0.20$	$S_1 = 0.30$	$S_1 = 0.40$	$S_1 = 0.50$	$S_1 \geq 0.60$
ZA	0.8	0.8	0.8	0.8	0.8	0.8
ZB	0.8	0.8	0.8	0.8	0.8	0.8
ZC	1.5	1.5	1.5	1.5	1.5	1.4
ZD	2.4	2.2	2.0	1.9	1.8	1.7
ZE	**4.2**	**3.3**	**2.8**	**2.4**	**2.2**	**2.0**
ZF	Field- specific ground behavior analysis will be carried out (See 16.5)					

5.4. Soil Classification According to Turkish Seismic Code

To be able to use the values in Table 5.1, a local ground classification has been initially made using Table 5.3 in Specification Part 16.4.

Table 5.3. Local Ground Classes

Local Ground Class	Type of Ground	Average for the top 30 meters		
		$(V_S)_{30}$ [m/s]	$(N_{60})_{30}$ [blow /30 cm]	$(C_u)_{30}$ [kPa]
ZA	strong, hard rocks	> 1500	-	-
ZB	semi-weathered, medium strength rocks	760 - 1500	-	-
ZC	weathered sand, gravel and solid clay layers or weathered, multi-cracked weak rocks	360 ? 760	> 50	> 250
ZD	medium- hard, hard sand, gravel or very hard clay layers	180 ? 360	15 ? 50	70 ? 250
ZE	loose sand and gravel, or soft, hard clay layers or profiles consisting of soft clay layers (Cu ¡ 25 kPa) thicker than 3 metres in total that meet the requirements of PI>20 and w>40%	< 180	< 15	< 70
ZF	grounds requiring field specific assessment and evaluation 1. Grounds that carry the risk of collapse or potential collapse under the influence of an earthquake (blemish grounds, highly sensitive clays, weak cement ground that is likely to collapse, etc.) 2.Turba clays that are thicker than 3 meters in total and/or clays with high organic content 3. High plasticide clays (PI¿50) that are thicker than (meters in total 4.Very thick (>35m) soft or medium- hard clays			

5.5. The Specification Part 2.3.4. Horizontal Elastic Design Spectrum

In Seismic Specification Part 2.3.4.1, for a given seismic earth movement, the coordinates of horizontal elastic design acceleration spectrum, namely horizontal elastic design spectral accelerations Sae(T), have been identified in Equation 5.2 in terms of their gravitational acceleration (g) according to the natural vibration period.

$$\begin{aligned} S_{ae}(T) &= \left(0.4 + 0.6\tfrac{T}{T_A}\right) S_{DS} && (0 \le T \le T_A) \\ S_{ae}(T) &= S_{DS} && (\mathrm{T}_A \le T \le T_B) \\ \mathrm{S}_{ae}(\mathrm{T}) &= \tfrac{S_{D1}}{T} && (T_B \le T \le T_L) \\ \mathrm{S}_{ae}(\mathrm{T}) &= \tfrac{S_{D1}T_L}{T^2} && (\mathrm{T}_L \le \mathrm{T}) \end{aligned} \tag{5.2}$$

Here, S_{DS} and S_{D1} show the design spectral acceleration coefficients described in Specification part 2.3.2.2 and T refers the natural vibration period. Horizontal design spectrum corner periods T_A and T_B are defined in Equation 5.3 according to S_{DS} and S_{D1}:

$$T_A = 0.2\frac{S_{D1}}{S_{DS}} \quad ; \quad T_B = \frac{S_{D1}}{S_{DS}} \tag{5.3}$$

Fixed Replacement Area Transition period will be taken as T_L=6 s.

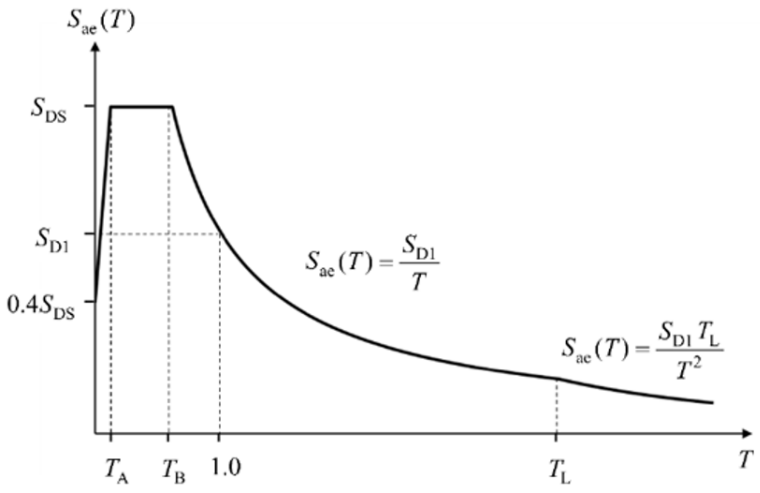

Figure 5.2. Horizontal elastic design spectral accelerations Sae(T).

The values for the Equation 5.1 given in Specification part 2.3.2.2., the Equation 5.2 and Equation 5.3 in Specification part 2.3.4 as well as the related coefficients in Table 5.1 and Table 5.2 have been adapted and horizontal elastic design spectrum acceleration graphs have been prepared following their calculation for different types of ground acceleration (0.1g PGA, 0.2g PGA, 0.3g PGA, 0.4g PGA). Figure 5.3, Figure 5.4, Figure 5.5, Figure 5.6 show the relevant design spectrum acceleration graphs obtained from the Finite Element analysis. In order to check the correctness of the calculations, a comparison of the horizontal elastic design acceleration spectrum for the model and a representative chosen point on the AFAD map has been made. The horizontal elastic design acceleration spectrum of the model, with a ground acceleration value of 0.2g, as shown in Figure 5.4, is in line with the horizontal elastic design spectrum acceleration of a representative chosen point on the AFAD map in Figure 5.7 with a value of 0.2g PGA.

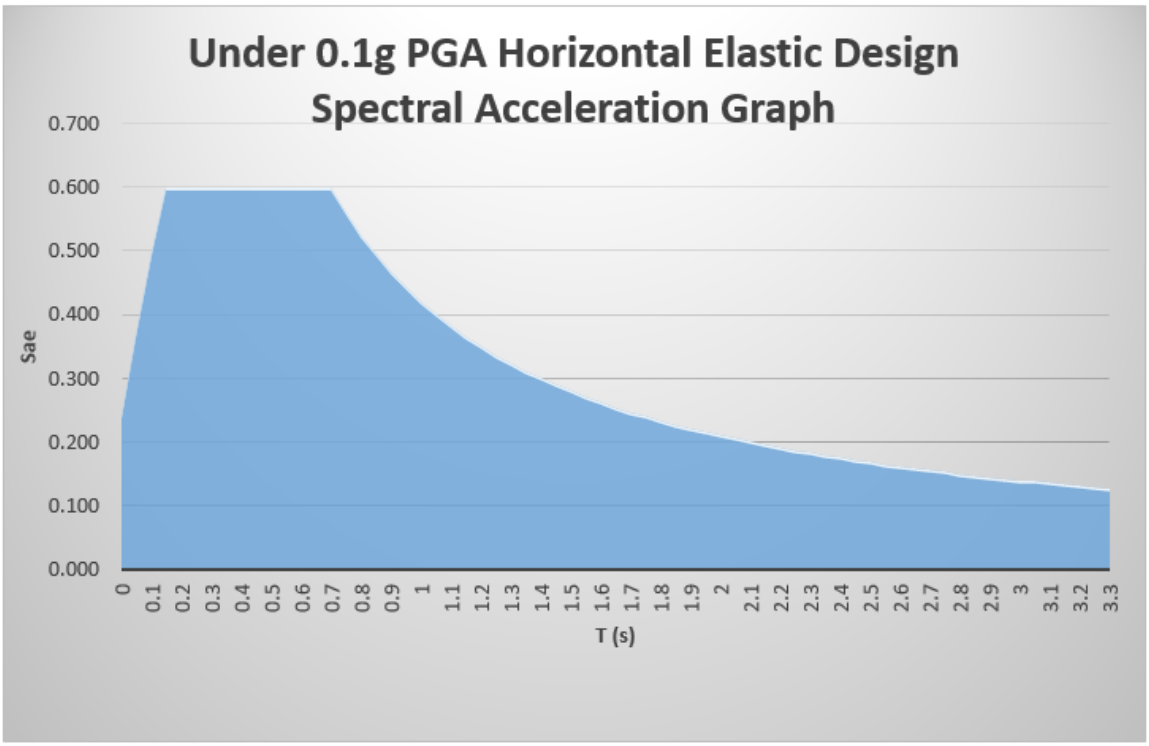

Figure 5.3. Under 0.1g PGA, Horizontal Elastic Design Spectrum.

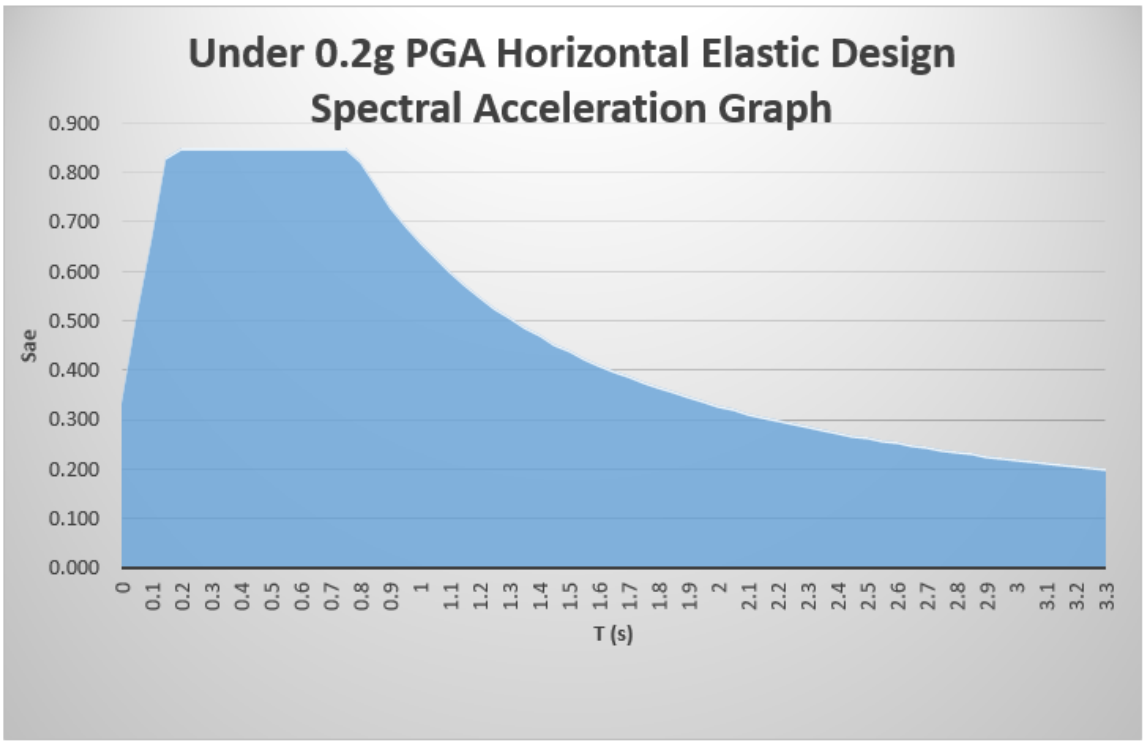

Figure 5.4. Under 0.2g PGA, Horizontal Elastic Design Spectrum.

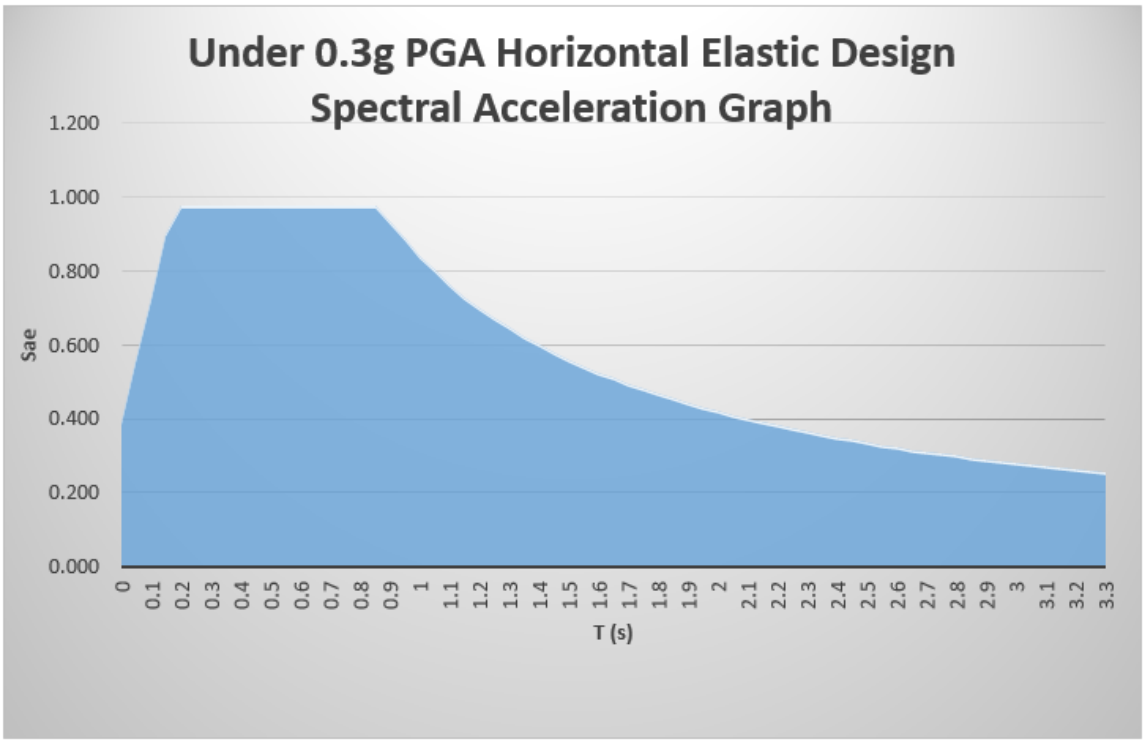

Figure 5.5. Under 0.3g PGA, Horizontal Elastic Design Spectrum.

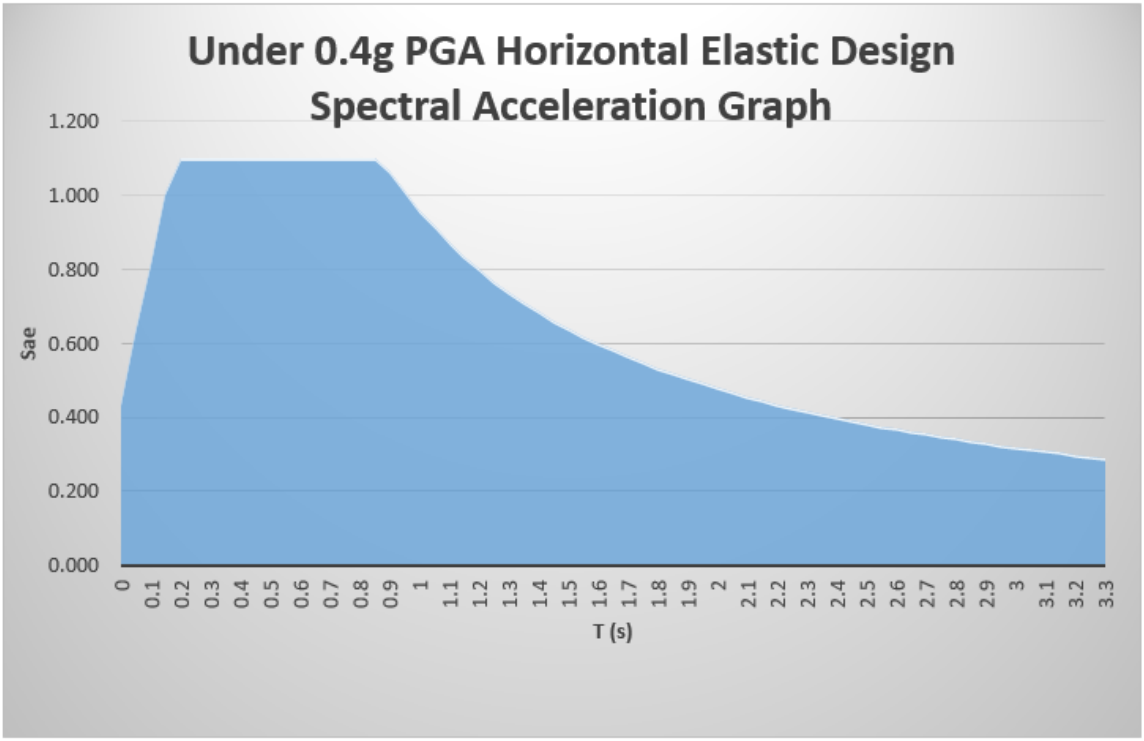

Figure 5.6. Under 0.4g PGA, Horizontal Elastic Design Spectrum.

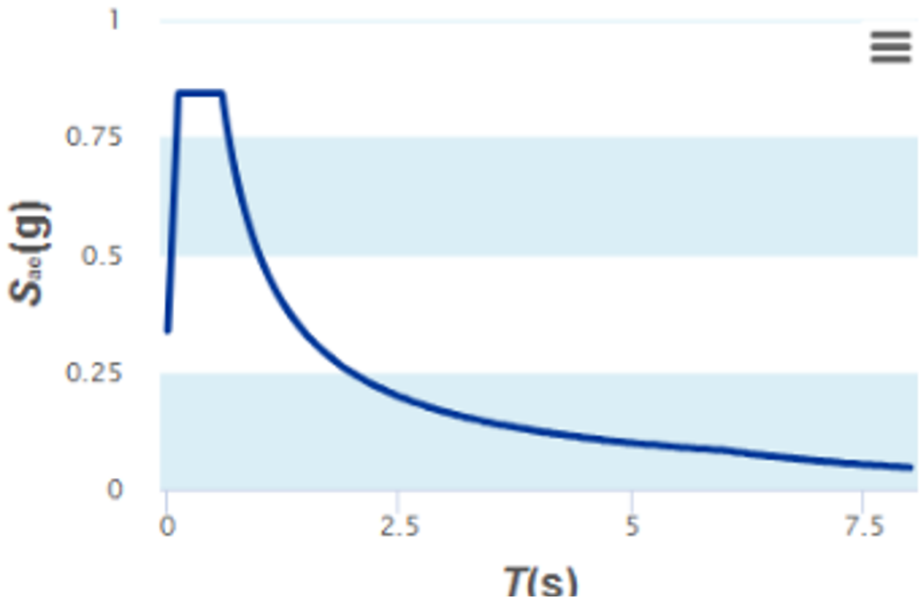

Figure 5.7. Under 0.2g PGA, Horizontal Elastic Design Spectrum of selected location of the Turkish Seismic Hazard Map.

6. LITERATURE REVIEW

There are a great number of studies on geosynthetics. Until now, several numerical and experimental studies have been performed regarding the seismic performance of geosynthetic reinforced soil retaining structures, slopes, and embankments. Nevertheless, the current dynamic studies on geosynthetics come short of explaining the behavior of geosynthetics under earthquake loadings in terms of energy and accelerations. Especially for earthquake hazard mitigation, researchers have focused on seismic base isolation, and unfortunately there are not sufficient number of studies attempting to explain the behavior of geosynthetic reinforced fill underlying the foundation under dynamic loads. Since the idea behind the use of geosynthetics in base isolation and the geosynthetic reinforced ground underlying the foundation are similar for the dynamic cases, base isolation studies will be also mentioned below to cover the concept of earthquake hazard mitigation.

6.1. Geosynthetic Seismic Isolation

Geosynthetics can be used for hazard mitigation against earthquakes, and it was first investigated by Kavazanjian *et al.* (1991).

Yegian and Lahlaf (1992) maintained that a horizontally located geosynthetic system which can restrict the transmission of acceleration to 0.2g can be of crucial advantage in seismic hazard mitigation, as most facilities are able to resist an acceleration of 0.2g. The shaking table test revealed decreasing dynamic-shear forces. Such an acceleration was able to travel from ground to the superstructure located above two sheets of geomembrane. Shaking table tests also revealed that two sheets of smooth HDPE geomembrane, a geosynthetic material, can be a good alternative base isolator for seismic hazard mitigation. It is understood that by means of slip deformation, the interface diminishes the dynamic energy transferred, decreasing the seismic response of the structure. In this study, the proposed scheme is capable of decreasing the transferred lateral ground acceleration by an average of 40%, as can be seen in Figure 6.1

and Figure 6.2.

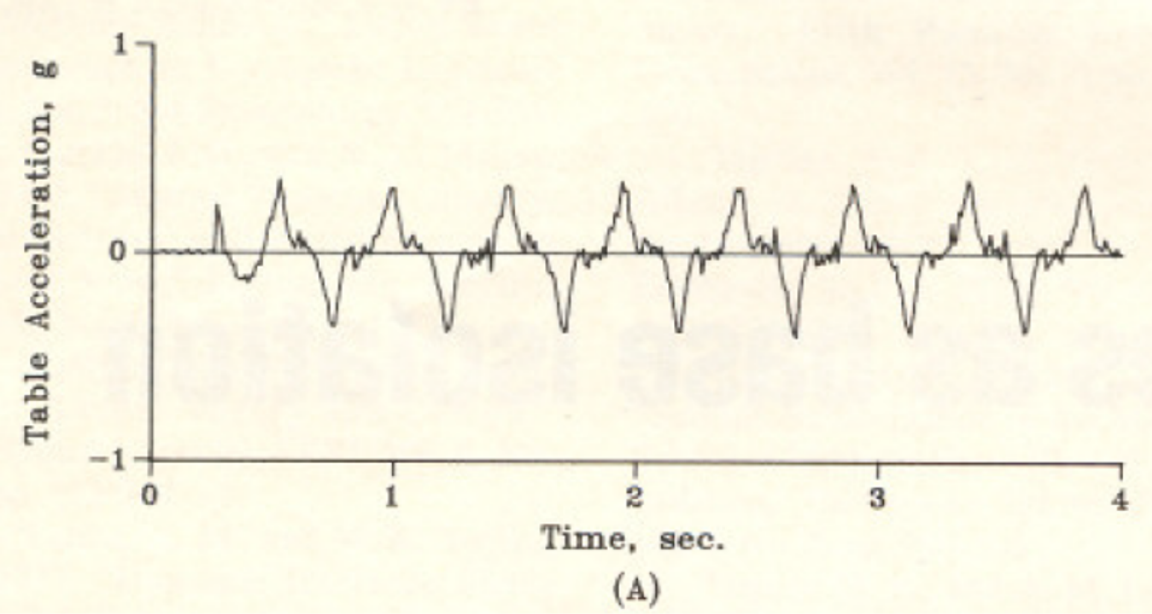

Figure 6.1. Shaking Table acceleration versus time, Yegian and Lahlaf (1992).

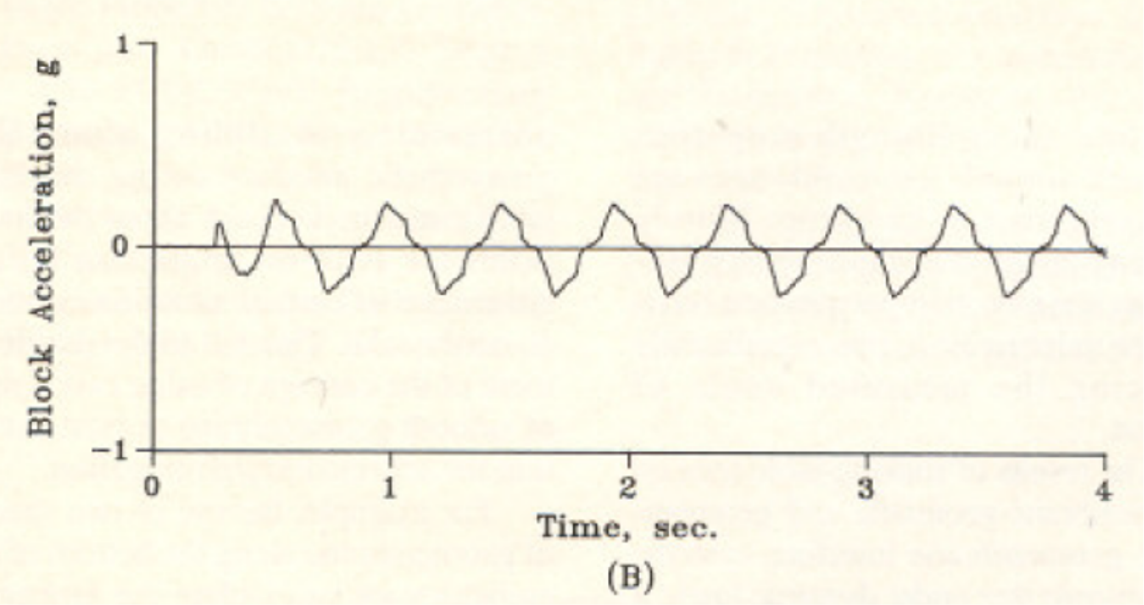

Figure 6.2. Block acceleration versus time, Yegian and Lahlaf (1992).

Kavazanjian *et al.* (1991), Yegian and Lahlaf (1992) and Zimmie (1995) asserted that geosynthetics base isolation is a good and effective means of decreasing the dynamic response of structural systems. The findings by Kavazanjian *et al.* (1991),

Yegian and Lahlaf (1992) and Zimmie (1995) suggest that under dynamic shear stimulations, slip deformations take place along smooth geosynthetic interfaces. The slip leads to a reduction in the energy transmitted throughout the interfaces. This way, it is thought, seismically excited slip deteriorations through a base geosynthetic liner will produce diminished accelerations transmitted to the landfill. By the same token, it can be said that geosynthetics placed in ground can diminish the amount of energy transmitted to the above superstructure.

Yegian *et al.* (1999) holds that geosynthetics placed under foundations are capable of absorbing seismic energy. Therefore, they transmit fewer excitations to a superstructure. Geosynthetics, as a foundation isolation, can be a cost-effective when it comes to reducing earthquake hazards. Yegian *et al.* (1999) performed a series of tests using a shaking table to see whether geosynthetics can be used as barrier against seismic energy or not. The tests were conducted on a single story building model. The accelerations of the model with and without geosynthectics were measured under earthquake motions. Yegian *et al.* (1999) concluded that the use of geosynthetics as a foundation isolation lessened the column shear forces in the tested model by 30%. The results obtained by Yegian *et al.* (1999) were compatible with those of Kavazanjian *et al.* (1991), Yegian and Lahlaf (1992) and Zimmie (1995) in terms of the effectiveness of geosynthetics base isolation as a solution for diminishing the dynamic response of structural systems.

Yegian and Kadakal (2004) focused on isolation of foundation for seismic protection via smooth synthetic liner. The solution for a low-cost seismic foundation isolation technique was investigated using synthetic materials developed by Hushmand and Martin (1991), Kavazanjian *et al.* (1991) and Yegian and Lahlaf (1992a,b).The aim of this study was to elaborate on the proposed concept of smooth geosynthetics liner used beneath foundations of buildings for dissipation of seismic energy as a results of sliding throughout the geosynthetic interfaces and hence propagating diminished accelerations to the superstructure. In this study, shaking table as well as cyclic loading tests were performed on various synthetic interfaces to determine the proper liner to be used in foundation isolation. Rigid block experiments were applied initially under sinusoidal

excitations. The aim was to figure out how accelerations are transferred along each interface and identify the variation between propagated accelerations, slips, slip rate for every interface as a function of harmonic excitation frequency and amplitude. Careful examination of the figure reveals the variation between transmitted acceleration versus table acceleration (g). Indeed, almost no change is observed in the acceleration transmitted under different frequencies. Subsequently, rigid block tests were performed again using more realistic earthquake-type shaking table excitations. It was understood that a high strength, nonwoven geotextile located over an ultrahigh molecular weight polyethylene , UHMWPE (Geotextile/ UHMWPE) forms a liner that matches well with this application. A single story structural model with and without foundation isolation test were analyzed and examined using a shaker table. The findings indicate that the function of foundation isolation substantially decreases the seismic shear forces and slip deformations (see Figure 6.4) in the model. The results point to the technical feasibility of using a smooth synthetic liner in earthquake disaster mitigation. The results further highlight that application of regular sinusoidal excitations does not affect at all the accelerations transferred under different frequencies (see Figure 6.3). In the presented thesis, the given excitations are shown to be sinusoidal excitations at the same time, and no noticeable sudden change in the amount of energy was observed.

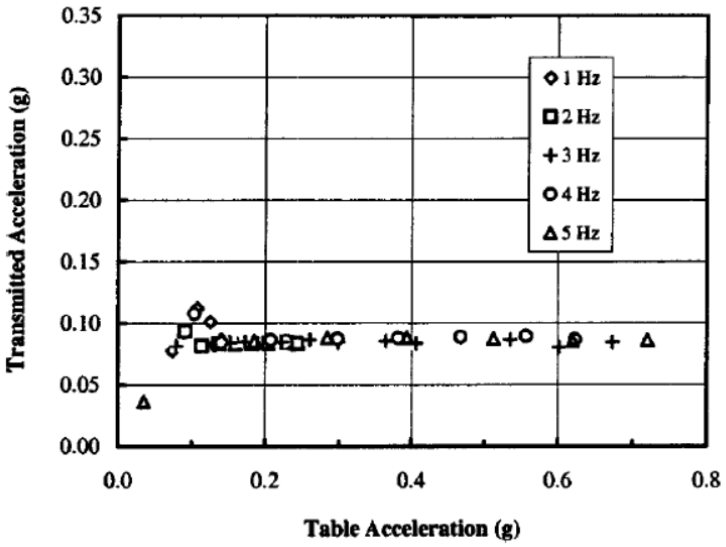

Figure 6.3. Variation of transmitted acceleration with table acceleration from rigid block teste on geotextile/ UHMWPE interface.

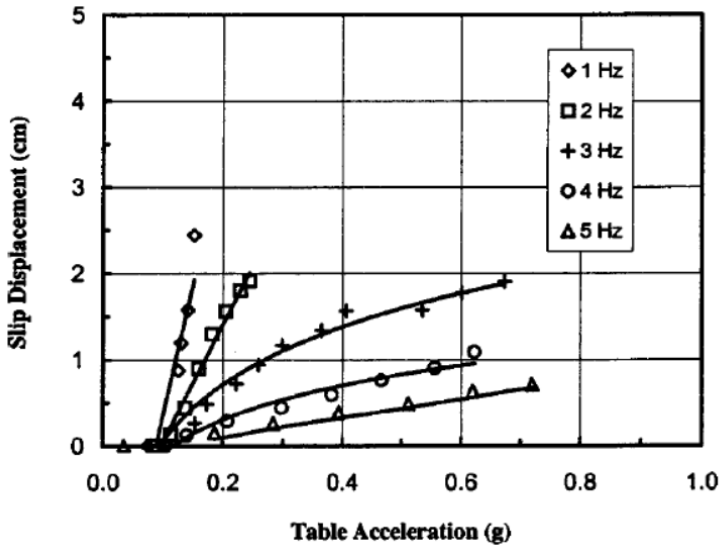

Figure 6.4. Variation of slip displacement with table acceleration from rigid block tests on geotextile / UHMWPE interface.

Another study performed by Yegian, Georgarakos, Gazetas (2005) indicated that seismic isolation that is made up of geotextile and a high molecular weight polyethylene put into the ground below the superstructure forms isolated soil wedge. The geosynthetic interface between the isolated and underlying soil, characterized by low as well as constant friction coefficient, restricts the acceleration transferred into the isolated soil, though some differential displacements may occur. The study was conducted using the finite element method. It basically investigated the effects of the shape of geosynthetic interface on the isolation impacts.

6.2. Geosynthetic Reinforced Ground against Seismic Loads

Verma *et al.* (2000) reported the results of a study on geogrid reinforced subgrades under seismic loading. To figure out the behavior of geogrid reinforced subgrade under simulated earthquake loading, different frequencies of 0.2, 0.6, 1 Hz were given as input and the dynamic loads as well as the settlements of the footing were reported. They discovered that frequency of seismic loadings has no impact whatsoever on the dynamic bearing capacity of both unreinforced and reinforced subgrades. However, the number of reinforcement layers, the dimensions of the reinforcements as well as their spacing

have a great influence on the dynamic bearing capacity of the subgrades. A critical decrease was observed in the settlement of the reinforced subgrade.

Santhkumar *et al.* (2001) carried out additional work on the dynamic behavior of geogrid reinforced soil , which examined in detail the increase in earthquake resistance of the foundation soil system under cyclic loadings. According to researchers, the dynamic behavior of the reinforced soil beneath foundation has not been fully understood yet; therefore, dynamic plate loading tests with different frequencies were performed. Analyses revealed that there is an important influence of the number of reinforcement layers, the dimensions of the reinforcement, and spacing of the reinforcement of dynamic loading on the bearing capacity of the subgrades. Frequency of cyclic load does not seem to have a great impact on the bearing capacity of sandy subgrade. A Significant decrease was observed in the settlement of reinforced sandy subgrades due to containment of geogrid in the foundation soil while dynamic bearing capacity followed an upward trend.

Gohil *et al.* (2013) investigated the effect of geogrid reinforced soil under seismic loading in order to explain energy dissipation in soil reinforced with geosynthetics. Shallow foundation model exposed to long period and short period earthquakes was investigated by means of a numerical model utilizing MIDAS-GTS software. Multilayer geogrids under foundation were modelled. Time history analyses were conducted. The dynamic properties of soil like stiffness for several damping ratios were used for the soil-geosynthetic -structure interaction. The overall dimensions of the model were 58.4 m x 24 m and the rectangular shallow foundation size was 1.8 m x 3.2 m. Five different magnitudes, five different PGA values and five different periods of earthquakes were performed at the ground base. Displacement, stresses, forces, acceleration and velocity were analyzed for all soft and medium stiff soils. For long period ground motions, the percentage of reduction in acceleration was found to be more than that in the short period ground motions when the soil beneath the foundation was reinforced. In this study, it was indicated that in the presence of geogrid reinforcement, reduction in pseudo acceleration, pseudo velocity and relative displacement can be seen but the differences are negligible. The problem here is that analyses were done only in the form

of time history analysis and one cannot be sure whether a similar result would have been obtained if response spectrum analysis had been carried out.

Clement (2015) did experimental research on a block foundation on sand reinforced with geogrid under dynamic excitation. Forced- and free- vertical vibration tests were performed on the model overlying dense sand. The experiment was performed on a tank model that had a square footing of 10 cm*10 cm*4.4 cm, which was exposed to dynamic loading by means of an electromagnetic shaker. To examine the geogrid reinforcement effect, both unreinforced and geogrid - reinforced sand cases were tested. External force of different frequencies was applied and the dynamic acceleration response of the foundation was obtained at corresponding frequencies. During free- and forced- vibration tests, dynamic response was recorded using accelerometers. At the end of the study, natural frequency/ resonant frequency ratios and damping ratios were calculated. Results indicated that the soil reinforced with geogrid raised the natural frequency of the soil-foundation system and at the same time diminished peak amplitude of vibration. Finally, vibration analysis was performed to identify the resonance condition which could cause failure to the system. It was understood that (relative) displacement would decrease if the natural frequency content exceeded the forcing frequency (frequency of the applied force). The experiment demonstrated that geogrid increases stiffness of the system and the dynamic shear modulus. Here, more than one resonance frequency was observed. It could be because of wave reflection brought about by tank walls, although, a large sized tank, with a flexible mesh and absorbing system, namely saw dust, was used.

Sreedhar and Abhiskek (2016) studied the impact of geosynthetic reinforcement on the dynamic characteristics by means of model block resonance tests. The test block measured 0.6m *0.5m *0.4m. The study was conducted to figure out the dynamic response of geosynthetic reinforced soil underlying a model of machine foundation. Vibration tests were performed both with and without geosynthetic reinforcement composed of a non-woven geotextile and a bi-axial geogrid. The resonant frequency and the peak amplitude were examined. When the resonant frequency was changed, there was a definite decrease in peak amplitude. It was concluded that geosynthetics

underlying machine foundations provide adjustment of the frequency content and limit peak amplitude. In addition, a crucial decrease was observed in the peak vertical displacement of the resonant condition. A further outcome was that geogrid was seen to perform relatively better than geotextile on all examined parameters.

Agarwal and Jakka (2016) examined a geosynthetic reinforced bearing layer for both static and dynamic cases. Under shallow foundations and working platforms, which are used for installing weighty construction machines and vehicles, reinforced layer soil system can be used to provide additional bearing capacity with the purpose of preventing shear failure as well as excessive deformations. Static and dynamic cases were analyzed by means of Plaxis 2D-Finite Element Software- on a two layered unreinforced and reinforced system. They tried to understand the impact of geogrid on bearing capacity and settlement. Two layered soil system composed of soft clay soil was laid under compacted granular fill. At the end of the study, geogrid was seen to perform well when it comes to increasing bearing capacity and decreasing the settlement behavior of soil. The effects of the parameters, namely position, number and stiffness of geogrid were also investigated. The study failed to examine acceleration and energy, though.

Sekman (2016) did an experimental study on mitigation of earthquake hazards by means of geosynthetics. His main goal was to investigate an applicable, low-cost alternative seismic isolation (SI), namely Geotechnical Seismic Isolation (GSI), for low-rise and mid-rise buildings. The SI system is made up of a geotextile laid on the geomembrane placed in the soil profile under the superstructure. The proposed seismic isolation technique is different from an ordinary base isolation as it directly has to do with geotechnics. 1:10 scaled low-rise and mid-rise building models were utilized to perform shaking table experiments. The effects of the suggested method were evaluated through comparison of with and without proposed Seismic Isolation system. The researchers found that GSI system was an effective tool to lower base shear, base moment, horizontal accelerations, horizontal drifts and Arias Intensity. With the help of the suggested GSI system, the seismic energy transferred from ground to the superstructure was eliminated by means of slip displacements among geotextile

and geomembrane. To sum up, it can be said that the suggested GSI system can increase resistance and thus durability of the structure against strong seismic motions. In this study, test results were surprising in that the suggested GSI system had a more positive impact on the 5-story building model rather than the 3-story building model. Another surprising outcome was the authors' tendency to associate the result with the effect of lower base reactions of shear and moment values due to slip displacement. The authors further proposed that high rise building models should be investigated in future studies.

Liu *et al.* (2018) performed a study to understand the relationship between Arias Intensity and the reactions of reinforced soil retaining walls exposed to near-field ground motions. Since it deals with ways of retaining walls, it does not have direct relevance to this study. However, examination of Arias Intensity under seismic excitations can offer useful insights. In the study, the dynamic finite element study concentrated on the relationship between the ground motion parameters, loadings and residual displacements. The findings of the study showed no relationship between Arias Intensity and residual facing displacement.

Hedge (2018) performed a numerical study of machine foundation overlying reinforced soil. Unreinforced, geogrid reinforced and geocell reinforced cases were examined. Foundation beds can be frequently exposed to dynamic loads because of several reasons like earthquakes, machine vibration and traffic load. Today, it is a well-known fact that geosynthetics are effective in limiting (relative) displacements and settlements of foundations under static loads. The influence of geosynthetics on soil behavior under dynamic load has not been fully understood yet. A finite element software Plaxis 2D was used for analysis and Mohr-Coulomb failure criteria was adopted. To see the performance of machine foundations overlain on the geocell reinforced soil beds, unreinforced geogrid reinforced cases were compared. Diverse frequencies of dynamic excitation and constant force sustenance were applied to all cases. The optimum performance location of the geocell and geogrid differed as well. At the optimum location of the geocell, a 61% decrease in displacement was recorded. Similarly, there was a 50% reduction in displacement in the presence of geocell. From the findings, one can easily realize that

geogrid is one of the ways of restricting settlements under dynamic loading. However, accelerations or energy dissipation in the soil system was not investigated at all.

7. NUMERICAL STUDY

The aim here was to see the effects of geosynthetic reinforced fill on the frequency content of seismic waves reaching the surface. Numerical studies are performed for both reinforced and unreinforced cases. The geosynthetic reinforced and unreinforced soils are modelled under same sinusoidal waves with different frequencies (0.5, 1, 2, 3 and 5 Hz) and different PGA's (0.1g, 0.2g, 0.3g, 0.4g) using a numerical dynamic analysis program, namely PLAXIS 2D, which utilizes the finite element method, and this way a lot of real geotechnical applications can be modelled. By means of PLAXIS 2D, acceleration data at marked points becomes accessible, which is then used to calculate the energy in terms of Arias Intensity at specified points with the help of Matlab. In addition, the average values for absolute accelerations of the intermediate 250 steps of the analysis were obtained to see if there is any link/correlation between the results. This enabled us to examine in detail the impacts of geogrid reinforcement, peak ground acceleration and frequency of the motion on the soft clayey soil underlying gravel in terms of average accelerations and energy.

7.1. Finite Element Model

Soft clayey soil, with a 30 m depth and 100 m width was chosen to represent the natural soil. 5 meter thick gravel fill was foreseen for soil improvement. Thus, a soft clay underlying gravel was used for the model. The scheme of the model is given in Figure 7.1. Gravel was selected for drainage purposes under foundation as well. Unreinforced and reinforced cases were investigated for comparison. 9 points were selected on the model. The points A,B,C were at the center of the gravel layer (and also 2.5 m above the geogrid reinforcement), the points D,E,F were nearly 3.5 m below the gravel layer (and also below the geogrid reinforcement) and the points G,H,I were just above the bottom. All of the selected points were sufficiently distant from the horizontal boundaries and structural elements. In other words, the points were located not on/near the geogrid, or on/near boundaries in order to achieve accurate results, since effects of boundaries, namely reflection of waves, could produce misleading results.

This way, results were expected to indicate whether the seismic response of reinforced soft soils under foundation would alter a soil response under a superstructure or not.

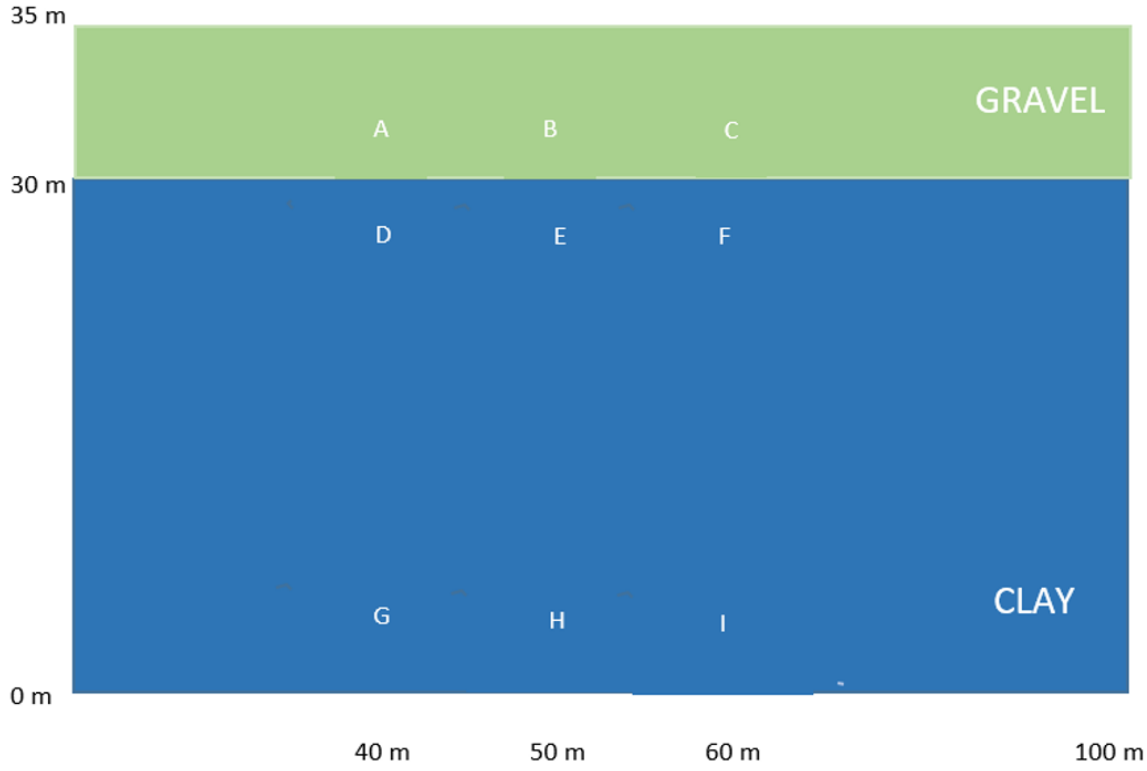

Figure 7.1. The scheme of soil layers and selected points.

7.1.1. Material Properties

The input parameters of soft clayey soil and gravel are given in Table 7.1.

Table 7.1. The input parameters of soft clayey soil and gravel.

Material	Material Model	Material Type	General Properties	Permeability	Stiffness	Strength
Clay	Mohr Coulomb	Undrained	γ_{unsat}=14 kN/m^2 γ_{sat}=16 kN/m^2	K$_{x,y}$=10^{-8} m/day	Eref=7E+03 kN/m^2 γ(nu)=0,35	Cref=24kN/m^2 Φ(phi)=3^o
Gravel	Mohr Coulomb	Undrained	γ_{unsat}=17 kN/m^2 γ_{unsat}=22 kN/m^2	K$_{x,y}$=10^{-2} m/day	Eref=1.5E+05 kN/m^2 γ(nu)=0,35	Cref≈0kN/m^2 Φ(phi)=35^o

7.1.2. Boundary conditions of the Finite Element model

In the Input part of the Plaxis, following the assignment of the predefined material to the soil strata of the model, boundaries were specified. The right and left side of the model were defined with absorbent boundaries.

At the far vertical boundaries, absorbent boundary conditions are applied to absorb outgoing waves. Plaxis has a convenient default setting to generate standard boundary conditions for earthquake loading (Plaxis Version 8 Dynamics Manual).

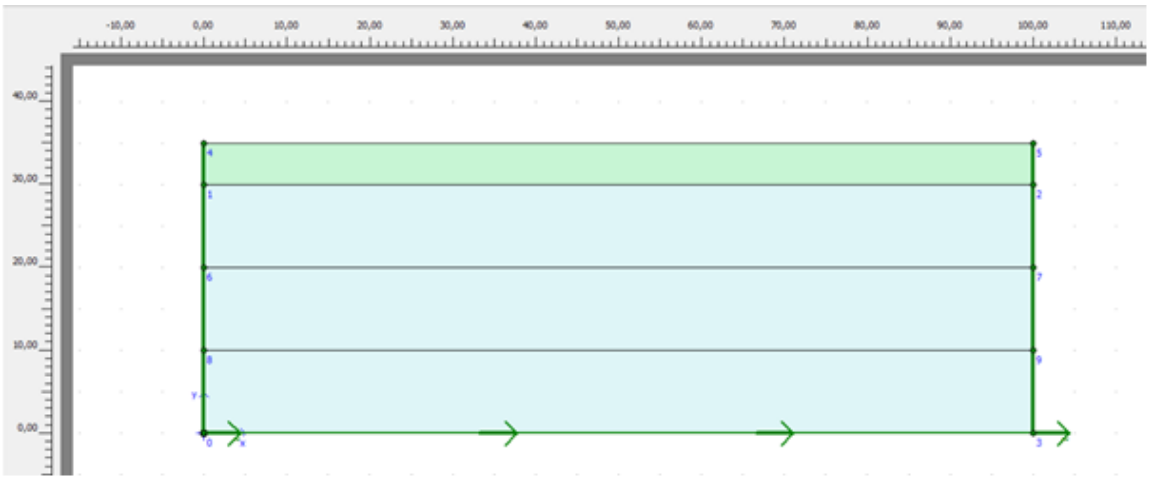

Figure 7.2. The model with absorbent boundaries defined at right and left side.

7.1.3. Loads

Since the materials are described with their densities, the program automatically adds the weight of the soils.

The only load applied was “prescribed displacement (dynamic)” and it was applied to the bottom of the model. Prescribed displacement is defined with a negligible size of 0.01 m in the x-axis.

The procedure followed for unreinforced model applies to the generation of the reinforced model as well. The difference between the unreinforced and reinforced case

is in the placement of the reinforcement between clayey soil and gravel and in the introduction of the interface. The interface was used for the interaction between the soil and structural elements for the purpose of decreasing the friction between the soil and structural elements. The prescribed displacement at bottom and the differences mentioned in the geogrid reinforced model are shown in Figure 7.3.

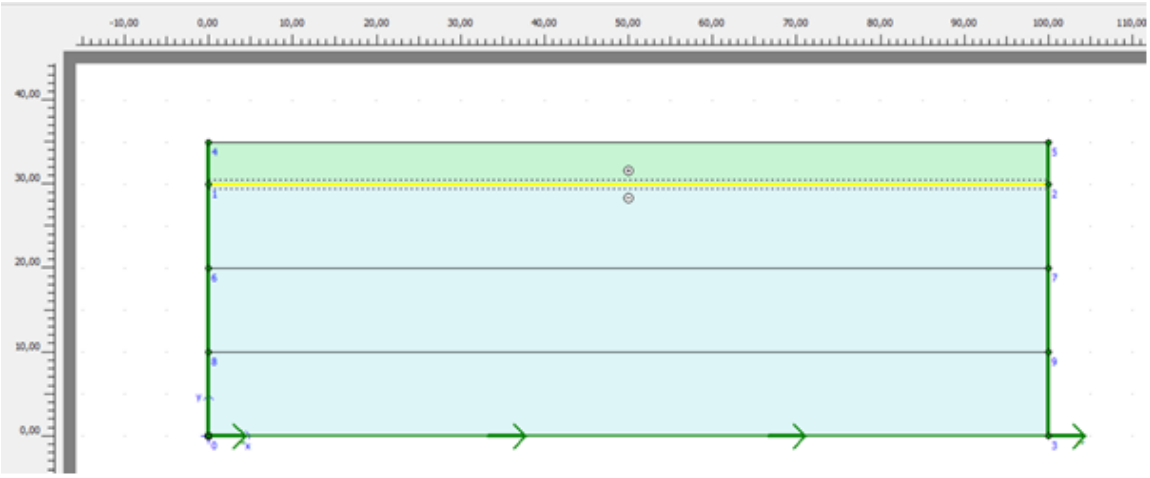

Figure 7.3. The prescribed displacement at the bottom of the geogrid reinforced model and the interface between geogrid and soil strata.

7.1.4. Mesh Generation

In Plaxis, the finite element model mesh must be generated for each calculation. As can be seen in the coarseness of the mesh in figure 4.1.2, the medium used for fine meshing has been defined for clayey soil, and the one used for very fine meshing has been defined for gravel in order to better capture the effect of geosynthetic reinforcement. The generated mesh for the unreinforced model is presented in Figure 7.4. Generation of mesh follows exactly the same procedure utilized for the reinforced case.

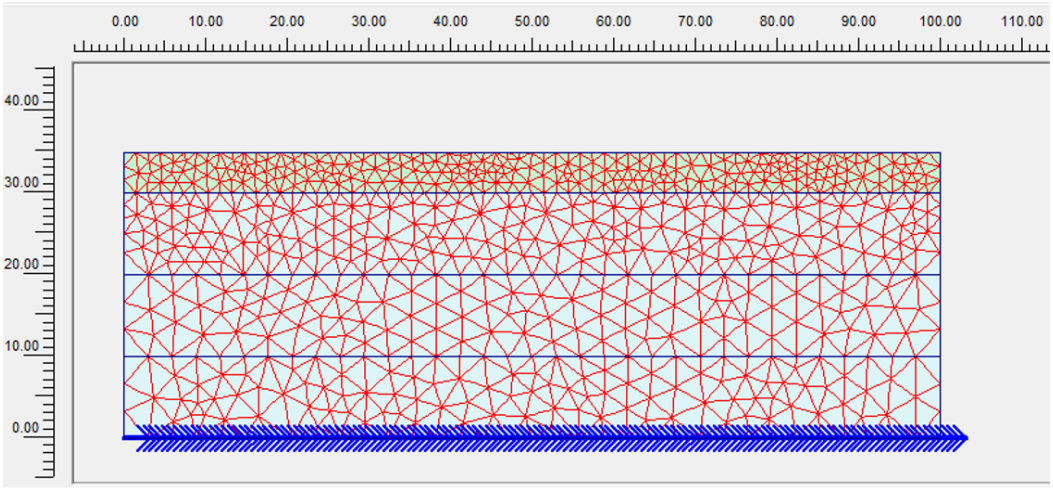

Figure 7.4. Finite Element Model Mesh for the Unreinforced Model.

7.1.5. Defining Geogrid for the Reinforced Case

Geogrid is defined at a height of 30 m from the ground, and it is at a distance of 5 meters to the surface. It is this feature of gravel that distinguishes it from clayey soil.

The geogrid is assumed to be an Elastic material in the Finite Element analysis. Geogrid properties are represented in the Finite element model with only one parameter, namely normal stiffness, and for the purposes of this study, a single constant value, EA: 2000 kN/m was chosen.

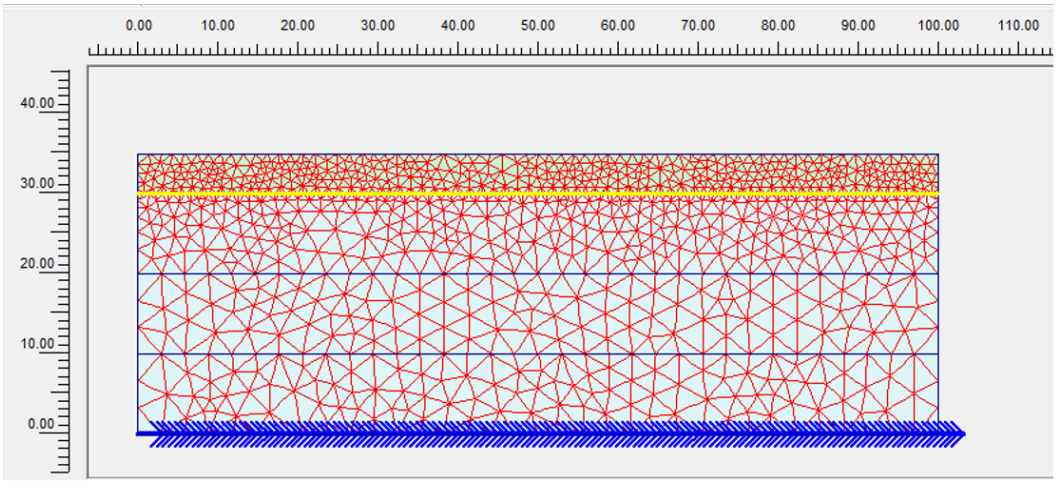

Figure 7.5. Meshed Model of Geogrid Reinforced Soil.

7.1.6. Coordinates of Selected Points

Since the selections are done manually on the mesh of the finite element analysis, nodes lead to change in the selected location of the points. The initial aim was to choose a depth of 32.5 m for the points A,B,C were at the center of the gravel layer (and also 2.5 m above the geogrid reinforcement), 27.5m for the points D,E,F were nearly 3.5 m below the gravel layer (and also below the geogrid reinforcement) and for the points G,H,I above the fault line, but the points selected turned out to be the ones given in Table 7.2. Same points apply to reinforced and unreinforced cases.

Table 7.2. The coordinates of the selected points.

Points	X COORDINATE (meter)	Z COORDINATE(meter)
A	40.00	32.20
B	50.00	32.00
C	60.00	32.40
D	40.00	26.80
E	50.00	26.60
F	60.00	26.50
G	40.00	3.70
H	50.00	3.75
I	60.00	2.14

7.1.7. Calculation

In the calculation of Plaxis, dynamic analysis was defined with parameters of 250 step and 5 sec. The amplitude and frequency of the earthquake was determined based on the multipliers. Artificial sinusoidal seismic waves with 0.5, 1, 2, 3, 5 Hz frequencies were created this way for the whole analysis by means of prescribed displacement at the bottom boundary.

7.2. Calculation of the Energy Via Arias Intensity

Arias Intensity specifies the intensity of an earthquake by measuring the acceleration of transferred seismic waves. It was suggested by Chilean engineer Arturo Arias in 1970. The time-integral of the square of the ground acceleration is considered to be:

$$I_A = \frac{\pi}{2g} \int_0^{T_d} a(t)^2 dt (m/s) \tag{7.1}$$

where g is the acceleration due to gravity and Td is the duration of signal above the threshold.

On Matlab, the Arias Intensity formula is used to get the energy values of selected points with the accelerations resulting from finite analysis. The utilized code is provided in Appendix B.

8. RESULTS OF THE ANALYSIS

The acceleration versus time figures for reinforced and unreinforced cases under 0.1g, 0.2g, 0.3g, 0.4g peak ground acceleration (PGA) with 0.5, 1, 2, 3, 5 Hz frequency of motions for the selected 9 points are given in Appendix A. Utilizing acceleration data, average acceleration values of the top points locating gravel layer, the middle points locating weak clayey soil and the bottom locating weak clayey soil have been calculated and plotted on curves with a horizontal average acceleration line as shown in Appendix C. The calculated Arias Intensity values are differentiated in the following subsection 8.1.

Direct comparison of the maximum peak accelerations between unreinforced and geogrid reinforced cases is avoided since the frequent extreme rises sharply in acceleration measurements. Examples of these irregular peaks can be seen in Figure 8.1 and Figure 8.2. Therefore, deciding which acceleration the real maximum application is can be rather subjective, which can lead to a faulty evaluation.

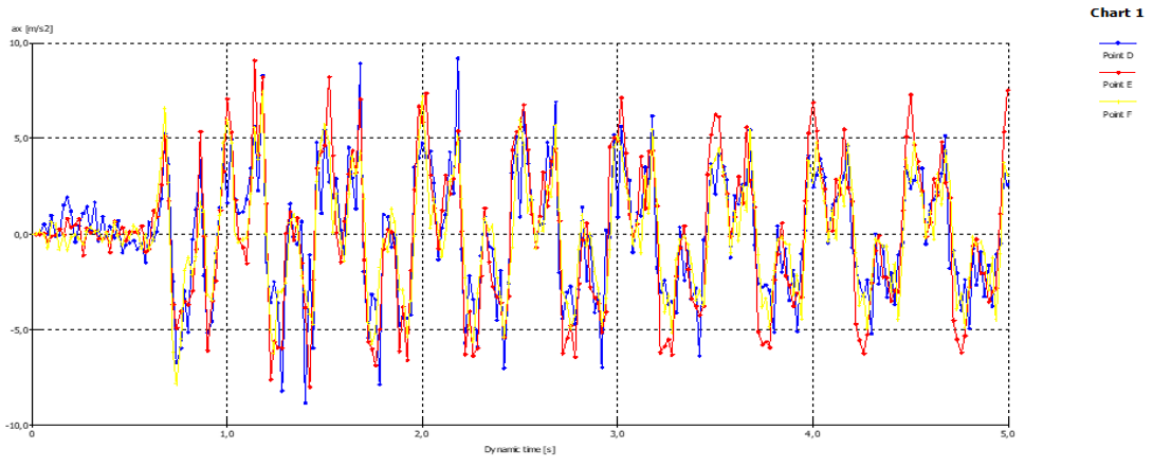

Figure 8.1. Frequent extreme jumps in the acceleration Figure of numerical analysis results for unreinforced case under 0.4g PGA with 2 hz frequency.

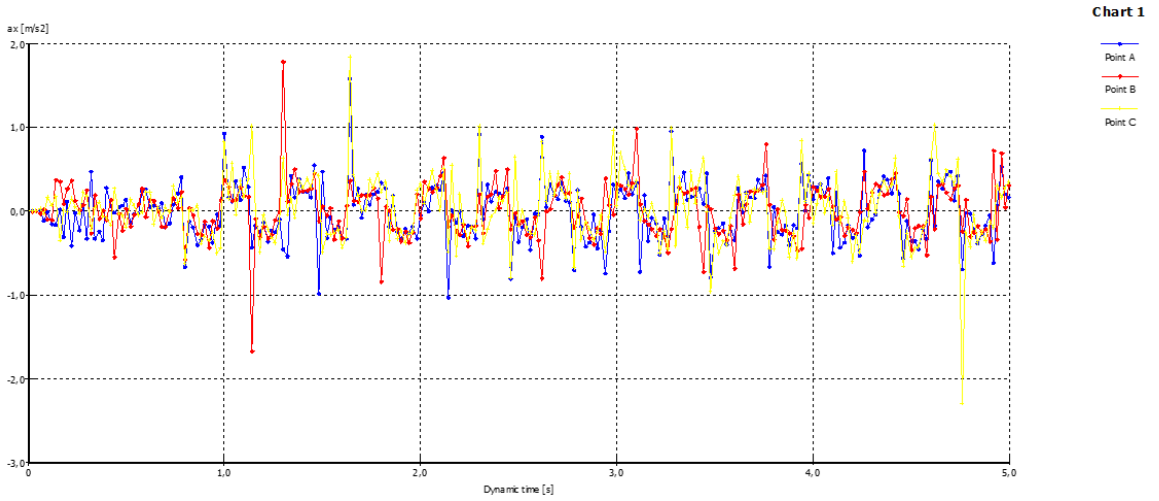

Figure 8.2. Frequent extreme jumps in the acceleration Figure of numerical analysis results for unreinforced case under 0.1g PGA with 3 hz of frequency.

In the presented thesis, to obtain an objective and a scientific comparison of geogrid reinforced and unreinforced cases, results of the analysis are examined for average accelerations as well as energies, namely Arias Intensity.

In Plaxis V8, analyses are made by means of 250 steps described as a default. Sub steps provide more accurate results for finite element analysis. As can be seen in Figure 8.3 and Figure 8.4, the marked points specify substeps of Plaxis calculation. Following Plaxis analysis, the acceleration values for substeps were transferred to excel and the average values of absolute accelerations of the intermediate 250 steps were found for the selected points. The comparison of average acceleration responses of the reinforced and unreinforced cases for all selected top, middle and bottom points under 0.1g, 0.2g, 0.3g, 0.4g ground accelerations (PGA) with a frequency of 0.5, 1, 2, 3, 5 Hz motions will be provided in the following section 8.1. Similarly, average acceleration curves for the selected top, middle and bottom points with overall average acceleration represented by a horizontal line can be seen in Appendix C.

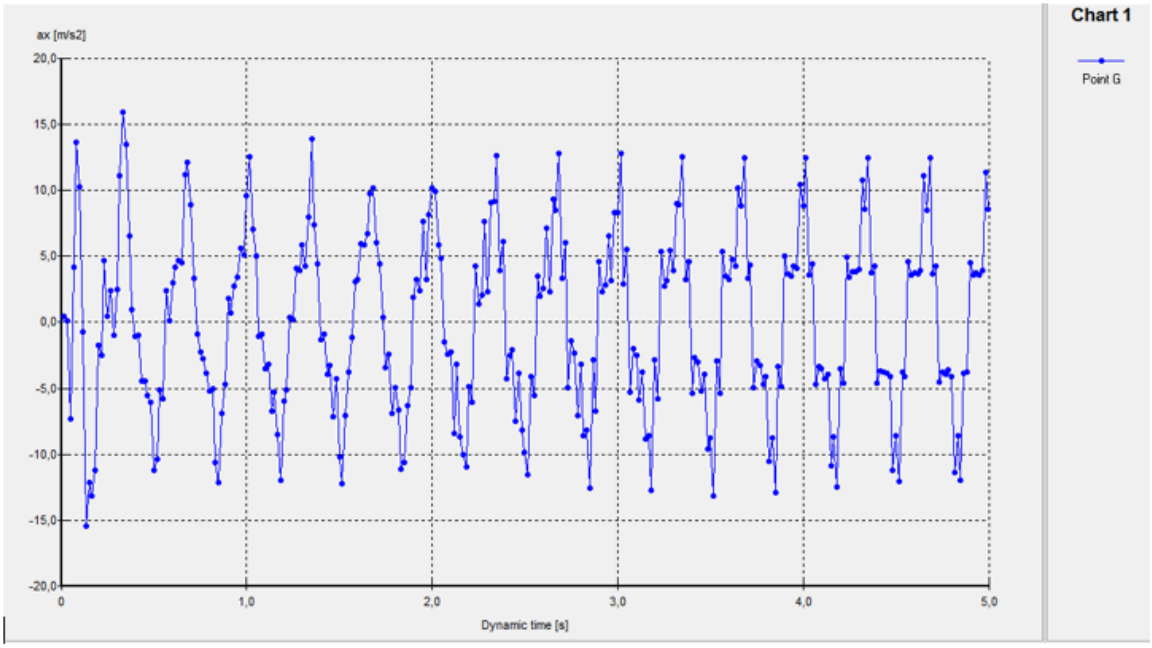

Figure 8.3. Marked points specify substeps of horizontal acceleration vs time figure of numerical analysis results of point G for reinforced case under 0.3g PGA with 3 hz frequency.

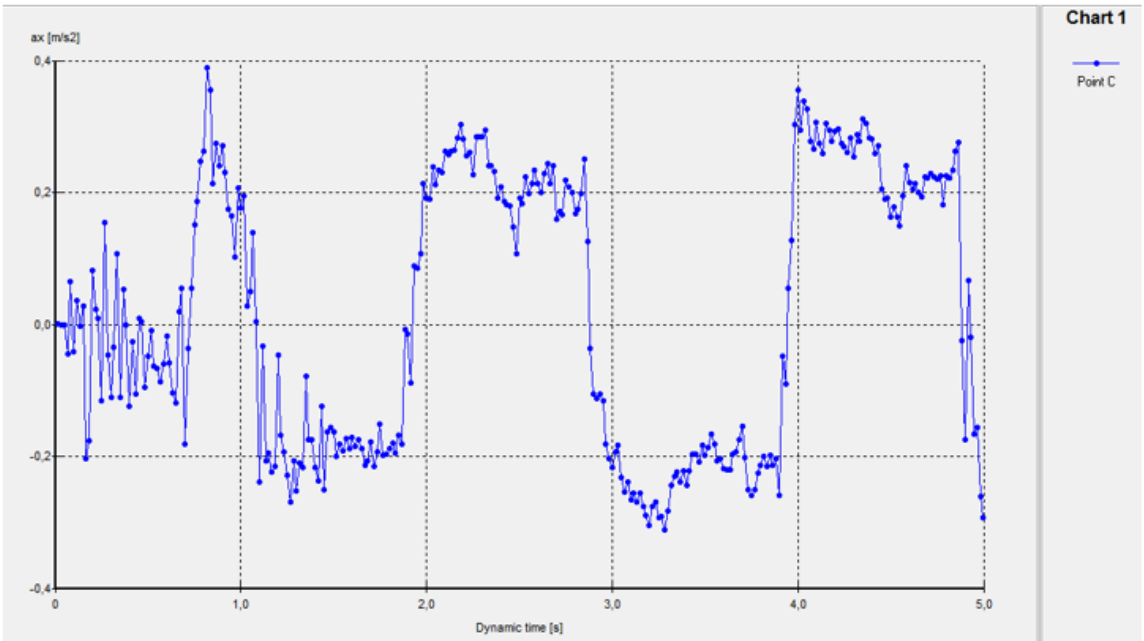

Figure 8.4. Marked points specify substeps of horizontal acceleration vs time figure of numerical analysis results of point C for unreinforced case under 0.3g PGA with 0.5 hz frequency.

To figure out energy absorption, the Arias Intensity values showed in subsection of 8.1 were examined. The ratios of Arias Intensity values obtained by means of comparison of reinforced and unreinforced cases are listed in Table 8.1. Geogrid is expected to provide energy absorption for soil. Hence, the diminished Arias intensity for the geogrid case may indicate that geogrid absorbs seismic energy.

To better understand the effects of the frequency content, PGA and geogrid reinforcement on acceleration and Arias Intensity of the clay and gravel, results were examined in detail according to their PGA and frequency values given in the following subsection 8.1. Since in Spectral Acceleration Figures, the frequency of the cyclic loads are represented with periods, it should be noted that 5 Hz frequency corresponds to 0.2 second period, 3 Hz frequency corresponds to 0.33 second period, 2 Hz frequency corresponds to 0.5 second period, 1 Hz frequency corresponds to 1 second period, and 0.5 Hz frequency corresponds to 2 second period.

8.1. Comparison of Numerical Analysis Data Under Different PGA Values with Different Frequencies

8.1.1. Comparison of Numerical Analysis Data Under 0.1g PGA

8.1.1.1. Under 0.5 Hz of Motion. When a sinusoidal acceleration with a peak of 0.1g is applied, the average acceleration at the base for a frequency of 0.5 Hz is much smaller than 0.1g, and is seen to be 0.083 m/s^2. As the wave moved upward the vibration deamplified with minimal differences. Same results are obtained for unreinforced and geogrid reinforced cases. Hence, it can be concluded that under low PGA as well as frequency, no influence of geogrid reinforcement on acceleration is observed.

Table 8.1. Average Acceleration (m/s^2) Values of Selected Points Under 0.1g PGA with 0.5 Hz of Frequency.

POINTS	With geogrid	Without geogrid
A,B,C	0.078	0.078
D,E,F	0.081	0.081
G,H,I	0.083	0.083

Table 8.2. Average Arias Intensity (m/s) Values of Selected Points Under 0.1g PGA with 0.5 Hz of Frequency.

POINTS	With geogrid	Without geogrid
A,B,C	0.0070	0.0071
D,E,F	0.0084	0.0084
G,H,I	0.1100	0.1100

The same comparison was made for the change in the Arias Intensity from bottom to top. The Arias intensity values decrease both for unreinforced and geogrid reinforced cases. Same Arias intensity values at the bottom and below the geogrid are obtained for unreinforced and geogrid reinforced cases. For the gravel layer, Arias Intensity of the reinforced case is slightly smaller than that for the unreinforced one.

8.1.1.2. Under 1 Hz of Motion. When a sinusoidal acceleration with a peak of 0.1g is applied, the average acceleration at the base for a frequency of 1 Hz is much smaller than 0.1g and is seen to be 0.322 m/s^2. As the wave moves upward, vibration first amplifies in the clay and then de-amplifies in the gravel. The average accelerations obtained for geogrid cases at the top and middle of the model are slightly smaller than those for unreinforced ones. At the bottom, identical acceleration values are observed.

Table 8.3. Average Acceleration (m/s2) Values of Selected Points Under 0.1g PGA with 1 Hz of Frequency.

POINTS	With geogrid	Without geogrid
A,B,C	0.197	0.198
D,E,F	0.411	0.413
G,H,I	0.322	0.322

Table 8.4. Average Arias Intensity (m/s) Values of Selected Points Under 0.1g PGA with 1 Hz of Frequency.

POINTS	With geogrid	Without geogrid
A,B,C	0.0396	0.0398
D,E,F	0.2243	0.2254
G,H,I	0.1331	0.1331

The Arias Intensity values from bottom to top, first increased in the clay and then decreased in the gravel layer both for unreinforced and geogrid reinforced cases. Same Arias intensity values at the bottom are obtained for unreinforced and geogrid reinforced cases. For the gravel and top of the clay layers, Arias Intensity values of the reinforced cases are smaller than those for the unreinforced cases.

8.1.1.3. Under 2 Hz of Motion. When a sinusoidal acceleration with a peak of 0.1g is applied, the average acceleration at the base for a frequency of 2 Hz is slightly smaller than 0.1g and is seen to be 0.718 m/s^2. As the wave moves upward, vibration deamplifies. The average accelerations obtained for geogrid cases at the middle of the model are slightly smaller and at the top slightly higher than those for unreinforced cases. At the bottom, identical acceleration values are observed.

Table 8.5. Average Acceleration (m/s^2) Values of Selected Points Under 0.1g PGA with 2 Hz of Frequency.

POINTS	With geogrid	Without geogrid
A,B,C	0.214	0.210
D,E,F	0.677	0.680
G,H,I	0.718	0.718

Table 8.6. Average Arias Intensity (m/s) Values of Selected Points Under 0.1g PGA with 2 Hz of Frequency.

POINTS	With geogrid	Without geogrid
A,B,C	0.0505	0.0500
D,E,F	0.5727	0.5817
G,H,I	0.6683	0.6683

From the bottom to the top, the Arias intensity values decreased for both unreinforced and geogrid reinforced cases. Same Arias intensity values at the bottom are obtained for unreinforced and geogrid reinforced cases. Arias Intensity of geogrid cases at the middle of the model is slightly smaller and at the top, it is slightly higher than in unreinforced cases.

8.1.1.4. Under 3 Hz of Motion. When a sinusoidal acceleration with a peak of 0.1g is applied, the average acceleration at the base for a frequency of 3 Hz is higher than 0.1g and is seen to be 3.215 m/s^2.As the wave moves upward, vibration de-amplifies. The average accelerations obtained for geogrid cases at the middle of the model acceleration are slightly smaller and at the top slightly higher than those for unreinforced cases. At the bottom, identical acceleration values are observed.

Table 8.7. Average Acceleration (m/s^2) Values of Selected Points Under 0.1g PGA with 3 Hz of Frequency.

POINTS	With geogrid	Without geogrid
A,B,C	0.290	0.269
D,E,F	1.012	1.030
G,H,I	3.215	3.215

Table 8.8. Average Arias Intensity (m/s) Values of Selected Points Under 0.1g PGA with 3 Hz of Frequency.

POINTS	With geogrid	Without geogrid
A,B,C	0.1295	0.1017
D,E,F	1.5417	1.6067
G,H,I	11.4433	11.4433

From the bottom to the top, the Arias intensity values decreased for both unreinforced and geogrid reinforced cases. Same Arias intensity values at the bottom have been obtained for unreinforced and geogrid reinforced cases. Arias Intensity of geogrid cases at the middle of the model is slightly smaller and at the top of the model slightly higher than that of unreinforced cases.

8.1.1.5. Under 5 Hz of Motion . When a sinusoidal acceleration with a peak of 0.1g is applied, the average acceleration at the base for a frequency of 5 Hz is much higher than 0.1g and is seen to be 4.233 m/s^2. As the wave moves upward, vibration first amplifies in the clay and then de-amplifies in the gravel. The average accelerations obtained for geogrid cases at the top and middle of the model are slightly smaller than those for unreinforced ones. At the bottom, identical acceleration values are observed.

Table 8.9. Average Acceleration (m/s^2) Values of Selected Points Under 0.1g PGA with 5 Hz of Frequency.

POINTS	With geogrid	Without geogrid
A,B,C	0.305	0.340
D,E,F	4.946	4.967
G,H,I	4.233	4.233

Table 8.10. Average Arias Intensity (m/s) Values of Selected Points Under 0.1g PGA with 5 Hz of Frequency.

POINTS	With geogrid	Without geogrid
A,B,C	0.1337	0.2067
D,E,F	30.6067	30.8200
G,H,I	19.6800	19.6800

From the bottom to the top, the Arias intensity values firstly increased in the clay and then decreased in the gravel layer for both unreinforced and geogrid reinforced cases. It should be noted that the Arias Intensity values from the bottom to the top of the clay layer increase from an order of 20 m/s to an order of 30 m/s, and then a sharp decrease occurs in the gravel. Same Arias intensity values at the bottom have been obtained for unreinforced and geogrid reinforced cases. For the gravel and top of the clay layers, the Arias Intensity values of the reinforced cases is smaller than that of the unreinforced case.

8.1.2. Comparison of Numerical Analysis Data under 0.2g PGA

8.1.2.1. Under 0.5 Hz of Motion. When a sinusoidal acceleration with a peak of 0.2g is applied, the average acceleration at the base for a frequency of 0.5 Hz is much smaller than 0.2g and is seen to be 0.178 m/s^2. As the wave moves upward, vibration first amplifies in the clay and then deamplifies in the gravel. Same results are obtained at the top and bottom points for unreinforced and geogrid reinforced cases. The average

acceleration for the geogrid case at the middle of the model is slightly smaller than those for the unreinforced case.

Table 8.11. Average Acceleration (m/s^2) Values of Selected Points Under 0.2g PGA with 0.5 Hz of Frequency.

POINTS	With geogrid	Without geogrid
A,B,C	0.154	0.154
D,E,F	0.195	0.196
G,H,I	0.178	0.178

Table 8.12. Average Arias Intensity (m/s) Values of Selected Points Under 0.2g PGA with 0.5 Hz of Frequency.

POINTS	With geogrid	Without geogrid
A,B,C	0.0242	0.0244
D,E,F	0.0459	0.0460
G,H,I	0.0497	0.0497

From the bottom to the top, the Arias intensity values decreased for both unreinforced and geogrid reinforced cases. Same Arias intensity values at the bottom have been obtained for unreinforced and geogrid reinforced cases. Arias Intensity of geogrid cases at the middle and top of the model is slightly smaller than that of unreinforced cases.

8.1.2.2. Under 1 Hz of Motion. When a sinusoidal acceleration with a peak of 0.2g is applied, the average acceleration at the base for a frequency of 1 Hz is much smaller than 0.2g and is seen to be 0.718 m/s^2. As the wave moves upward, vibration first amplifies in the clay and then de-amplifies in the gravel. The average accelerations obtained for geogrid cases at the top and middle of the model are slightly smaller than those for unreinforced cases. At the bottom, identical acceleration values are observed.

Table 8.13. Average Acceleration (m/s^2) Values of Selected Points Under 0.2g PGA with 1 Hz of Frequency.

POINTS	With geogrid	Without geogrid
A,B,C	0.239	0.238
D,E,F	1.100	1.103
G,H,I	0.718	0.718

Table 8.14. Average Arias Intensity (m/s) Values of Selected Points Under 0.2g PGA with 1 Hz of Frequency.

POINTS	With geogrid	Without geogrid
A,B,C	0.0612	0.0602
D,E,F	1.5880	1.6060
G,H,I	0.6593	0.6593

The Arias Intensity values from bottom to top, first increased in the clay and then decreased in the gravel layer for both unreinforced and geogrid reinforced cases. Same Arias intensity values at the bottom have been obtained for unreinforced and geogrid reinforced cases. The Arias Intensity values for geogrid cases at the middle of the model are slightly smaller and at the top slightly higher than those for the unreinforced case.

8.1.2.3. Under 2 Hz of Motion. When a sinusoidal acceleration with a peak of 0.2g is applied, the average acceleration at the base for a frequency of 2 Hz is slightly smaller than 0.2g and is seen to be 1.357 m/s^2. As the wave moves upward, vibration de-amplifies. The average accelerations obtained for geogrid cases at the middle and at the top of the model are slightly higher than those for unreinforced cases. At the bottom, identical acceleration values are observed.

Table 8.15. Average Acceleration (m/s^2) Values of Selected Points Under 0.2g PGA with 2 Hz of Frequency.

POINTS	With geogrid	Without geogrid
A,B,C	0.224	0.219
D,E,F	1.179	1.178
G,H,I	1.357	1.357

Table 8.16. Average Arias Intensity (m/s) Values of Selected Points Under 0.2g PGA with 2 Hz of Frequency.

POINTS	With geogrid	Without geogrid
A,B,C	0.0681	0.0632
D,E,F	1.8087	1.8203
G,H,I	2.3833	2.3833

From the bottom to the top, the Arias intensity values decreased for both unreinforced and geogrid reinforced cases. Same Arias intensity values at the bottom have been obtained for unreinforced and geogrid reinforced cases. Arias Intensity of geogrid cases at the middle of the model is slightly smaller and at the top slightly higher than that of unreinforced case.

8.1.2.4. Under 3 Hz of Motion. When a sinusoidal acceleration with a peak of 0.2g is applied, the average acceleration at the base for a frequency of 3 Hz is higher than 0.2g and is seen to be 5.071 m/s^2. As the wave moves upward, vibration de-amplifies. The average accelerations obtained for geogrid cases at the middle of the model are slightly smaller and at the top slightly higher than those for the unreinforced case. At the bottom, identical acceleration values are observed.

Table 8.17. Average Acceleration (m/s^2) Values of Selected Points Under 0.2g PGA with 3 Hz of Frequency.

POINTS	With geogrid	Without geogrid
A,B,C	0.280	0.270
D,E,F	1.604	1.631
G,H,I	5.071	5.071

Table 8.18. Average Arias Intensity (m/s) Values of Selected Points Under 0.2g PGA with 3 Hz of Frequency.

POINTS	With geogrid	Without geogrid
A,B,C	0.0999	0.0913
D,E,F	3.9913	4.2437
G,H,I	25.9933	25.9933

From the bottom to the top, the Arias intensity values decreased for both unreinforced and geogrid reinforced cases. Same Arias intensity values at the bottom have been obtained for unreinforced and geogrid reinforced cases. Arias Intensity of geogrid cases at the middle of the model is slightly smaller and at the top slightly higher than that of the unreinforced case.

8.1.2.5. Under 5 Hz of Motion. When a sinusoidal acceleration with a peak of 0.2g is applied, the average acceleration at the base for a frequency of 5 Hz is much higher than 0.2g and is seen to be 7.287 m/s^2. As the wave moves upward, vibration de-amplifies. The average accelerations obtained for geogrid cases at the middle of the model are slightly higher and at the top slightly smaller than those for the unreinforced case. At the bottom, identical acceleration values are observed.

Table 8.19. Average Acceleration (m/s^2) Values of Selected Points Under 0.2g PGA with 5 Hz of Frequency.

POINTS	With geogrid	Without geogrid
A,B,C	0.287	0.302
D,E,F	6.158	5.983
G,H,I	7.287	7.287

Table 8.20. Average Arias Intensity (m/s) Values of Selected Points Under 0.2g PGA with 5 Hz of Frequency.

POINTS	With geogrid	Without geogrid
A,B,C	0.1216	0.1263
D,E,F	44.3500	44.1567
G,H,I	56.4967	56.4967

From the bottom to the top, the Arias intensity values decreased for both unreinforced and geogrid reinforced cases. Same Arias intensity values at the bottom have been obtained for unreinforced and geogrid reinforced cases. Arias Intensity of geogrid cases at the middle of the model is slightly higher and at the top slightly smaller than that of the unreinforced case.

8.1.3. Comparison of Numerical Analysis Data under 0.3g PGA

8.1.3.1. Under 0.5 Hz of Motion. When a sinusoidal acceleration with a peak of 0.3g is applied, the average acceleration at the base for a frequency of 0.5 Hz is much smaller than 0.3g and is seen to be 0.286 m/s^2. As the wave moves upward, vibration first amplifies in the clay and then de-amplifies in the gravel. Same analysis results have been obtained for unreinforced and geogrid reinforced cases. Hence, under low PGA as well as frequency, no influence of geogrid reinforcement on acceleration is observed.

Table 8.21. Average Acceleration (m/s^2) Values of Selected Points Under 0.3g PGA with 0.5 Hz of Frequency.

POINTS	With geogrid	Without geogrid
A,B,C	0.184	0.184
D,E,F	0.321	0.321
G,H,I	0.286	0.286

Table 8.22. Average Arias Intensity (m/s) Values of Selected Points Under 0.3g PGA with 0.5 Hz of Frequency.

POINTS	With geogrid	Without geogrid
A,B,C	0.0323	0.0323
D,E,F	0.1293	0.1297
G,H,I	0.1207	0.1207

The Arias Intensity values from bottom to top, first increased in the clay and then decreased in the gravel layer for both unreinforced and geogrid reinforced cases. Same Arias intensity values at bottom and top of the model have been obtained for unreinforced and geogrid reinforced cases. Average Arias Intensity of geogrid cases at middle of the model is slightly smaller than that of unreinforced cases.

8.1.3.2. Under 1 Hz of Motion. When a sinusoidal acceleration with a peak of 0.3g is applied, the average acceleration at the base for a frequency of 1 Hz is much smaller than 0.3g and is seen to be 1.121 m/s^2. As the wave moves upward, vibration first amplifies in the clay and then de-amplifies in the gravel. The average accelerations obtained for geogrid cases at the top of the model are slightly smaller than those for unreinforced ones. At the bottom and the middle, identical acceleration values are observed.

Table 8.23. Average Acceleration (m/s^2) Values of Selected Points Under 0.3g PGA with 1 Hz of Frequency.

POINTS	With geogrid	Without geogrid
A,B,C	0.246	0.243
D,E,F	1.582	1.582
G,H,I	1.121	1.121

Table 8.24. Average Arias Intensity (m/s) Values of Selected Points Under 0.3g PGA with 1 Hz of Frequency.

POINTS	With geogrid	Without geogrid
A,B,C	0.0625	0.0610
D,E,F	3.1167	3.0633
G,H,I	1.5033	1.5033

The Arias Intensity values from bottom to top, first increased in the clay and then sharply decreased in the gravel layer for both unreinforced and geogrid reinforced cases. Same Arias intensity values at the bottom have been obtained for unreinforced and geogrid reinforced cases. For the gravel and top of the clay layers, the Arias Intensity values of the reinforced cases are slightly higher than that of the unreinforced cases.

8.1.3.3. Under 2 Hz of Motion. When a sinusoidal acceleration with a peak of 0.3g is applied, the average acceleration at the base for a frequency of 2 Hz is slightly smaller than 0.3g and is seen to be 2.105 m/s^2. As the wave moves upward, vibration de-amplifies. The average accelerations obtained for geogrid cases at middle and at top of the model are slightly smaller than those for unreinforced cases. At the bottom, identical acceleration values are observed.

Table 8.25. Average Acceleration (m/s^2) Values of Selected Points Under 0.3g PGA with 2 Hz of Frequency.

POINTS	With geogrid	Without geogrid
A,B,C	0.241	0.244
D,E,F	1.931	1.948
G,H,I	2.105	2.105

Table 8.26. Average Arias Intensity (m/s) Values of Selected Points Under 0.3g PGA with 2 Hz of Frequency.

POINTS	With geogrid	Without geogrid
A,B,C	0.0764	0.0773
D,E,F	4.7997	4.8610
G,H,I	5.6097	5.6097

From the bottom to the top, the Arias intensity values decreased for both unreinforced and geogrid reinforced cases. Same Arias intensity values at the bottom have been obtained for unreinforced and geogrid reinforced cases. Arias Intensity of geogrid cases at middle and at top of the model are slightly smaller than that of unreinforced cases.

8.1.3.4. Under 3 Hz of Motion. When a sinusoidal acceleration with a peak of 0.3g is applied, the average acceleration at the base for a frequency of 3 Hz is higher than 0.3g and is seen to be 5.537 m/s^2. As the wave moves upward, vibration de-amplifies. The average accelerations obtained for geogrid cases at middle of the model acceleration are slightly smaller and at the top slightly higher than those for unreinforced cases. At the bottom, identical acceleration values are observed.

Table 8.27. Average Acceleration (m/s^2) Values of Selected Points Under 0.3g PGA with 3 Hz of Frequency.

POINTS	With geogrid	Without geogrid
A,B,C	0.311	0.291
D,E,F	2.011	2.021
G,H,I	5.537	5.537

Table 8.28. Average Arias Intensity (m/s) Values of Selected Points Under 0.3g PGA with 3 Hz of Frequency.

POINTS	With geogrid	Without geogrid
A,B,C	0.1246	0.1076
D,E,F	6.6743	6.7490
G,H,I	37.5433	37.5433

From the bottom to the top, the Arias intensity values decreased for both unreinforced and geogrid reinforced cases. Same Arias intensity values at the bottom have been obtained for unreinforced and geogrid reinforced cases. Arias Intensity of geogrid cases at the middle of the model is slightly smaller and at top of the model slightly higher than that of unreinforced cases.

8.1.3.5. Under 5 Hz of Motion. When a sinusoidal acceleration with a peak of 0.3g is applied, the average acceleration at the base for a frequency of 5 Hz is much higher than 0.3g and is seen to be 7.582 m/s^2. As the wave moves upward, vibration deamplifies. The average accelerations obtained for geogrid cases at the middle of the model acceleration are slightly higher and at the top slightly smaller than those for unreinforced cases. At the bottom, identical acceleration values are observed.

Table 8.29. Average Acceleration (m/s^2) Values of Selected Points Under 0.3g PGA with 5 Hz of Frequency.

POINTS	With geogrid	Without geogrid
A,B,C	0.323	0.327
D,E,F	5.949	5.810
G,H,I	7.582	7.582

Table 8.30. Average Arias Intensity (m/s) Values of Selected Points Under 0.3g PGA with 5 Hz of Frequency.

POINTS	With geogrid	Without geogrid
A,B,C	0.1654	0.1603
D,E,F	41.5000	42.3067
G,H,I	66.9667	66.9667

From the bottom to the top, the Arias intensity values decreased for both unreinforced and geogrid reinforced cases. Same Arias intensity values at the bottom have been obtained for unreinforced and geogrid reinforced cases. Arias Intensity of geogrid cases at top of the model is slightly higher and at the middle slightly smaller than that of the unreinforced case.

8.1.4. Comparison of Numerical Analysis Data under 0.4g PGA

8.1.4.1. Under 0.5 Hz of Motion. When a sinusoidal acceleration with a peak of 0.4g is applied, the average acceleration at the base for a frequency of 0.5 Hz is much smaller than 0.4g and is obtained as 0.380 m/s^2. As the wave moves upward, vibration first amplifies in the clay and then de-amplifies in the gravel. The average accelerations obtained for geogrid cases at the top and the middle of the model are slightly smaller than those for unreinforced ones. At the bottom, same acceleration values are observed. Hence, under low frequency with high PGA, only a slight influence of geogrid reinforcement on acceleration was observed.

Table 8.31. Average Acceleration (m/s2) Values of Selected Points Under 0.4g PGA with 0.5 Hz of Frequency.

POINTS	With geogrid	Without geogrid
A,B,C	0.199	0.200
D,E,F	0.459	0.460
G,H,I	0.380	0.380

Table 8.32. Average Arias Intensity (m/s) Values of Selected Points Under 0.4g PGA with 0.5 Hz of Frequency.

POINTS	With geogrid	Without geogrid
A,B,C	0.0371	0.0370
D,E,F	0.2593	0.2607
G,H,I	0.2203	0.2203

The Arias Intensity values from bottom to top, first increased in the clay and then decreased in the gravel layer for both unreinforced and geogrid reinforced cases. Same Arias intensity values at the bottom have been obtained for unreinforced and geogrid reinforced cases. For the top of the clay layer, average Arias Intensity of the reinforced cases is slightly smaller than that of the unreinforced one. For the gravel layer, however, Arias Intensity of the reinforced case turns out to be slightly higher than that of the unreinforced case.

8.1.4.2. Under 1 Hz of Motion. When a sinusoidal acceleration with a peak of 0.4g is applied, the average acceleration at the base for a frequency of 1 Hz is much smaller than 0.4g and is seen to be 1.440 m/s^2. As the wave moves upward, vibration first amplifies in the clay and then de-amplifies in the gravel. The average accelerations obtained for geogrid cases at the middle of the model are slightly smaller and at the top slightly higher than those for unreinforced cases. At the bottom, identical acceleration values are observed.

Table 8.33. Average Acceleration (m/s2) Values of Selected Points Under 0.4g PGA with 1 Hz of Frequency.

POINTS	With geogrid	Without geogrid
A,B,C	0.260	0.257
D,E,F	1.812	1.821
G,H,I	1.440	1.440

Table 8.34. Average Arias Intensity (m/s) Values of Selected Points Under 0.4g PGA with 1 Hz of Frequency.

POINTS	With geogrid	Without geogrid
A,B,C	0.0750	0.0797
D,E,F	4.0033	4.0747
G,H,I	2.4993	2.4993

The Arias Intensity values from bottom to top, first increased in the clay and then decreased in the gravel layer for both unreinforced and geogrid reinforced cases. Same Arias intensity values at the bottom are obtained for unreinforced and geogrid reinforced cases. For the gravel and top of the clay layers, Arias Intensity of the reinforced cases are smaller than that of the unreinforced cases.

8.1.4.3. Under 2 Hz of Motion. When a sinusoidal acceleration with a peak of 0.4g is applied, the average acceleration at the base for a frequency of 2 Hz is slightly smaller than 0.4g and is seen to be 3.226 m/s^2. As the wave moves upward, vibration de-amplifies. The average accelerations obtained for geogrid cases at middle of the model are slightly smaller and at the top slightly higher than those for unreinforced cases. At the bottom, identical acceleration values are observed.

Table 8.35. Average Acceleration (m/s^2) Values of Selected Points Under 0.4g PGA with 2 Hz of Frequency.

POINTS	With geogrid	Without geogrid
A,B,C	0.261	0.259
D,E,F	2.601	2.624
G,H,I	3.226	3.226

Table 8.36. Average Arias Intensity (m/s) Values of Selected Points Under 0.4g PGA with 2 Hz of Frequency.

POINTS	With geogrid	Without geogrid
A,B,C	0.0838	0.0860
D,E,F	8.7670	8.9023
G,H,I	12.7900	12.7900

From the bottom to the top, the Arias intensity values decreased for both unreinforced and geogrid reinforced cases. Same Arias intensity values at the bottom have been obtained for unreinforced and geogrid reinforced cases. For the gravel and top of the clay layers, Arias intensity values of the reinforced cases are smaller than that of the unreinforced cases.

8.1.4.4. Under 3 Hz of Motion. When a sinusoidal acceleration with a peak of 0.4g is applied, the average acceleration at the base for a frequency of 3 Hz is higher than 0.4g and is seen to be 5.536 m/s^2. As the wave moves upward, vibration de-amplifies. The average accelerations obtained for geogrid cases at the middle of the model acceleration are slightly smaller and at the top slightly higher than those for unreinforced cases. At the bottom, identical acceleration values are observed.

Table 8.37. Average Acceleration (m/s^2) Values of Selected Points Under 0.4g PGA with 3 Hz of Frequency.

POINTS	With geogrid	Without geogrid
A,B,C	0.323	0.311
D,E,F	2.181	2.234
G,H,I	5.536	5.536

Table 8.38. Average Arias Intensity (m/s) Values of Selected Points Under 0.4g PGA with 3 Hz of Frequency.

POINTS	With geogrid	Without geogrid
A,B,C	0.1413	0.1347
D,E,F	7.5557	7.4833
G,H,I	43.0067	43.0067

From the bottom to the top, the Arias intensity values decreased for both unreinforced and geogrid reinforced cases. Same Arias intensity values at the bottom have been obtained for unreinforced and geogrid reinforced cases. For the gravel and top of the clay layers, Arias Intensity values of the reinforced cases are smaller than that of the unreinforced cases.

8.1.4.5. Under 5 Hz of Motion. When a sinusoidal acceleration with a peak of 0.4g is applied, the average acceleration at the base for a frequency of 5 Hz is much higher than 0.4g and is seen to be 8.069 m/s^2. As the wave moves upward, vibration de-amplifies. The average accelerations obtained for geogrid cases at the top and the middle of the model are slightly higher than those for unreinforced ones. At the bottom, identical acceleration values are observed.

Table 8.39. Average Acceleration (m/s^2) Values of Selected Points Under 0.4g PGA with 5 Hz of Frequency.

POINTS	With geogrid	Without geogrid
A,B,C	0.440	0.430
D,E,F	5.907	5.783
G,H,I	8.069	8.069

Table 8.40. Average Arias Intensity (m/s) Values of Selected Points Under 0.4g PGA with 5 Hz of Frequency.

POINTS	With geogrid	Without geogrid
A,B,C	0.2973	0.8010
D,E,F	39.8100	40.5333
G,H,I	75.6367	75.6367

From the bottom to the top, the Arias intensity values decreased for both unreinforced and geogrid reinforced cases. Same Arias intensity values at the bottom have been obtained for unreinforced and geogrid reinforced cases. For the gravel and top of the clay layers, Arias Intensity values of the reinforced cases are smaller than that of the unreinforced cases.

In order to gain a better insight into all the results, the average Arias Intensity values given in Table 8.41. can be examined. Arias Intensity Ratios have been provided in the Table 8.42 as well.

Table 8.41. Under acceleration of 0.1g, 0.2g, 0.3g, 0.4g with frequency of 0.5, 1, 2, 3, 5 Hz, Average Arias Intensity Comparison with reinforced and unreinforced case for the top points, middle points and bottom points respectively.

FOR THE POINTS A,B,C AVERAGE ARIAS INTENSITY COMPARISON										
PGA	0.5 Hz reinforced	0.5 Hz unreinforced	1 HZ reinforced	1 HZ unreinforced	2 HZ reinforced	2 HZ unreinforced	3 HZ reinforced	3 HZ unreinforced	5 HZ reinforced	5 HZ unreinforced
0.1g	0.007	0.0071	0.0396	0.0398	0.0505	0.05	0.1295	0.1017	0.1337	0.2067
0.2g	0.0242	0.0244	0.0612	0.0602	0.0681	0.0632	0.0999	0.0913	0.1216	0.1263
0.3g	0.0323	0.0323	0.0625	0.061	0.0764	0.0773	0.1246	0.1076	0.1654	0.1603
0.4g	0.037	0.037	0.075	0.0797	0.0838	0.086	0.1413	0.1347	0.2973	0.801
FOR THE POINTS D.E.F AVERAGE ARIAS INTENSITY COMPARISON										
PGA	0.5 Hz reinforced	0.5 Hz unreinforced	1 HZ reinforced	1 HZ unreinforced	2 HZ reinforced	2 HZ unreinforced	3 HZ reinforced	3 HZ unreinforced	5 HZ reinforced	5 HZ unreinforced
0.1g	0.0084	0.0084	0.2243	0.2254	0.5727	0.5817	1.5417	1.6067	30.6067	30.82
0.2g	0.046	0.046	1.588	1.606	1.8087	1.8203	3.9913	4.2437	44.35	44.1567
0.3g	0.1293	0.1297	3.1167	3.0633	4.7997	4.861	6.6743	6.749	41.5	42.3067
0.4g	0.2593	0.2607	4.0033	4.0747	8.767	8.9023	7.5557	7.4833	39.81	40.5333
FOR THE POINTS G.H.I AVERAGE ARIAS INTENSITY COMPARISON										
PGA	0.5 Hz reinforced	0.5 Hz unreinforced	1 HZ reinforced	1 HZ unreinforced	2 HZ reinforced	2 HZ unreinforced	3 HZ reinforced	3 HZ unreinforced	5 HZ reinforced	5 HZ unreinforced
0.1g	0.11	0.11	0.1331	0.1331	0.6683	0.6683	11.4433	11.4433	19.68	19.68
0.2g	0.0497	0.0497	0.6593	0.6593	2.3833	2.3833	25.9933	25.9933	56.4967	56.4967
0.3g	0.1207	0.1207	1.5033	1.5033	5.6097	5.6097	37.5433	37.5433	66.9667	66.9667
0.4g	0.2203	0.2203	2.4993	2.4993	12.79	12.79	43.0067	43.0067	75.6367	75.6367

Table 8.42. Under acceleration of 0.1g, 0.2g, 0.3g, 0.4g with frequency of 0.5, 1, 2, 3, 5 Hz, Arias Intensity Ratios for reinforced and unreinforced cases of top points/ bottom points and middle points/bottom poi.

ARIAS INTENSITY RATIOS FOR THE POINTS OF (A,B,C)/(G,H,I)										
PGA	0.5 Hz reinforced	0.5 Hz unreinforced	1 HZ reinforced	1 HZ unreinforced	2 HZ reinforced	2 HZ unreinforced	3 HZ reinforced	3 HZ unreinforced	5 HZ reinforced	5 HZ unreinforced
0.1g	0.064	0.065	0.298	0.299	0.076	0.075	0.011	0.009	0.007	0.011
0.2g	0.487	0.491	0.093	0.091	0.029	0.027	0.004	0.004	0.002	0.002
0.3g	0.268	0.268	0.042	0.041	0.014	0.014	0.003	0.003	0.002	0.002
0.4g	0.168	0.168	0.030	0.032	0.007	0.007	0.003	0.003	0.004	0.011
ARIAS INTENSITY RATIOS FOR THE POINTS OF (D,E,F)/(G,H,I)										
PGA	0.5 Hz reinforced	0.5 Hz unreinforced	1 HZ reinforced	1 HZ unreinforced	2 HZ reinforced	2 HZ unreinforced	3 HZ reinforced	3 HZ unreinforced	5 HZ reinforced	5 HZ unreinforced
0.1g	0.076	0.076	**1.685**	**1.693**	0.857	0.870	0.135	0.140	**1.555**	**1.566**
0.2g	0.925	0.926	**2.409**	**2.436**	0.759	0.764	0.154	0.163	0.785	0.782
0.3g	**1.072**	**1.075**	**2.073**	**2.038**	0.856	0.867	0.178	0.180	0.620	0.632
0.4g	**1.177**	**1.183**	**1.602**	**1.630**	0.685	0.696	0.176	0.174	0.526	0.536

Table 8.42 displays the calculated Arias Intensity ratios. When the ratio is above one, it is considered an indication of soil amplification and when it is lower than one, soil de-amplification is thought to occur. Table readings of average Arias Intensity ratio values for geogrid reinforced and unreinforced cases as well as the bolded ratios implying soil amplification suggest that for both geogrid reinforced and unreinforced cases, the average Arias Intensity of the points at the bottom is smaller than that for the points top of the clay. To be precise, the Arias Intensity values from the bottom to the points top of the clay increase from an order of 20 m/s to an order of 30 m/s in the analysis of 0.1g PGA under frequency of 5 Hz motion. In other words, the Arias Intensity ratio of 1.56 points to the existence of soil amplification for soft soil under high frequency of motion. In addition, for both geogrid reinforced and unreinforced cases of 0.3g PGA under frequency of 0.5 Hz, 0.4g PGA under frequency of 0.5 Hz and for all PGA values under frequency of 1 Hz, soil amplification has been observed for the points at the top of the clay. However, soil amplification did not occur at the gravel layer. To the contrary, a sharp decrease in accelerations and energies was observed during the transfer of the vibrations from top of the clay to the gravel layer. Another important point is that geogrid reinforcement functioned best under 3 Hz frequency of motion since in this case the de-amplification ratio is largest, the Arias Intensity ratio ranges between 13%-18%.

8.1.5. Arias Intensity Ratios of Geogrid Reinforced/ Unreinforced Cases

Table 8.43. Arias Intensity Ratios of Geogrid Reinforced/ Unreinforced Cases.

FOR POINTS ABC AI RATIO (GEOGRID/(NON-GEOGRID))CASES					
PGA (g)	0.5 Hz	1 Hz	2 Hz	3 Hz	5 Hz
0.1	0.989	0.994	1.010	1.273	0.647
0.2	0.992	1.017	1.077	1.094	0.963
0.3	1.000	1.025	0.988	1.158	1.031
0.4	1.001	0.941	0.974	1.049	0.371
FOR POINTS DEF AI RATIO (GEOGRID/(NON-GEOGRID))CASES					
PGA (g)	0.5 Hz	1 Hz	2 Hz	3 Hz	5 Hz
0.1	1.000	0.995	0.985	0.960	0.993
0.2	0.999	0.989	0.994	0.941	1.004
0.3	0.997	1.017	0.987	0.989	0.981
0.4	0.995	0.982	0.985	1.009	0.982
FOR POINTS GHI AI RATIO (GEOGRID/(NON-GEOGRID))CASES					
PGA (g)	0.5 Hz	1 Hz	2 Hz	3 Hz	5 Hz
0.1	1.000	1.000	1.000	1.000	1.000
0.2	1.000	1.000	1.000	1.000	1.000
0.3	1.000	1.000	1.000	1.000	1.000
0.4	1.000	1.000	1.000	1.000	1.000

Table 8.43 Under acceleration of 0.1g, 0.2g, 0.3g, 0.4g with frequency of 0.5, 1, 2, 3, 5 Hz, Arias Intensity Ratios between reinforced and unreinforced cases for the top points, middle points and bottom points respectively.

When a general glance is taken to Table 8.43, it can be seen that geogrid reinforcement did not work the same way for the points within the gravel and for the points top of the clay. Hence, different soil strata (gravel and clay) seems to lead to different average Arias Intensity ratios of geogrid reinforcement case over the unreinforced case.

Ground motions being equal, as far as the Arias Intensity ratios of geogrid reinforcement case over the unreinforced case are concerned, geogrid is thought to exhibit effective absorption behavior under 5 Hz frequency motion. Indeed, under 0.4g PGA

and 5 Hz motion, the ratio appears to be 37%. However, under a motion of 3 Hz frequency, geogrid presence will always cause an increase in the gravel layer.

Ground motions being equal, for the points at the middle, as far as the Arias Intensity ratios of geogrid reinforcement case over the unreinforced case are concerned, geogrid exhibits reductive absorption behavior under 5 Hz frequency of motion compared to the 3 Hz frequency of motion.

Ground motions being equal, for the points at the bottom, as far as the Arias Intensity ratios of geogrid reinforcement case over the unreinforced case are concerned, Arias Intensity values remain definitely the same and, as predicted, geogrid reinforcement has no effect whatsoever on the results obtained.

Overall, the average Arias Intensity ratio comparisons made between geogrid reinforced and unreinforced cases under same parameters (PGA, frequency... etc.) shows that the amount of energies is relatively close to one another for the middle part. However, the Arias Intensity values of the top points are in general very small. That is why, it would not be wrong to conclude that not geosynthetics but gravel laid on the soft clayey soil had a greater effect on the results. This may be because of the relatively high stiffness of the thick gravel layer. For future studies, the result should be further investigated.

8.2. Figurative View of the Arias Intensity Values

8.2.1. Arias Intensity values for reinforced and unreinforced cases of the top, middle and bottom points

Transition of the vibration from the bottom to top of the model and the illustration of the Arias Intensity values are given below in Figure 8.5, Figure 8.6, Figure 8.7, Figure 8.8 along with the top points, middle points and bottom points under different PGA values with different frequencies. Overall, the Arias Intensity of the geogrid reinforced cases seems to be lower than that of unreinforced cases. Although the Arias

Intensity general is slightly smaller for the geogrid cases, these differences in energy between the geogrid reinforced and unreinforced cases with same parameters are so small to be shown in Figure 8.5, Figure 8.6, Figure 8.7, Figure 8.8, which mainly deal with the top points, middle points and bottom points.

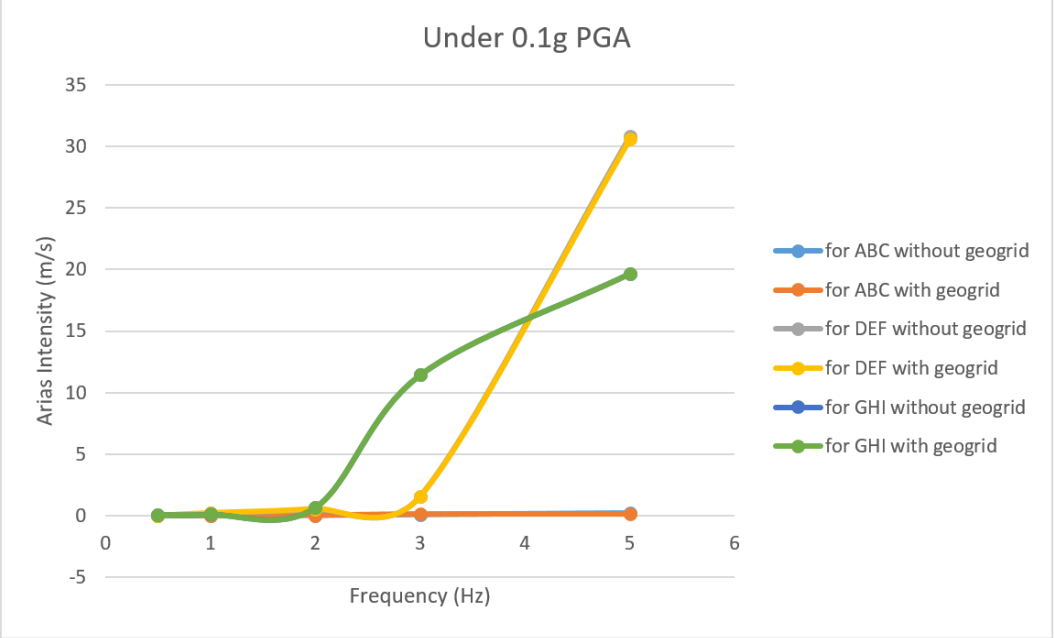

Figure 8.5. Arias Intensity values for reinforced and unreinforced cases of the top points, middle points and bottom points under an acceleration of 0.1g with a frequency of 0.5, 1, 2, 3, 5 Hz motions.

In Figure 8.5, the orange line representing top of the clay layer is above the green line representing the bottom at the frequency of 5 Hz motion. This points to the existence of soil amplification for soft soil under high frequency of motion. The Arias Intensity from the bottom to the top of the clay layer apparently increases from an order of 20 m/s to an order of 30 m/s as the analysis of 0.1g PGA under 5 Hz frequency indicates.

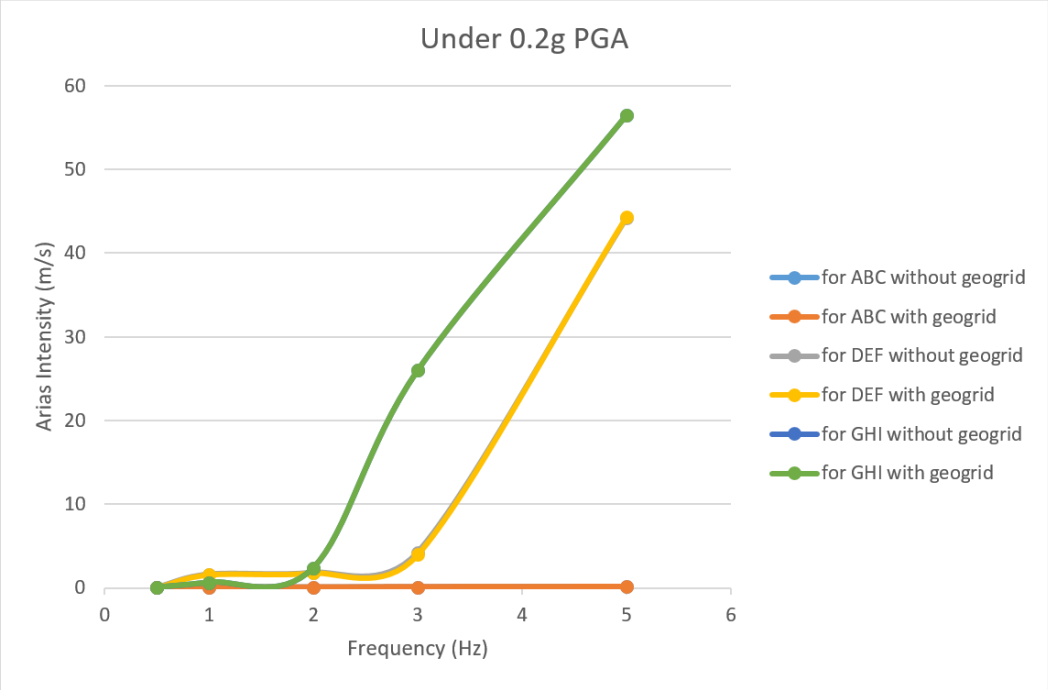

Figure 8.6. Arias Intensity values for reinforced and unreinforced cases of the top points, middle points and bottom points under an acceleration of 0.2g with a frequency of 0.5, 1, 2, 3, 5 Hz motions.

In Figure 8.6, the orange line representing top of the clay layer is above the green line representing the bottom at a frequency of 1 Hz motion. Therefore, soil amplification can be said to occur for a frequency of 1 Hz frequency under 0.2g PGA.

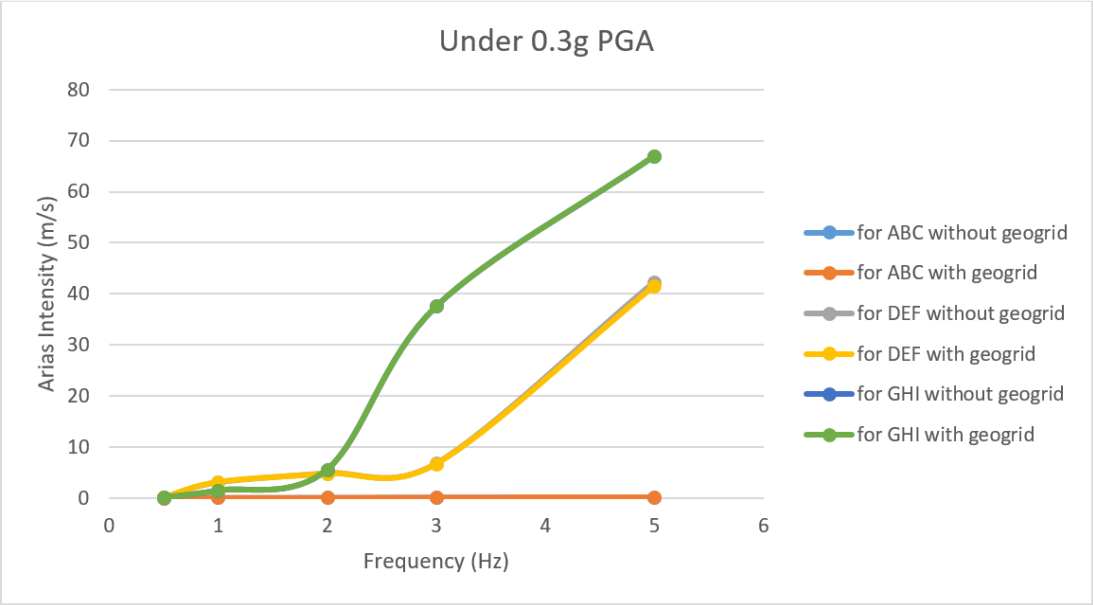

Figure 8.7. Arias Intensity values for reinforced and unreinforced cases of the top points, middle points and bottom points under an acceleration of 0.3g with a frequency of 0.5, 1, 2, 3, 5 Hz motions.

In Figure 8.7, the orange line representing top of the clay layer is above the green line representing the bottom at a frequency of 1 Hz motion. Hence, soil amplification can be said to occur for a frequency of 1 Hz motion under 0.3g PGA. Table 8.43 further demonstrates that minor soil amplification exists for a frequency of 0.5 Hz motion under 0.3g PGA; however, as it is too small, it cannot be differentiated in the Figure 8.7.

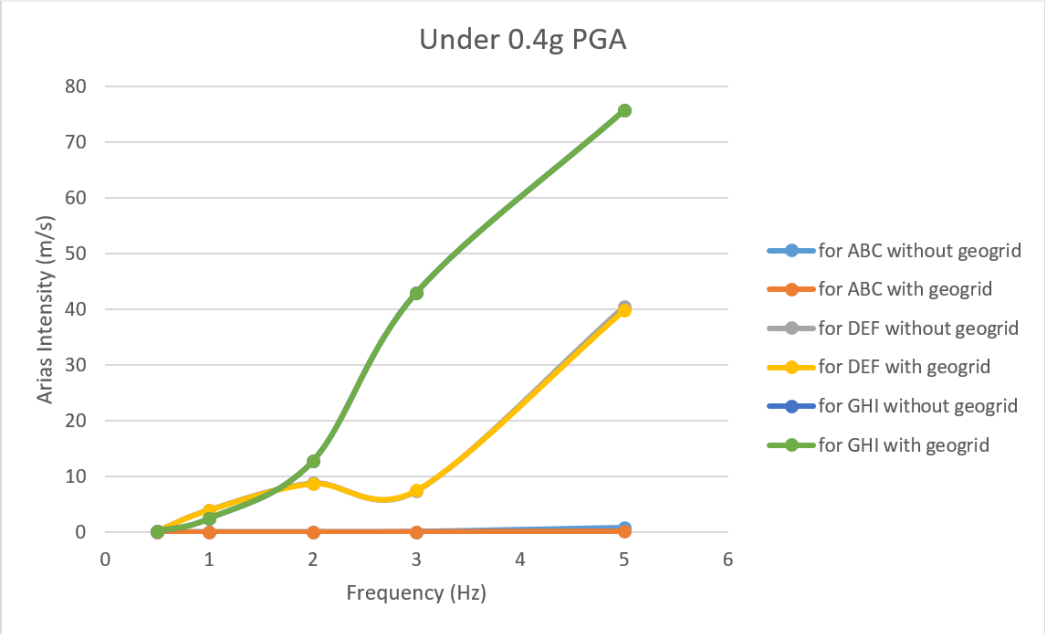

Figure 8.8. Arias Intensity values for reinforced and unreinforced cases of the top points, middle points and bottom points under an acceleration of 0.4g with a frequency of 0.5, 1, 2, 3, 5 Hz motions.

In Figure 8.8, the orange line representing top of the clay layer is above the green line representing the bottom at the frequency of 1 Hz motion. Hence, it can be easily noticed that there is soil amplification for a frequency of 1 Hz motion under 0.4g PGA. According to the Table 8.42, minor soil amplification exists for a frequency of 0.5 Hz motion under 0.4g PGA ; however, as it is too small, it cannot be differentiated in Figure 8.8.

8.2.2. Arias Intensity values for reinforced and unreinforced cases of the top and the middle points

Arias Intensity values for reinforced and unreinforced cases of the top points and middle points under an acceleration of 0.1g, 0.2g, 0.3g, 0.4g with a frequency of 0.5, 1, 2, 3, 5 Hz motions were plotted separately in order to see the effects of geogrid reinforcement on the selected points. Since the bottom points are exactly the same for reinforced and unreinforced cases, they are not included in the following figures.

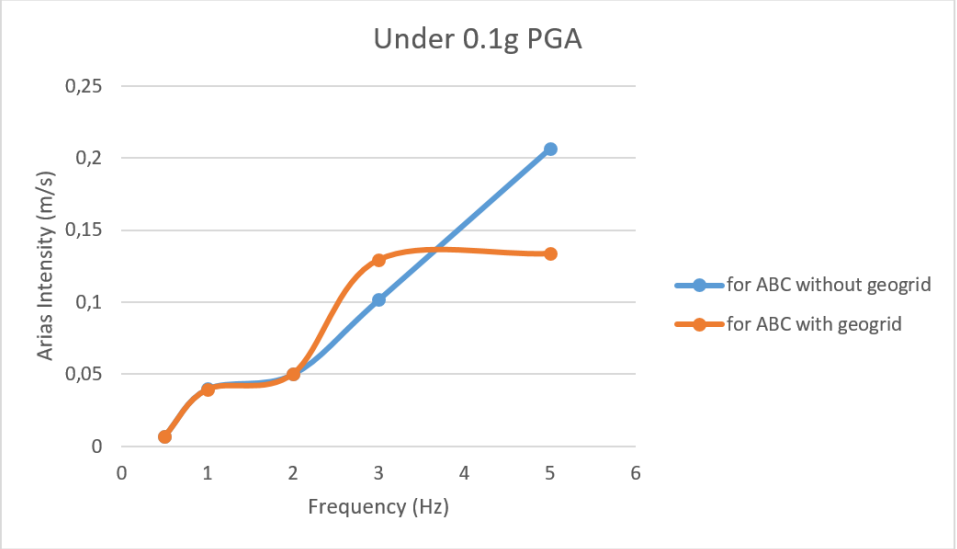

Figure 8.9. Arias Intensity values for reinforced and unreinforced cases of the top points under an acceleration of 0.1g with a frequency of 0.5, 1, 2, 3, 5 Hz motions.

In Figure 8.9, the orange line representing geogrid reinforcement case is above the blue line representing the unreinforced case at the frequency of 3 Hz motion for the gravel layer. Hence, it can be said that geogrid reinforcement has increased the acceleration for a frequency of 3 Hz motion under 0.1g PGA in the gravel layer. But for a frequency of 5 Hz, the geogrid has been able to reduce Arias Intensity considerably, when compared to the unreinforced case.

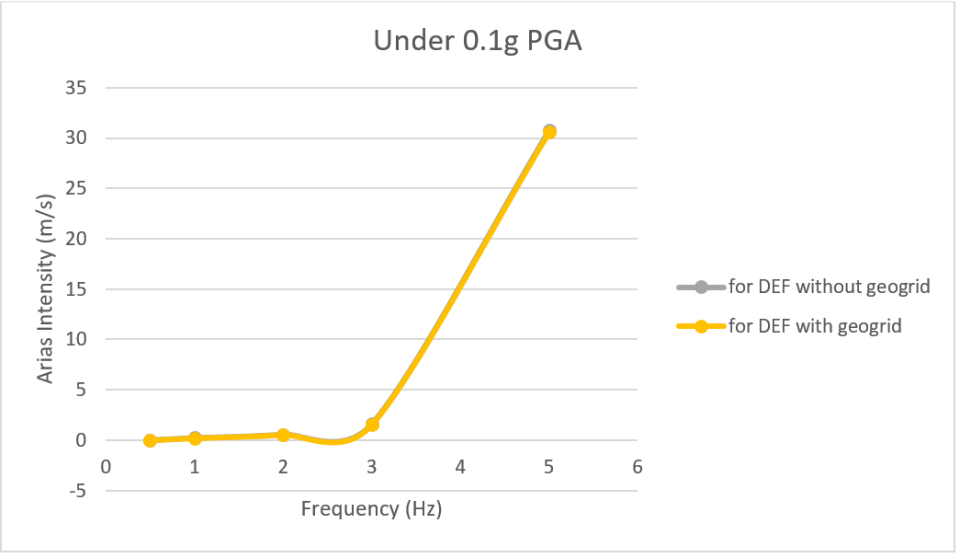

Figure 8.10. Arias Intensity values for reinforced and unreinforced cases of the middle points under an acceleration of 0.1g with a frequency of 0.5, 1, 2, 3, 5 Hz motions.

In Figure 8.10, the orange line representing the geogrid reinforcement case overlaps with the gray line representing the unreinforced case at all motions for the top of the clay layer. Therefore, geogrid reinforcement, as predicted, seems to have no influence on the acceleration for a frequency of 0.5, 1, 2, 3, 5 Hz motions under 0.1g PGA at the top of the clay layer.

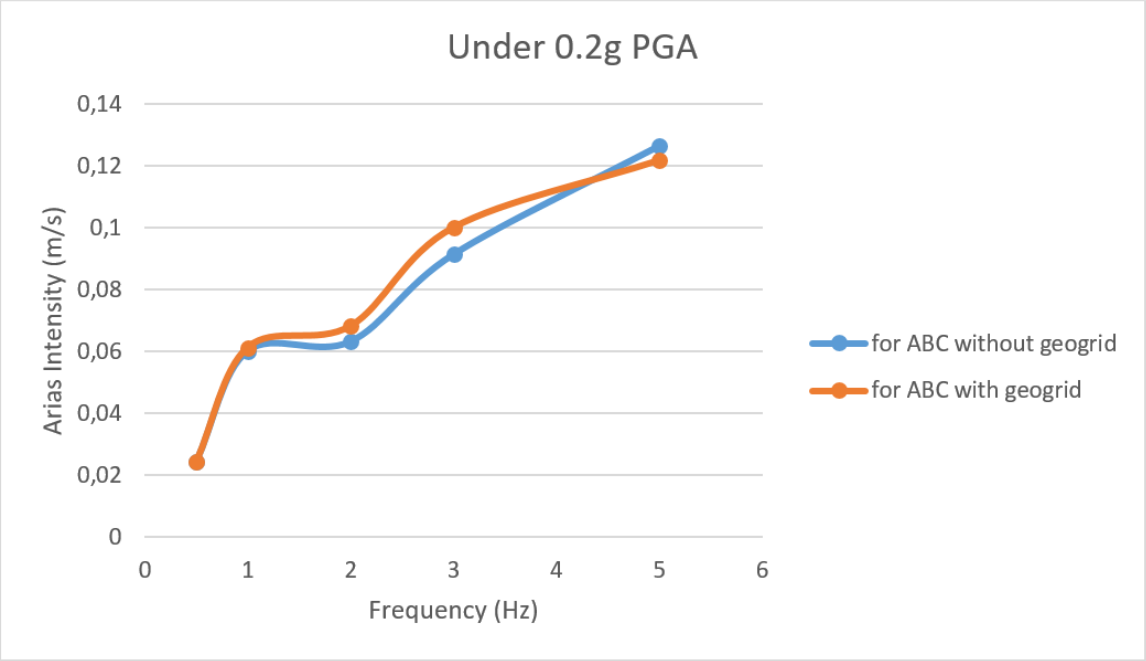

Figure 8.11. Arias Intensity values for reinforced and unreinforced cases of the top points under an acceleration of 0.2g with a frequency of 0.5, 1, 2, 3, 5 Hz motions.

In Figure 8.11, the orange line representing geogrid reinforcement case is above the blue line representing the unreinforced case at a frequency of 1, 2, 3 Hz motions for the gravel layer. Thus, geogrid reinforcement seems to have increased the acceleration for a frequency of 1, 2, 3 Hz motions under 0.2g PGA in the gravel layer.

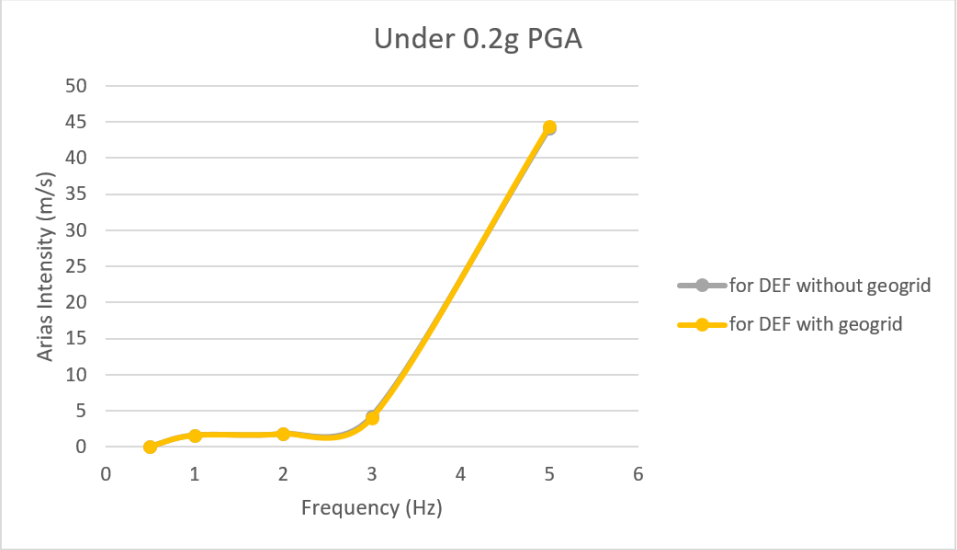

Figure 8.12. Arias Intensity values for reinforced and unreinforced cases of the middle points under an acceleration of 0.2g with a frequency of 0.5, 1, 2, 3, 5 Hz motions.

In Figure 8.12, the orange line representing geogrid reinforcement case seems to overlap with the gray line representing the unreinforced case at all motions for the top of the clay layer. Hence, it can be concluded that geogrid reinforcement has no considerable influence on the acceleration for a frequency of 0.5, 1, 2, 3, 5 Hz motions under 0.2g PGA at the top of the clay layer.

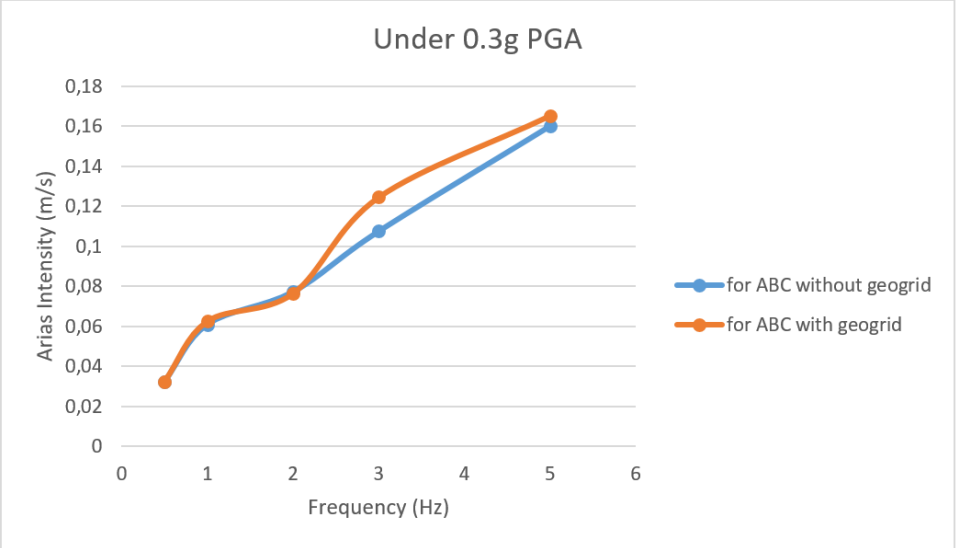

Figure 8.13. Arias Intensity values for reinforced and unreinforced cases of the top points under an acceleration of 0.3g with a frequency of 0.5, 1, 2, 3, 5 Hz motions.

In Figure 8.13, the orange line representing the geogrid reinforcement case is above the blue line representing the unreinforced case at a frequency of 1, 3, 5 Hz motions for the gravel layer. Hence, it can be noticed the geogrid reinforcement increases the acceleration slightly for a frequency of 1, 3, 5 Hz motions under 0.3g PGA in the gravel layer.

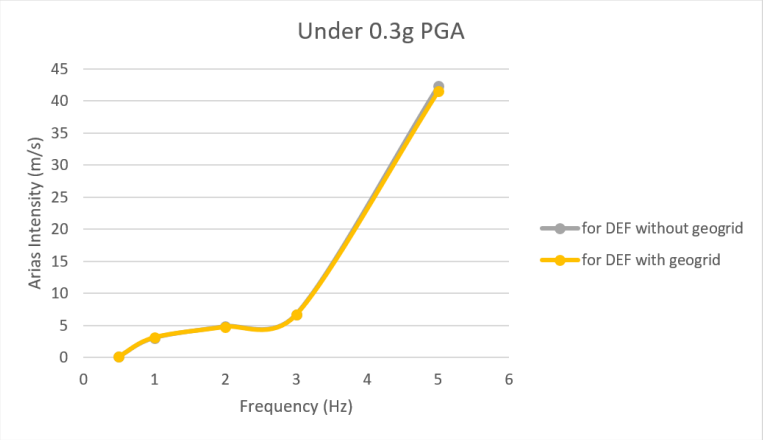

Figure 8.14. Arias Intensity values for reinforced and unreinforced cases of the middle points under an acceleration of 0.3g with a frequency of 0.5, 1, 2, 3, 5 Hz motions.

In Figure 8.14, the orange line representing the geogrid reinforcement case overlaps with gray line representing the unreinforced case at all motions for the top of the clay layer. Hence, it can be concluded the geogrid reinforcement has no considerable influence on the acceleration for a frequency of 0.5, 1, 2, 3, 5 Hz motions under 0.3g PGA at the top of the clay layer.

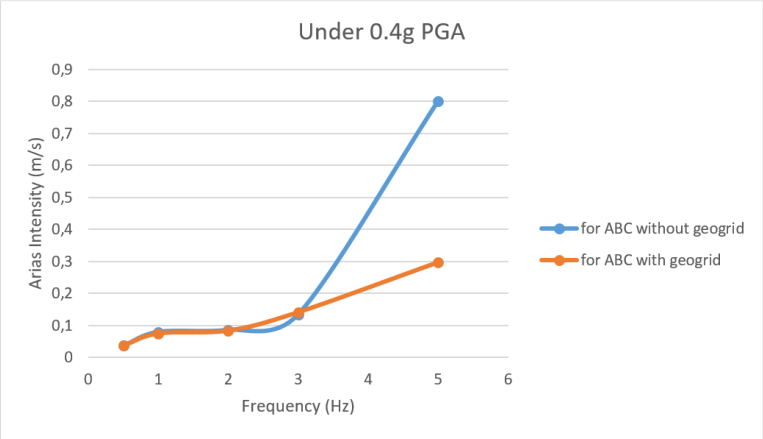

Figure 8.15. Arias Intensity values for reinforced and unreinforced cases of the top points under an acceleration of 0.4g with a frequency of 0.5, 1, 2, 3, 5 Hz motions.

In Figure 8.15, the orange line representing the geogrid reinforcement case is slightly above the blue line representing the unreinforced case at a frequency of 1, 2, 3 Hz motions for the gravel layer. Hence, it can be said the geogrid reinforcement led to a minor increase in the acceleration for a frequency of 1, 2, 3 Hz motions under 0.4g PGA in the gravel layer. Again here, the presence of geogrid has been able to reduce the Arias Intensity for a frequency of 5 Hz.

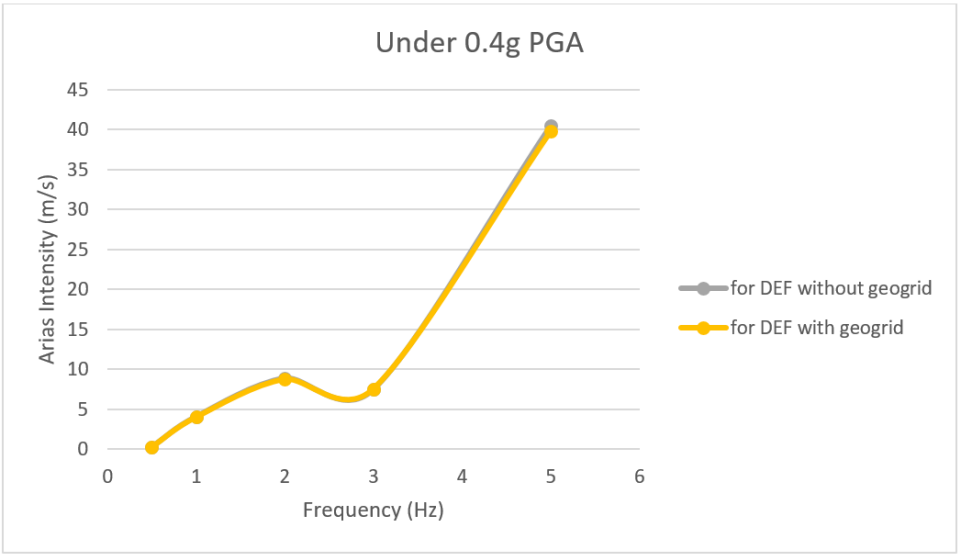

Figure 8.16. Arias Intensity values for reinforced and unreinforced cases of the middle points under an acceleration of 0.4g with a frequency of 0.5, 1, 2, 3, 5 Hz motions.

In Figure 8.16, the orange line representing the geogrid reinforcement case overlaps with the gray line representing the unreinforced case at all motions for top of the clay layer. Hence, it can be said that geogrid reinforcement has no considerable influence on the acceleration for a frequency of 0.5, 1, 2, 3, 5 Hz motions under 0.4g PGA at the top of the clay layer.

8.3. Figurative View of the Average Arias Intensity Ratio Values

Average Arias Intensity Ratio values for reinforced and unreinforced cases of the top points/ the bottom and middle points/ the bottom under an acceleration of 0.1g, 0.2g, 0.3g, 0.4g with a frequency of 0.5, 1, 2, 3, 5 Hz motions have been plotted separately in order to better observe the effects of geogrid reinforcement on the selected points locating different soil strata. Interpretation of Figure 8.17, Figure 8.18, Figure 8.19 and Figure 8.20 show that since unreinforced and geogrid reinforced cases of the top points/ the bottom and middle points/ the bottom differ from each other slightly, they overlap across all motions. Hence, it can be inferred that the geogrid reinforcement has no reasonably influence to differ the Arias Intensity ratio.

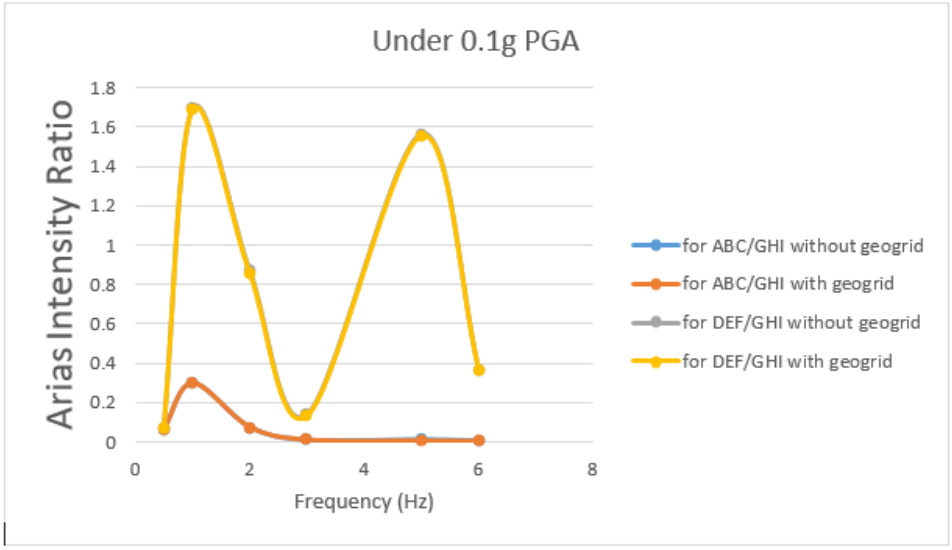

Figure 8.17. Average Arias Intensity Ratio values for reinforced and unreinforced cases of the top points/ the bottom and middle points/ the bottom under frequencies of 0.5, 1, 2, 3, 5 Hz with a ground motion of 0.1g PGA.

Under 0.1g PGA with a motion of 0.5 Hz, the Arias Intensity ratio of the middle points/ the bottom is close to zero. The maximum Arias Intensity ratio value is observed to be nearly 1.7 for the middle points/ the bottom under a frequency of 1 Hz. For this reason, there appears to be amplification on the weak ground. On the weak ground, under frequencies of 2 and 3 Hz a reduction in the amplitude occurs and between 3 Hz to 5 Hz motion, the Arias Intensity ratio rises It is seen that the amplification in magnitude occurs at 1 Hz and 5 Hz.

For the top points/ the bottom, under 0.1g PGA with a frequency of 0.5 Hz, the ratio remains the same as the one for the middle points/ the bottom. The maximum Arias Intensity ratio is observed to be at a motion frequency of 1 Hz. Then a reduction in the amplitude occurs and the ratio is almost zero for 3, 5 Hz motions.

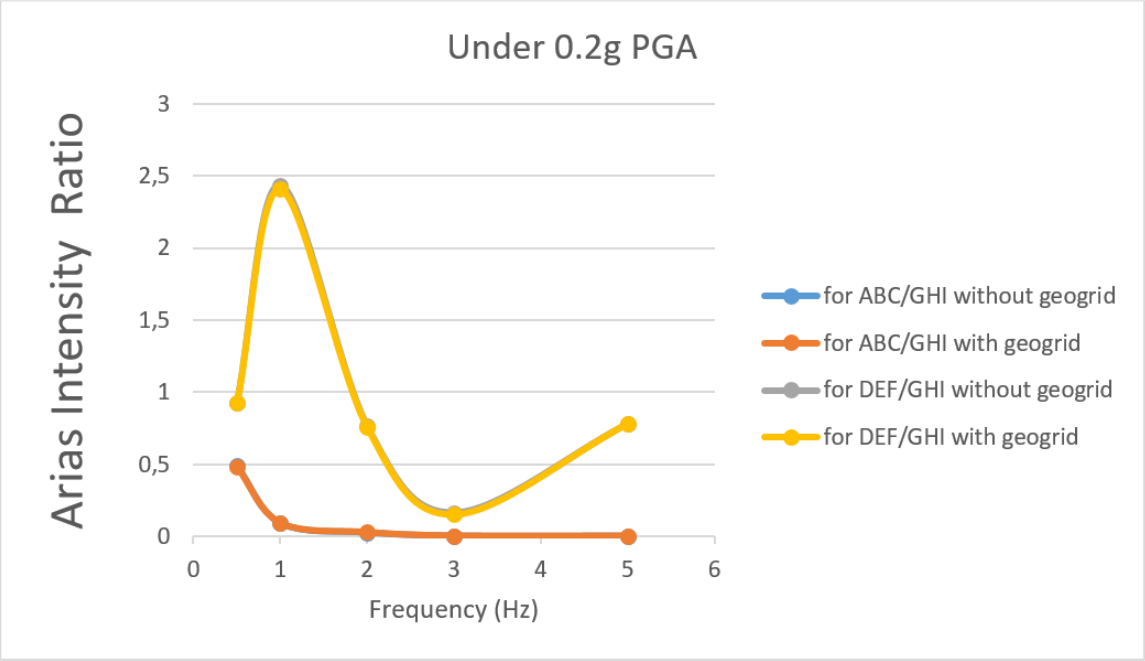

Figure 8.18. Average Arias Intensity Ratio values for reinforced and unreinforced cases of the top points/ the bottom and middle points/ the bottom under 0.5, 1, 2, 3, 5 Hz frequency with 0.2g PGA ground motion.

Under 0.2g PGA with a motion of 0.5 Hz, the Arias Intensity ratio of the middle points/ the bottom is nearly 1. The maximum Arias Intensity ratio value is observed to be nearly 2.5 for the middle points/ the bottom under a frequency of 1 Hz. For this

reason, amplification is said to occur on the weak ground. On the weak ground, under frequencies of 2 and 3 Hz, a reduction in the amplitude is observed and between 3 Hz to 5 Hz motion ,the Arias Intensity ratio shows an increase.

For the top points/ the bottom, under 0.2g PGA with a frequency of 0.5 Hz, the ratio is 0.5. The maximum Arias Intensity ratio is observed to be at a motion frequency of 0.5 Hz. Then the ratio begins to fall and reaches almost zero for 3, 5 Hz motions.

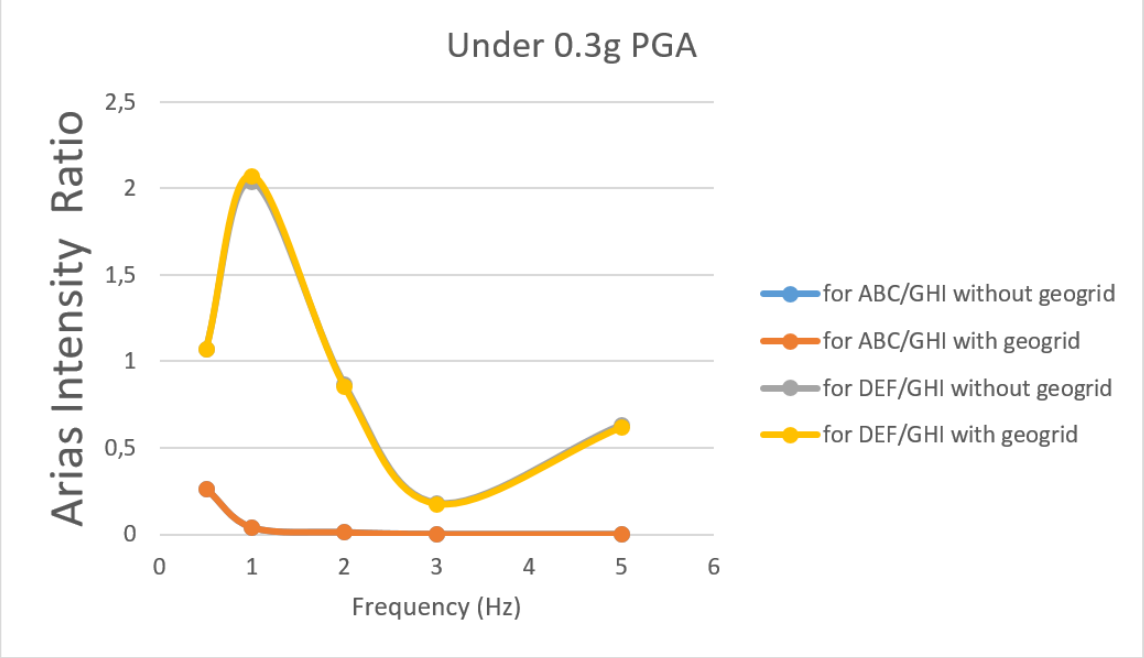

Figure 8.19. Average Arias Intensity Ratio values for reinforced and unreinforced cases of the top points/ the bottom and middle points/ the bottom under frequencies of 0.5, 1, 2, 3, 5 Hz with a ground motion of 0.3g PGA.

Under 0.3g PGA with a motion of 0.5 Hz, the Arias Intensity ratio of the middle points/ the bottom is nearly 1. The maximum Arias Intensity ratio value is observed to be nearly 2 for the middle points/ the bottom under a frequency of 1 Hz. For this reason, amplification is said to occur on the weak ground. Here, under frequencies of 2 and 3 Hz, a reduction in the amplitude happens and from 3 Hz to 5 Hz motion, the Arias Intensity ratio shows an increase.

For the top points/ the bottom, under 0.3g PGA with a frequency of 0.5 Hz, the ratio is 0.27, The maximum Arias Intensity ratio is observed to be at a motion frequency of 0.5 Hz. Then, the ratio begins to fall and reaches almost zero for 2, 3, 5 Hz motions.

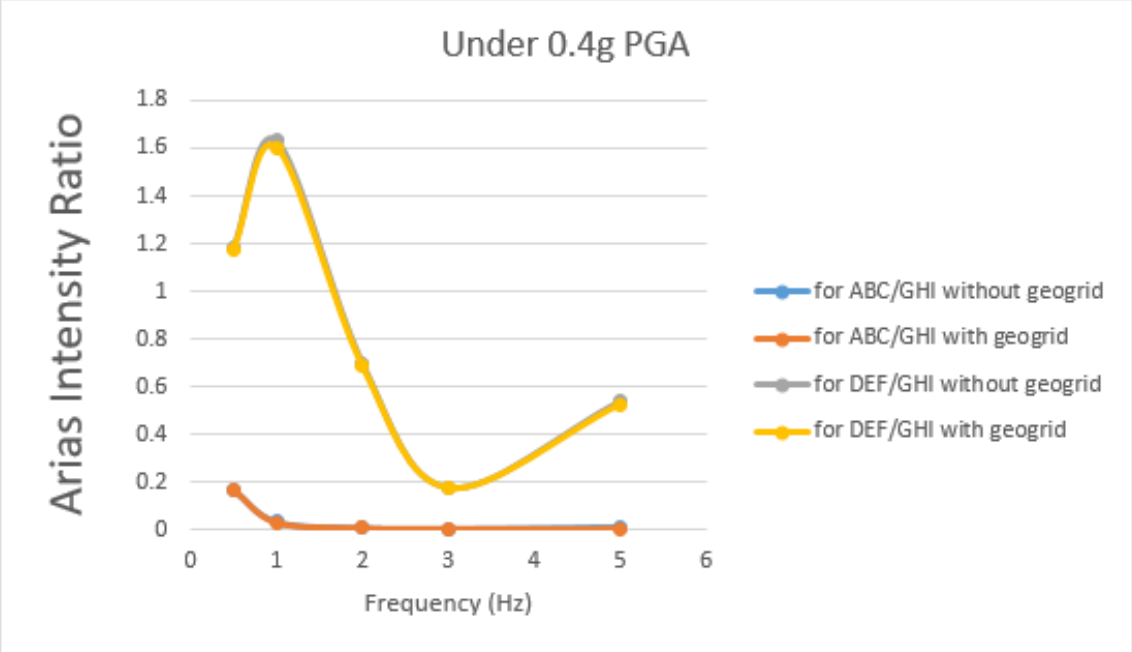

Figure 8.20. Average Arias Intensity Ratio values for reinforced and unreinforced cases of the top points/ the bottom and middle points/ the bottom under frequencies of 0.5, 1, 2, 3, 5 Hz with a ground motion of 0.3g PGA.

Under 0.4g PGA with a motion of 0.5 Hz, the Arias Intensity ratio of the middle points/ the bottom is nearly 1.2. The maximum Arias Intensity ratio value is observed to be nearly 1.6 for the middle points/ the bottom under 1 Hz frequency. For this reason, amplification is said to occur on the weak ground. On the weak ground, under frequencies of 2 and 3 Hz, a reduction in the amplitude happens and from 3 Hz to 5 Hz motion, the Arias Intensity ratio shows an increase.

For the top points/ the bottom, under 0.4g PGA with a frequency of 0.5 Hz, the ratio is around 0.2. The maximum Arias Intensity ratio is observed to be at a motion frequency of 0.5 Hz. Then, the ratio begins to fall and reaches almost zero for 2, 3, 5 Hz motions.

9. CONCLUSION

In many soil improvement projects involving soft clays, it is common practice to construct a granular layer on the surface reinforced with a geosynthetic. It is a known fact that this increases the bearing capacity and causes more even settlement. However the effect of these practices on the earthquake behavior have not been studied. So the main purpose of the presented thesis is to investigate the effect of the geogrid reinforced fill on the seismic behavior of the soft clayey soil. Since the seismic effects depend both on the frequency and amplitude of the earthquake waves, sinusoidal loads with varying frequencies and amplitudes have been applied on the model.

The soil model was defined to have a depth of 35 m and a width of 100 m. There was a 30 m soft clayey soil underlying 5 m thick gravel. The unreinforced and geogrid reinforced models were numerically modelled by means of the finite element software PLAXIS 2D (2012). To analyze the results 9 points were chosen on the mesh. 3 points were chosen to be above the geogrid reinforcement (at middle of the gravel layer), 3 points were chosen below the geogrid reinforcement (at top of the clayey soil) and three points were chosen right above the base as a reference.

Sinusoidal seismic waves with frequencies of 0.5, 1, 2, 3, 5 Hz and amplitudes of 0.1g, 0.2g, 0.3g and 0.4 g have been applied to the model and the seismic performance of unreinforced and reinforced cases of the same model was examined in detail. Comparison of unreinforced and reinforced cases for average acceleration and average energy values was made using Arias Intensity.

It was hypostasized that the geogrid would help in changing the natural frequency of the soil and absorb more energy at least for some frequencies for the points located in the middle of the gravel and above the geogrid reinforcement.

The results indicate that the assumption is true for 28 of the 40 cases studied, corresponding to a percentage of 70% of all analyses that have been performed. Hence,

one can easily infer from the findings that geogrid absorbs seismic energy. However, the observed change in the Arias Intensity between reinforced and unreinforced cases is minimal, almost negligible, for all cases but Arias Intensity values are nearly zero for the gravel layer, suggesting that gravel overlying soft clayey soil is likely to have more influence than geogrid reinforcement on the seismic behavior of the soil.

Under similar ground motions, for the points at the top, according to the Arias Intensity ratios, for geogrid reinforcement case over unreinforced case, geogrid exhibits effective absorption behavior below 5 Hz frequency. For under 0.4g PGA and 5 Hz motion, the ratio turns out to be 37%.

However, there are also exceptions. For the points at the top, for the motion of 3 Hz frequency, geogrid showed a negative effect in terms of energy absorption.

From the bottom to the top, similar PGA increasing and decreasing behavior in the acceleration and Arias Intensity values are generally in line with each other for reinforced and unreinforced cases. Under 0.1g, 0.2g, 0.3g, 0.4g ground motions with different frequencies of 0.5, 1, 2, 3, 5 Hz, the average acceleration at the base is not exactly the same as the given ground motion. Under 0.1g motion, acceleration first amplifies in the clay and de-amplifies in the gravel under 1 and 5 Hz motions for both unreinforced and geogrid reinforced cases. On the other hand, under 0.2g, 0.3g, 0.4g PGA, soil amplification occurs only at frequency motion of 1 Hz for both unreinforced and geogrid reinforced cases.

By looking at the average Arias Intensity values, it can be said that the Arias Intensity values have been reduced by the presence of the gravel layer more effectively than by the geogrid for the investigated geometry, material properties and conditions. For future studies, this fact should be taken into consideration. Also the possibility of using multi layers of geogrid should be investigated.

REFERENCES

Arvind K.V., Kumar S.A.R., Rao T.V.S.R, "Dynamic Behavior of Geogrid-Reinforced Soil", *4th International Conferences On Recent Advances In Geotechnical Earthquake Engineering and Soil Dynamics*, 2001.

Arvind K.V., Kumar S.A.R., Rao T.V.S.R, "Geogrid Reinforced Subgrades Simulated Earthquake Loading", *(12WCEE), World Conference on Earthquake Engineering*, 2000.

Clement, S., "Experimental Studies on Dynamic Response of a Block Foundation on Sand Reinforced with Geogrid", *Geosynthetics*, pp. 479-488, 2015.

Edinçliler, E., Y.S. Toksoy, Ö. Yıldız, "The Effect of Earthquake Characteristics on The Seismic Performance of Mid-Rise Structures on Geogrid Reinforced Soils", 4th International Earthquake Engineering and Seismology Conference, Anatolia University, Eskişehir, 2017.

Gohil D.P., C.H. Solanki, A.K. Desai, "Behaviour of Geogrid Reinforced Soil under Earthquake Loading", *In: Construction Engineering*, Vol. 1, No. 1, 2013.

Güler, E. A.K. Enünlü, "Investigation of Dynamic Behavior of Geosynthetic Reinforced Soil Retaining Structures Under Earthquake Loads", *Bulletin of Earthquake Engineering*, Vol. 7, No. 3, pp. 737-777, 2009.

Güler,E. E. Cicek, "Bearing Capacity of Strip Footing On Reinforced Layered Granular Soils", *Journal of Civil Engineering and Management*, Vol. 21, No. 5, pp. 605?614, 2018.

Jyoti A., Jakka, R.S. "Investigation On A Geosynthetic Reinforced Bearing Layer Under Static And Dynamic Loading", *Indian Geotechnical Conference IGC2016*, Vol. 15-17, 2006.

Liu, H., C. Hung, J. Cao, "Relationship between Arias Intensity and the responses of reinforced soil retaining walls subjected to near-field ground motions", *In: Soil Dynamics and Earthquake Engineering*, Vol.111, pp. 160-168, 2018.

Santhakumar, A.R., K.A. Verma, and Rao, T. V. S. R., "Dynamic Behavior of Geogrid-Reinforced Soil", *International Conferences on Recent Advances in Geotechnical Earthquake Engineering and Soil Dynamics*, Vol. 47, 2001.

Sekman M., *Experimental Study On Mitigation Of Earthquake Hazards Using Geosynthetics*, Boğaziçi University 2016.

Sreedhar, M.V.S., and J. Abhishek, "Effect of Geosynthetic Reinforcement on Dynamic Characteristics Through Model Block Resonance Tests", *Proceedings of Indian Geotechnical Conference*, pp. 1-4, 2016.

Stafford P.J., J.B. Berrill, J.R. Pettinga,"New Predictive Equations For Arias Intensity From Crustal Earthquakes In New Zea", *Journal of Seismology*, Vol. 13, No. 1, pp. 31?52, 2008.

Toksoy, Y.S. *Investigation of the Seismic Performance of Reinforced Highway Embankments*, M.S. Thesis, Boğaziçi University, 2014.

Venkateswarlu, H., A. Hegde, "Numerical Analysis of Machine Foundation Resting on the Geocell Reinforced Soil Beds", *Geotechnical Engineering Journal of the Seags and Agssea*, Vol. 49, No. 4, pp. 0046-5828, 2018.

Yegian, M. K., U. Kadakal, "Foundation Isolation for Seismic Protection using a Smooth Synthetic Liner", *American Society of Civil Engineers Journal of Geotechnical and Geoenvironmental Engineering*, Vol. 130, No. 11, pp. 1121-1130, 2004.

Yegian, M.K. and A. Lahlaf, "Geomembranes As Base-Isolation", *Geosynthetic Fabric Report*, 1992.

Yegian, M.K., G. Gazetas, and P. Geargarakos, "In-ground Isolation Using Geosyn-

thetic Liners, 9th World Seminar on Seismic Isolation", *Energy Dissipation and Active Vibration Control of Structures*, pp. 13-16, 2005.

Yegian, M.K., U. Kadakal, and M. Catan, "Geosynthetic for Earthquake Hazard Mitigation", *In: Geosynthetics ?99 Boston, Specifying Geosynthetics and Developing Design Details*, Vol. 1, pp. 87-100, 1999.

APPENDIX A: NUMERICAL ANALYSIS RESULTS OF ACCELERATION VERSUS DYNAMIC TIME FIGURES FOR THE SELECTED 9 POINTS

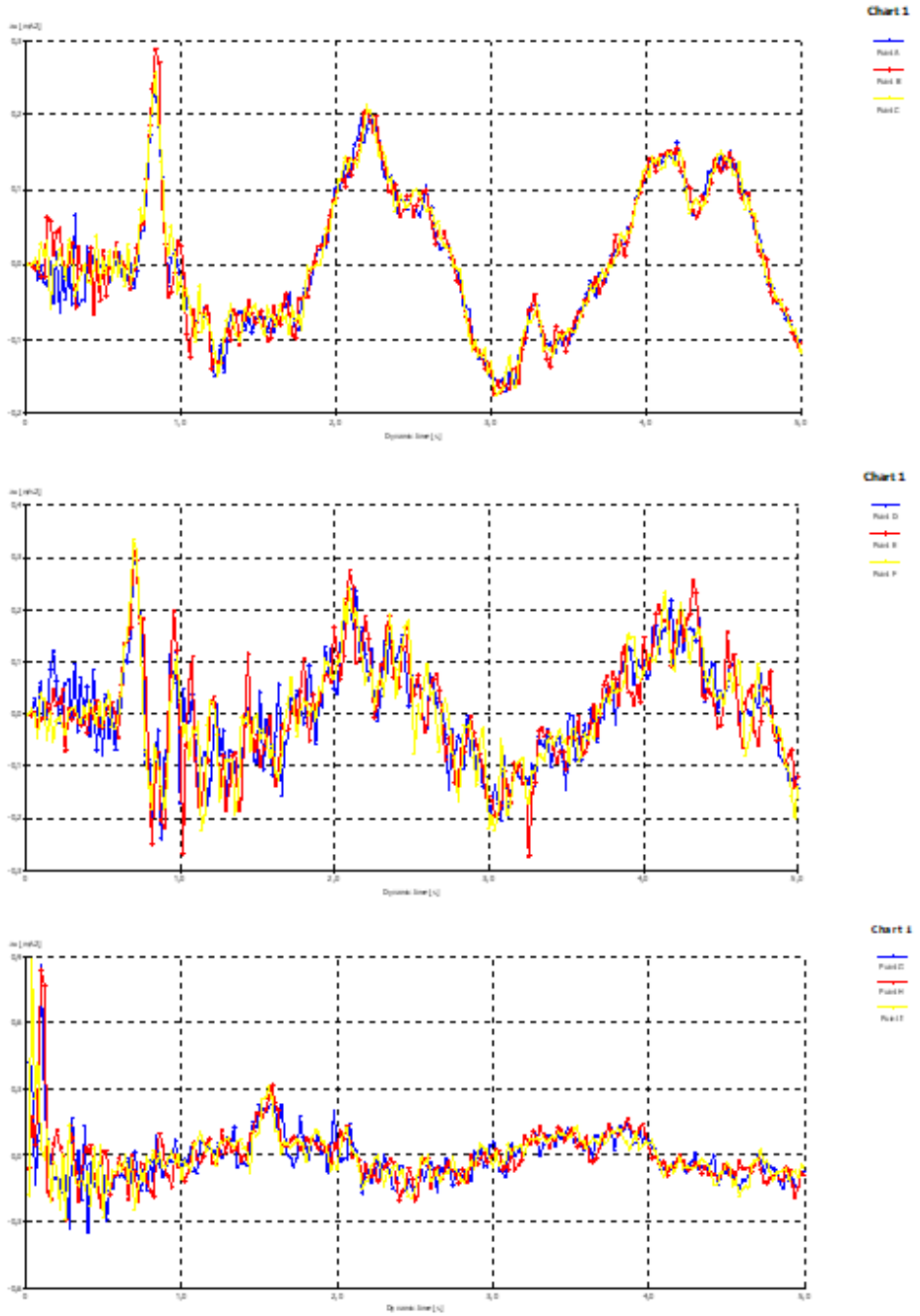

Figure A.1. Numerical Analysis Results for unreinforced case under 0.1g acceleration with 0.5 hz frequency.

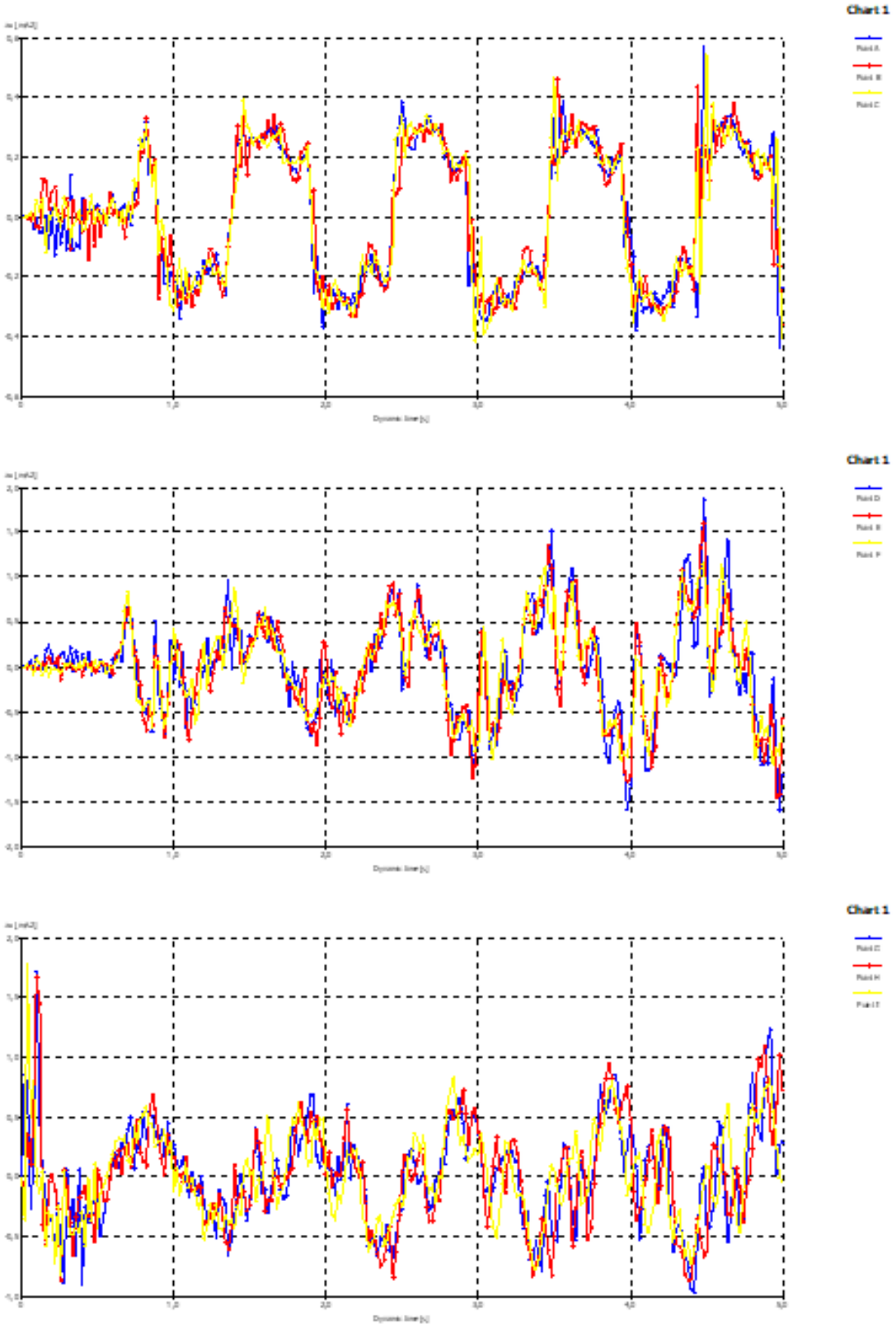

Figure A.2. Numerical Analysis results for unreinforced case under 0.1g acceleration with 1 hz frequency.

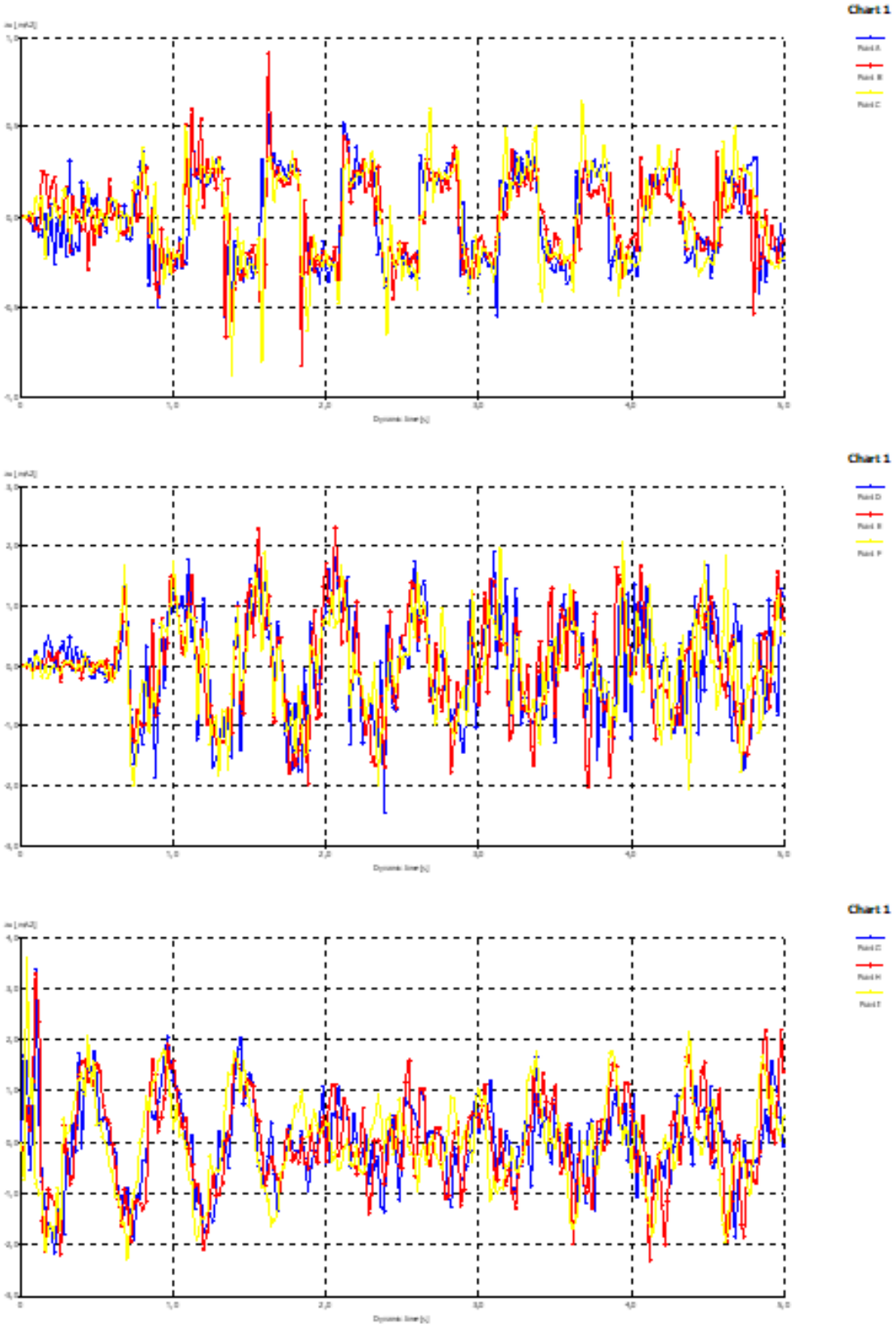

Figure A.3. Numerical Analysis results for unreinforced case under 0.1g acceleration with 2 hz frequency.

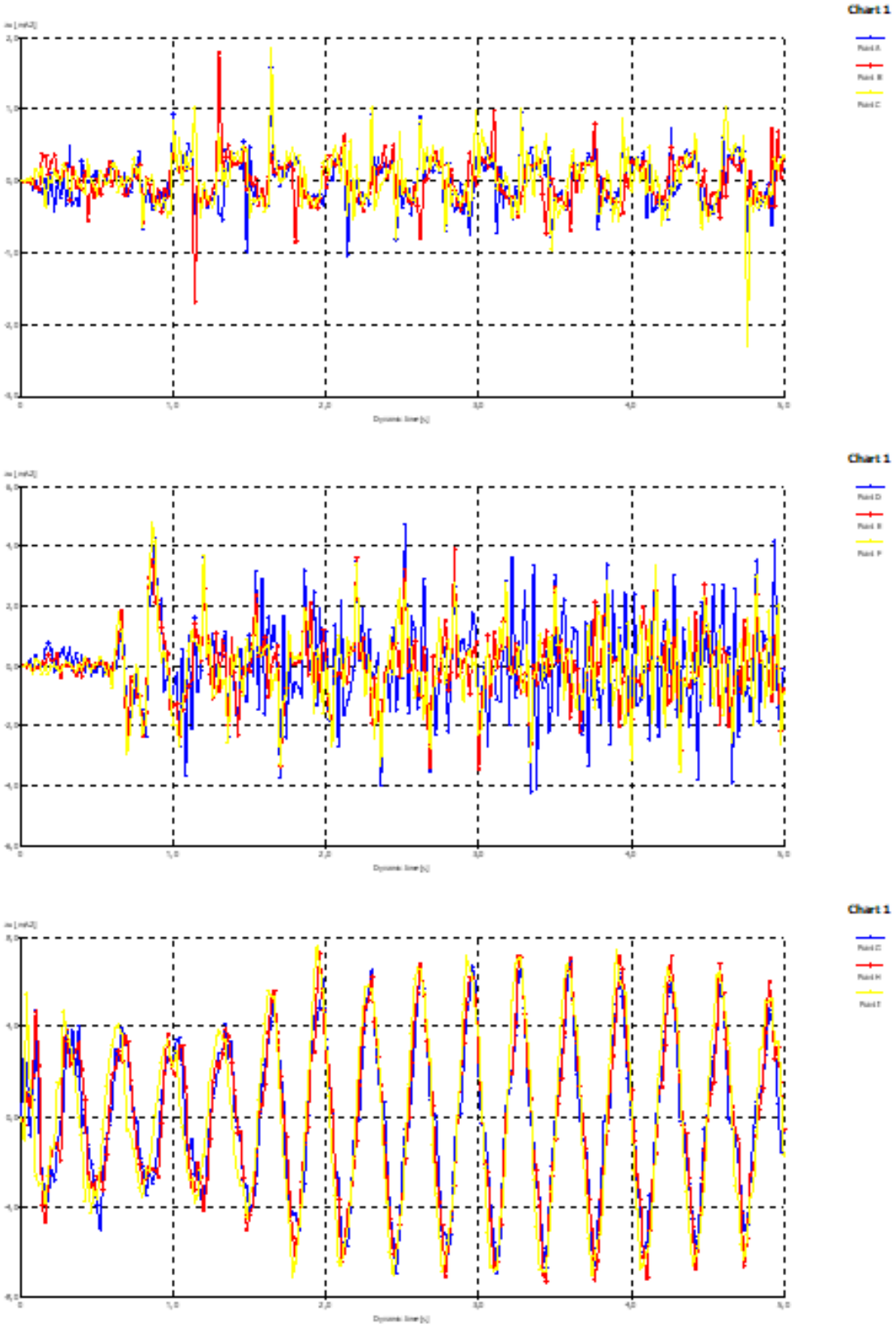

Figure A.4. Numerical Analysis results for unreinforced case under 0.1g acceleration with 3 hz frequency.

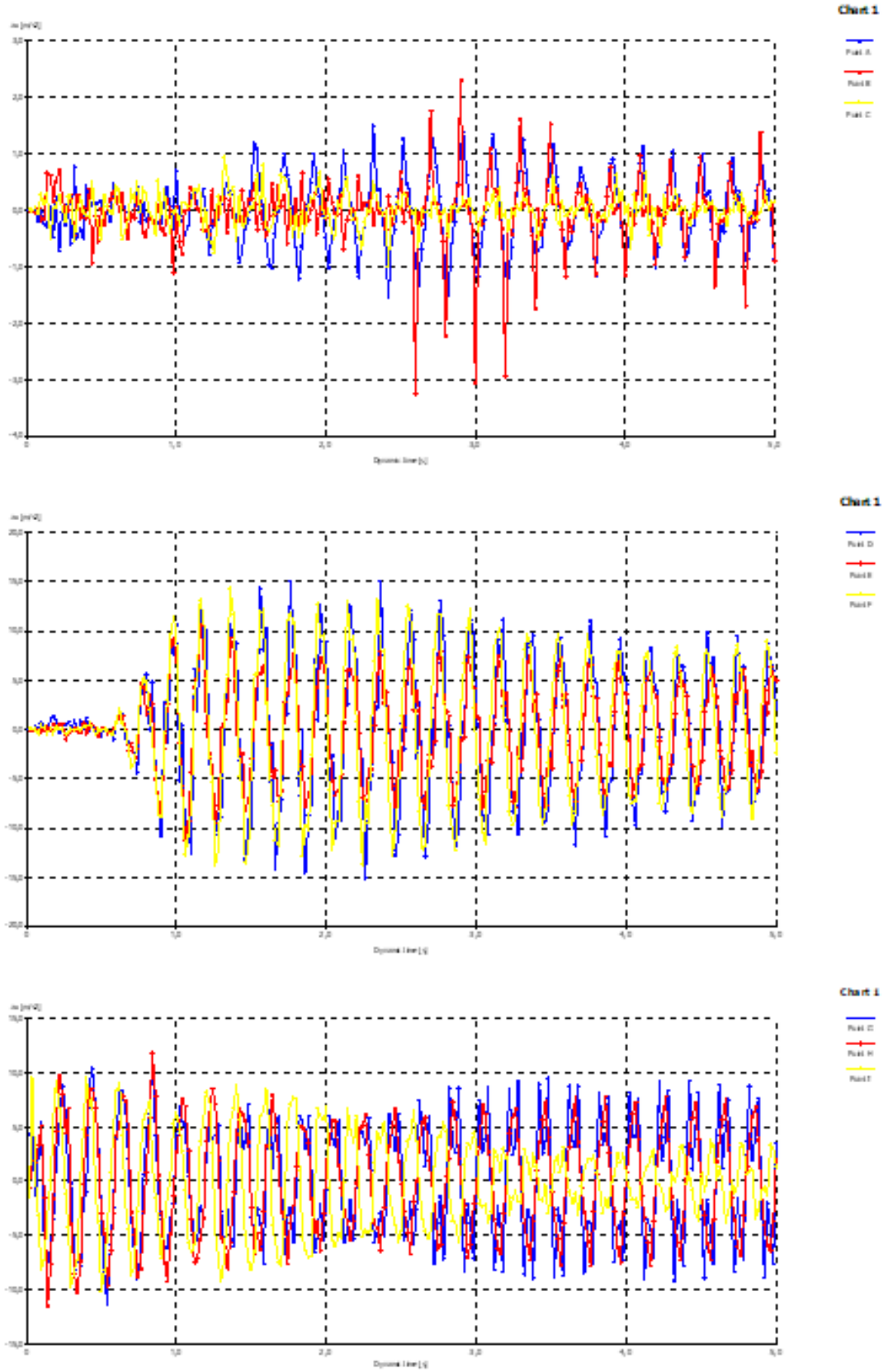

Figure A.5. Numerical Analysis results for unreinforced case under 0.1g acceleration with 5 hz frequency.

Figure A.6. Numerical Analysis results for unreinforced case under 0.2g acceleration with 0.5 hz frequency.

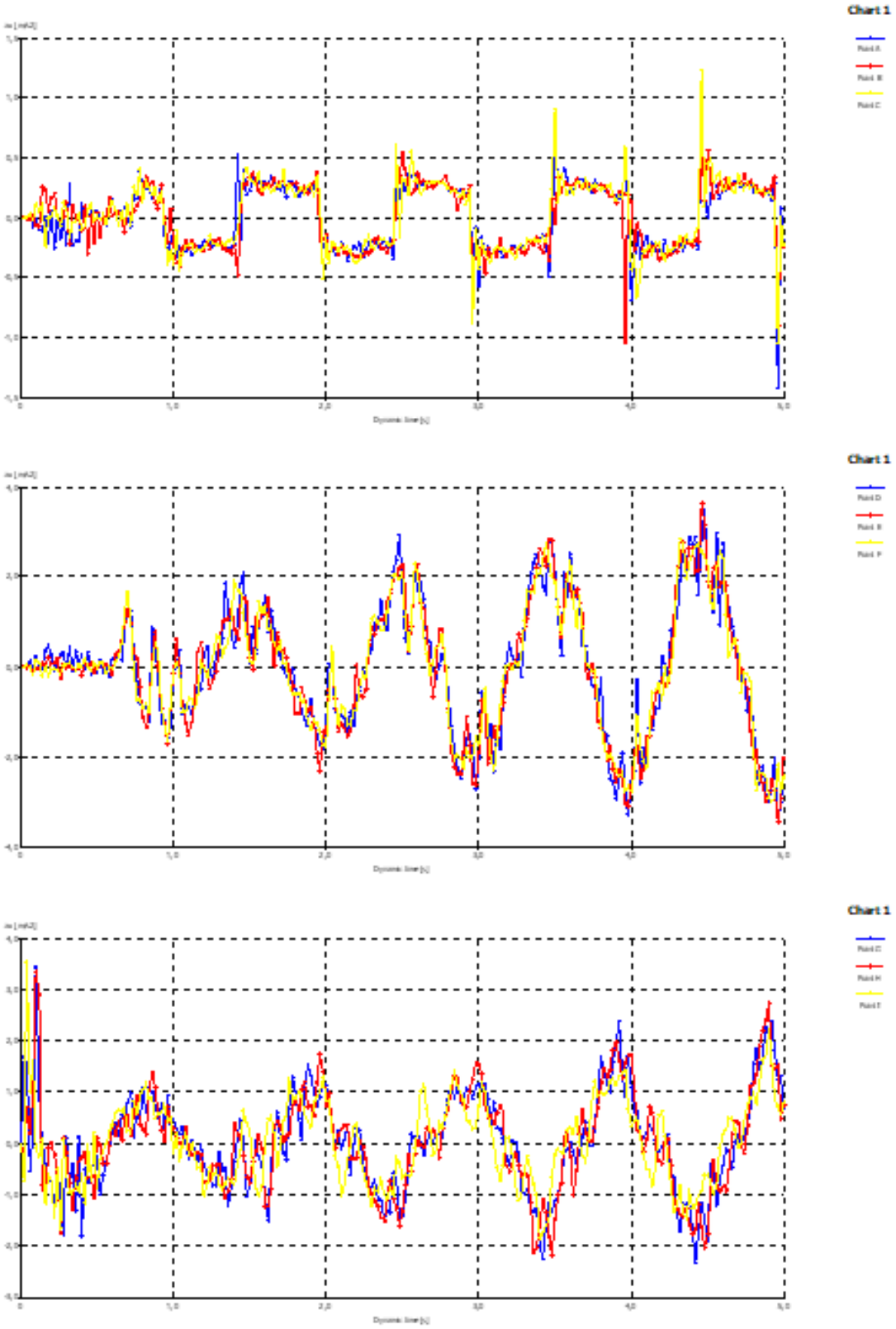

Figure A.7. Numerical Analysis results for unreinforced case under 0.2g acceleration with 1 hz frequency.

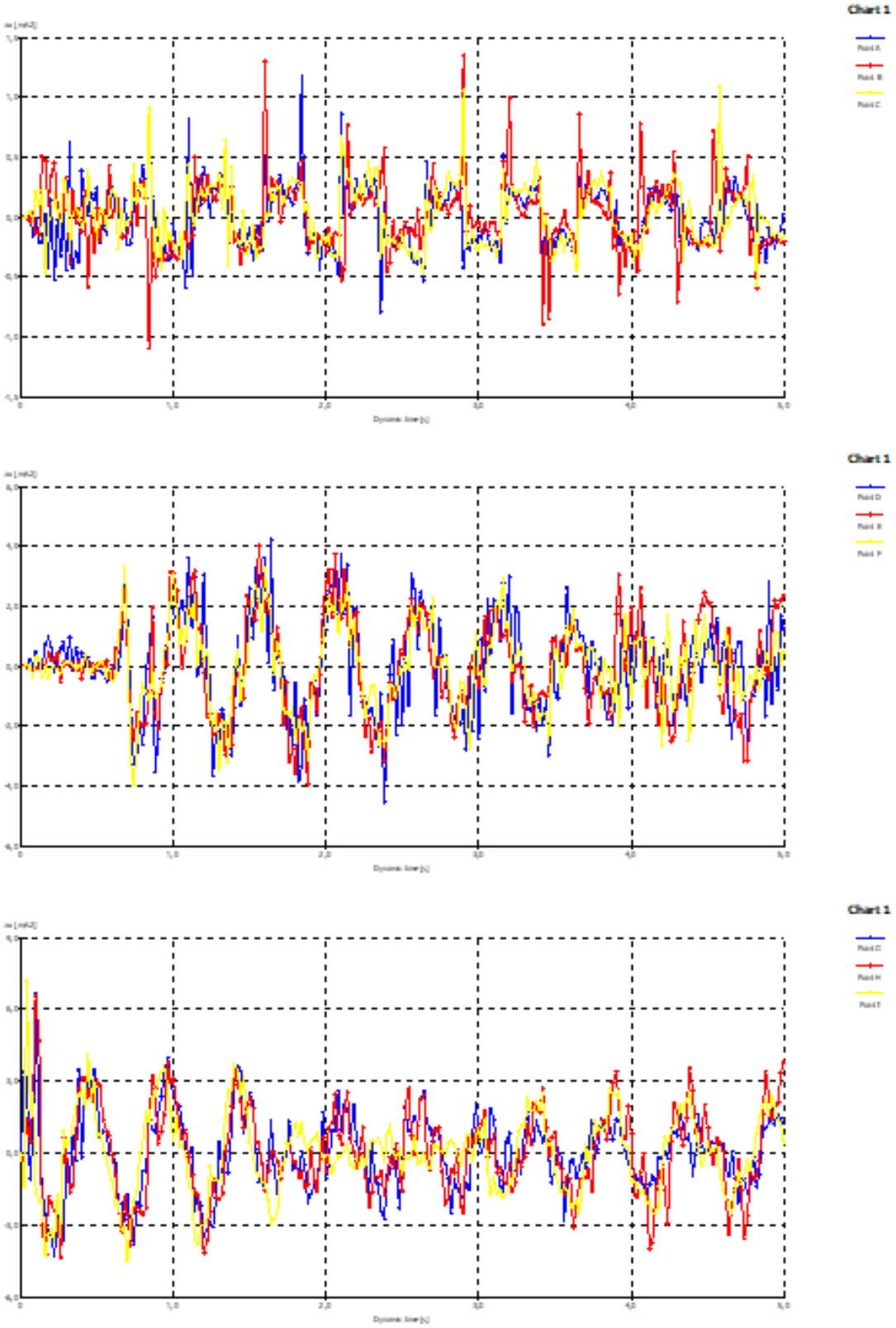

Figure A.8. Numerical Analysis results for unreinforced case under 0.2g acceleration with 2 hz frequency.

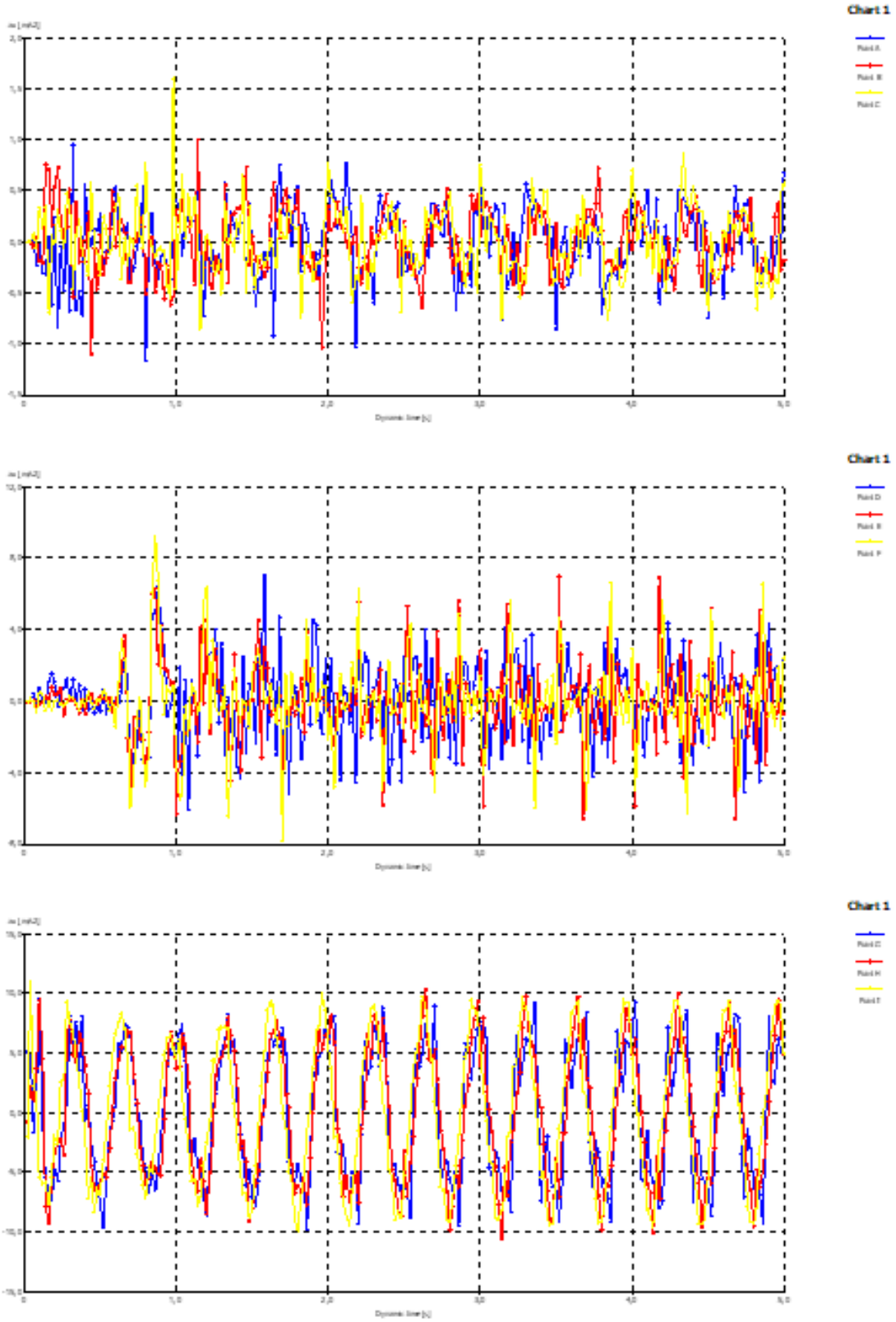

Figure A.9. Numerical Analysis results for unreinforced case under 0.2g acceleration with 3 hz frequency.

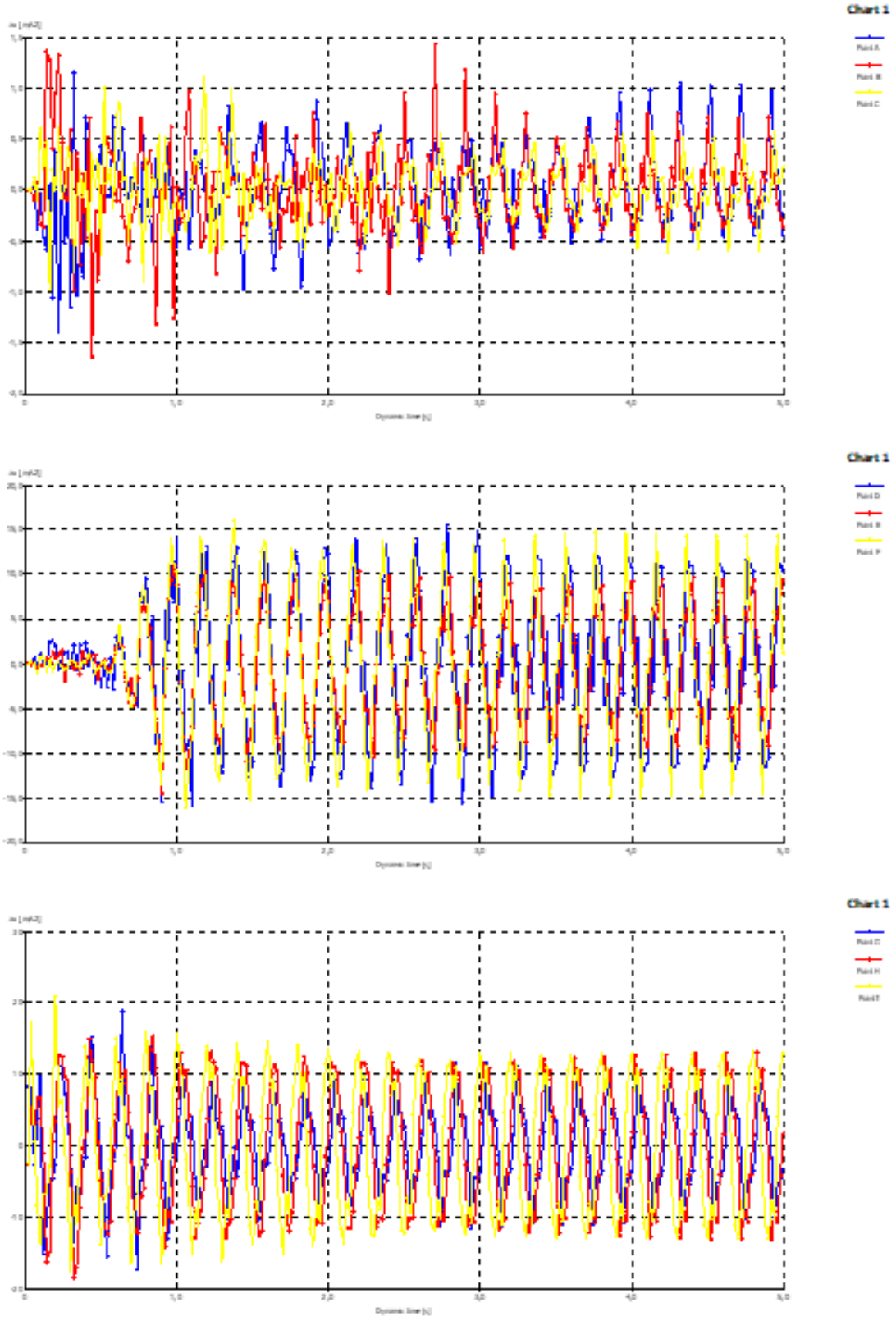

Figure A.10. Numerical Analysis results for unreinforced case under 0.2g acceleration with 5 hz frequency.

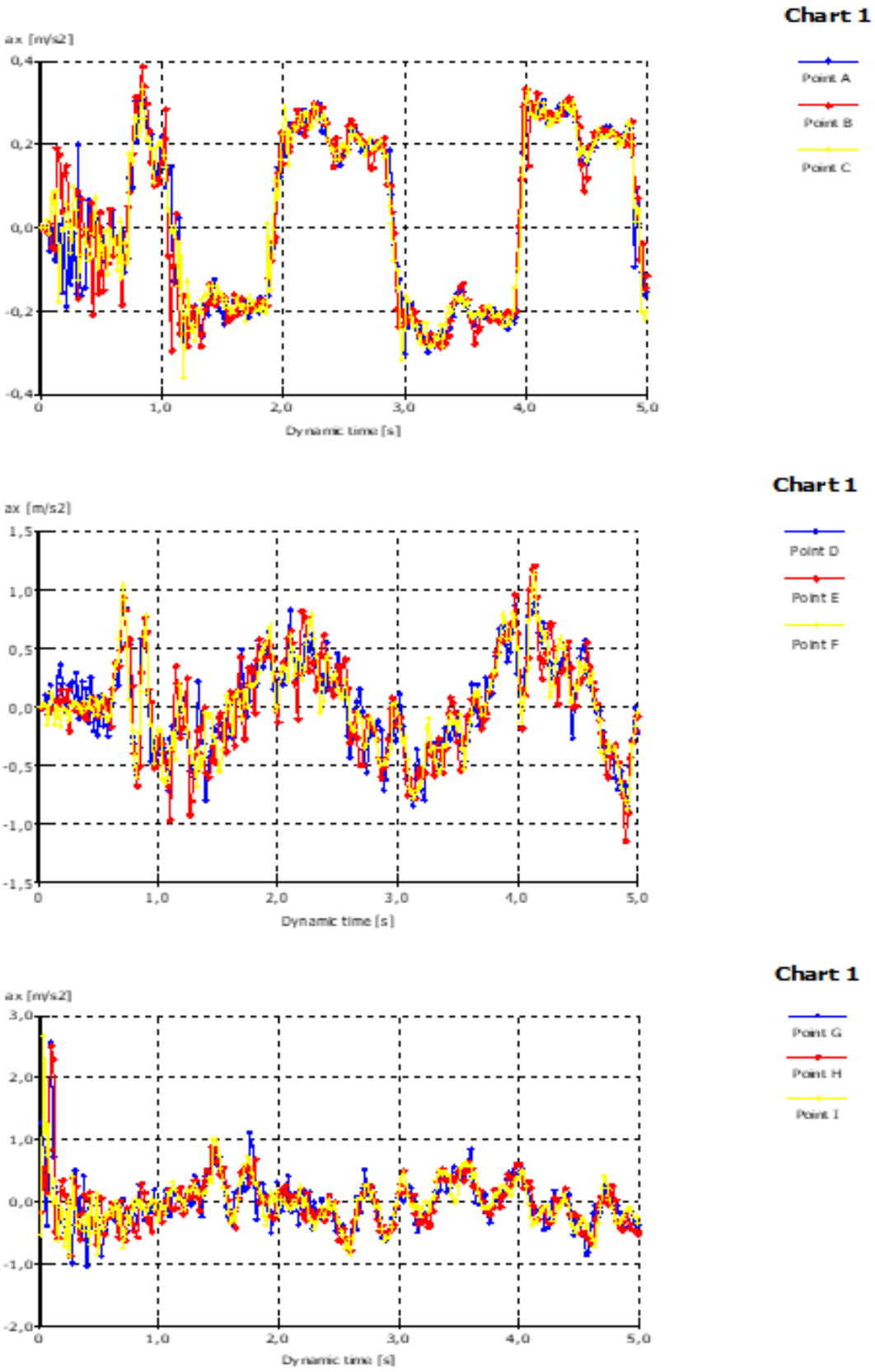

Figure A.11. Numerical Analysis results for unreinforced case under 0.3g acceleration with 0.5 hz frequency.

Figure A.12. Numerical Analysis results for unreinforced case under 0.3g acceleration with 1 hz frequency.

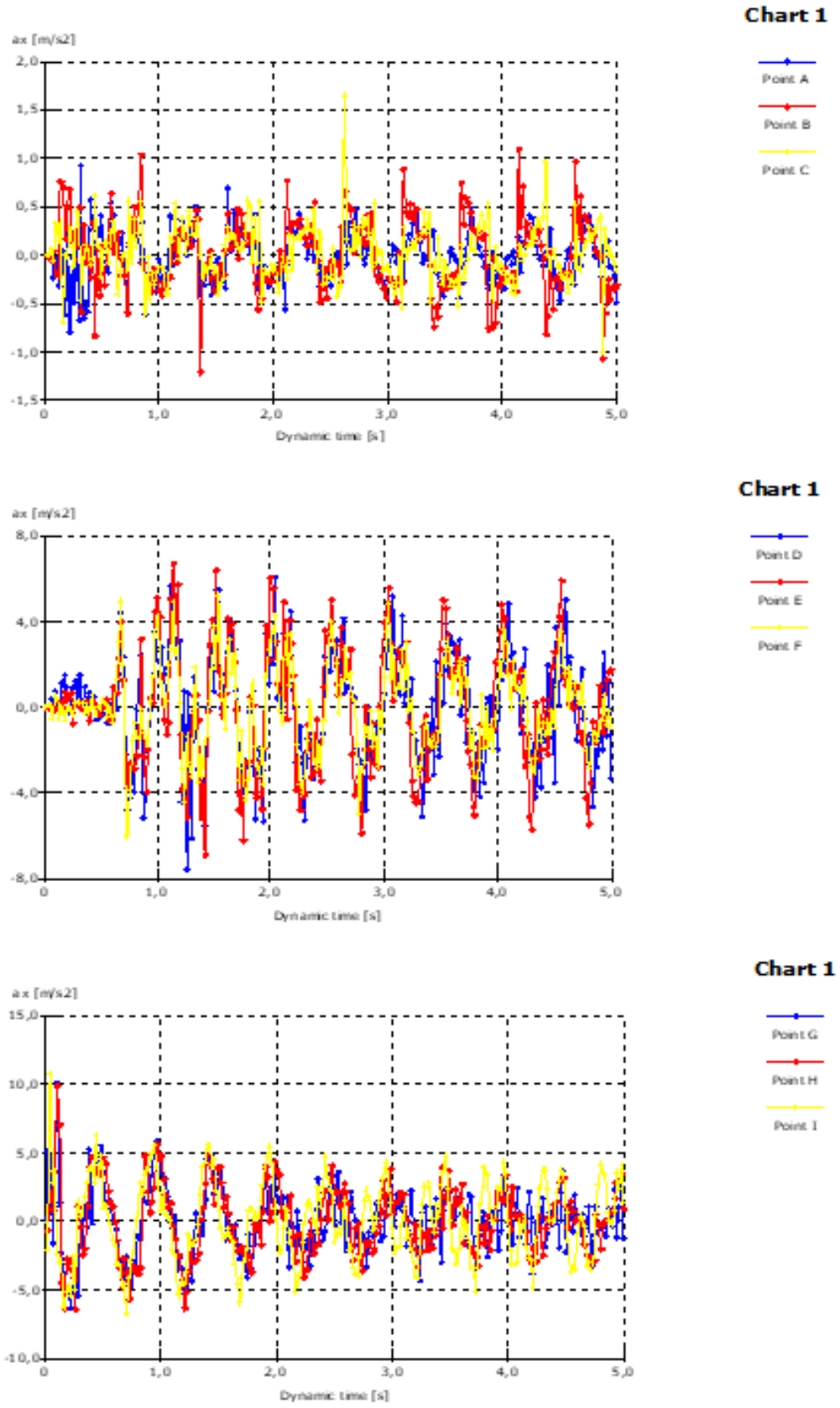

Figure A.13. Numerical Analysis results for unreinforced case under 0.3g acceleration with 2 hz frequency.

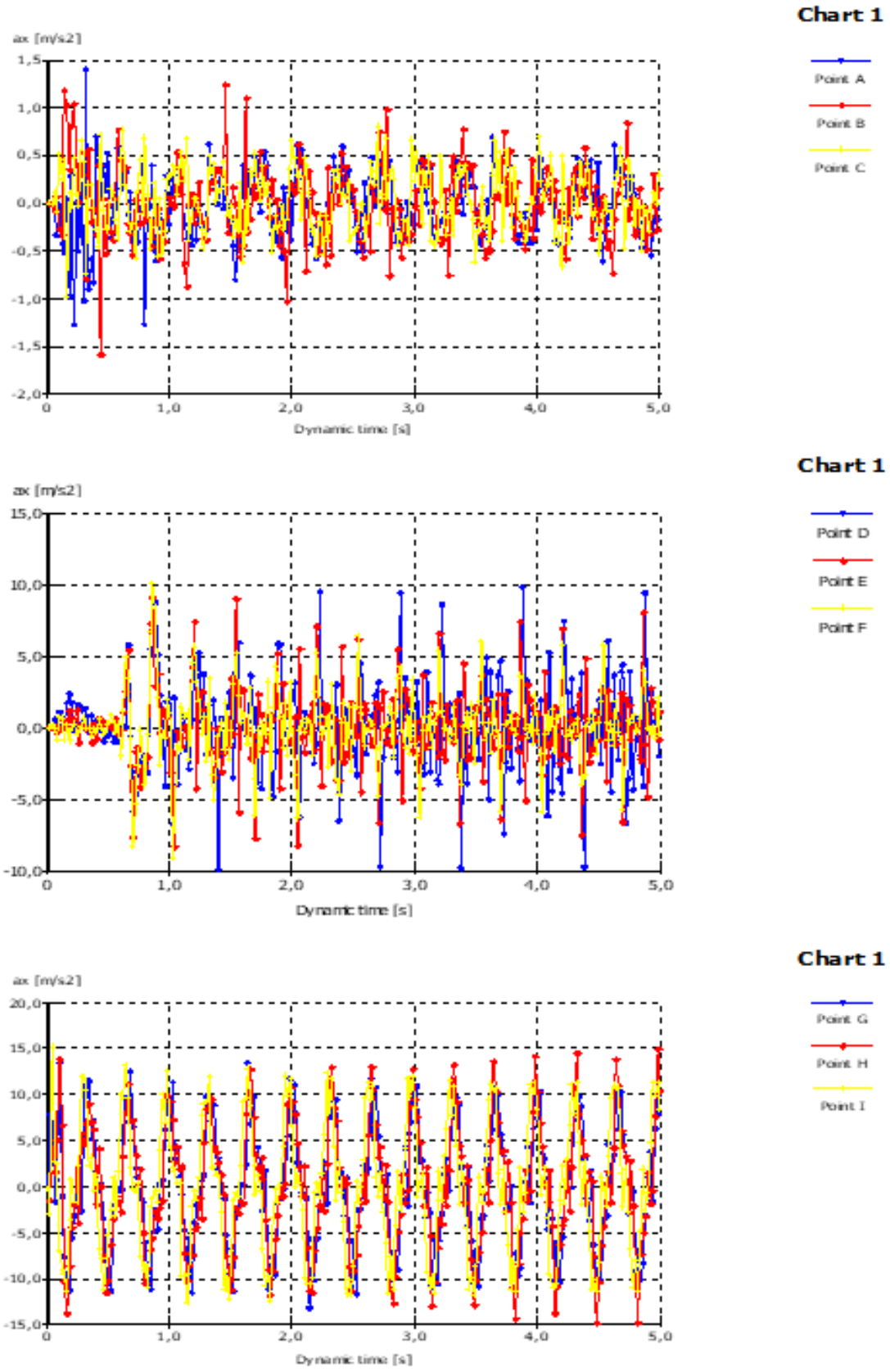

Figure A.14. Numerical Analysis results for unreinforced case under 0.3g acceleration with 3 hz frequency.

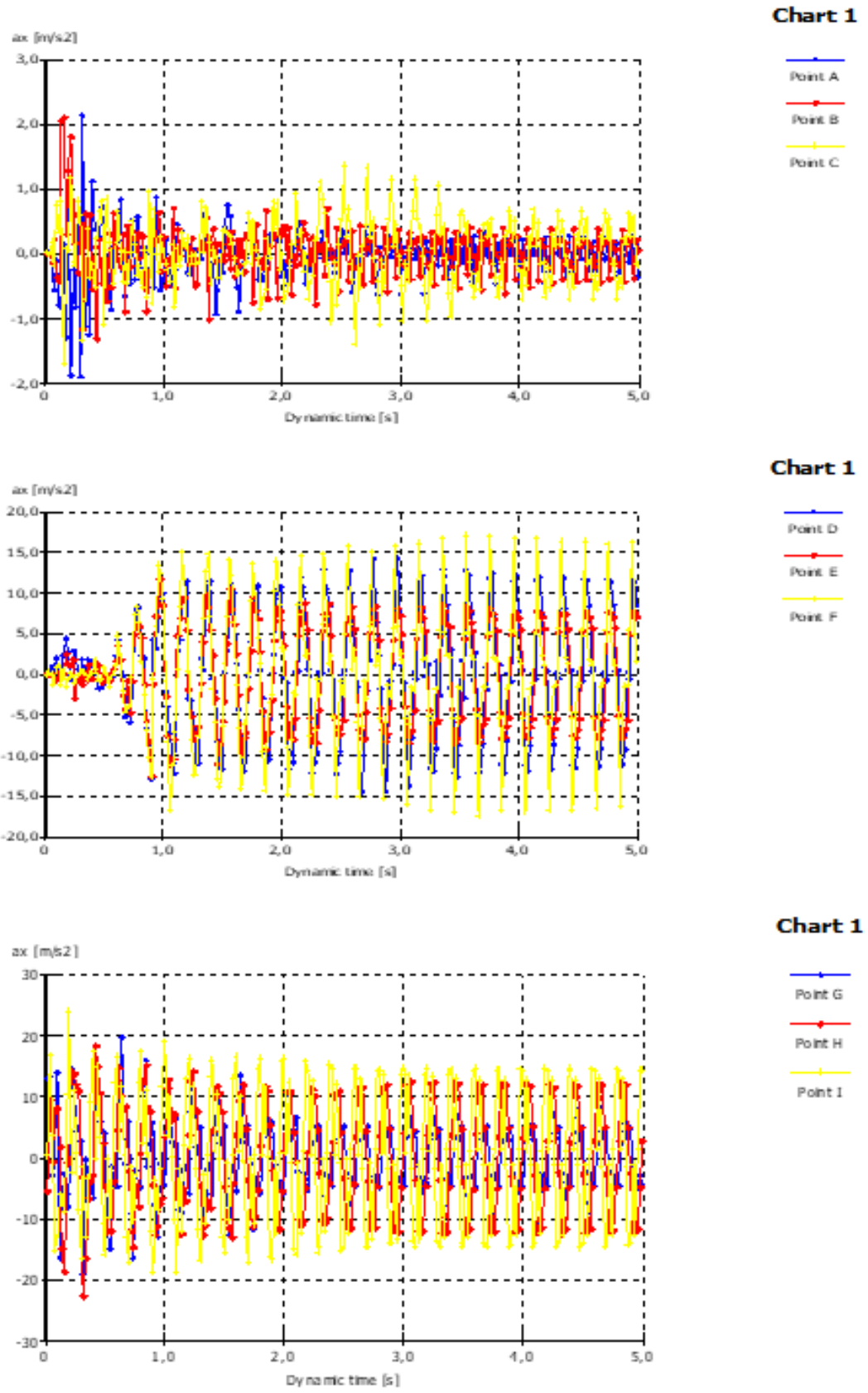

Figure A.15. Numerical Analysis results for unreinforced case under 0.3g acceleration with 5 hz frequency.

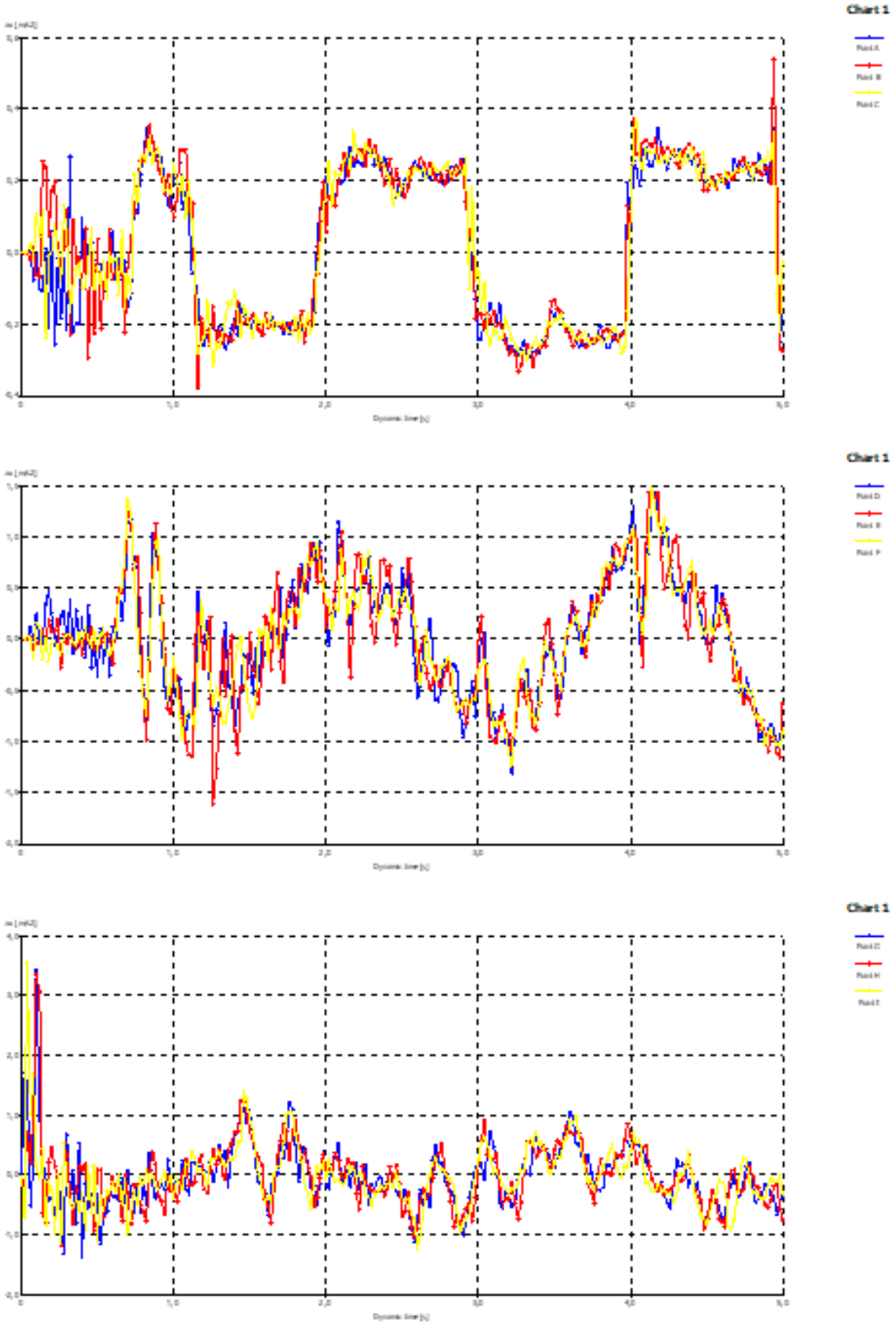

Figure A.16. Numerical Analysis results for unreinforced case under 0.4g acceleration with 0.5 hz frequency.

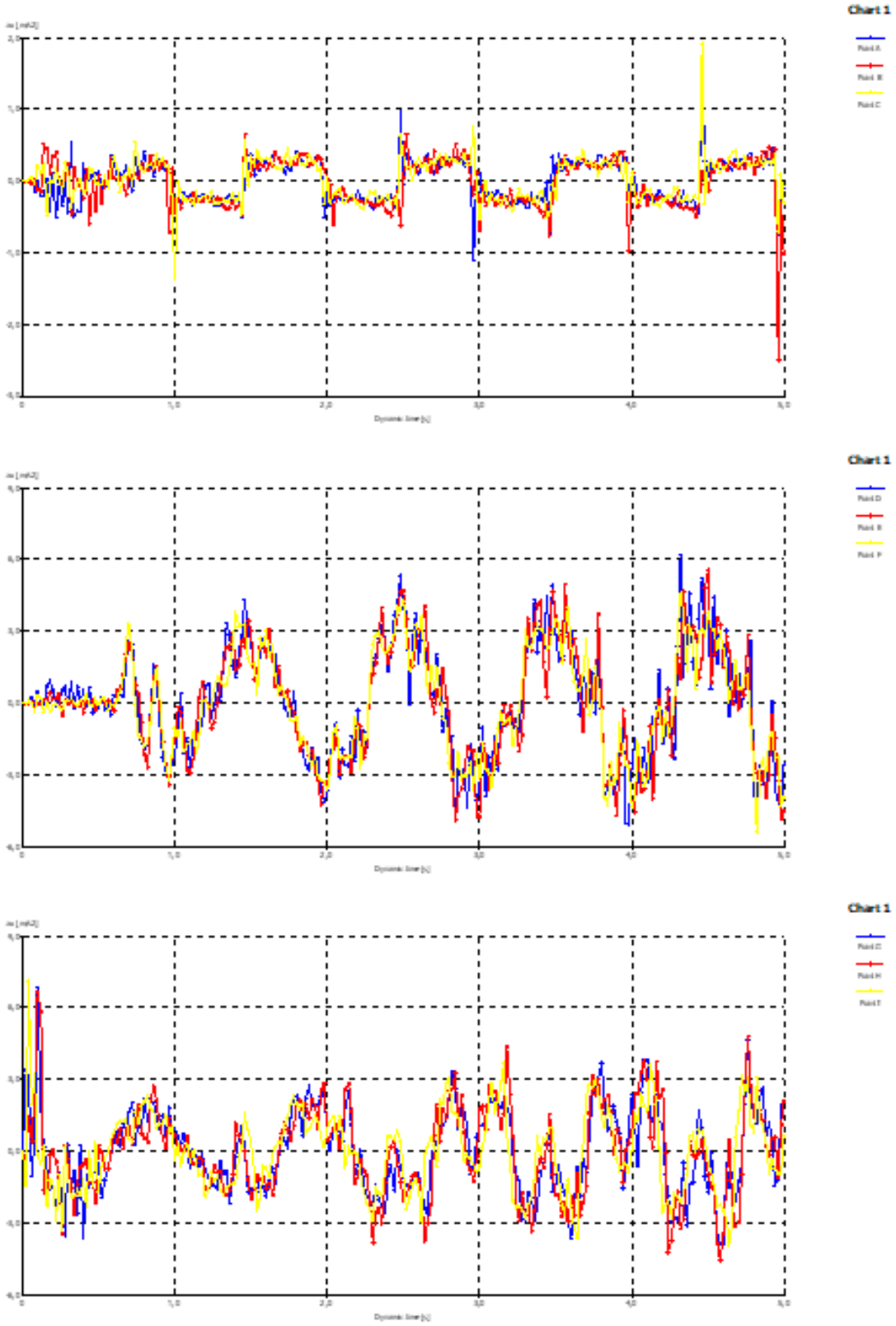

Figure A.17. Numerical Analysis results for unreinforced case under 0.4g acceleration with 1 hz frequency.

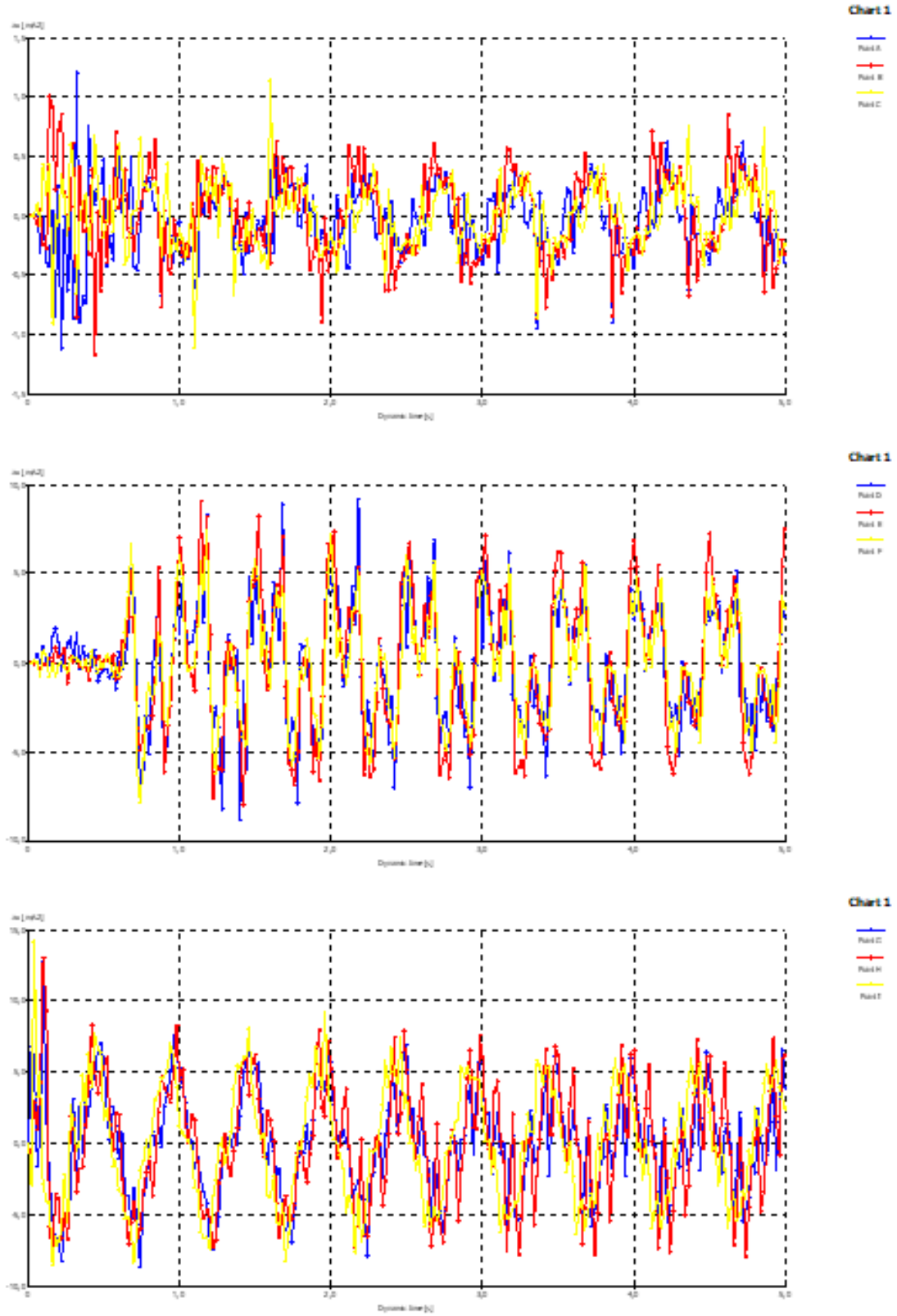

Figure A.18. Numerical Analysis results for unreinforced case under 0.4g acceleration with 2 hz frequency.

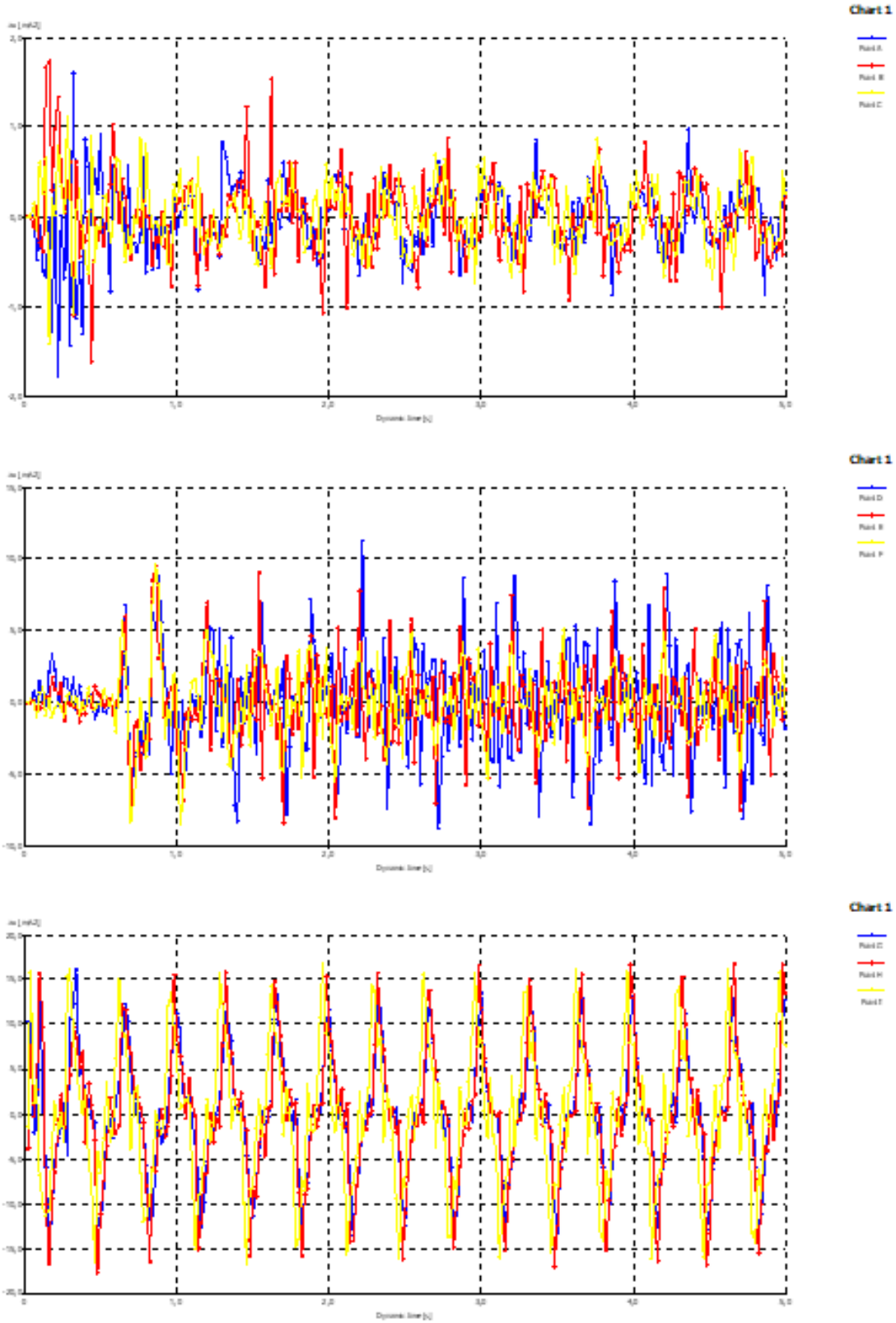

Figure A.19. Numerical Analysis results for unreinforced case under 0.4g acceleration with 3 hz frequency.

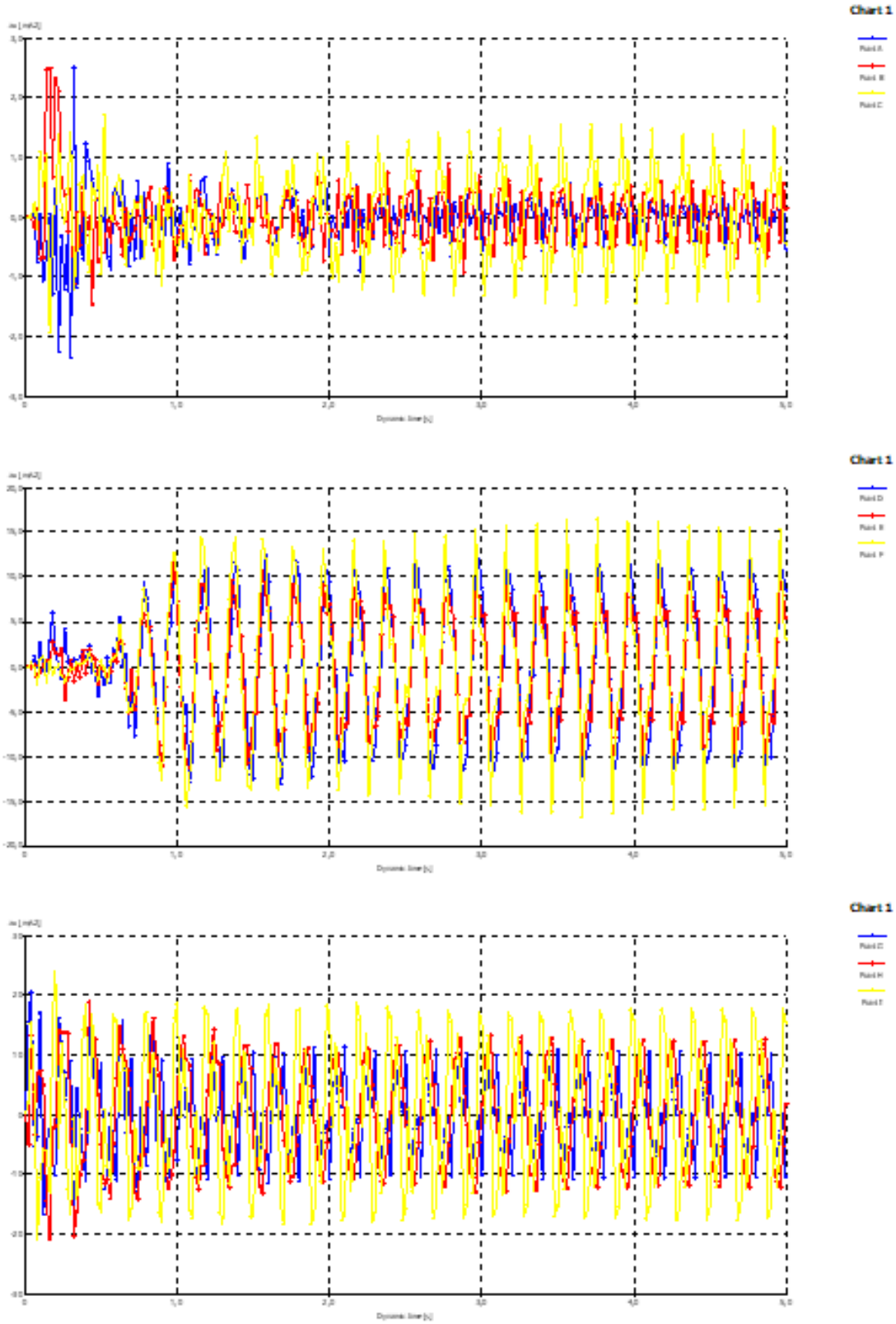

Figure A.20. Numerical Analysis results for unreinforced case under 0.4g acceleration with 5 hz frequency.

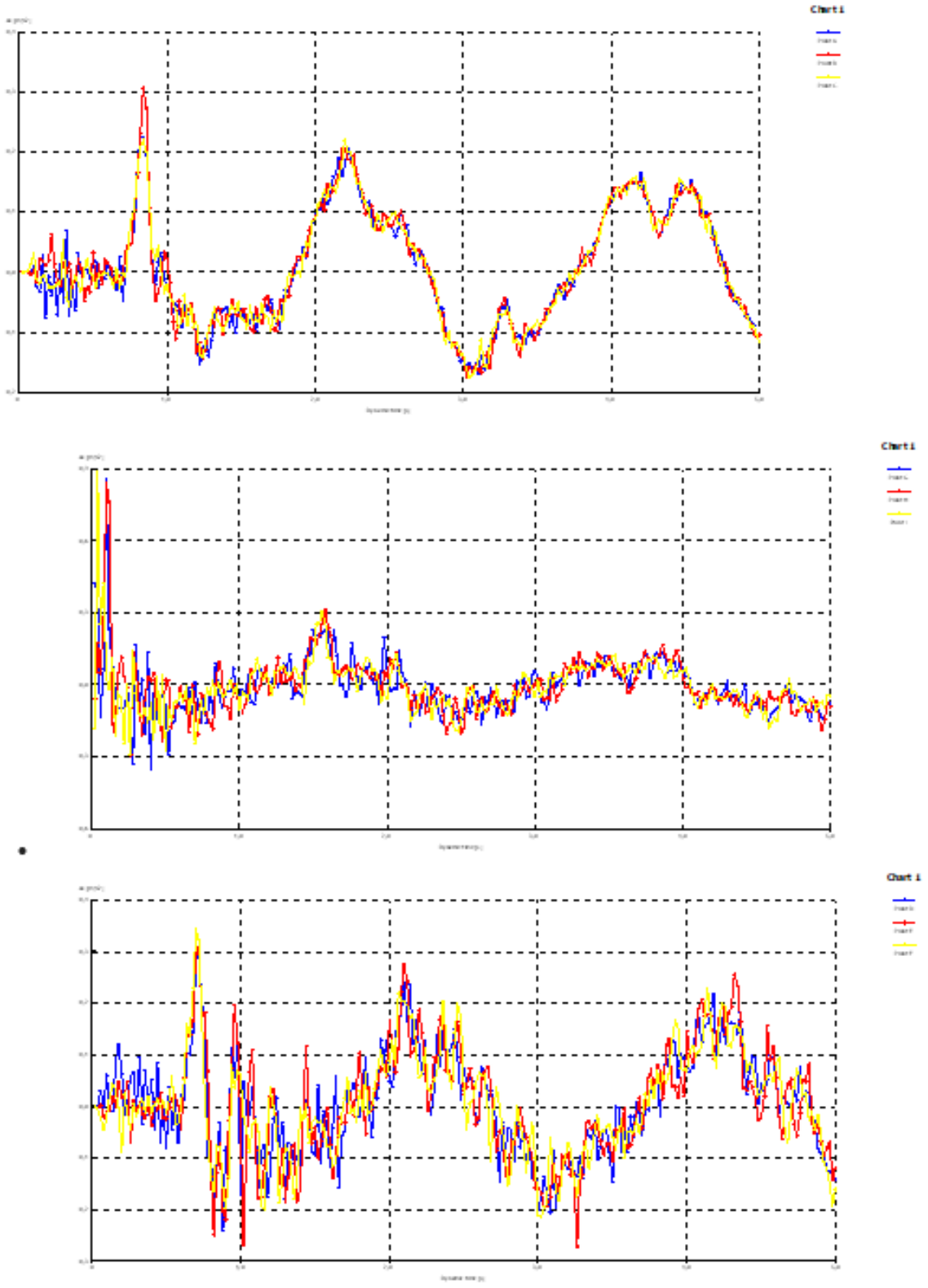

Figure A.21. Numerical Analysis results for the geogrid case under 0.1g acceleration with 0.5 hz frequency.

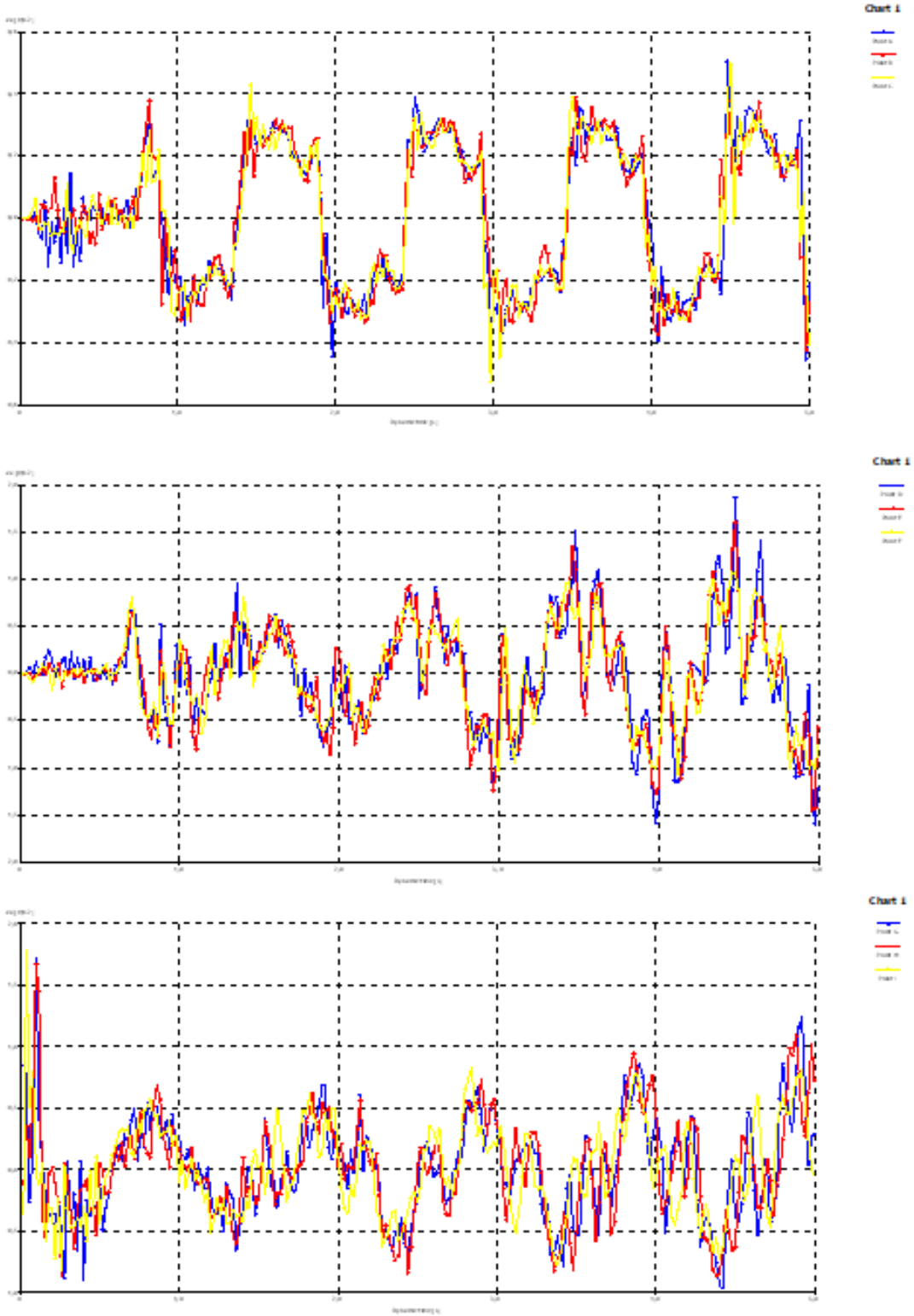

Figure A.22. Numerical Analysis results for the geogrid case under 0.1g acceleration with 1 hz frequency.

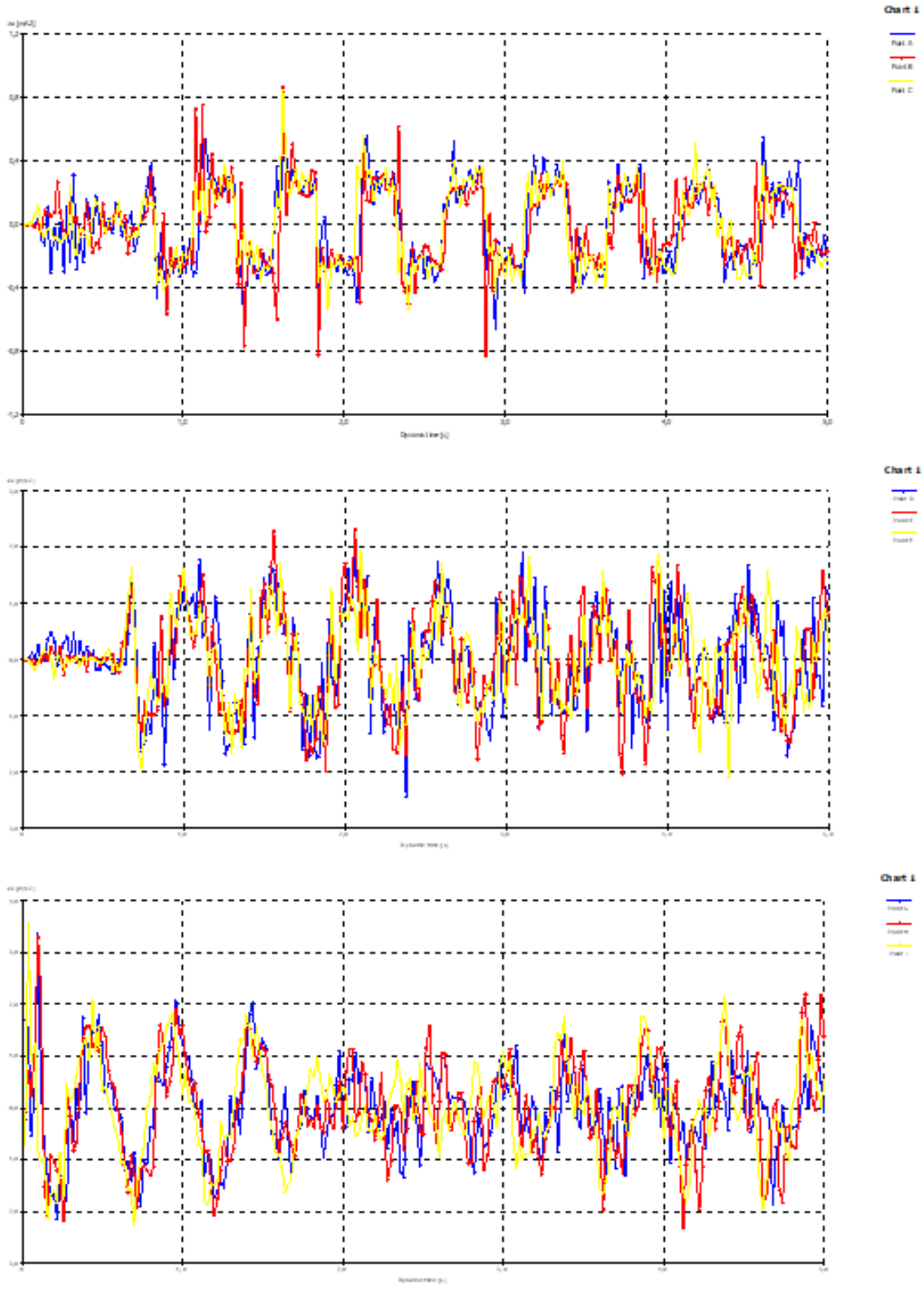

Figure A.23. Numerical Analysis results for the geogrid case under 0,1g acceleration with 2 hz frequency.

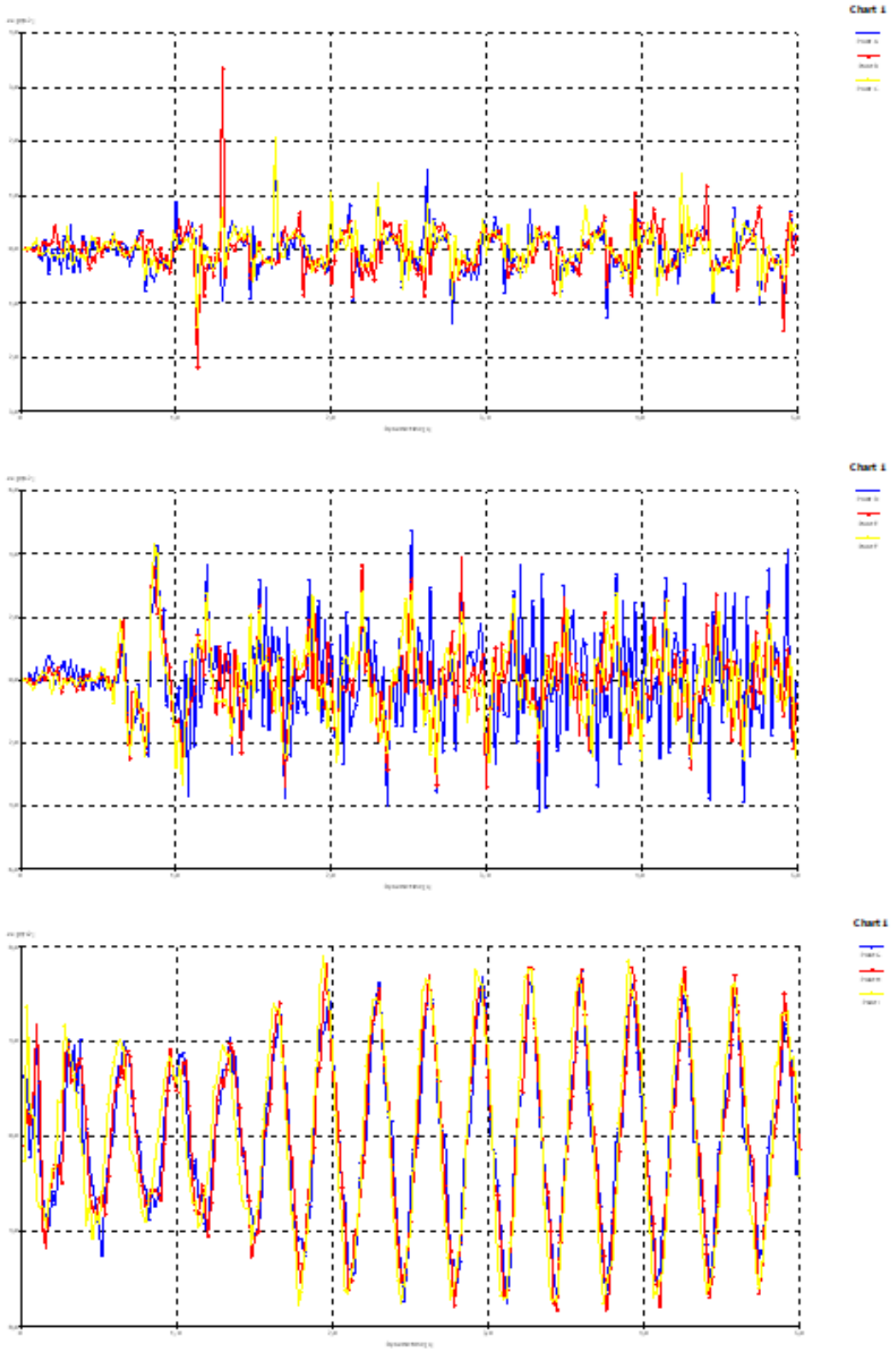

Figure A.24. Numerical Analysis results for the geogrid case under 0.1g acceleration with 3 hz frequency.

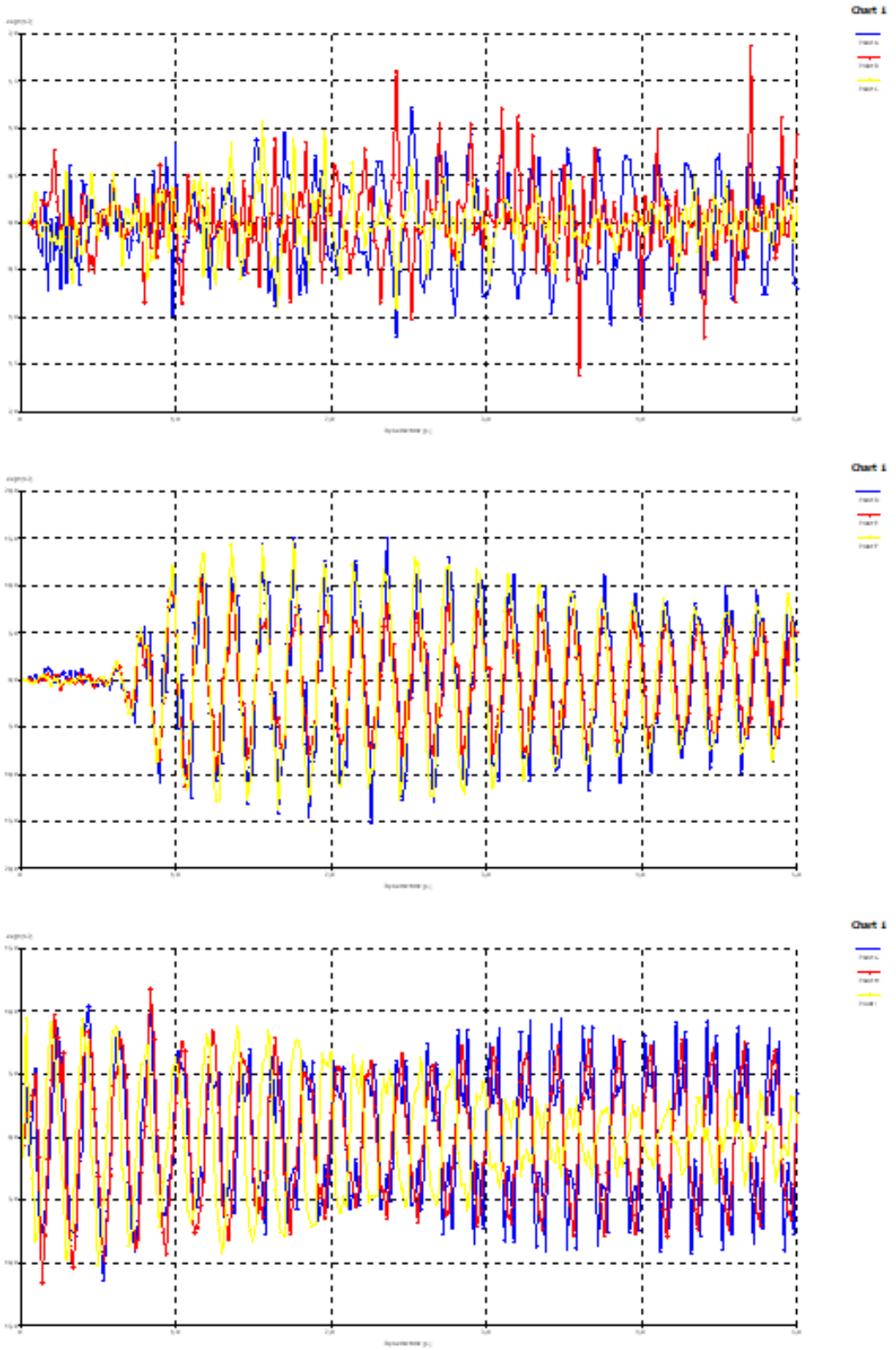

Figure A.25. Numerical Analysis results for the geogrid case under 0.1g acceleration with 5 hz frequency.

Figure A.26. Numerical Analysis results for the geogrid case under 0.2g acceleration with 0.5 hz frequency.

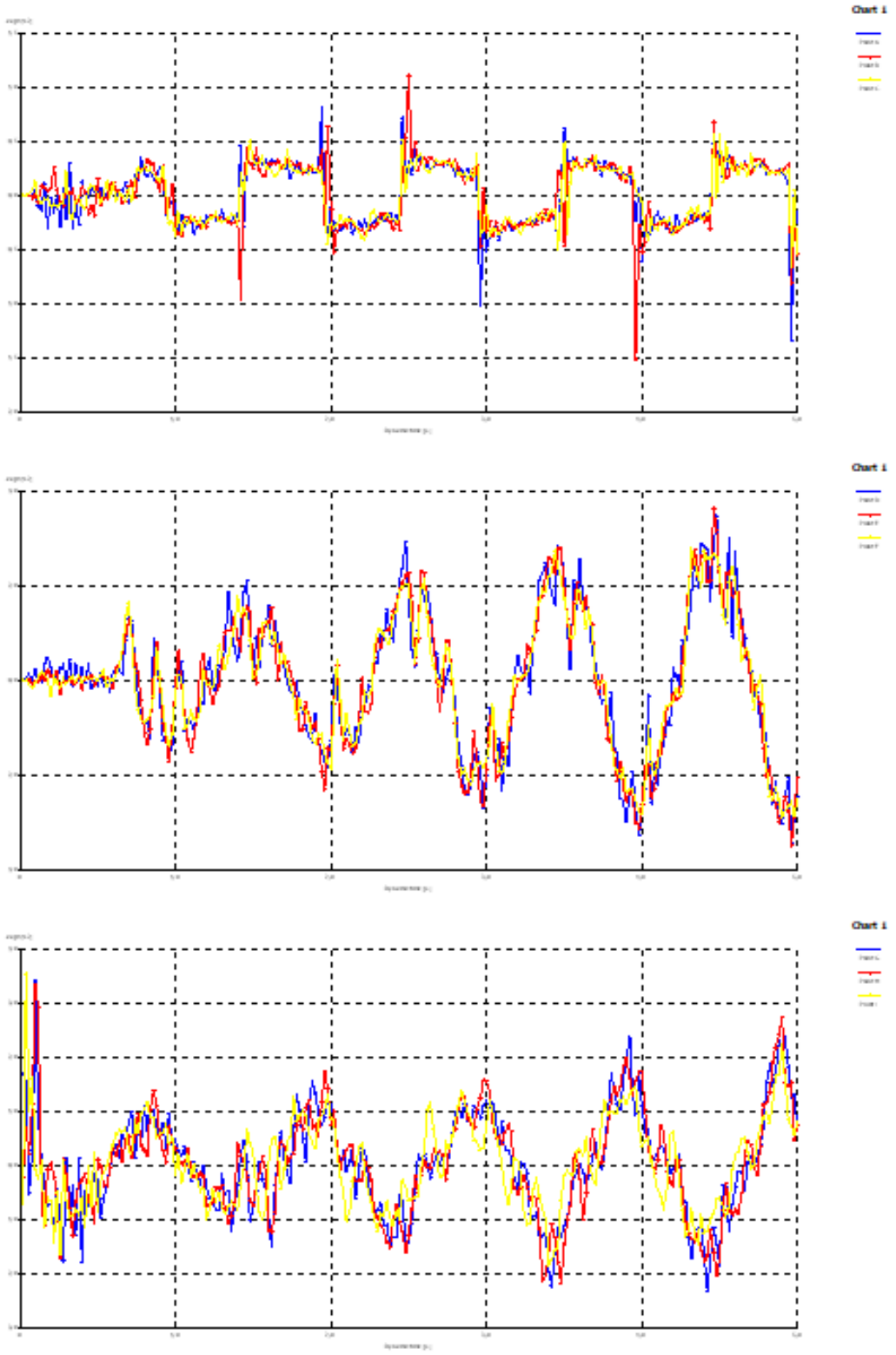

Figure A.27. Numerical Analysis results for the geogrid case under 0.2g acceleration with 1 hz frequency.

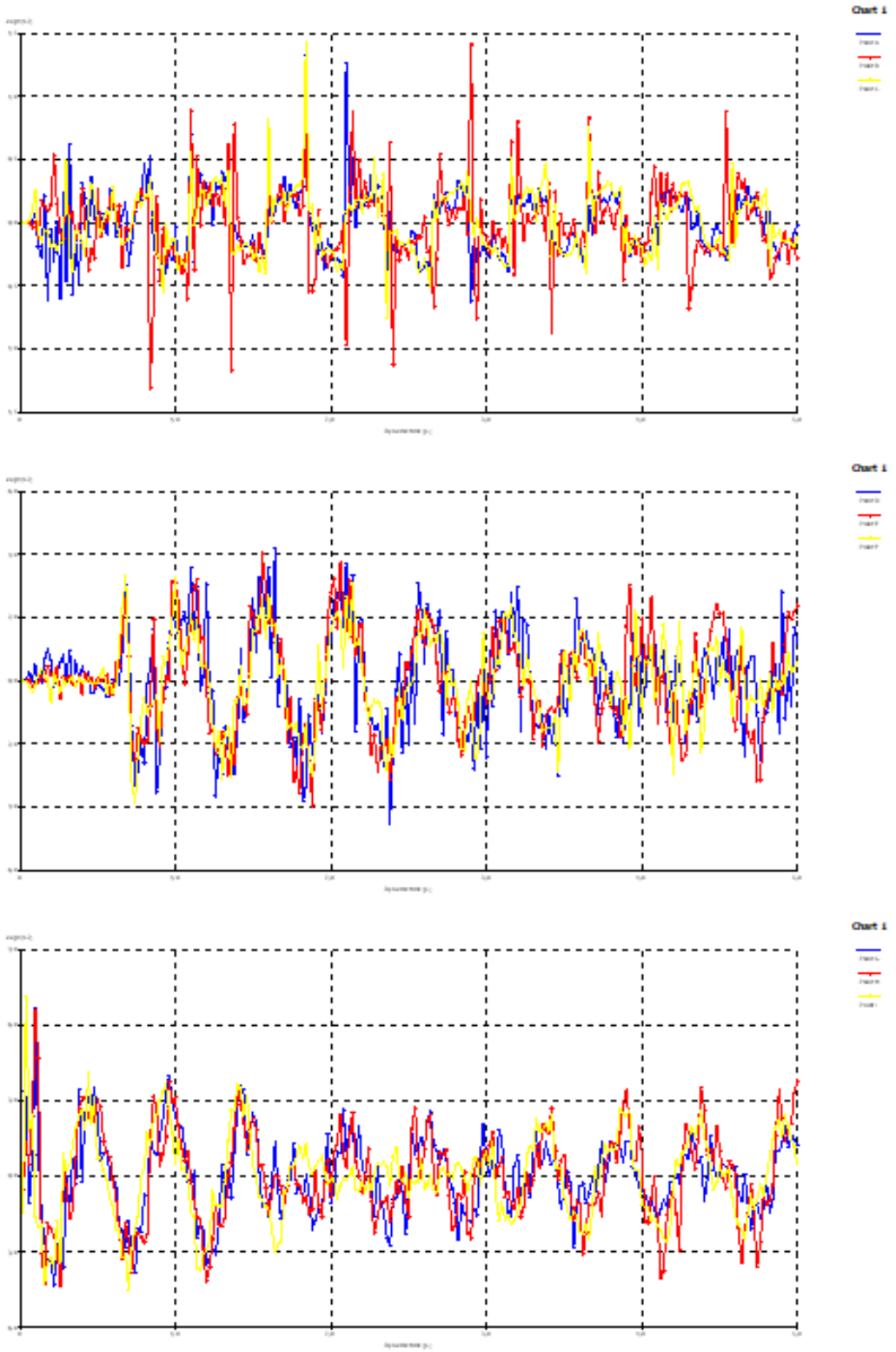

Figure A.28. Numerical Analysis results for the geogrid case under 0.2g acceleration with 2 hz frequency.

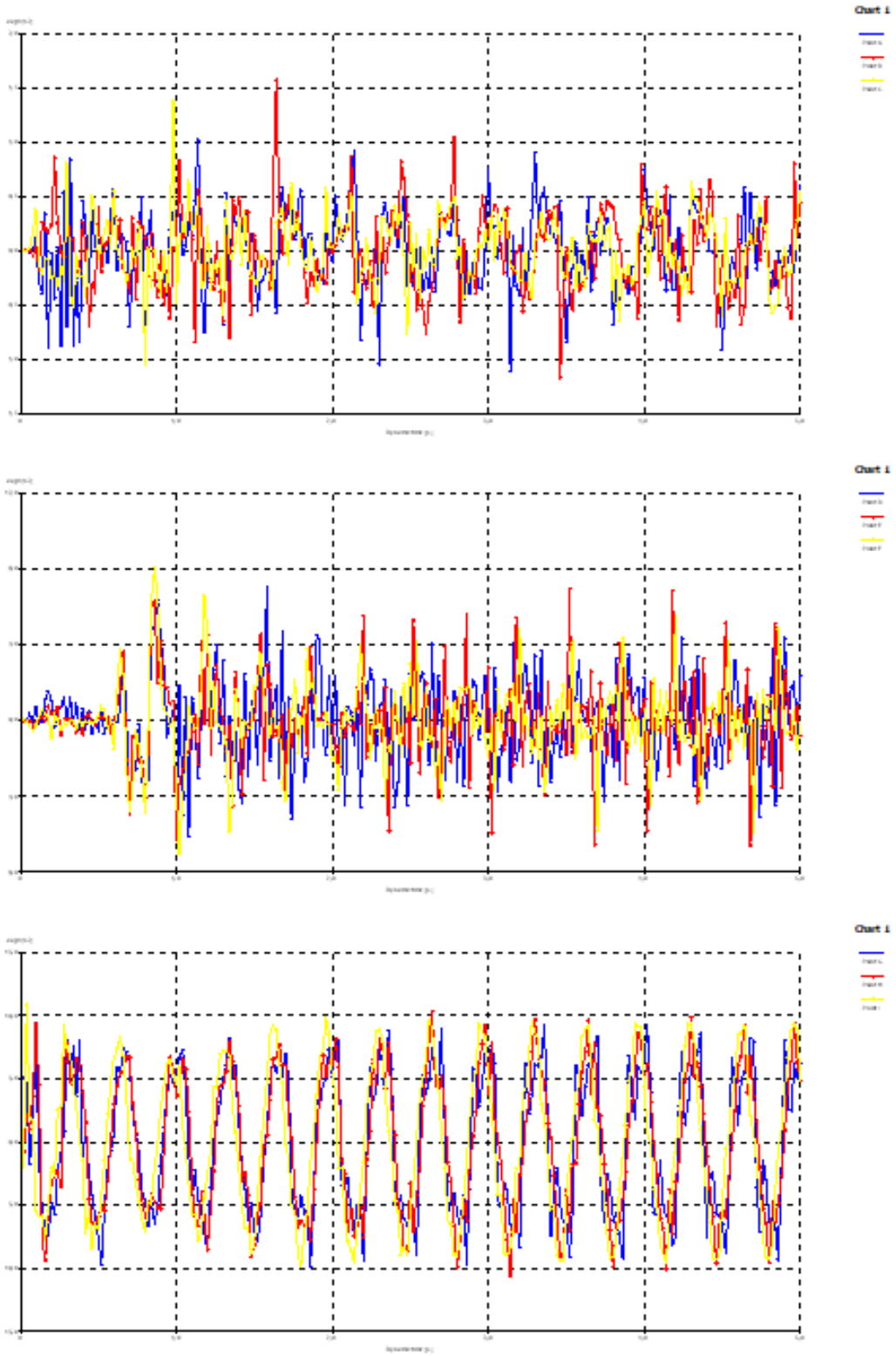

Figure A.29. Numerical Analysis results for the geogrid case under 0.2g acceleration with 3 hz frequency.

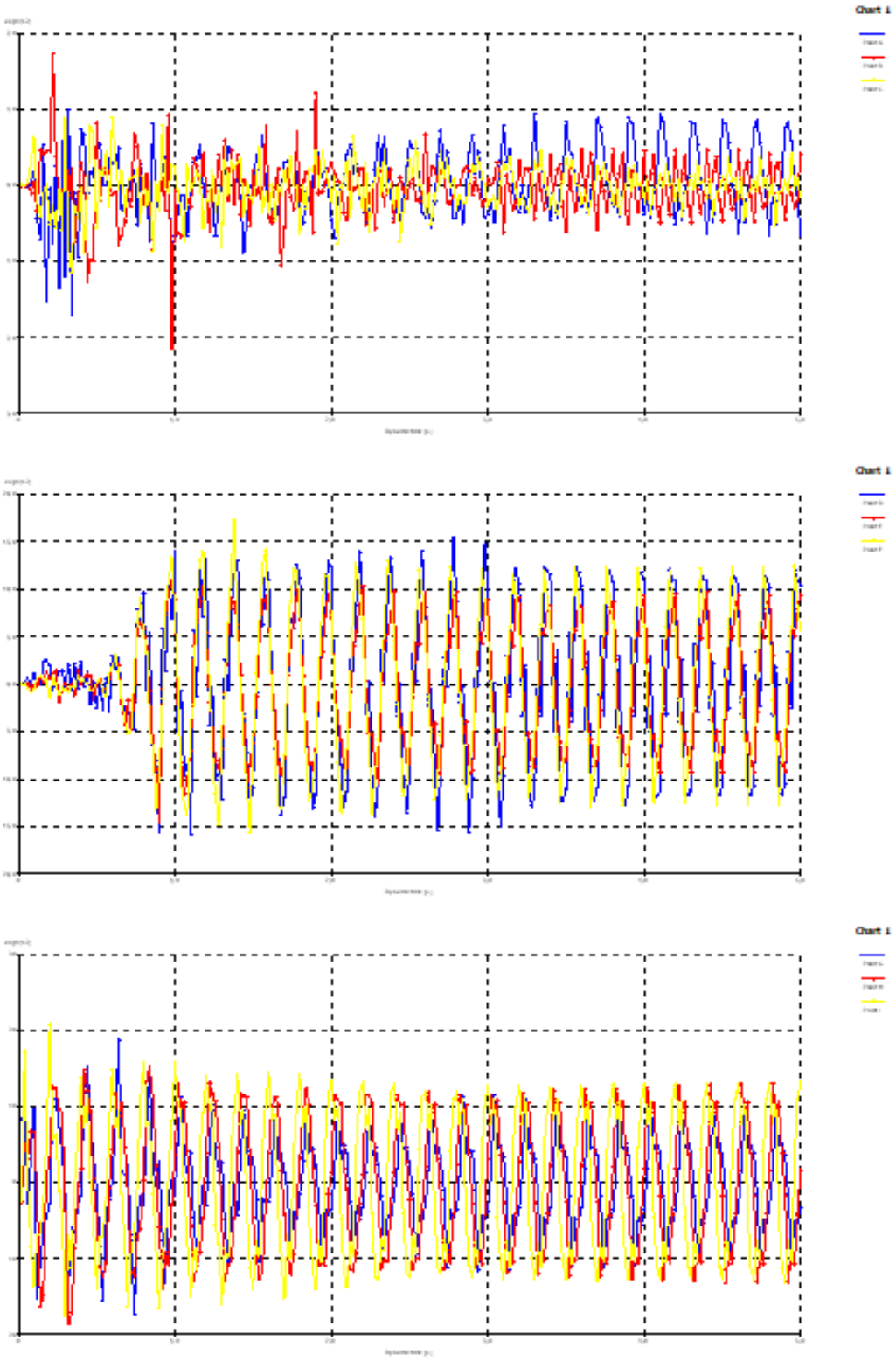

Figure A.30. Numerical Analysis results for the geogrid case under 0.2g acceleration with 5 hz frequency.

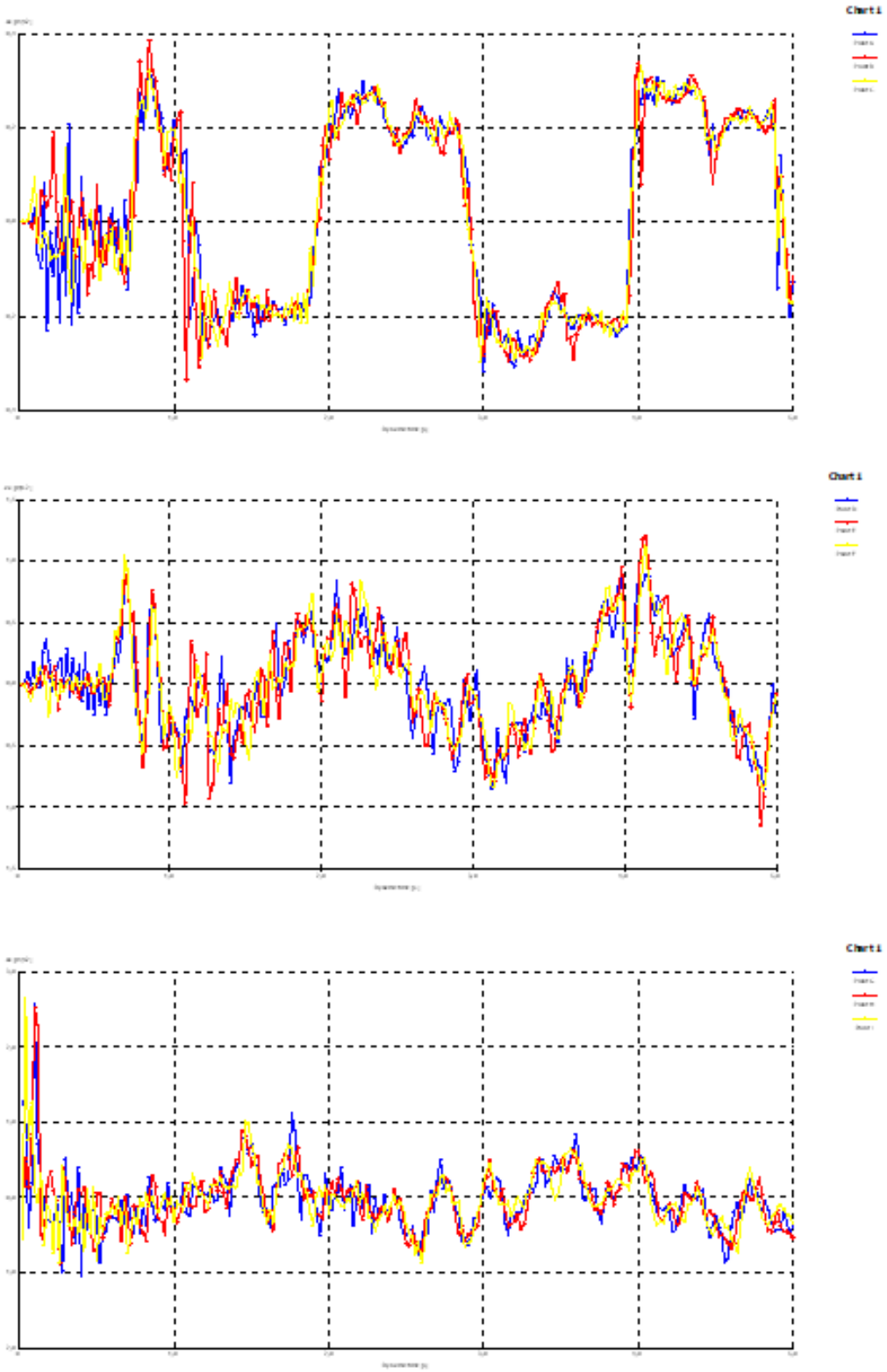

Figure A.31. Numerical Analysis results for the geogrid case under 0.3g acceleration with 0.5 hz frequency.

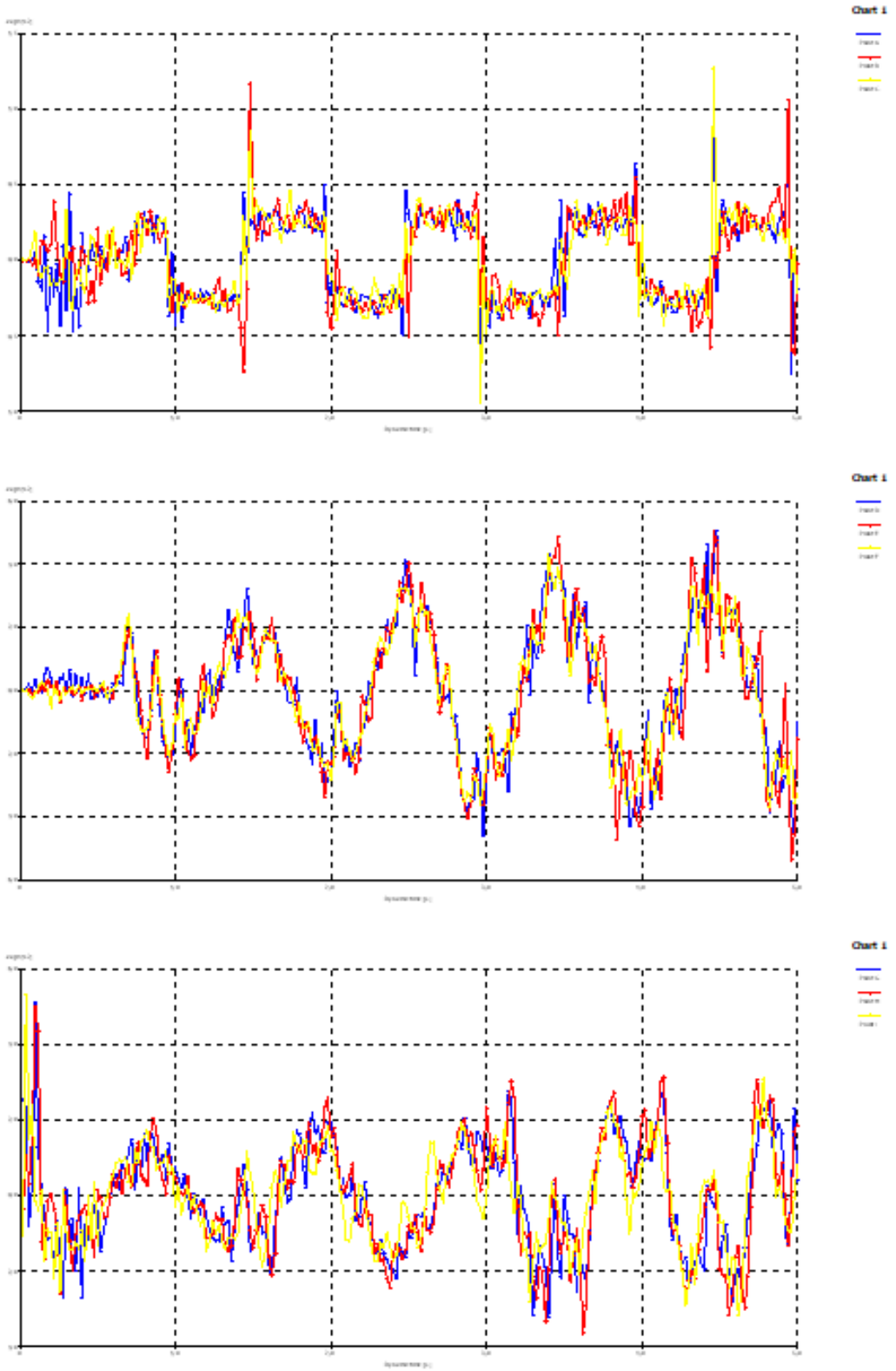

Figure A.32. Numerical Analysis results for the geogrid case under 0.3g acceleration with 1 hz frequency.

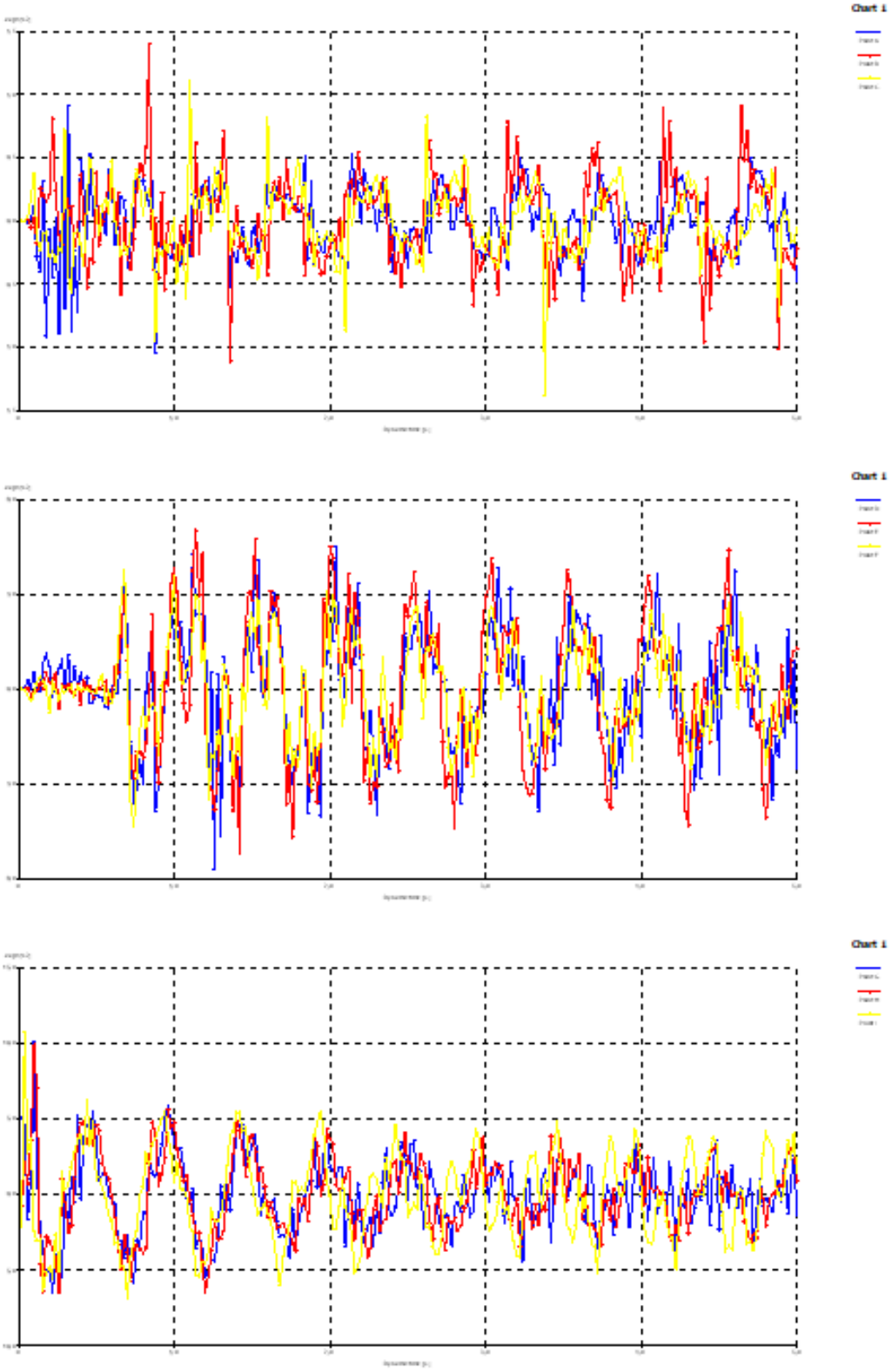

Figure A.33. Numerical Analysis results for the geogrid case under 0.3g acceleration with 2 hz frequency.

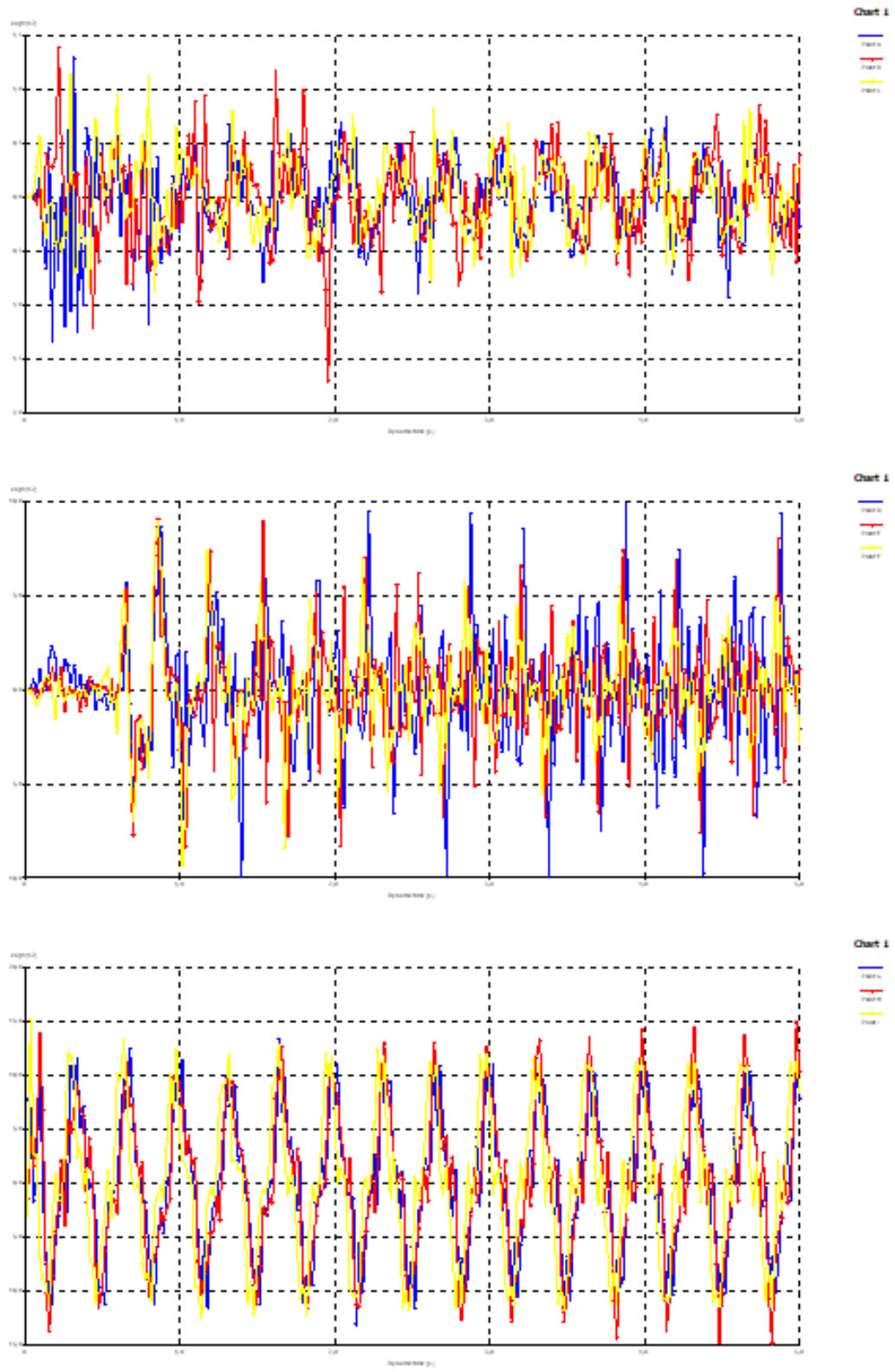

Figure A.34. Numerical Analysis results for the geogrid case under 0.3g acceleration with 3 hz frequency.

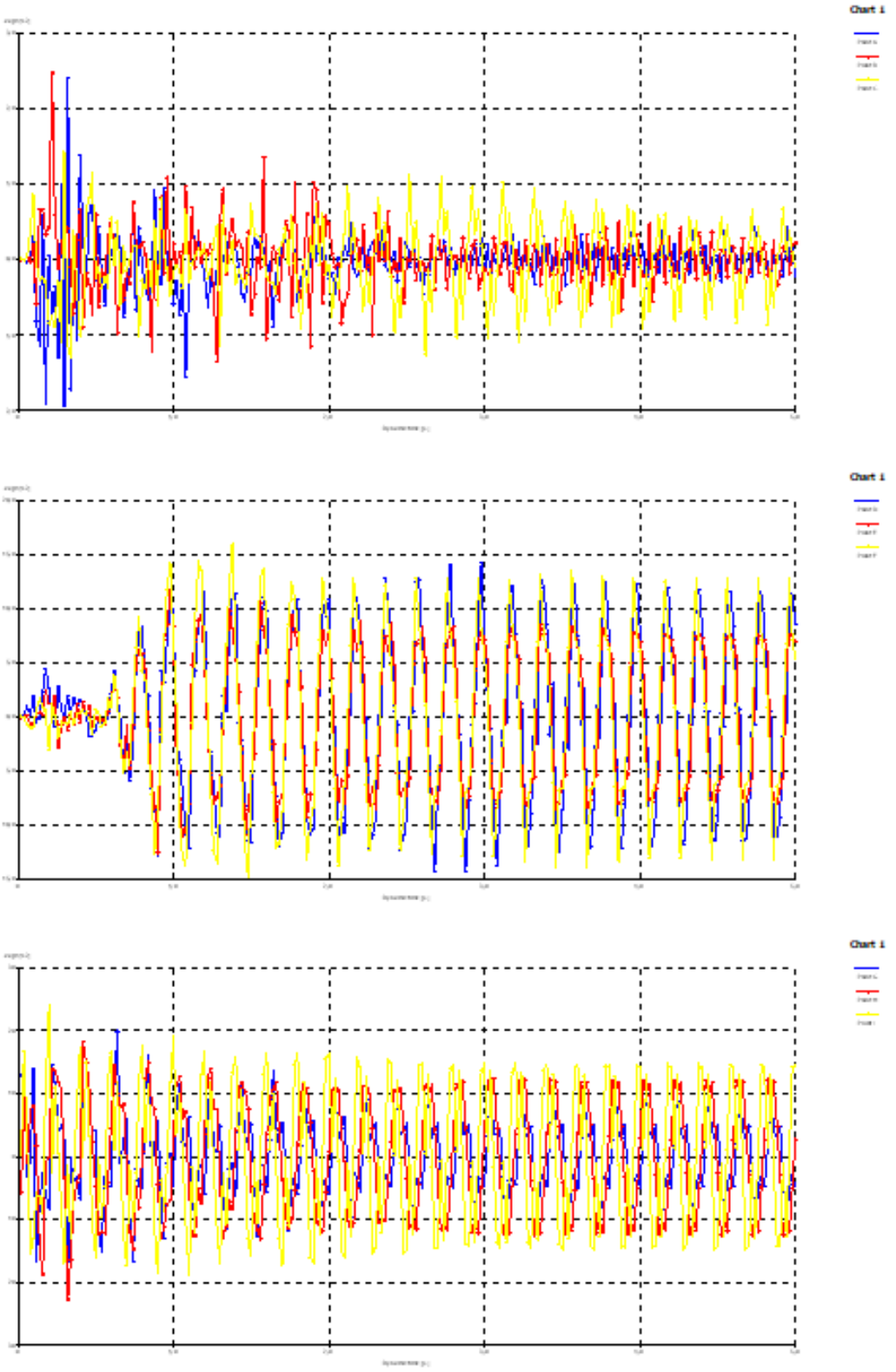

Figure A.35. Numerical Analysis results for the geogrid case under 0.3g acceleration with 5 hz frequency.

Figure A.36. Numerical Analysis results for the geogrid case under 0.4g acceleration with 0.5 hz frequency.

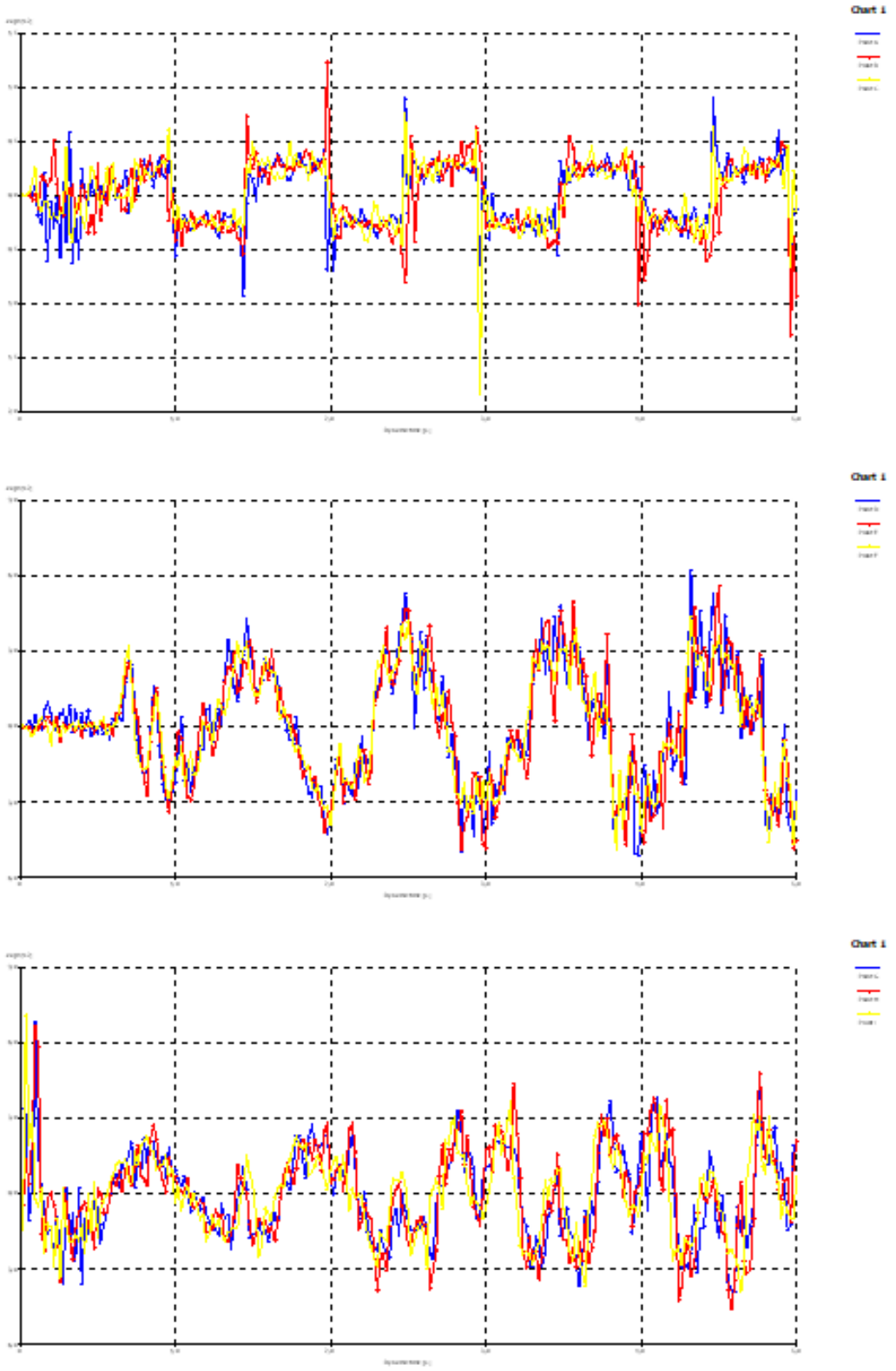

Figure A.37. Numerical Analysis results for the geogrid case under 0.4g acceleration with 1 hz frequency.

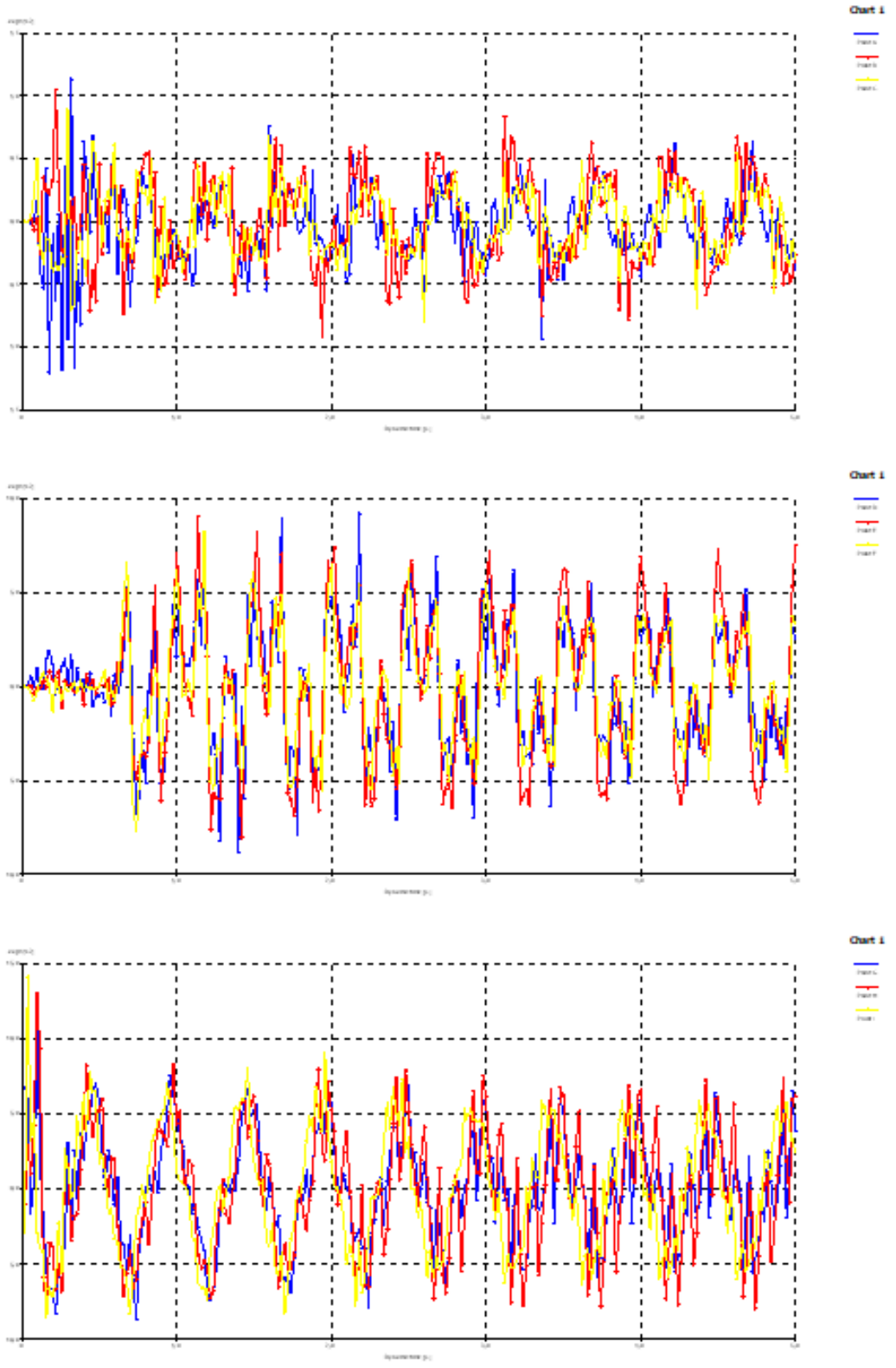

Figure A.38. Numerical Analysis results for the geogrid case under 0.4g acceleration with 2 hz frequency.

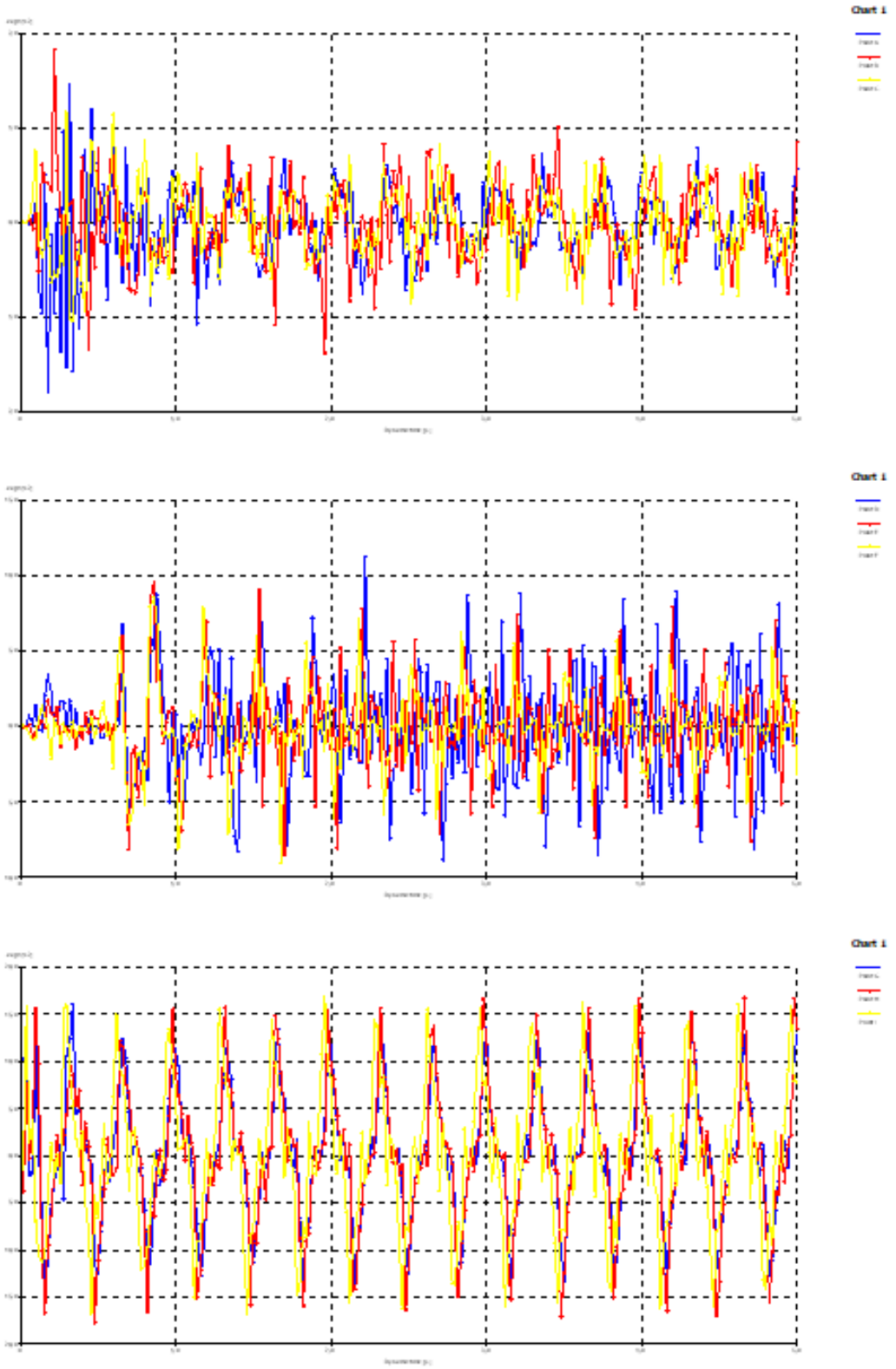

Figure A.39. Numerical Analysis results for the geogrid case under 0.4g acceleration with 3 hz frequency.

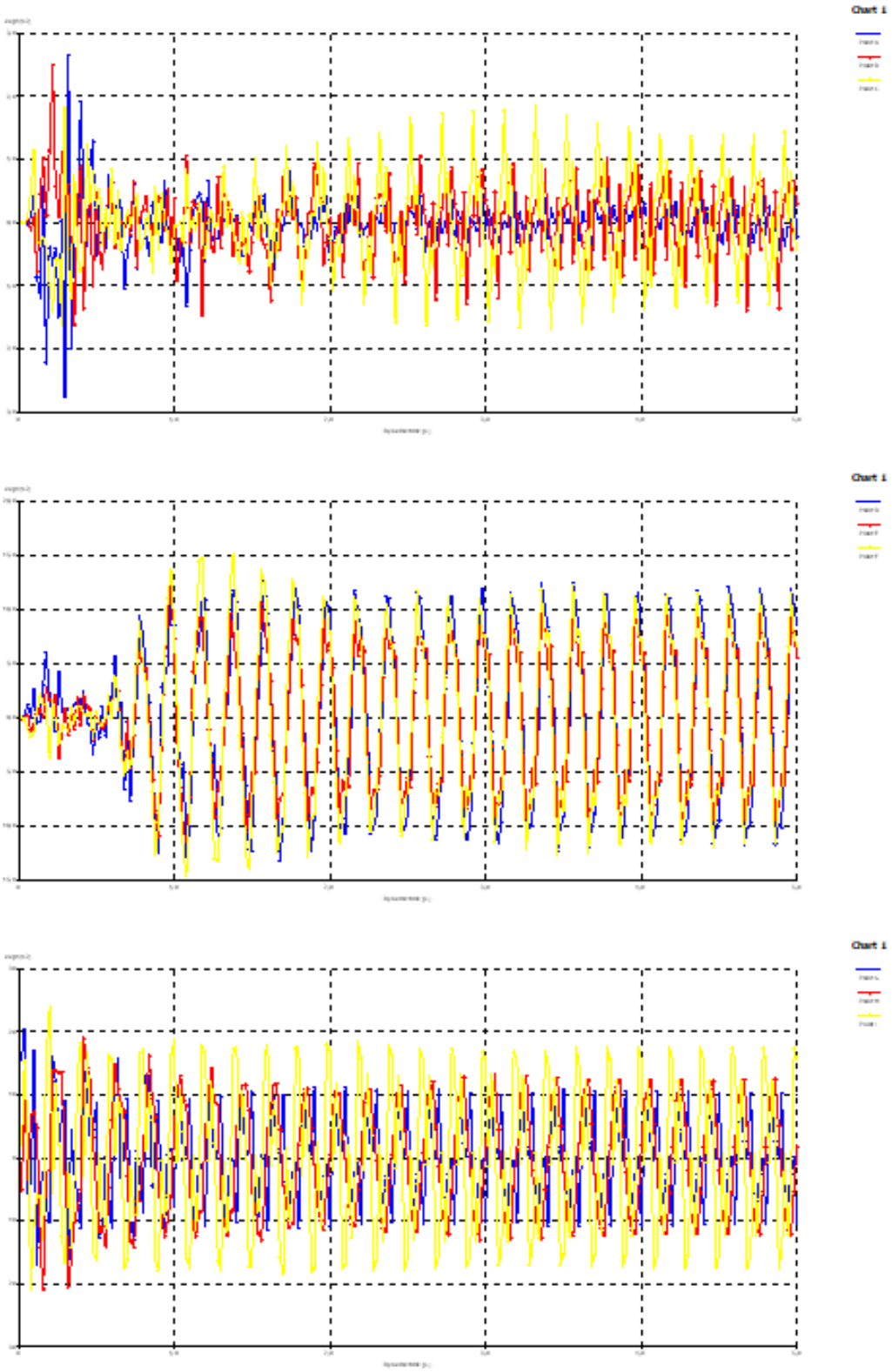

Figure A.40. Numerical Analysis results for the geogrid case under 0,4g acceleration with 5 hz frequency.

APPENDIX B: THE CODE OF ARIAS INTENSITY USED IN MATLAB

```
ivmeninoldugukolonnumarası
column ivme = 16;
zamanınoldugukolonnumarası
column time = 15;
k = 0;
filename =′ deneme.xlsx′;
sonucD = xlsread(filename);
exceldosyasının boyutları
dimension = size(sonucD);
row = dimension(1, 1);
column = dimension(1, 2);
zamanadım
dt = 0.02;
ariasintensitymatrix i
AI = zeros(row, 1);
zamankolonumatrixi
TIME = sonucD(:, column time);
ariasintensityhesab?
for i = 1 : row;
k = k + (3.14/(2 ∗ 9.81)) ∗ sonucD(i, column ivme)^2 ∗ dt;
AI(i) = k;
i = i + 1;
end
plot(TIME, AI);
```

APPENDIX C: AVERAGE ACCELERATION FIGURES FOR THE SELECTED POINTS LOCATING THE TOP, THE MIDDLE AND THE BOTTOM

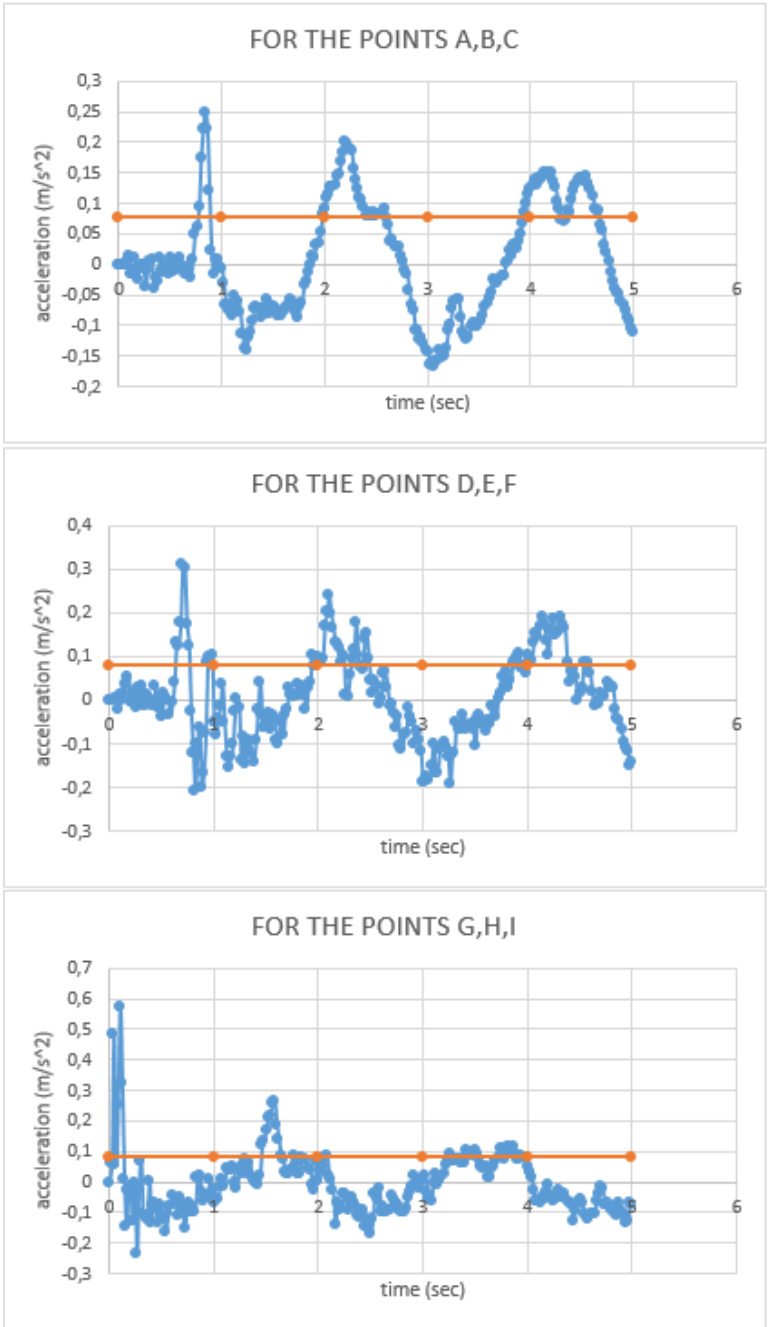

Figure C.1. Average Acceleration for unreinforced case under 0.1g PGA with 0.5 hz frequency.

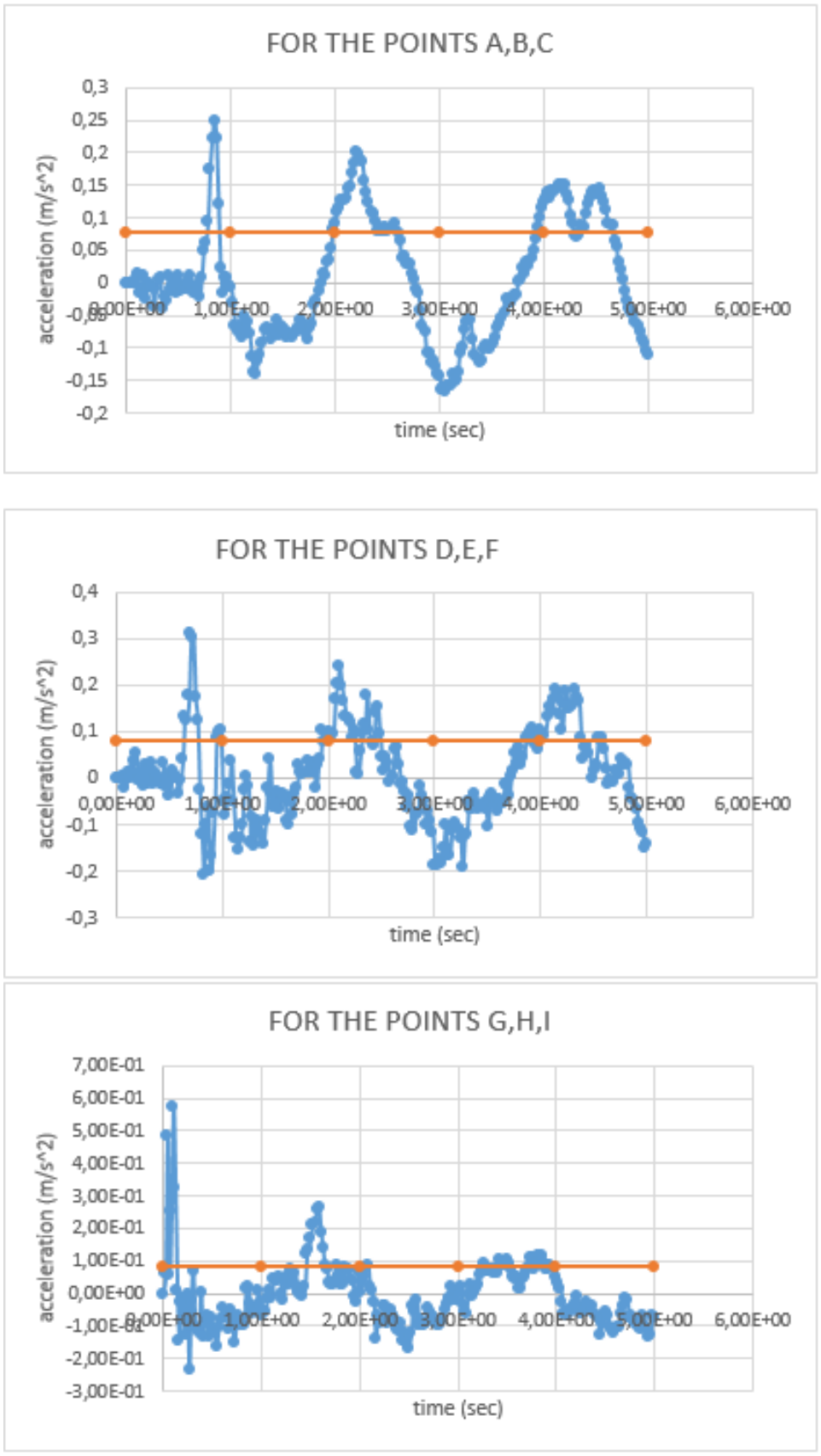

Figure C.2. Average Acceleration for reinforced case under 0.1g PGA with 0.5 hz frequency.

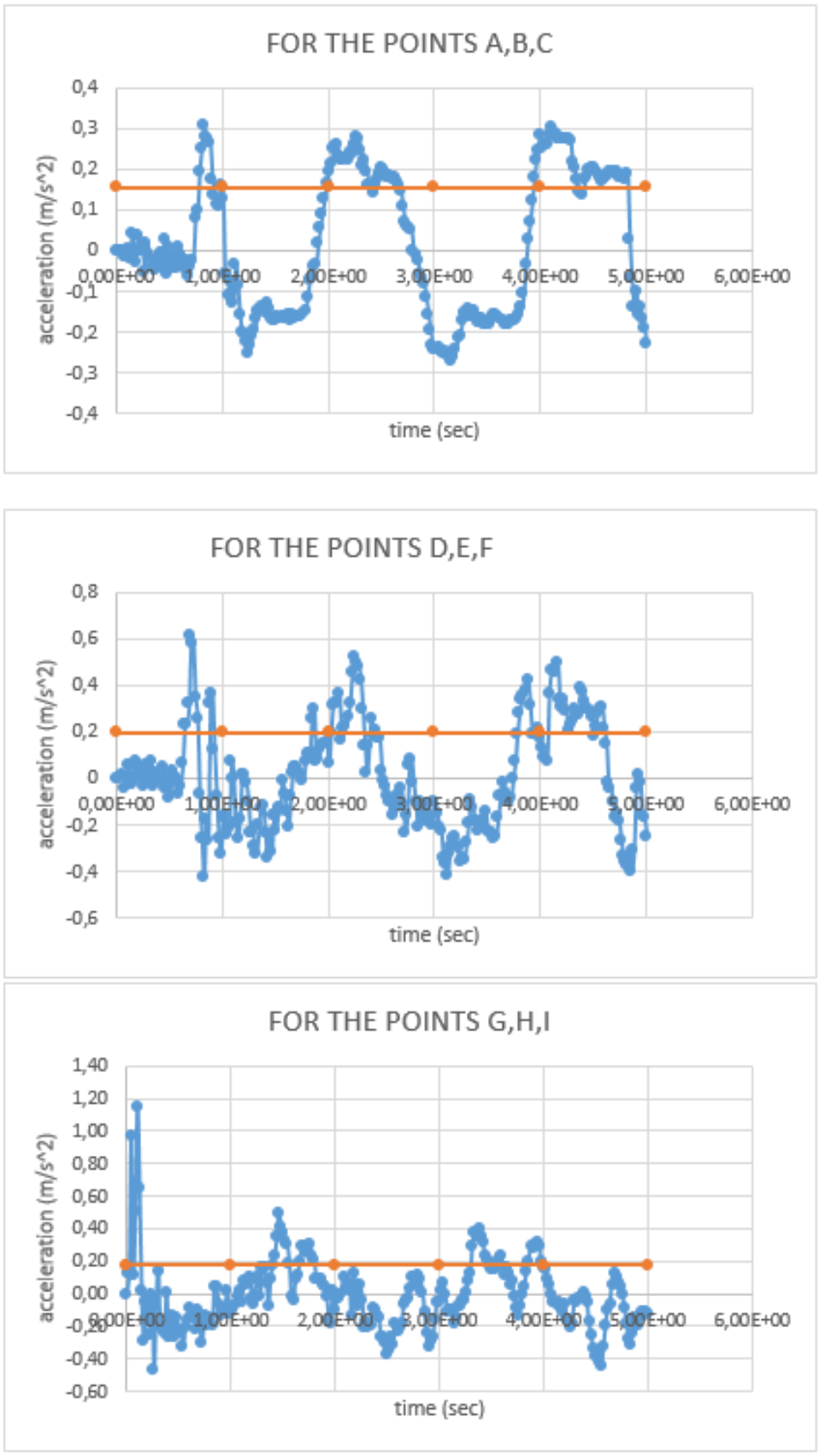

Figure C.3. Average Acceleration for unreinforced case under 0.2g PGA with 0.5 hz frequency.

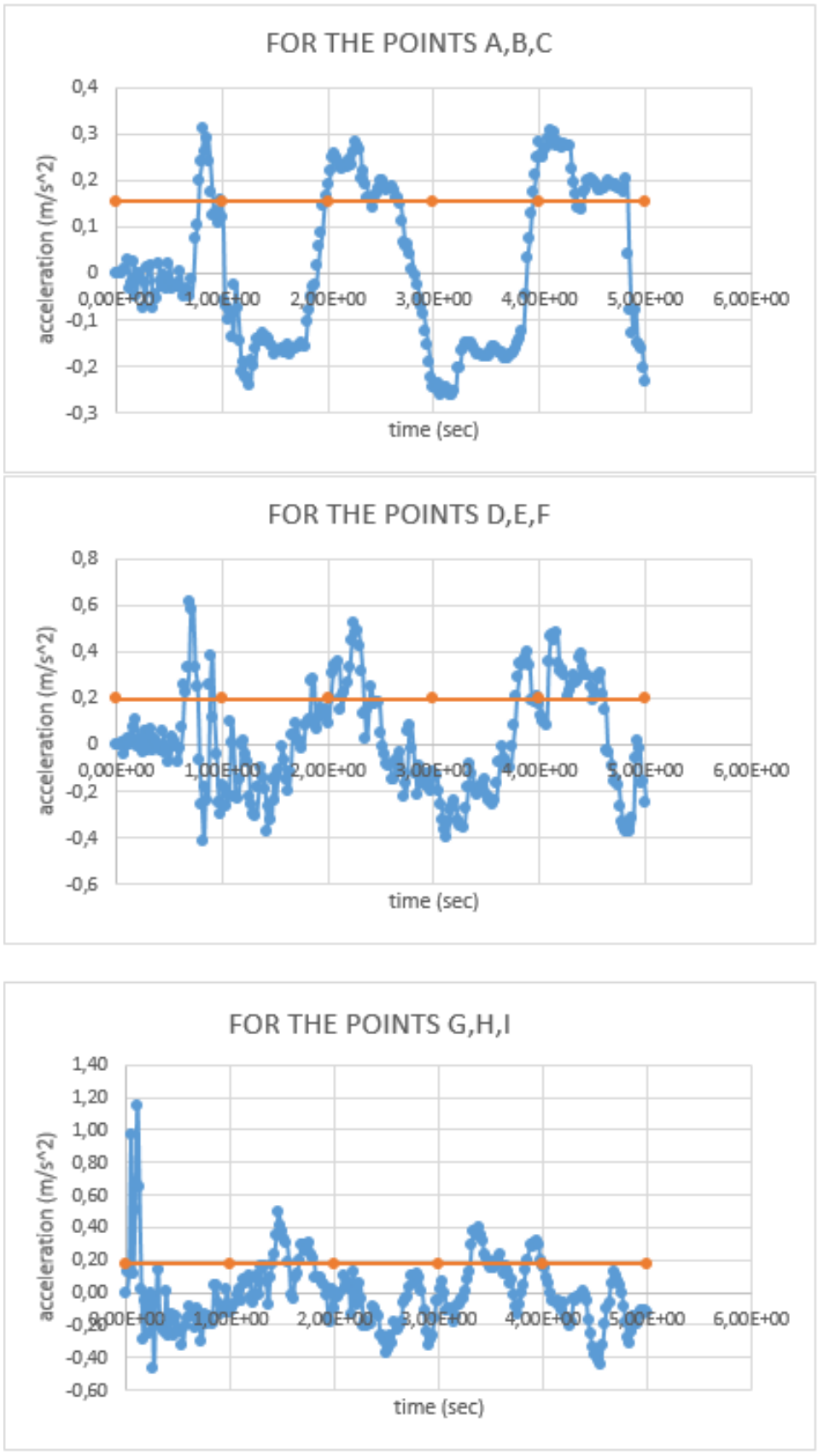

Figure C.4. Average Acceleration for reinforced case under 0.2g PGA with 0.5 hz frequency.

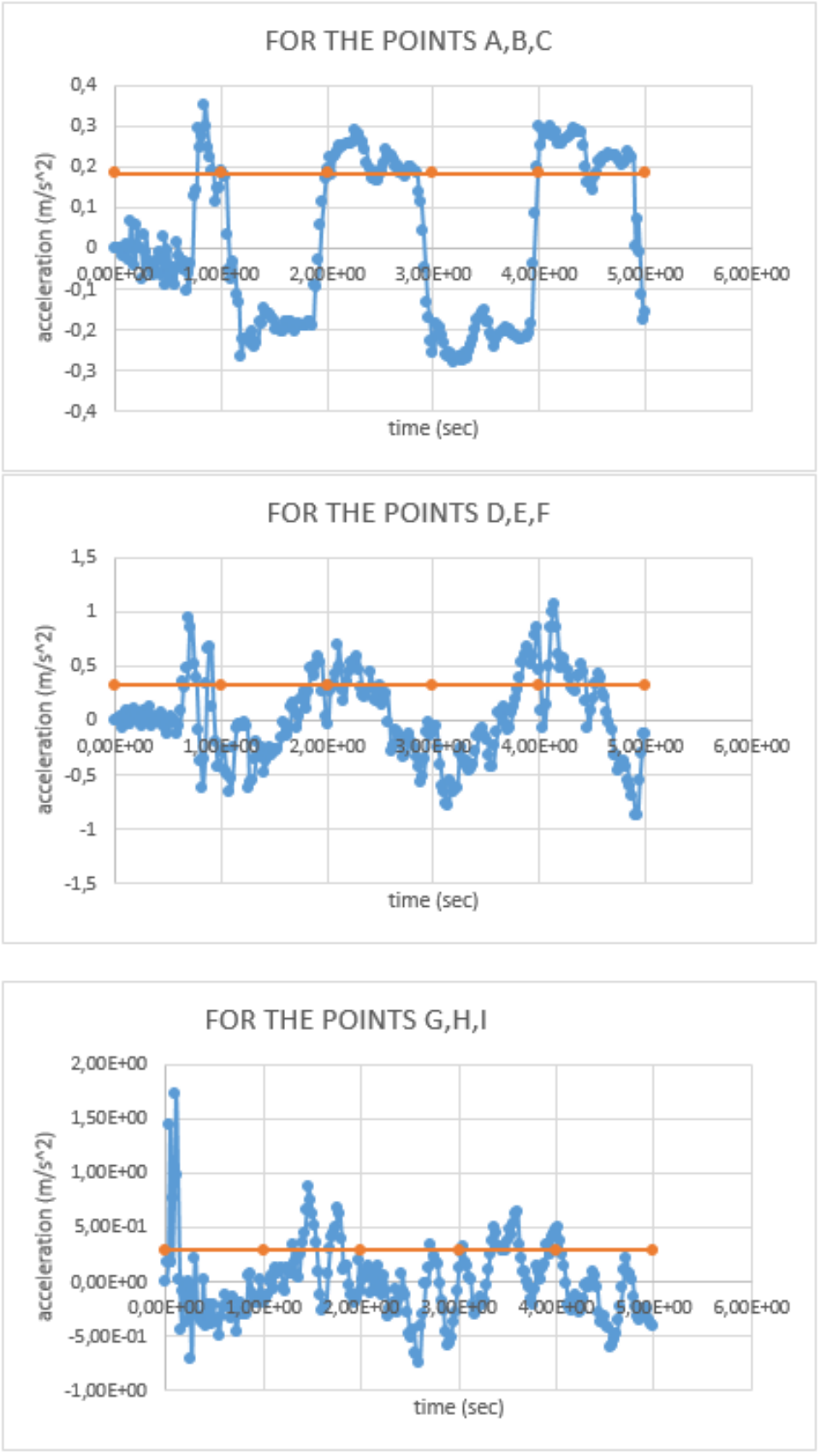

Figure C.5. Average Acceleration for unreinforced case under 0.3g PGA with 0.5 hz frequency.

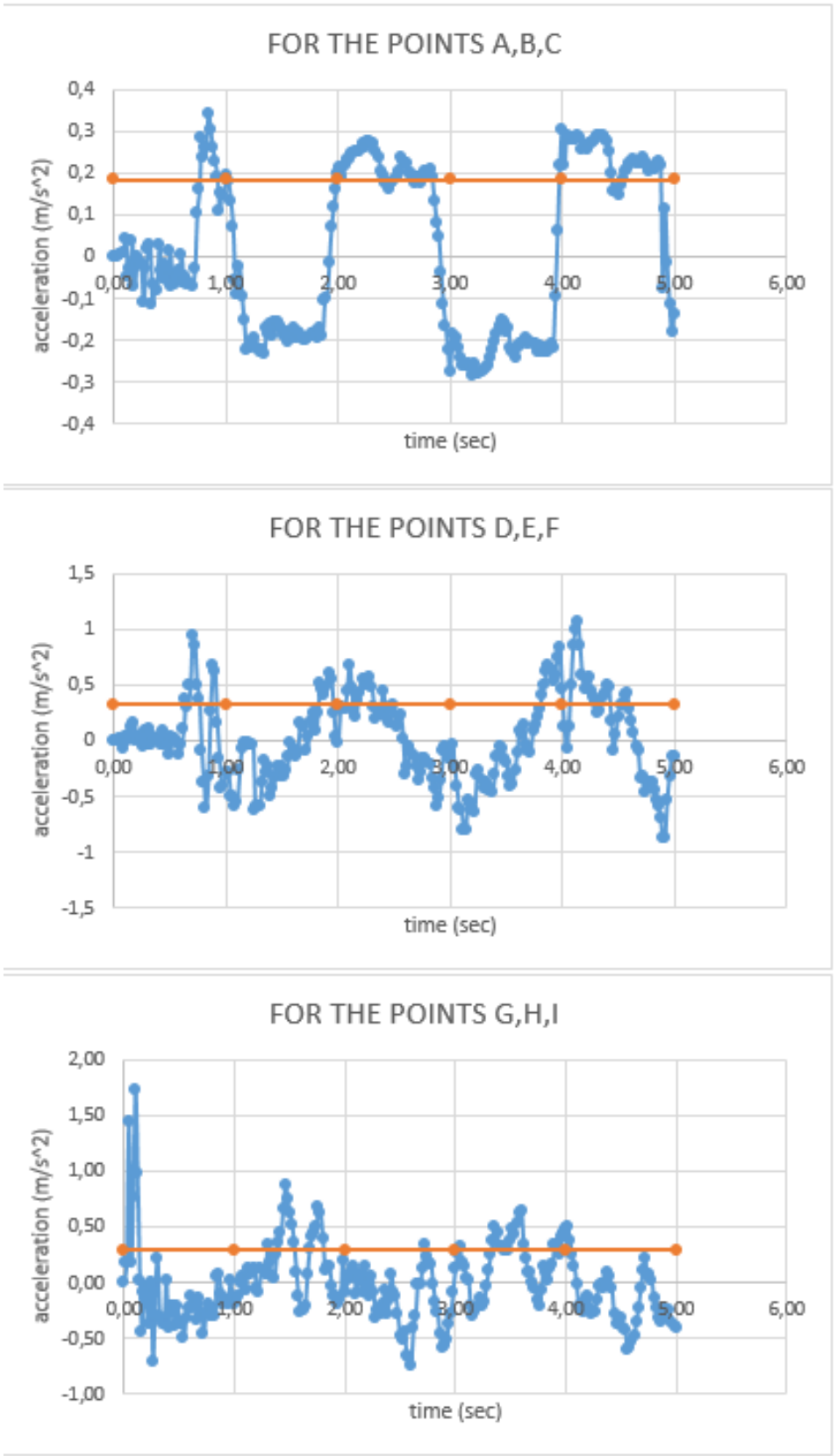

Figure C.6. Average Acceleration for reinforced case under 0.3g PGA with 0.5 hz frequency.

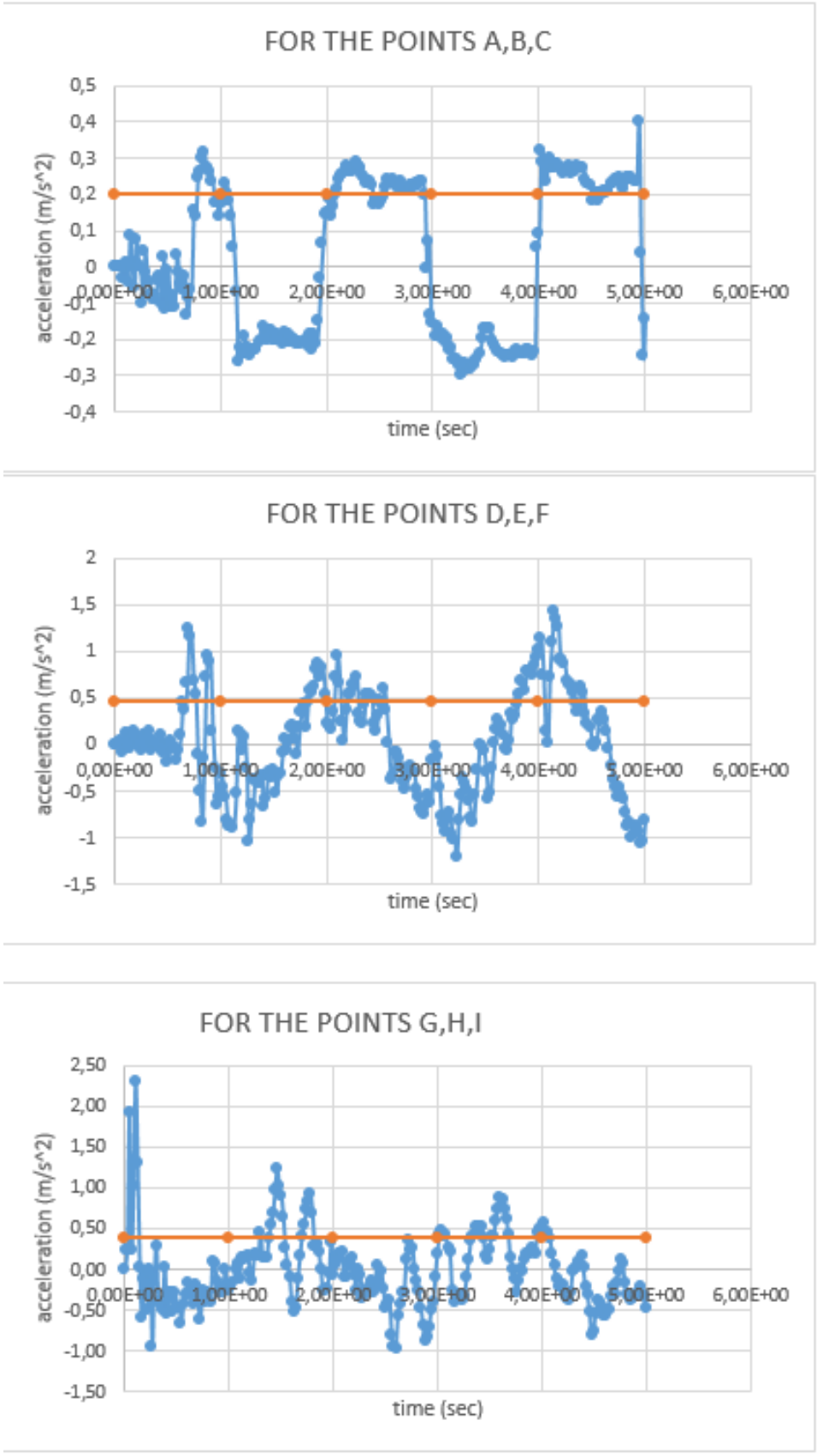

Figure C.7. Average Acceleration for unreinforced case under 0.4g PGA with 0.5 hz frequency.

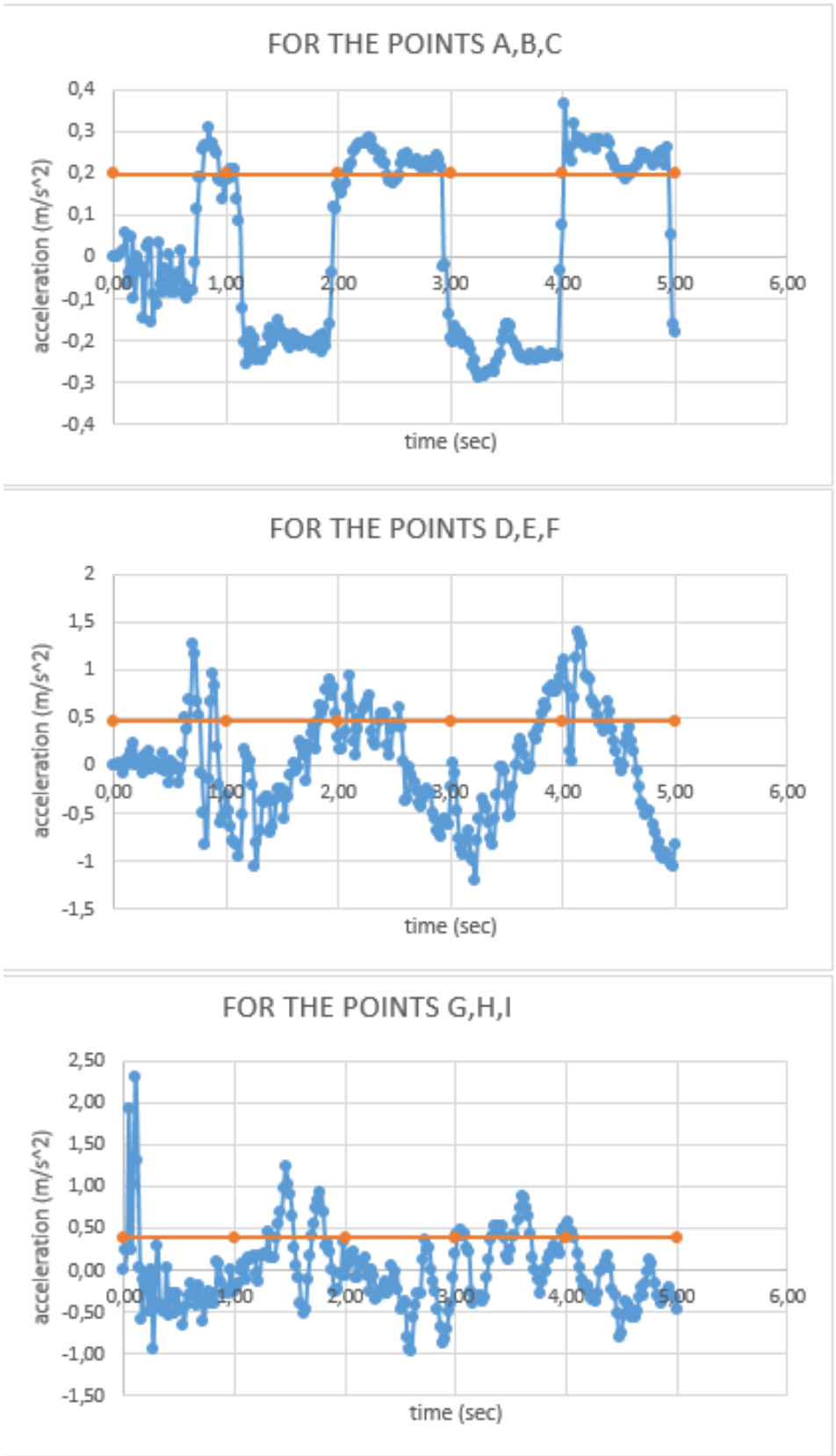

Figure C.8. Average Acceleration for reinforced case under 0.4g PGA with 0.5 hz frequency.

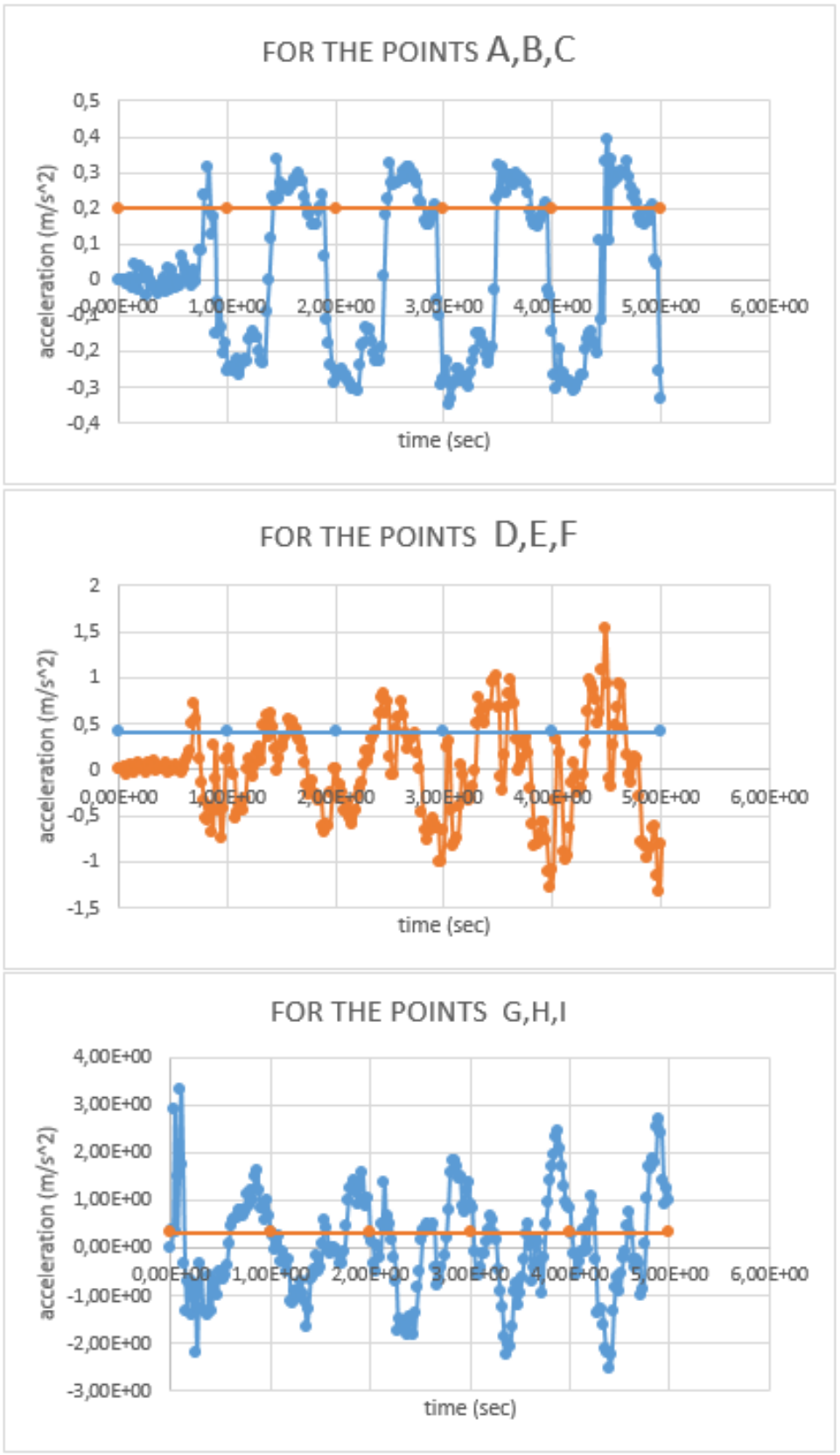

Figure C.9. Average Acceleration for unreinforced case under 0.1g PGA with 1 hz frequency.

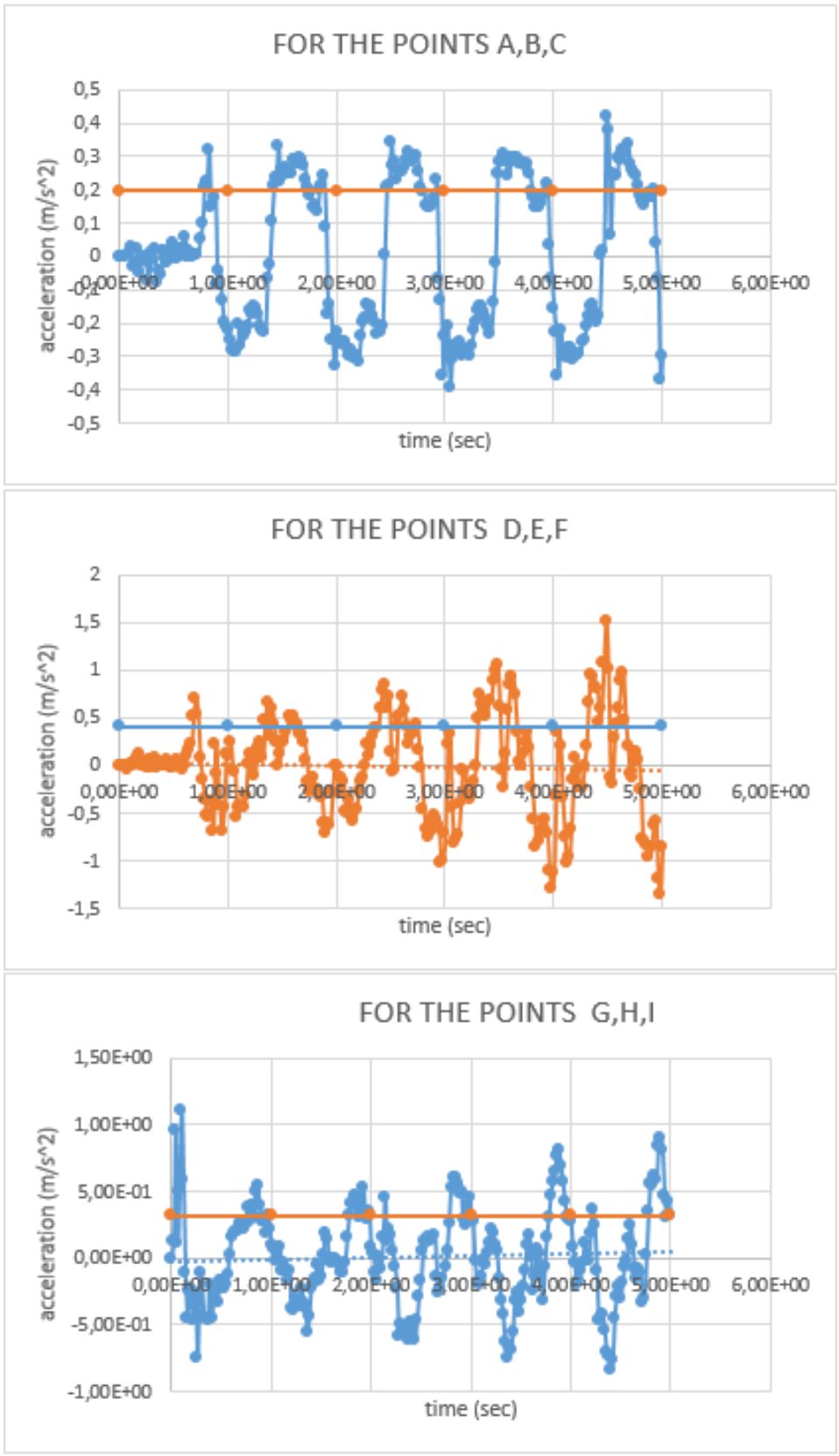

Figure C.10. Average Acceleration for reinforced case under 0.1g PGA with 1 hz frequency.

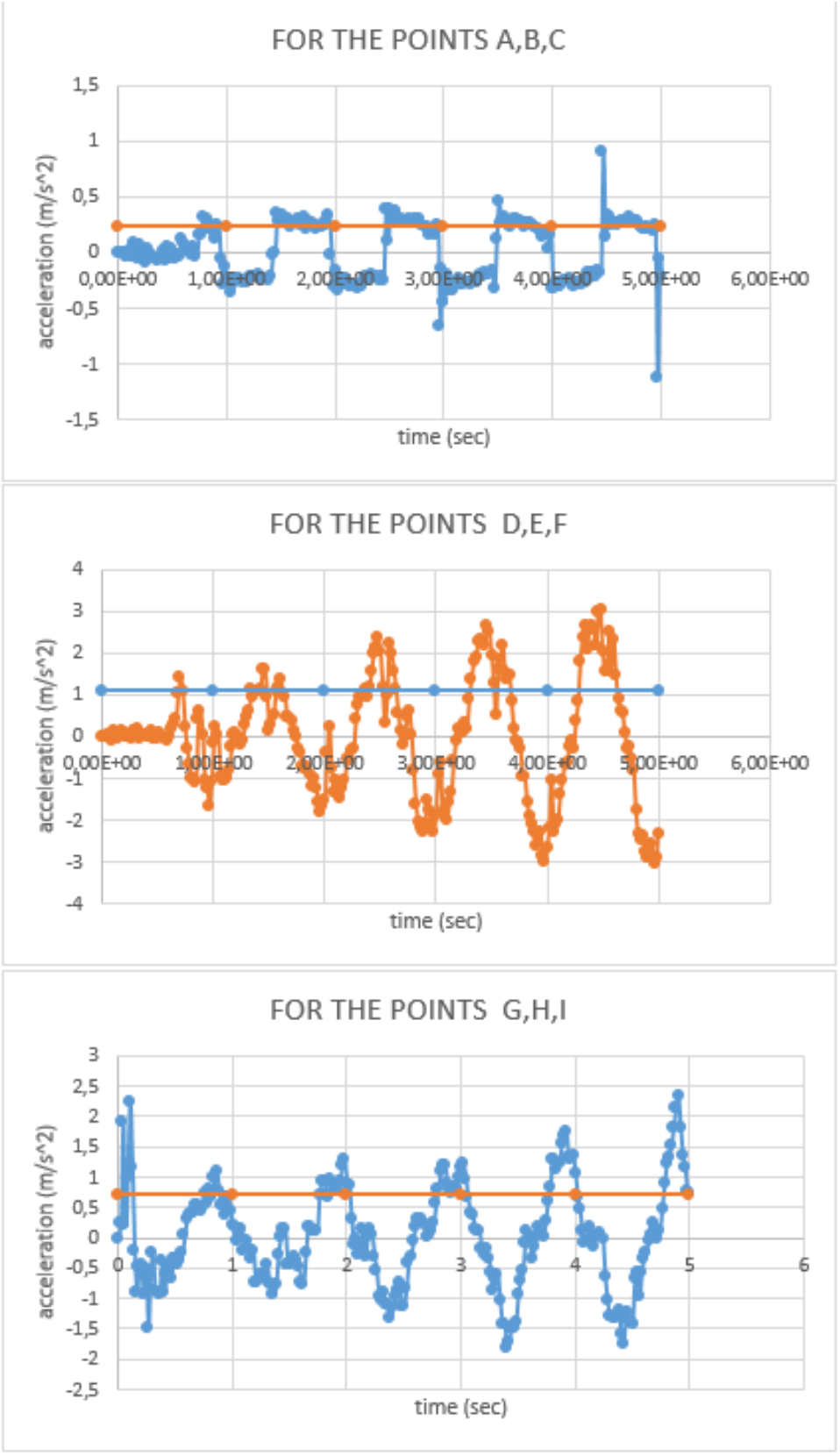

Figure C.11. Average Acceleration for unreinforced case under 0.2g PGA with 1 hz frequency.

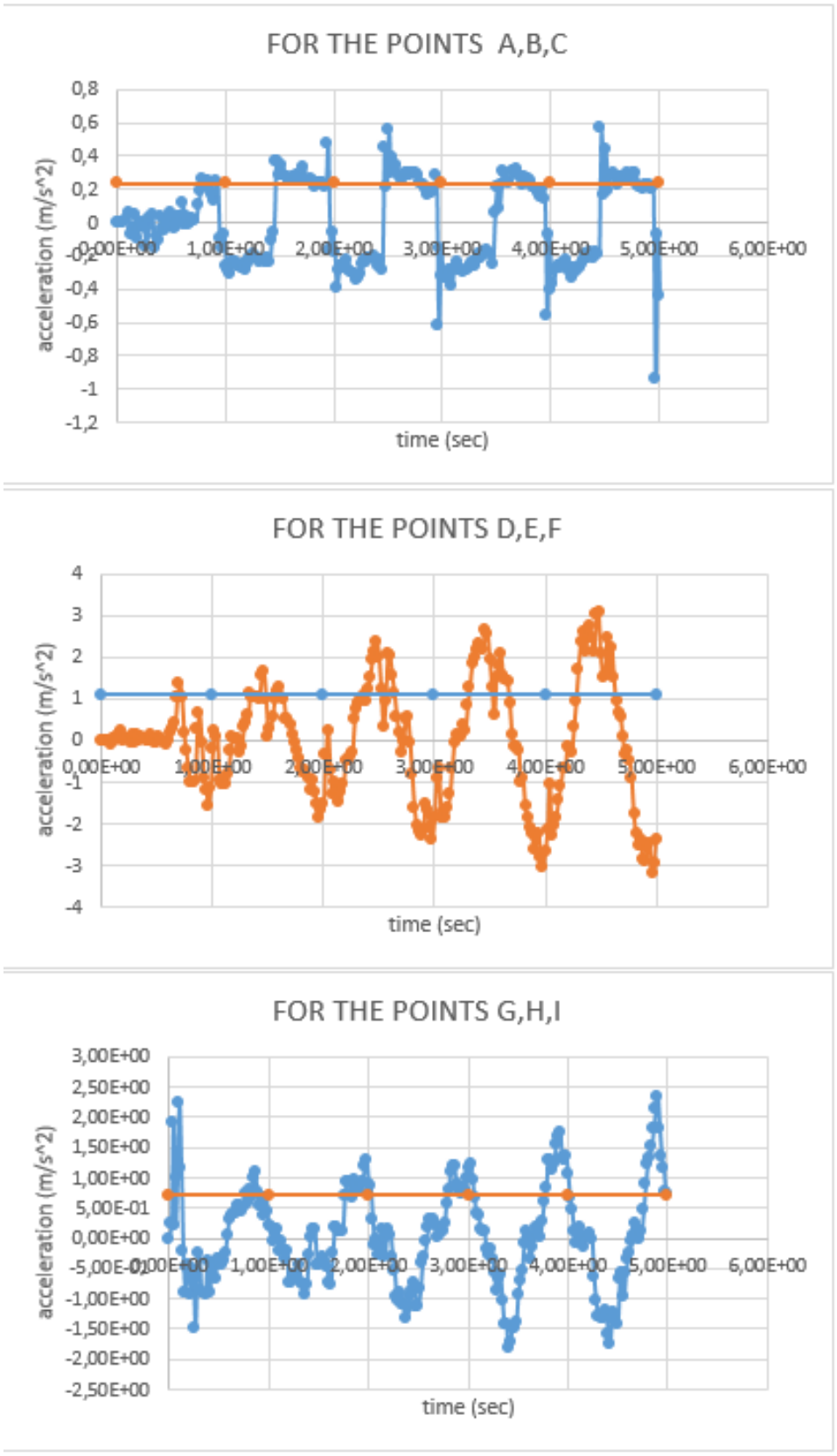

Figure C.12. Average Acceleration for reinforced case under 0.2g PGA with 1 hz frequency.

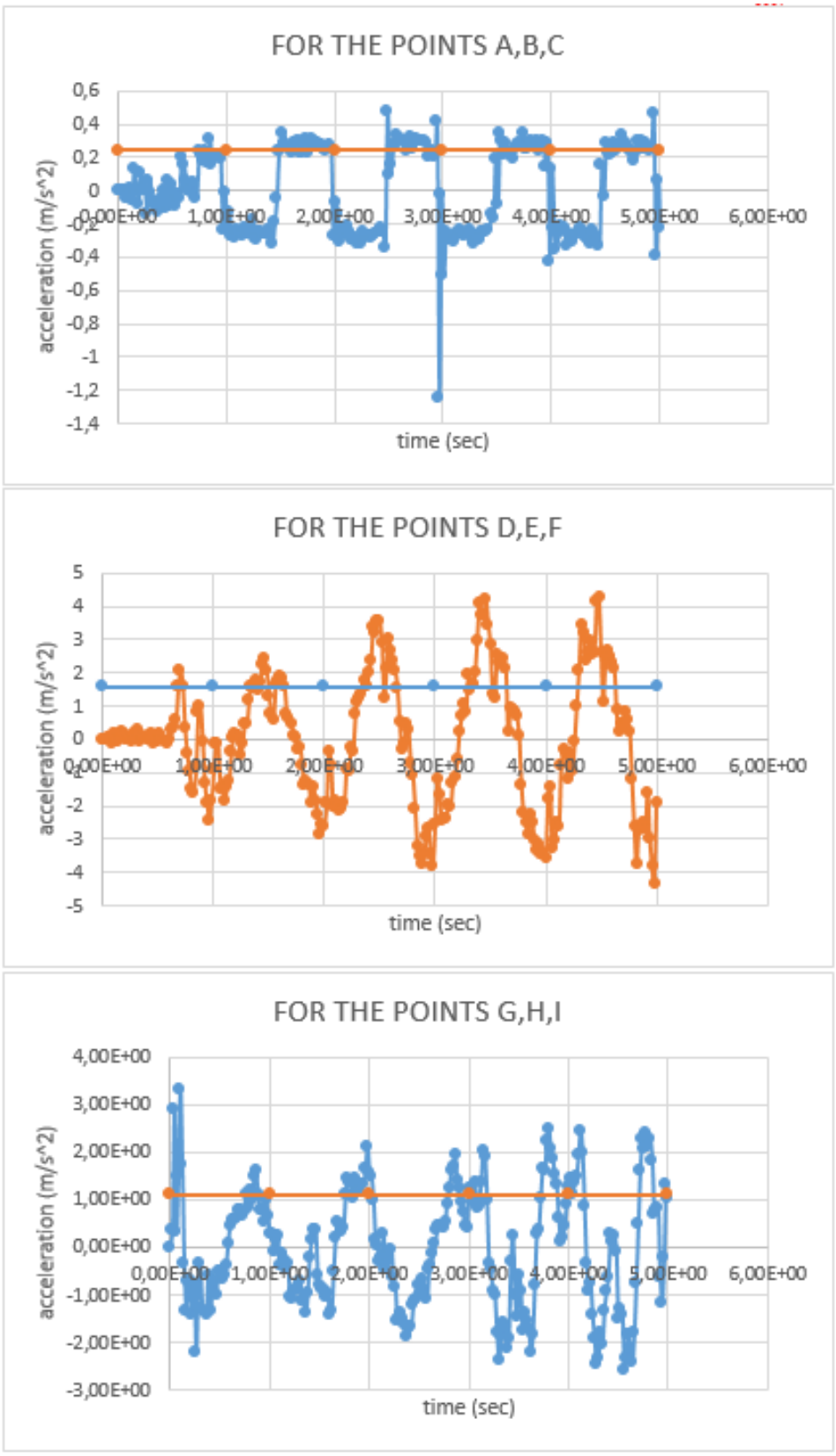

Figure C.13. Average Acceleration for unreinforced case under 0.3g PGA with 1 hz frequency.

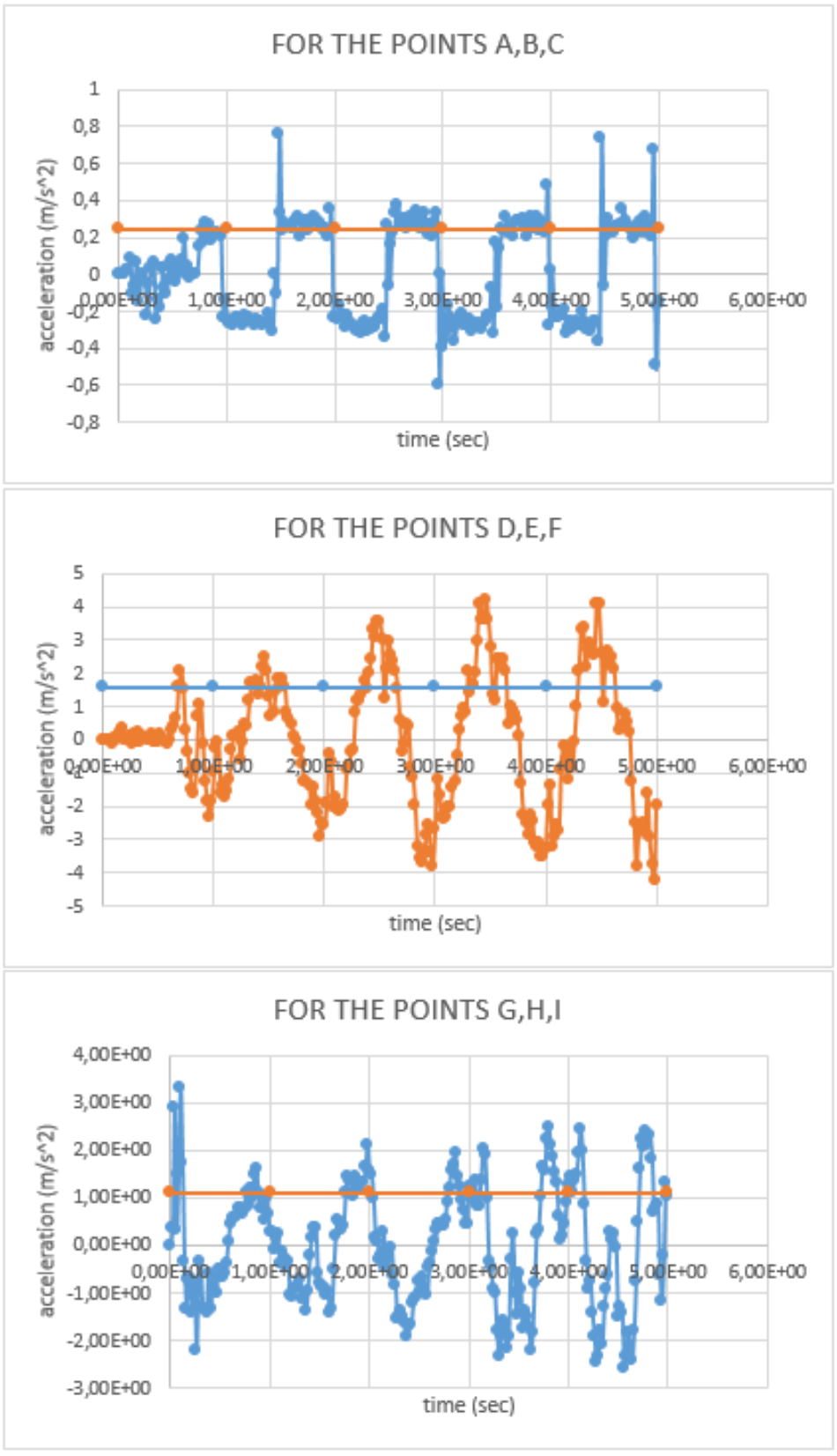

Figure C.14. Average Acceleration for reinforced case under 0.3g PGA with 1 hz frequency.

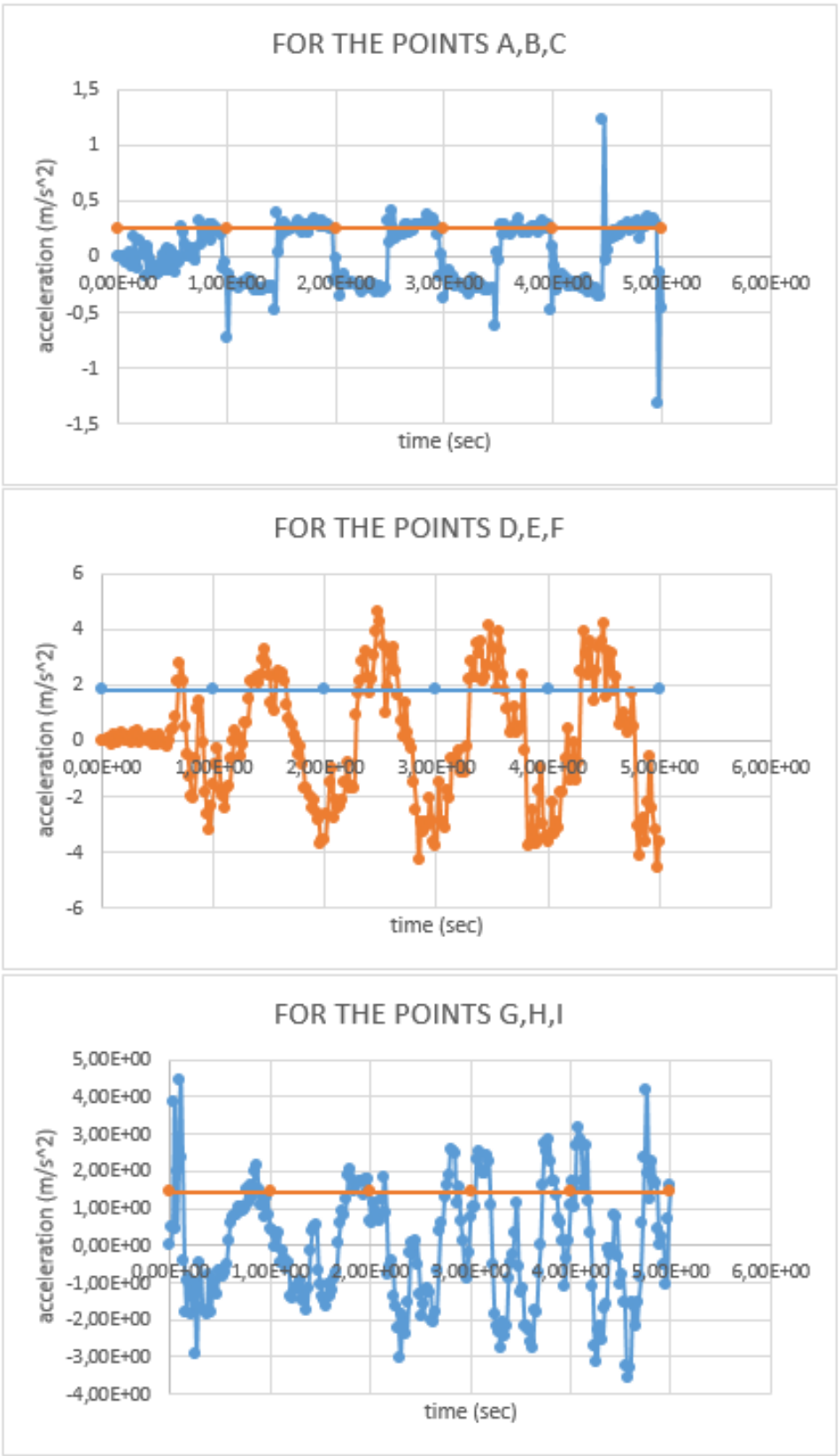

Figure C.15. Average Acceleration for unreinforced case under 0.4g PGA with 1 hz frequency.

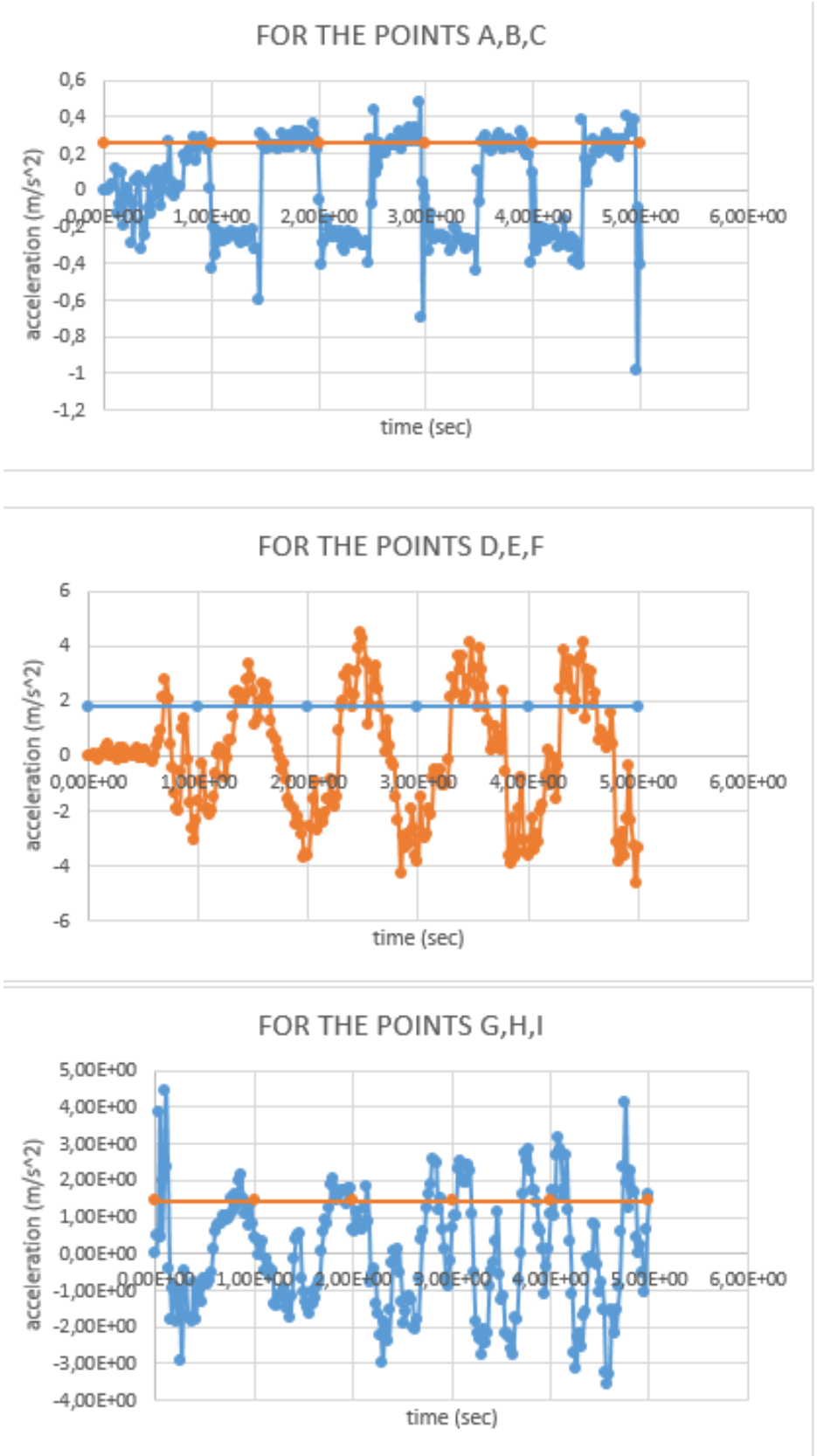

Figure C.16. Average Acceleration for reinforced case under 0.4g PGA with 1 hz frequency.

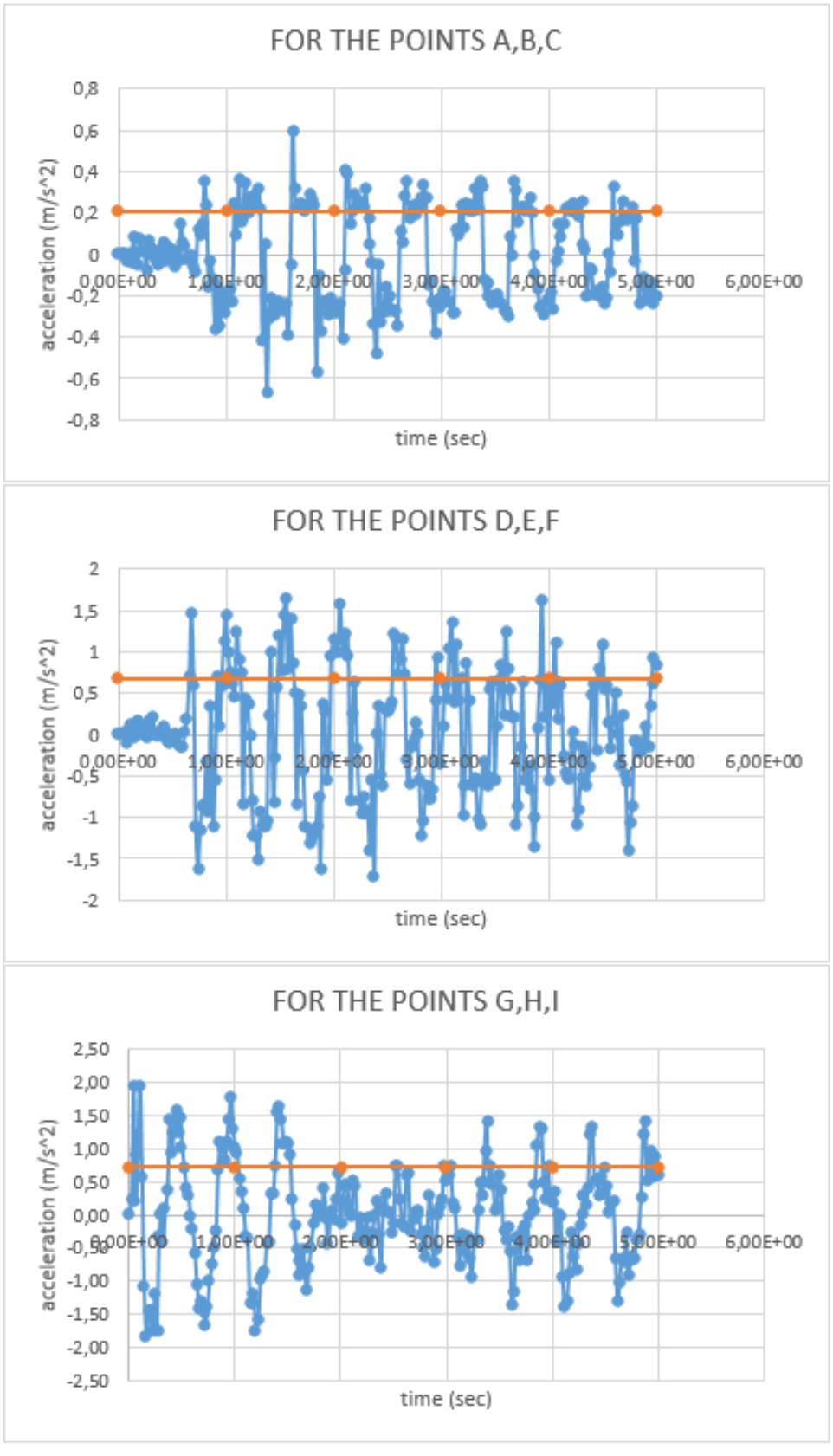

Figure C.17. ? Average Acceleration for unreinforced case under 0.1g PGA with 2 hz frequency.

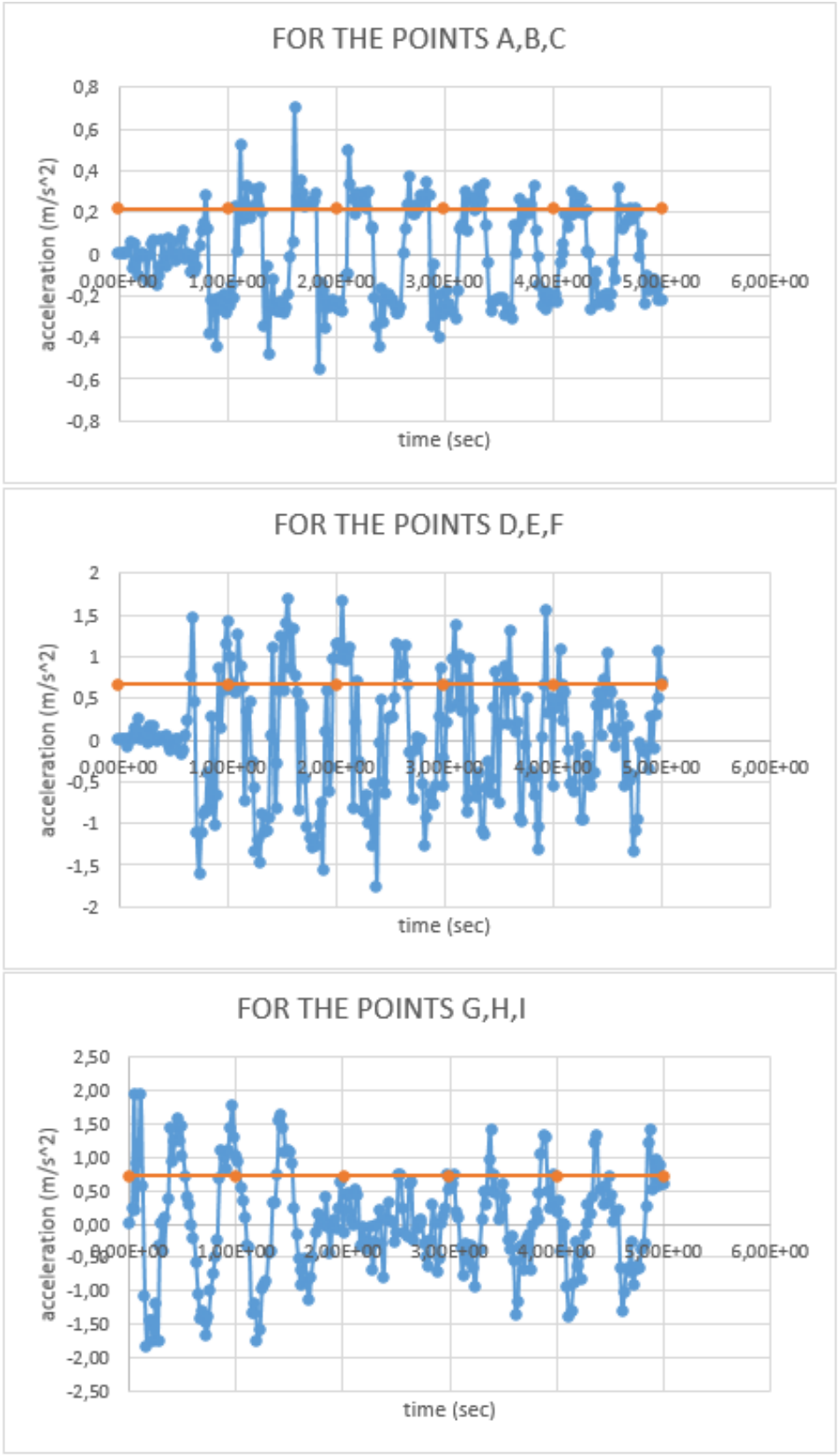

Figure C.18. Average Acceleration for reinforced case under 0.1g PGA with 2 hz frequency.

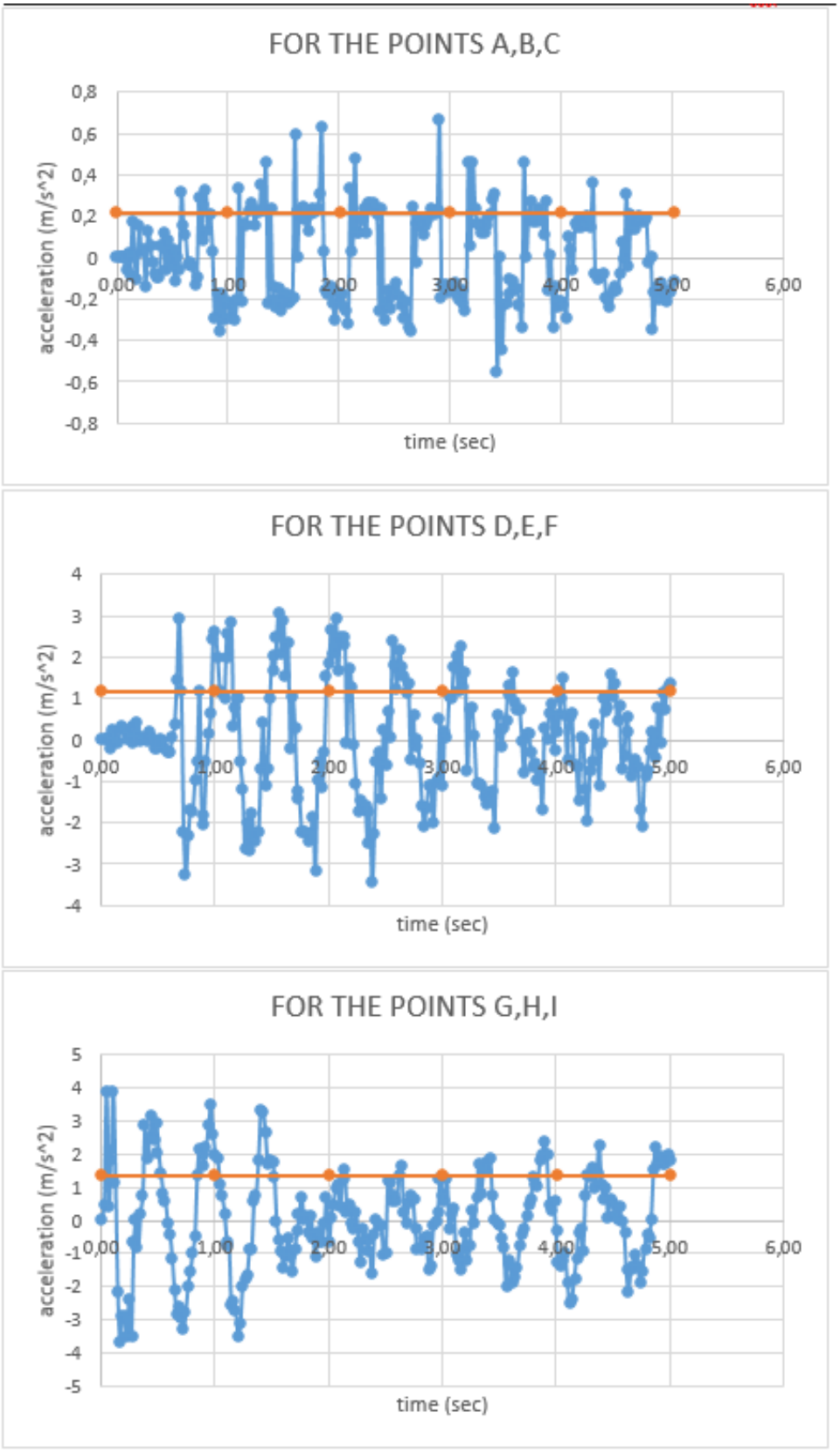

Figure C.19. Average Acceleration for unreinforced case under 0.2g PGA with 2 hz frequency.

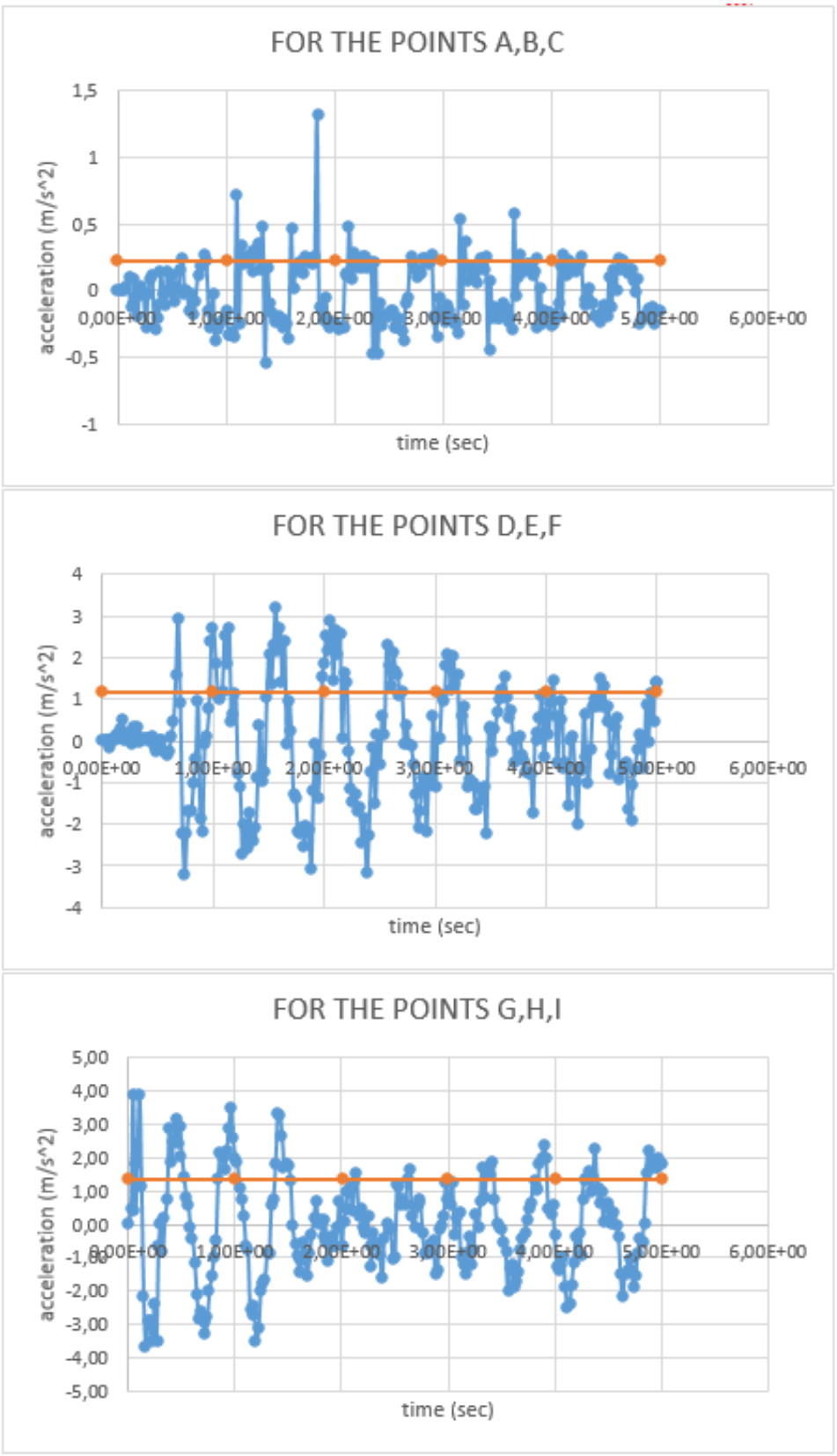

Figure C.20. Average Acceleration for reinforced case under 0.2g PGA with 2 hz frequency.

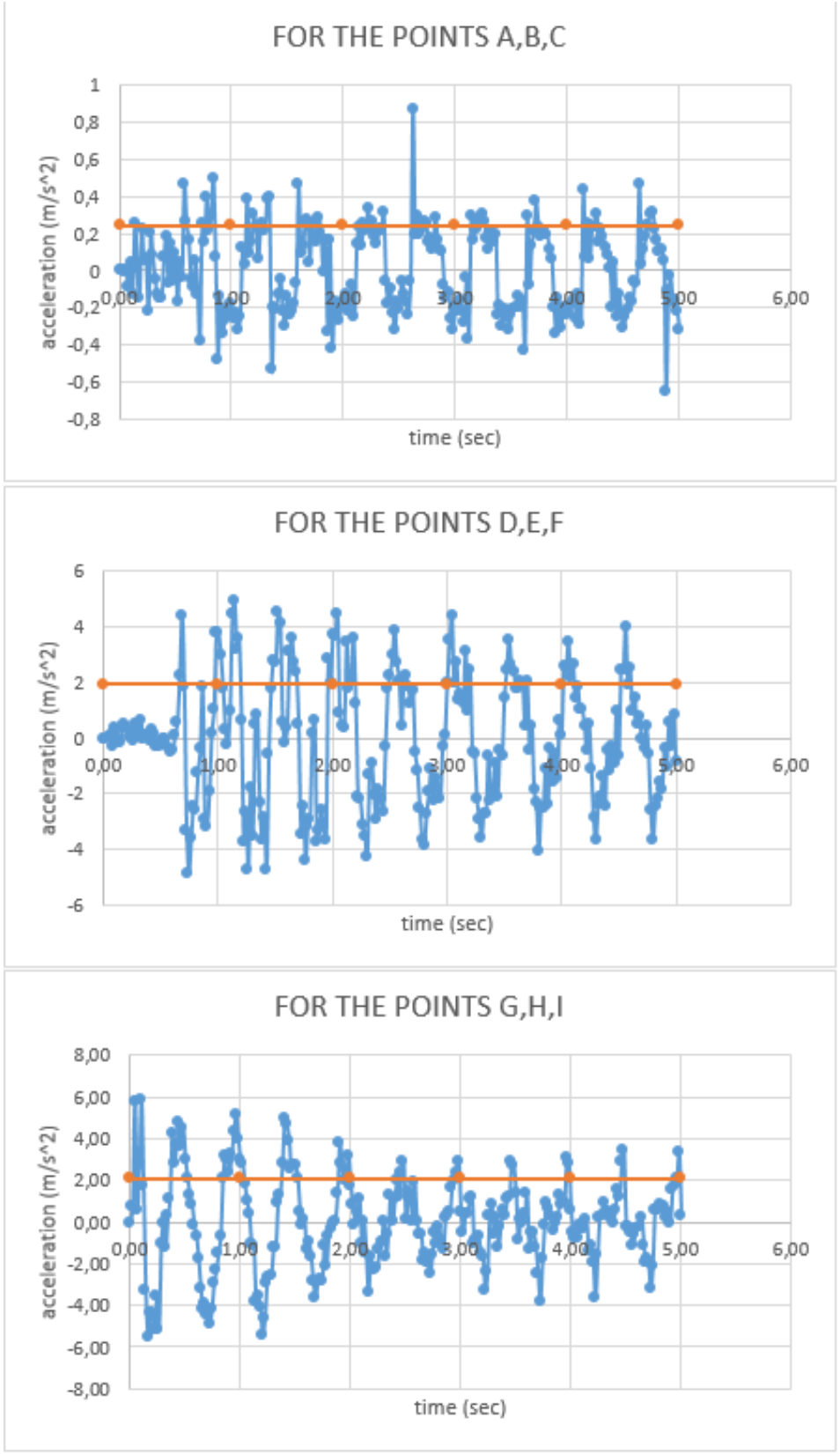

Figure C.21. Average Acceleration for unreinforced case under 0.3g PGA with 2 hz frequency.

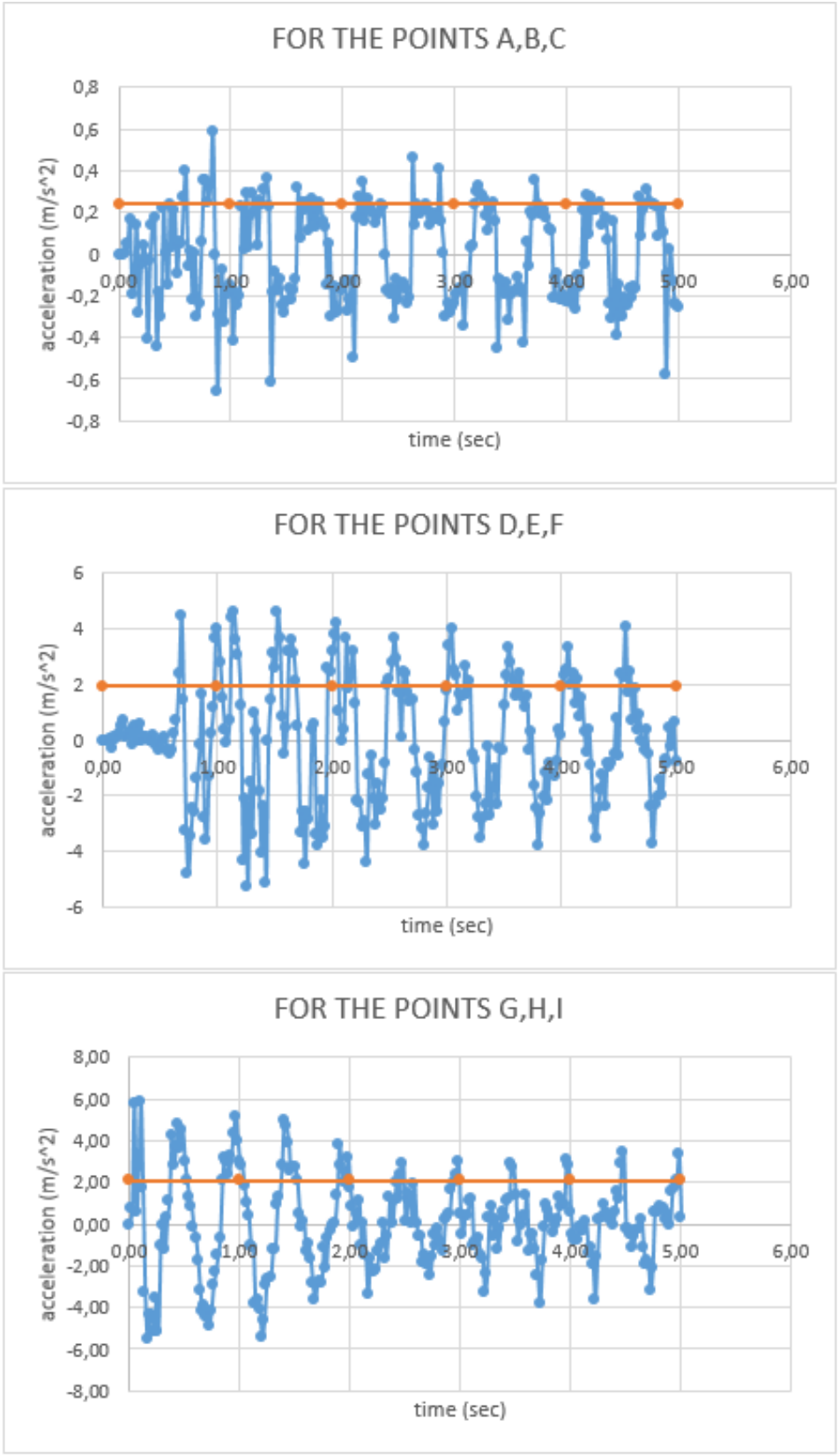

Figure C.22. Average Acceleration for reinforced case under 0.3g PGA with 2 hz frequency.

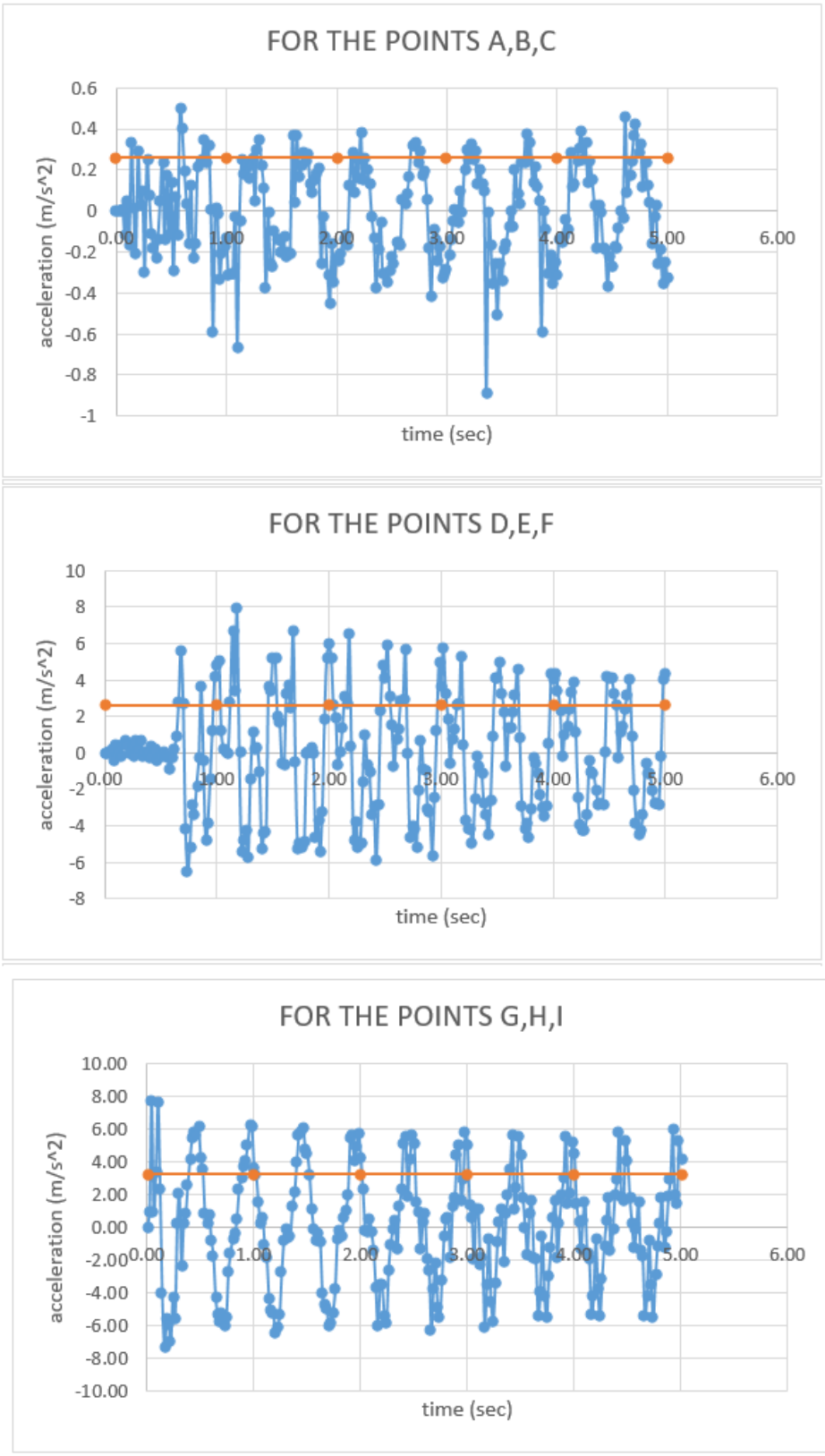

Figure C.23. Average Acceleration for reinforced case under 0.4g PGA with 2 hz frequency.

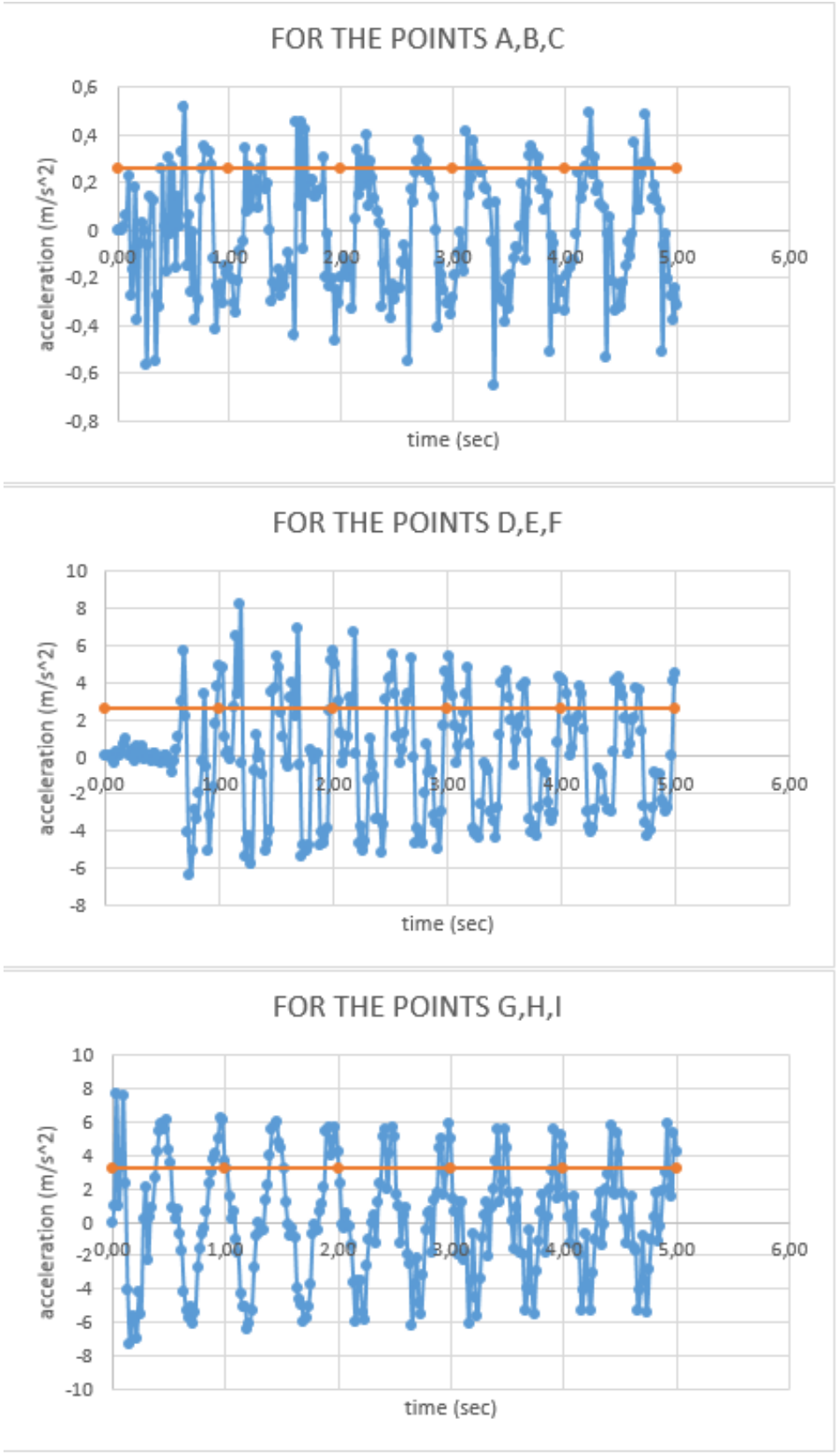

Figure C.24. Average Acceleration for unreinforced case under 0.1g PGA with 3 hz frequency.

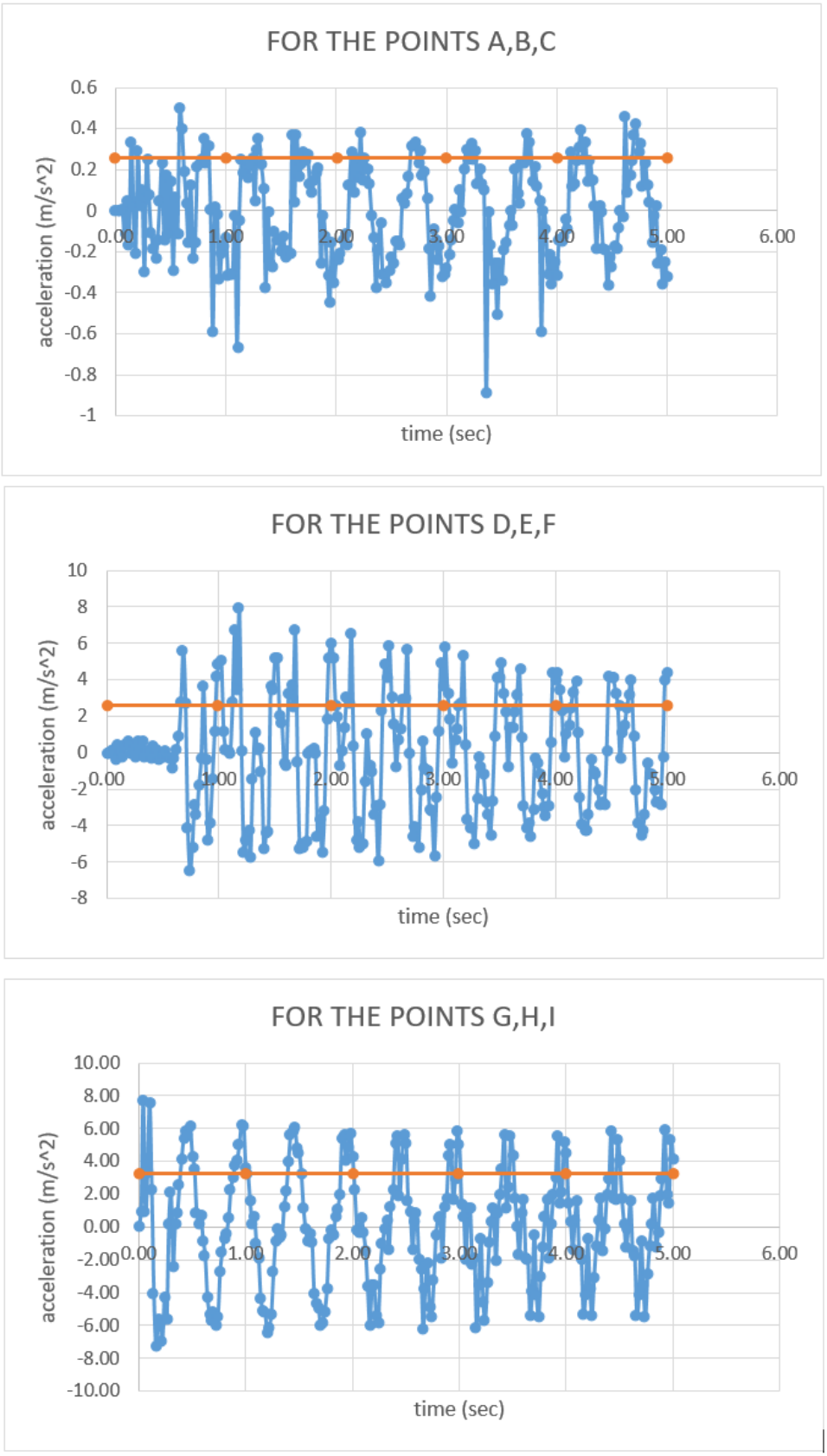

Figure C.25. Average Acceleration for reinforced case under 0.1g PGA with 3 hz frequency.

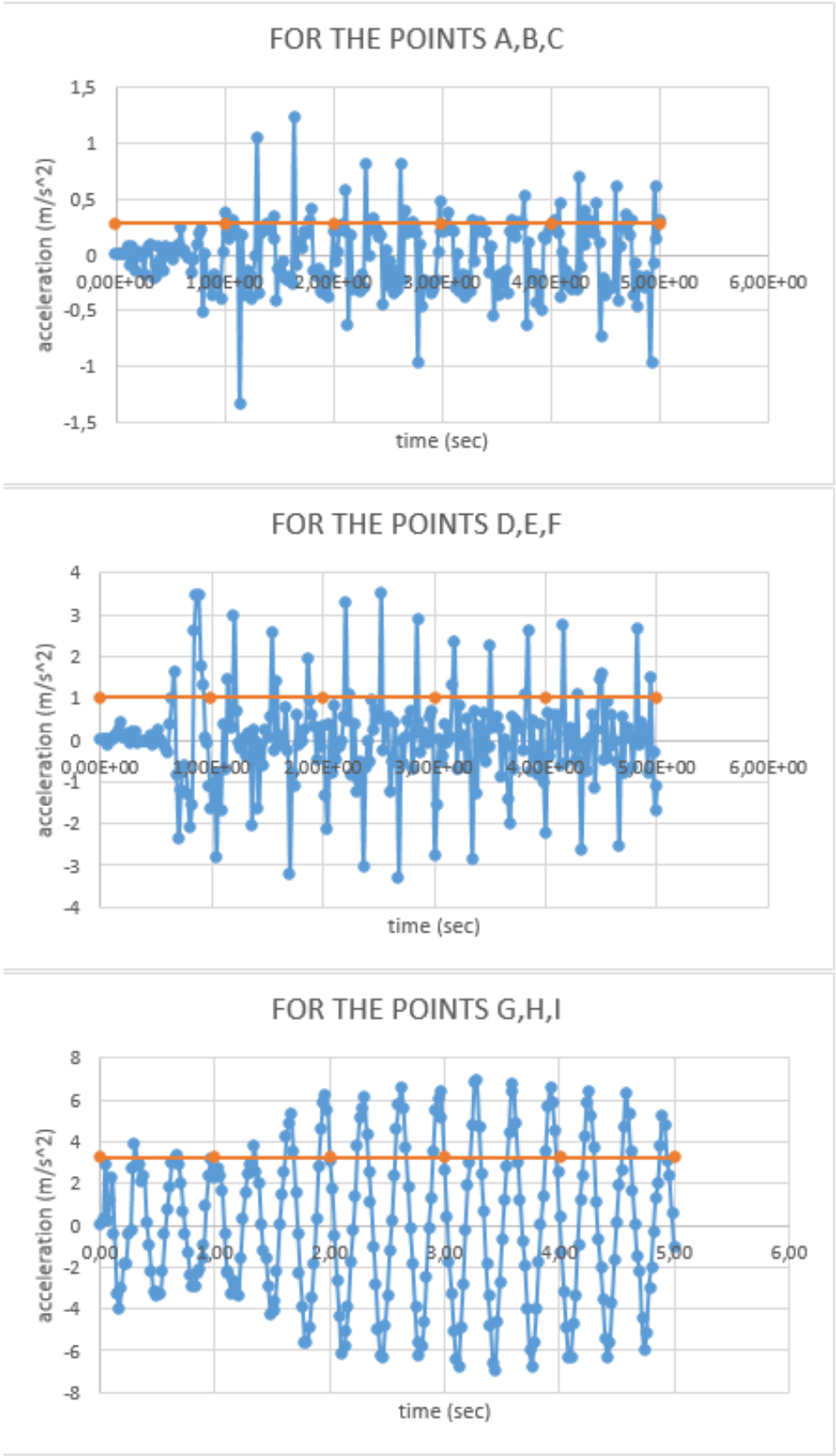

Figure C.26. Average Acceleration for unreinforced case under 0.2g PGA with 3 hz frequency.

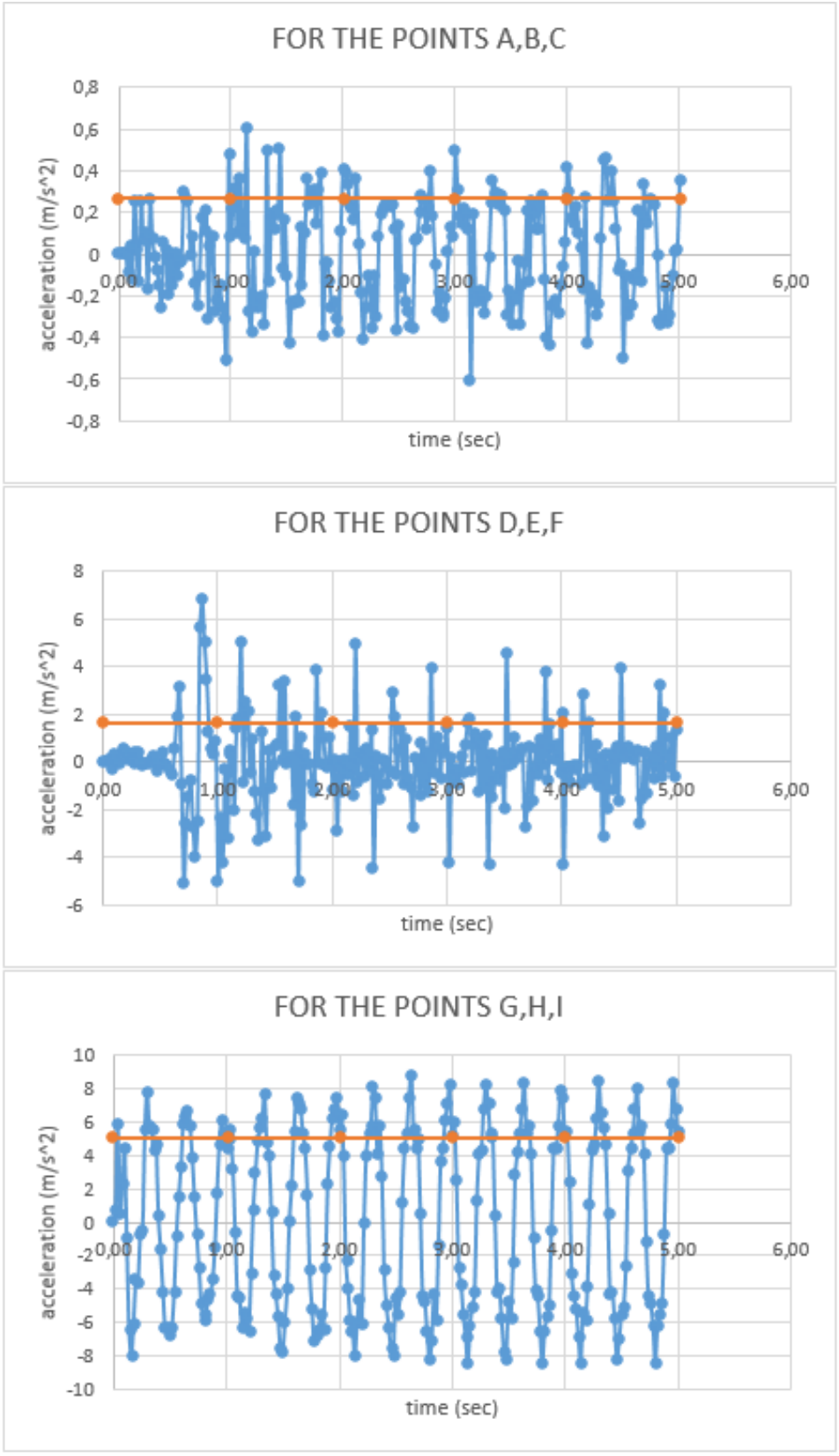

Figure C.27. Average Acceleration for reinforced case under 0.2g PGA with 3 hz frequency.

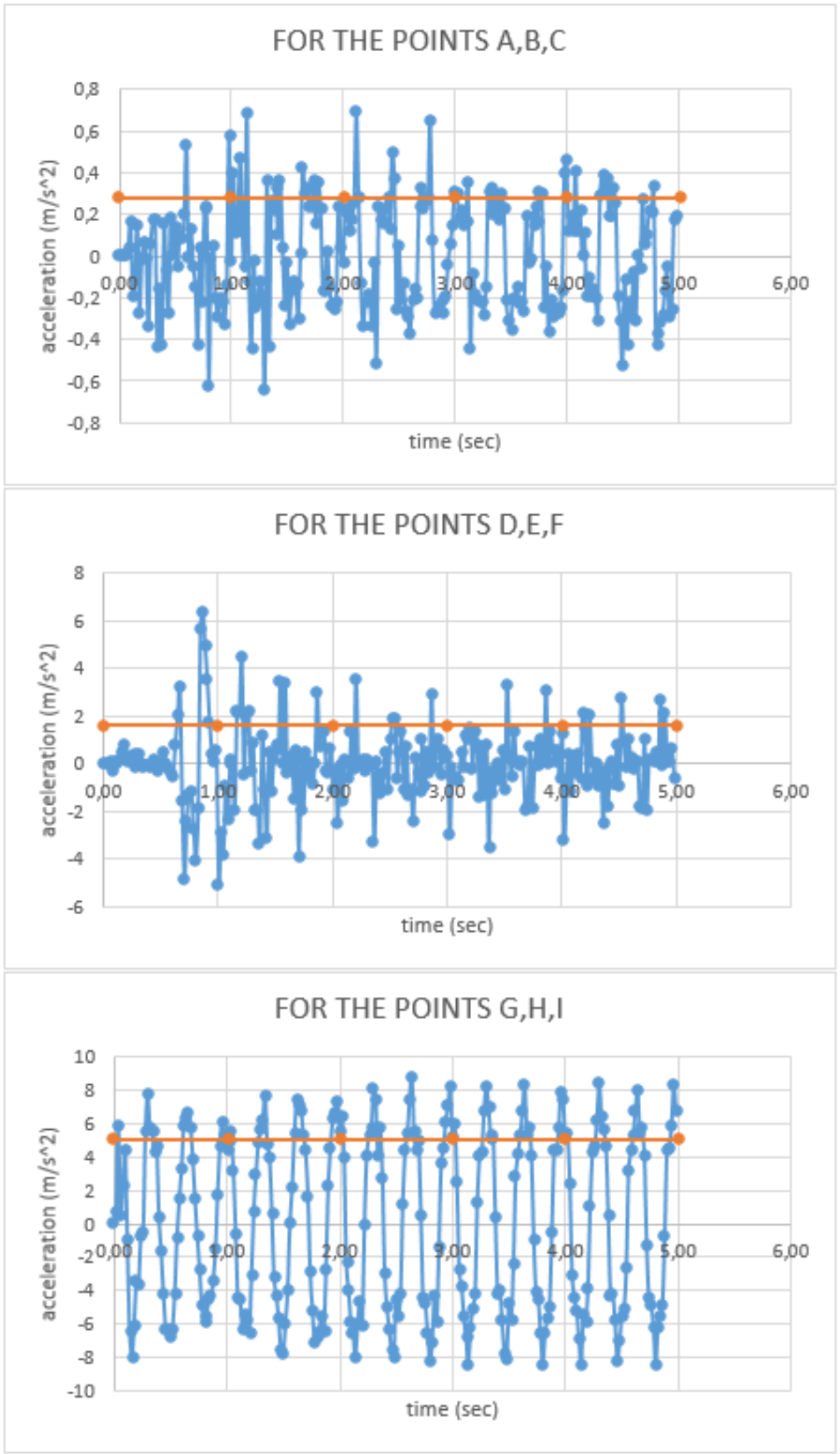

Figure C.28. Average Acceleration for unreinforced case under 0.3g PGA with 3 hz frequency.

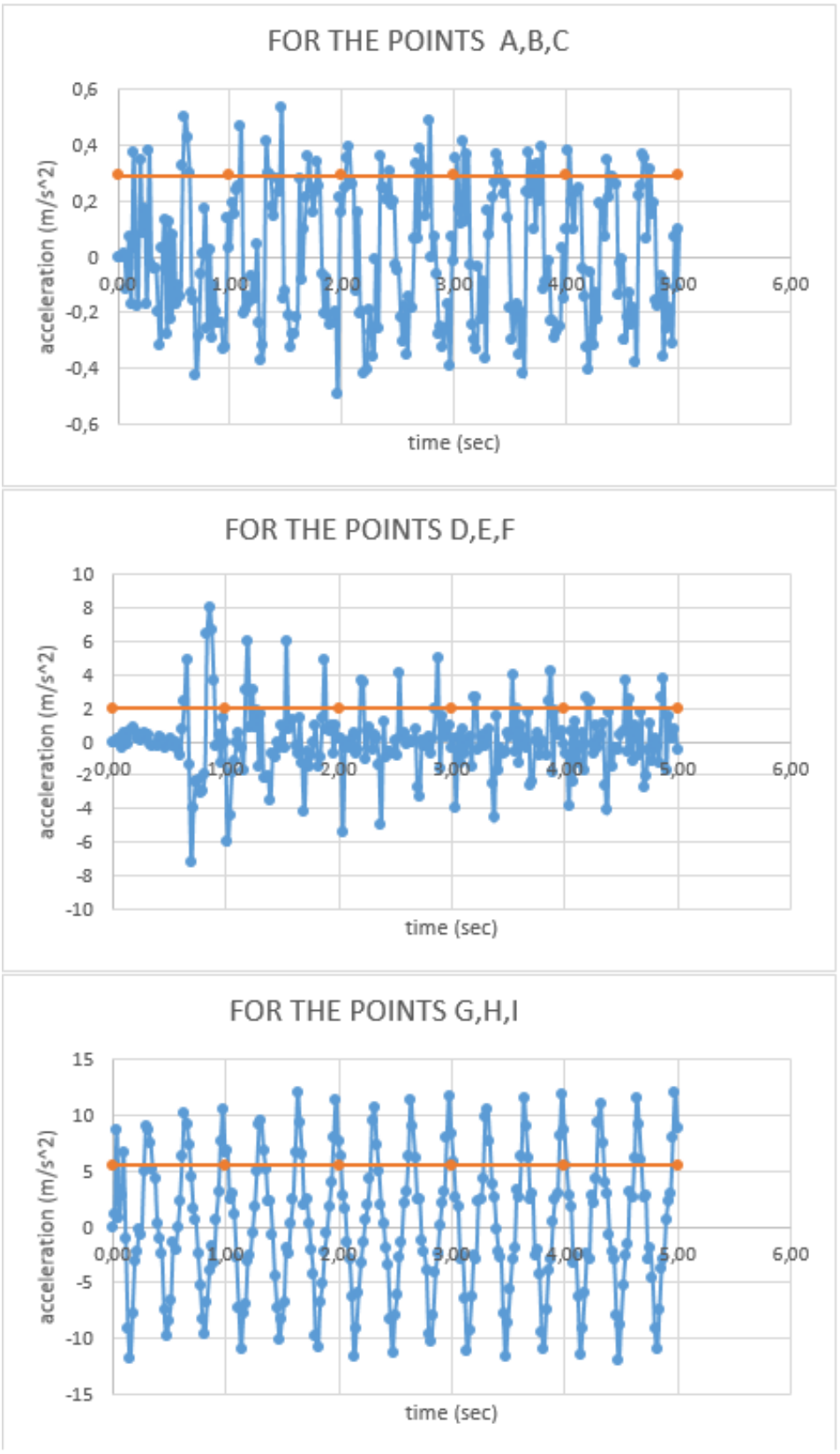

Figure C.29. Average Acceleration for reinforced case under 0.3g PGA with 3 hz frequency.

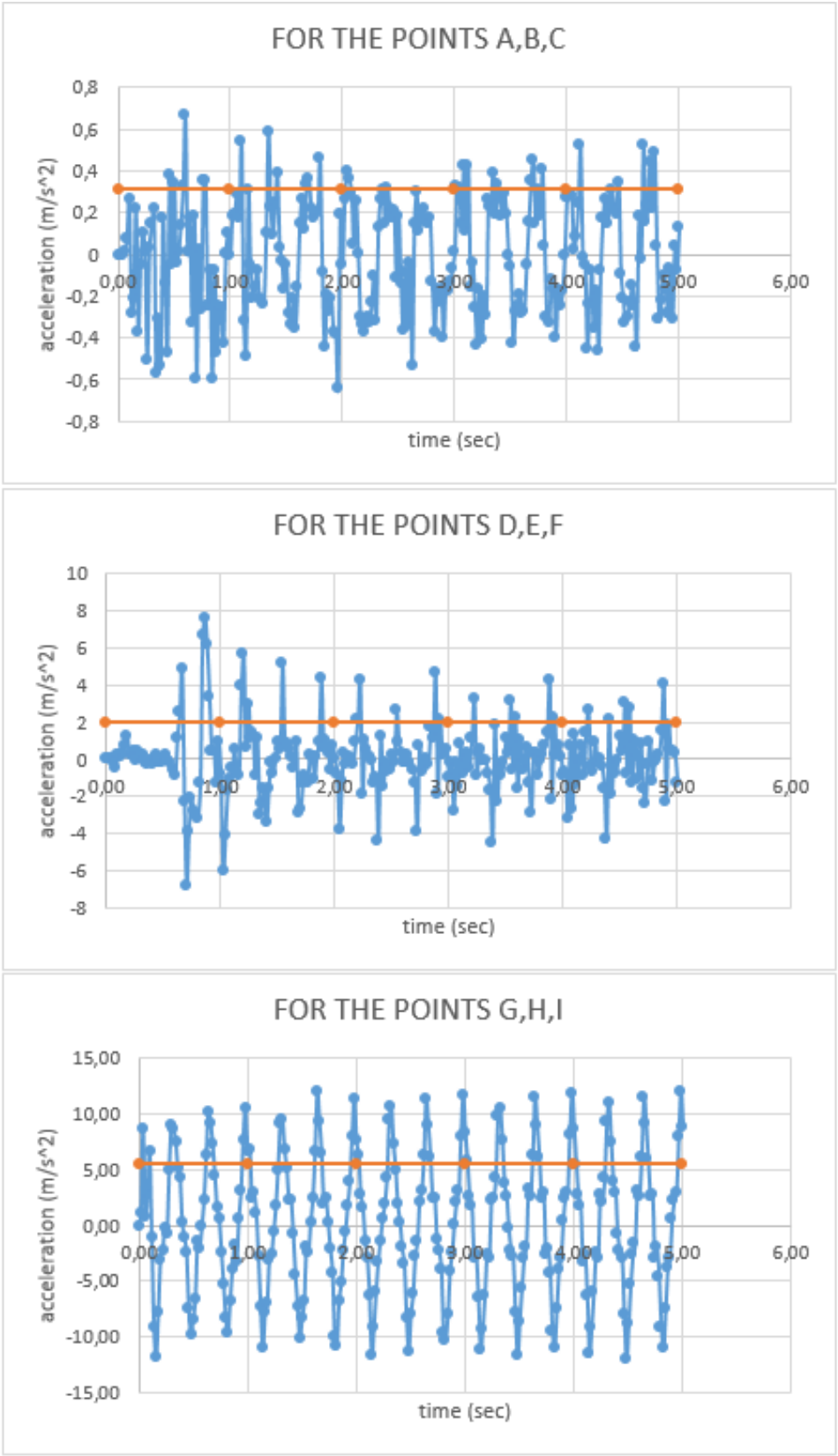

Figure C.30. Average Acceleration for unreinforced case under 0.4g PGA with 3 hz frequency.

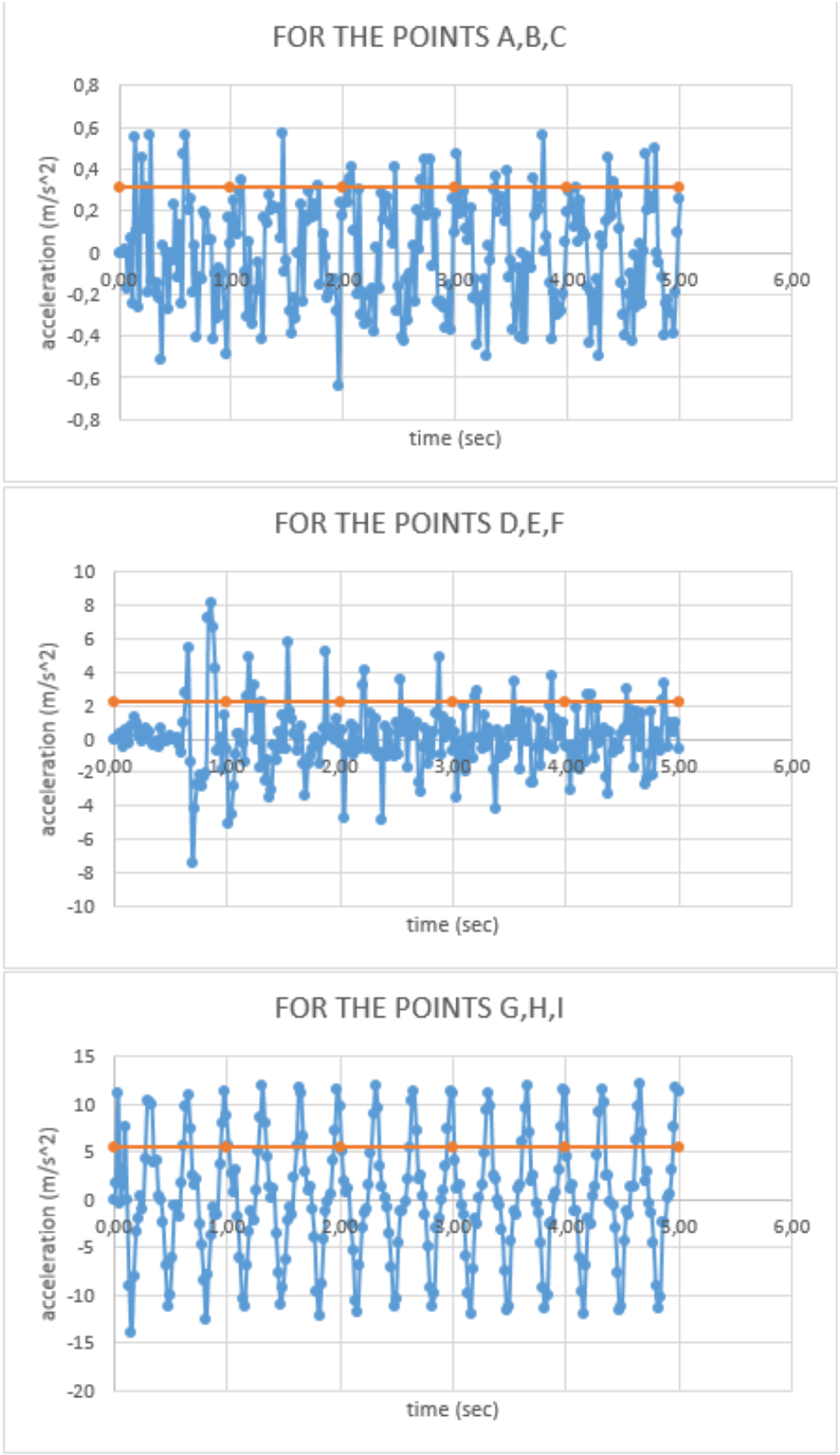

Figure C.31. Average Acceleration for reinforced case under 0.4g PGA with 3 hz frequency.

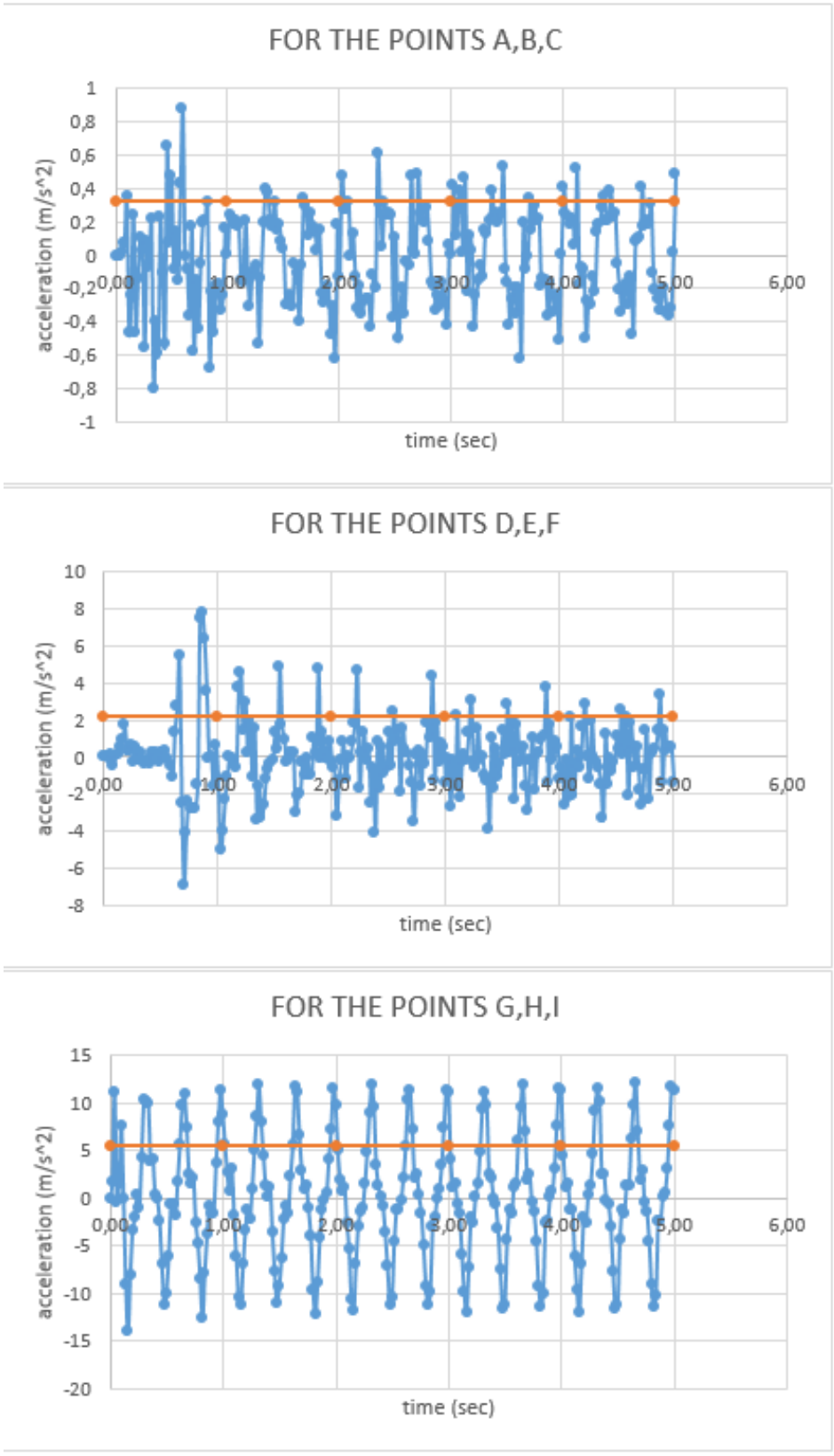

Figure C.32. Average Acceleration for unreinforced case under 0.1g PGA with 5 hz frequency.

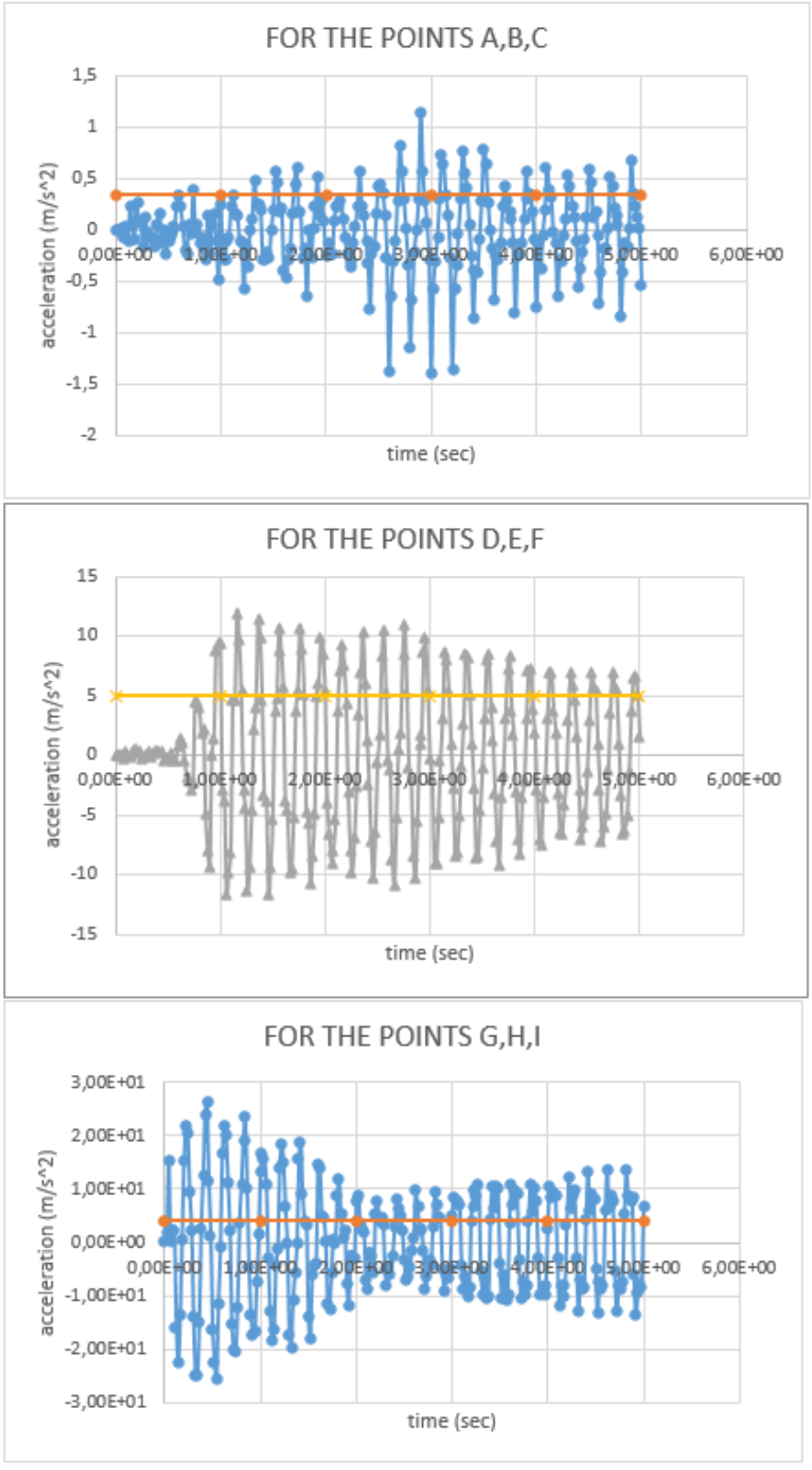

Figure C.33. Average Acceleration for reinforced case under 0.1g PGA with 5 hz frequency.

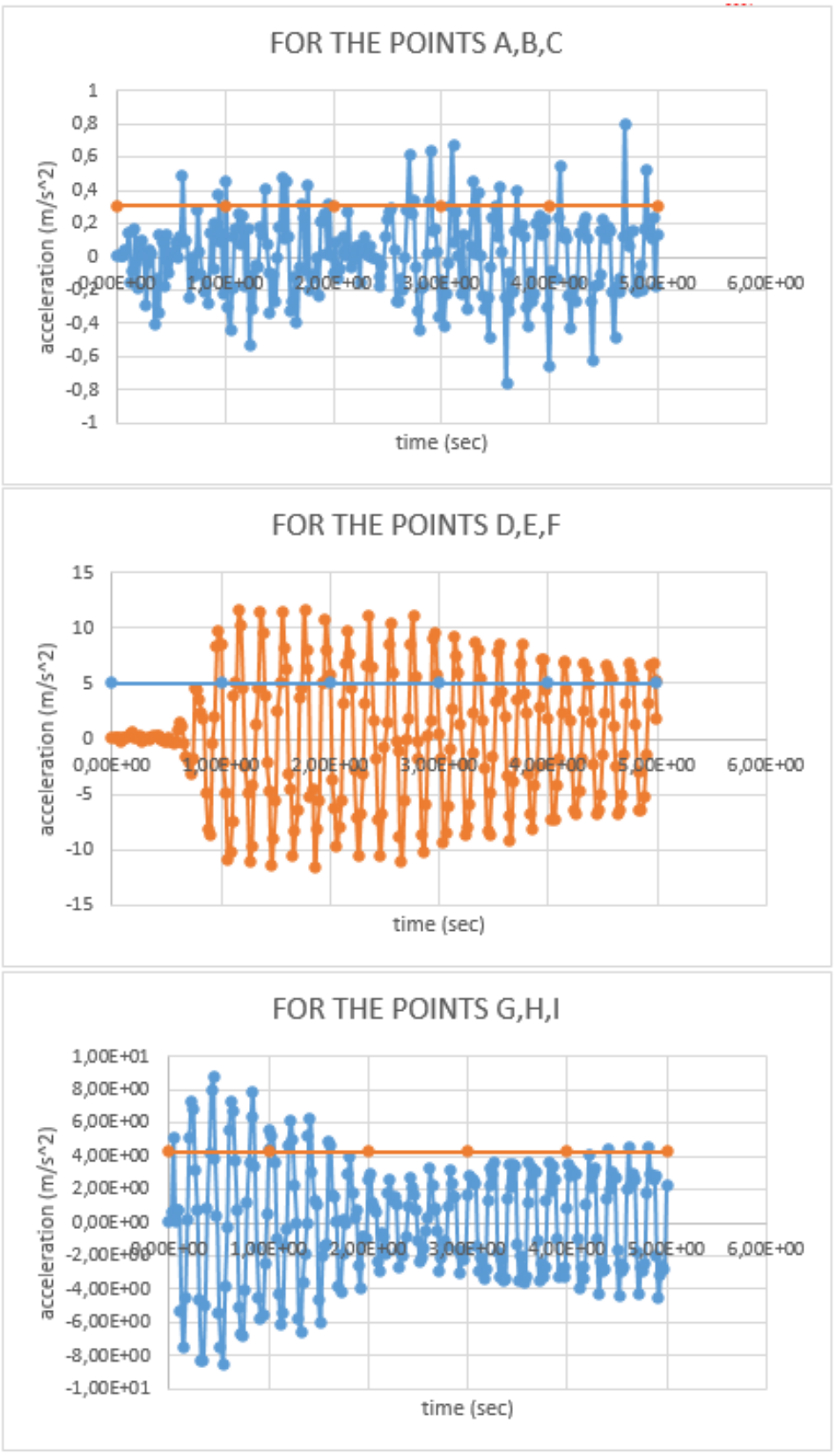

Figure C.34. Average Acceleration for unreinforced case under 0.2g PGA with 5 hz frequency.

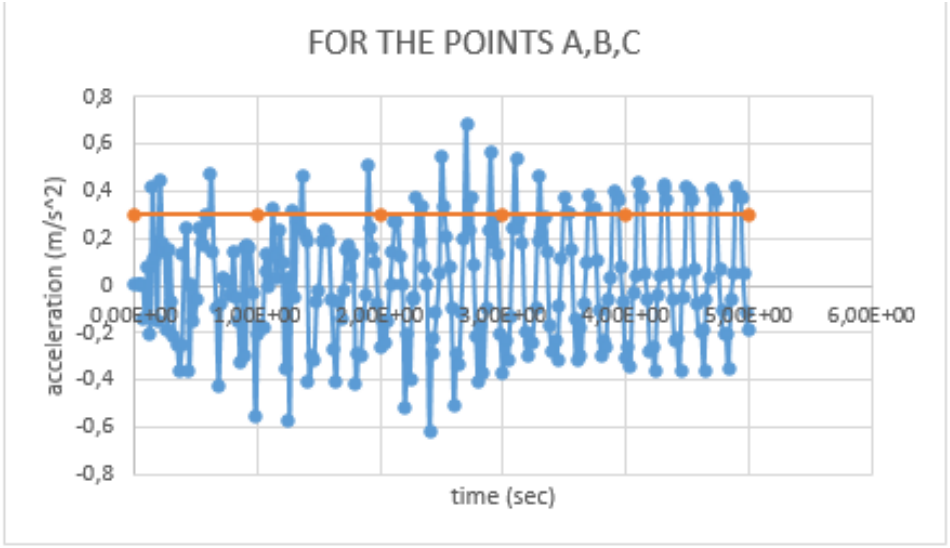

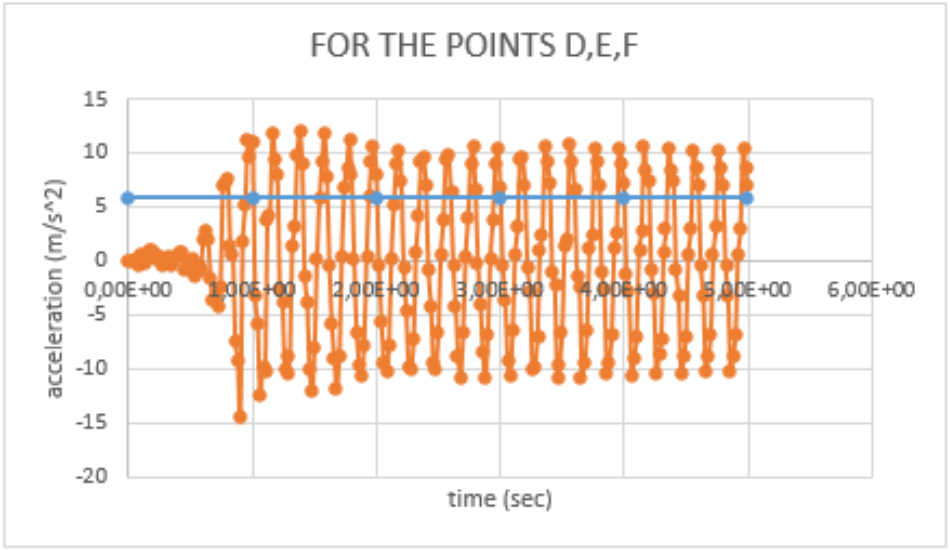

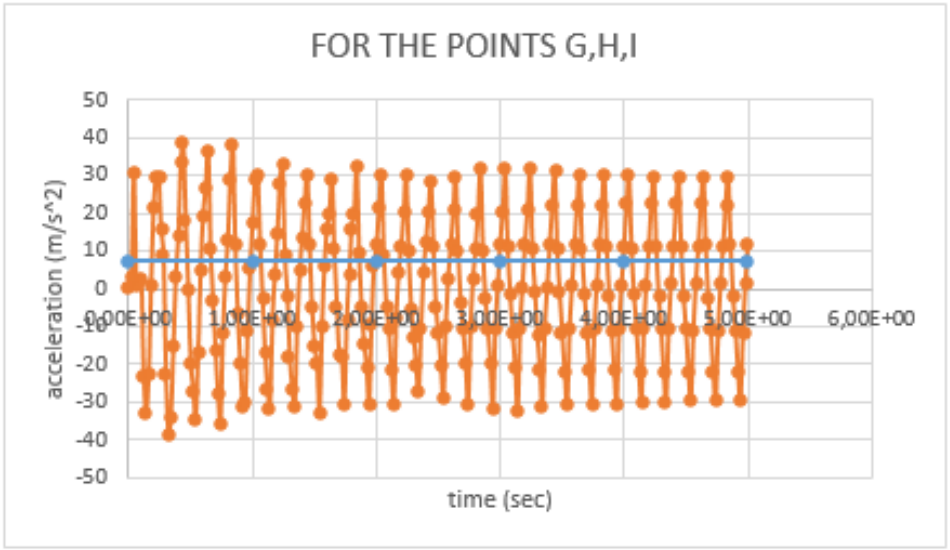

Figure C.35. Average Acceleration for reinforced case under 0.2g PGA with 5 hz frequency.

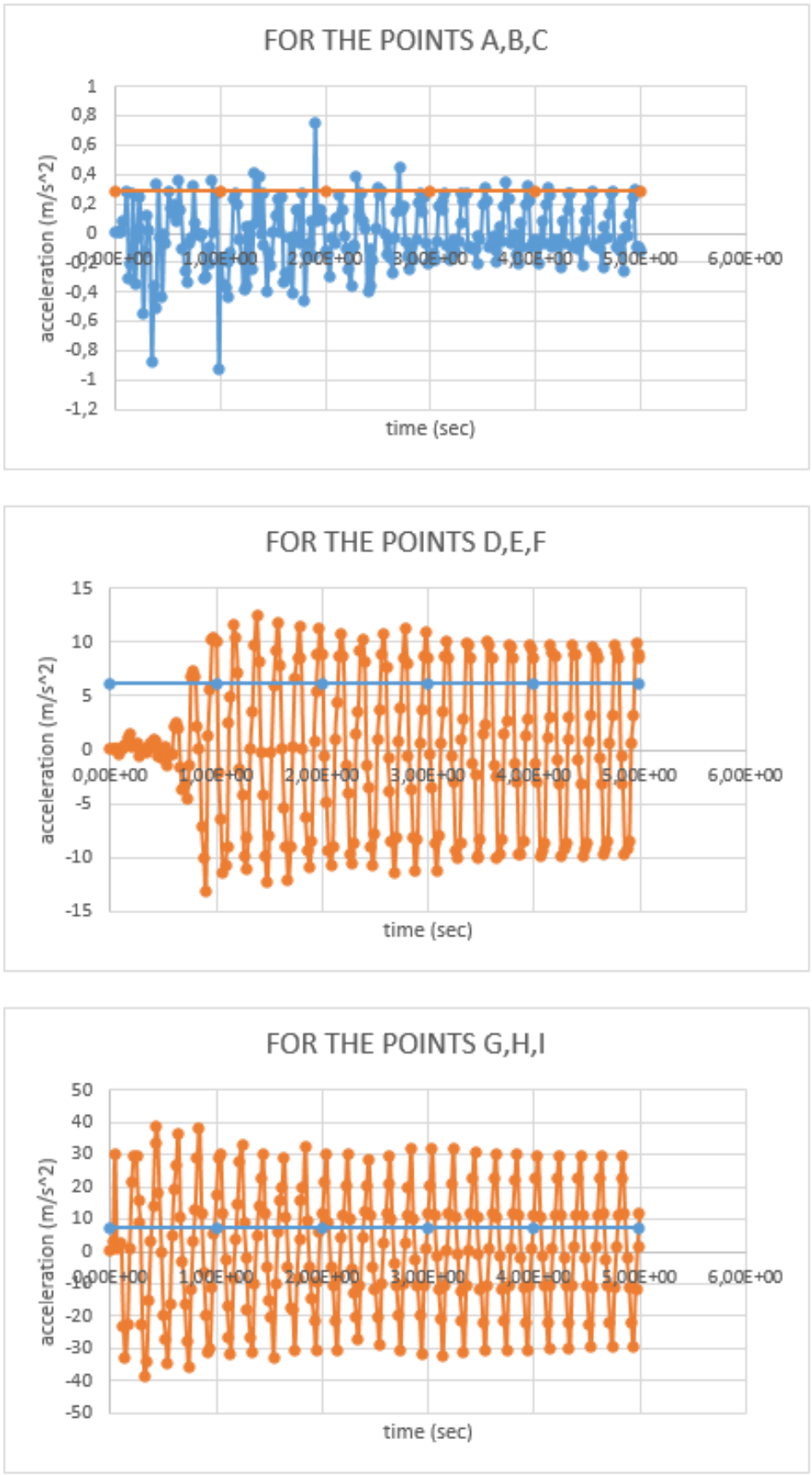

Figure C.36. Average Acceleration for unreinforced case under 0.3g PGA with 5 hz frequency.

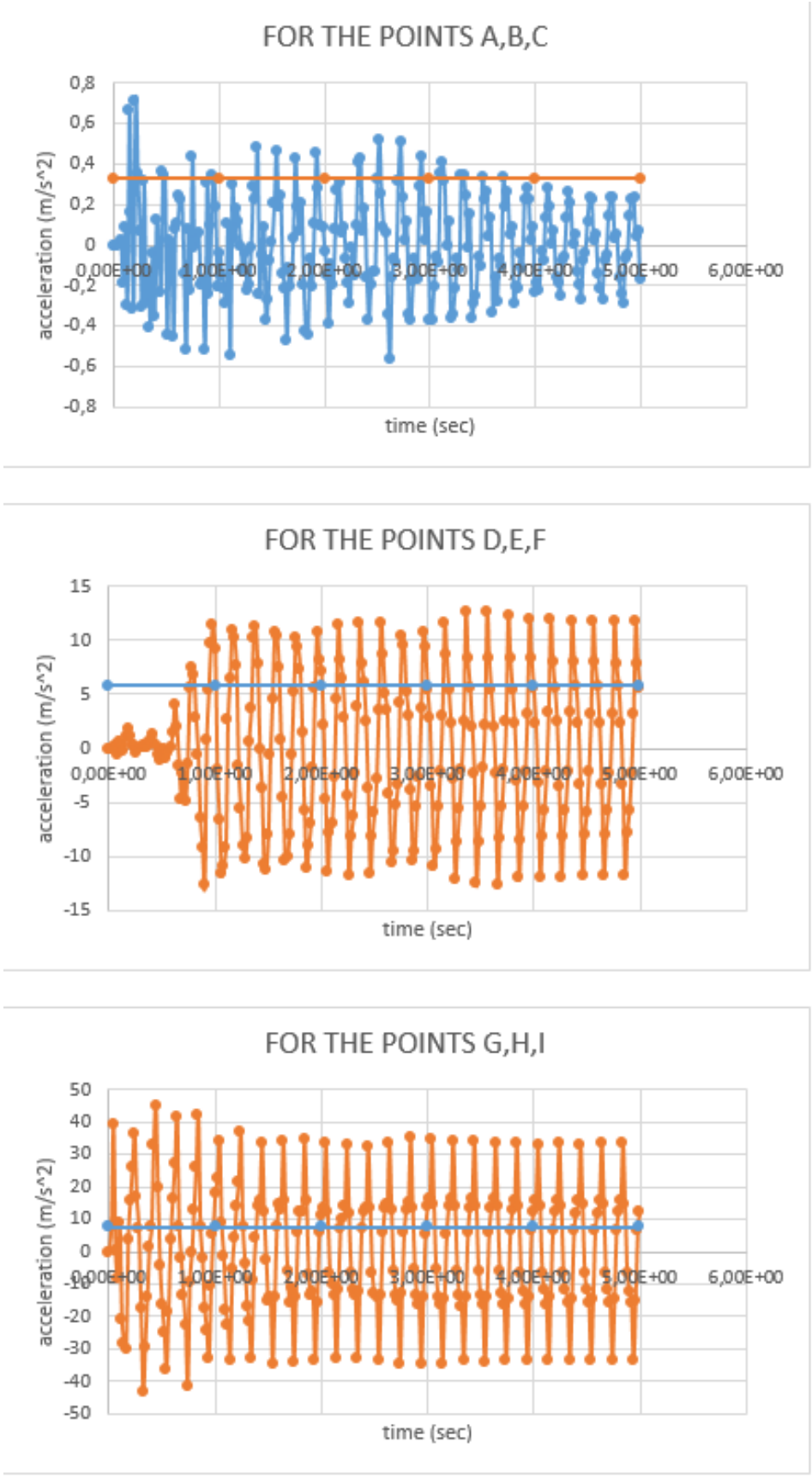

Figure C.37. Average Acceleration for reinforced case under 0.3g PGA with 5 hz frequency.

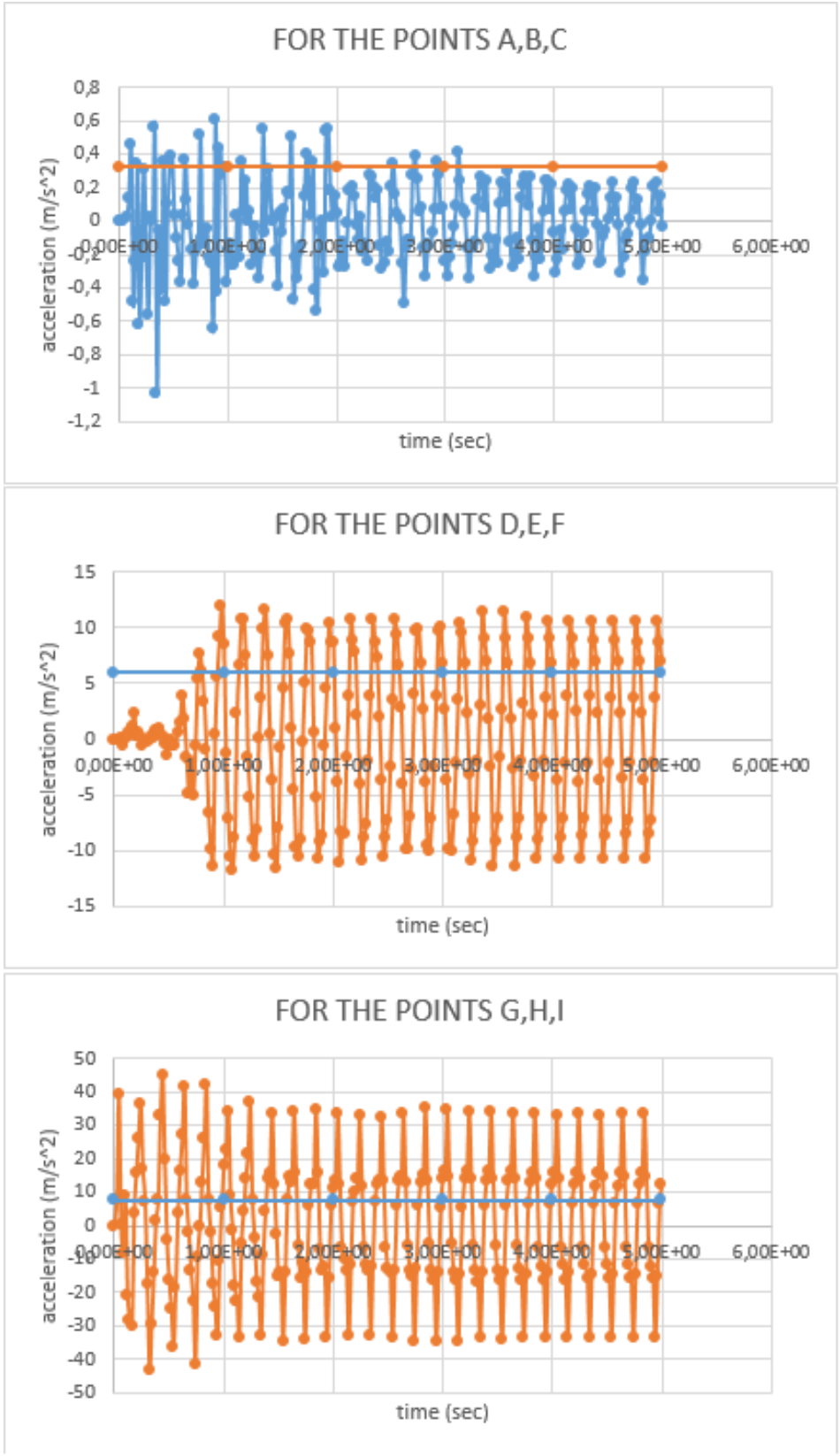

Figure C.38. Average Acceleration for unreinforced case under 0.4g PGA with 5 hz frequency.

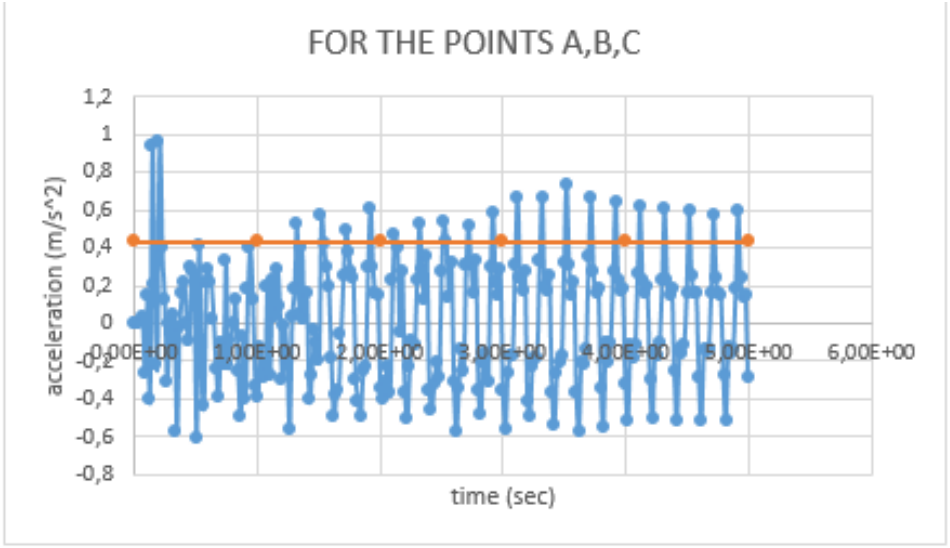

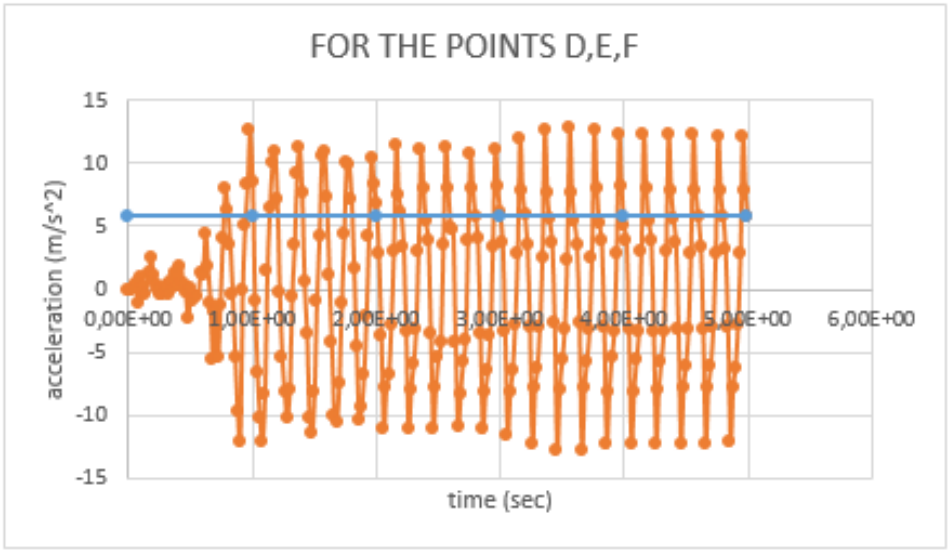

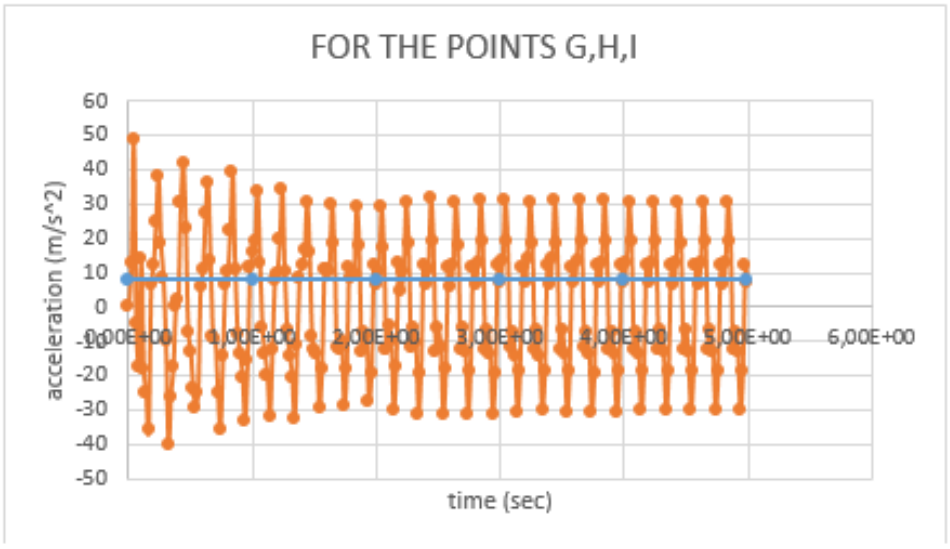

Figure C.39. Average Acceleration for reinforced case under 0.4g PGA with 5 hz frequency.